Universitat Politècnica de Catalunya

Stability and ligand binding properties of human cone visual pigments

A thesis submitted for the degree of

Doctor of Philosophy

by

Sundaramoorthy Srinivasan

This work has been carried out at the Molecular and Industrial Biotechnology Group, Department of Chemical Engineering, under the direction of Prof. Pere Garriga Solé.

Prof. Pere Garriga Solé

Terrassa, 2015

UNIVERSITAT POLITÈCNICA DE CATALUNYA BARCELONATECH

Curs acadèmic: 2014/2015

Acta de qualificació de tesi doctoral

Nom i cognoms
SUNDARAMOORTHY SRINIVASAN

Programa de doctorat
TECNOLOGIA AGROALIMENTÀRIA I BIOTECNOLOGIA

Unitat estructural responsable del programa
ENGINYERIA QUÍMICA

Resolució del Tribunal

Reunit el Tribunal designat a l'efecte, el doctorand / la doctoranda exposa el tema de la seva tesi doctoral titulada STABILITY AND LIGAND BINDING PROPERTIES OF HUMAN CONE VISUAL PIGMENTS

Acabada la lectura i després de donar resposta a les qüestions formulades pels membres titulars del tribunal, aquest atorga la qualificació:

☐ NO APTE ☐ APROVAT ☐ NOTABLE ☐ EXCEL·LENT

(Nom, cognoms i signatura) President/a		(Nom, cognoms i signatura) Secretari/ària
(Nom, cognoms i signatura) Vocal	(Nom, cognoms i signatura) Vocal	(Nom, cognoms i signatura) Vocal

_____, _____ d'/de _____ de _____

El resultat de l'escrutini dels vots emesos pels membres titulars del tribunal, efectuat per l'Escola de Doctorat, a instància de la Comissió de Doctorat de la UPC, atorga la MENCIÓ CUM LAUDE:

☐ SÍ ☐ NO

(Nom, cognoms i signatura) President de la Comissió Permanent de l'Escola de Doctorat	(Nom, cognoms i signatura) Secretari de la Comissió Permanent de l'Escola de Doctorat

Barcelona, _____ d'/de _____ de _____

To

my family
&
Shana

எப்பொருள் யார் யார் வாய் கேட்பினும்
அப்பொருள் மெய்பொருள் காண்பதறிவு

- *திருவள்ளுவர்*

The thing, whatsoever, is said by whomsoever,
discerning the truth of it, is wisdom

- ***Thiruvalluvar***

ABSTRACT

Human color perception is mediated by cone photoreceptor cells which mainly locate on the fovea of the eye. Bright light activates the photosensitive opsin pigments which are embedded in the outer segment membrane discs of cone retinal cells thereby initiating the complex process of photopic vision with a fast response. The cone visual pigments are G-protein coupled receptors which share analogous structure and functional features with rhodopsin, the most thoroughly studied G-protein coupled receptor from rod photoreceptor cells mediating scotopic vision and distributed throughout the retina. These visual pigments are believed to play an unique role in modulating spectral tuning of visible light depending on the molecular variance around the protein bound chromophore, 11-*cis*-retinal, which is a vitamin A derivative acting as an inverse agonist. Various mutations have been clinically identified in the cone opsin genes and associated with visual dysfunction ranging from mild color blindness to severe cone dystrophies. As the crystal structure of the cone pigments is yet to be resolved, identifying key molecular mechanisms that play major roles in optimal functioning of these photoreceptor proteins, should be helpful in providing a deeper understanding of their function and in designing novel therapeutic strategies for congenital retinal cone dysfunction.

In order to study such light sensitive, delicate membrane proteins, the human cone opsin genes have been transiently expressed in mammalian cells, regenerated with their natural chromophore and immunopurified in dark conditions. The purified recombinant chromophore-regenerated cone opsins in solution have been characterized in detail by means of biophysical approaches, including spectroscopic, biochemical, and functional analysis, in order to uncover novel properties that help in optimizing the function of these receptors. The studied molecular properties of cone opsins, include stability in solution, the mechanism of chromophore regeneration and their functional analysis have been compared to those of rhodopsin. Site-directed mutagenesis was employed to obtain the clinically identified mutations in cone opsins related to visual disorders and to compare the structure and function of these mutated opsins with the molecular properties of the wild-type cone opsins expressed in the same way.

The results of the present study indicate that the cone opsins are less stable in solution and their retinal binding site is more open than rhodopsin. The ligand binding studies using retinal analogs, show that the photoactivated rhodopsin loses its ability to regenerate with its natural chromophore with time but not with an analog, 9-*cis*-retinal and cone opsins show regeneration with both retinal analogs under the same experimental conditions.

The highly identical red and green cone opsins exhibit different ligand binding modes during regeneration with their natural chromophore, 11-*cis*-retinal. A secondary retinal uptake, with a

slower kinetics, has been also observed with the red and green cone pigments during regeneration with 11-*cis*-retinal which is altered in the case of blue cone opsin. The role of specific amino acids involved in the regeneration mechanism has also been clarified.

Most of the cone opsin mutants studied, associated with visual disorders, fail to regenerate with the ligand due to protein misfolding resulting in aggregation in solution. R330Q green cone opsin mutant show a regeneration ability similar to that of the native pigment but a compromised transducin binding efficiency. Though the N94K deuteranopic mutant apparently aggregates when expressed in mammalian, chromophore binding to opsin would be through an unprotonated Schiff base linkage.

Overall, in the present study the molecular properties of cone opsins have been compared among them and with the well-studied rhodopsin. This has led to the proposal of novel molecular mechanisms for cone opsins. The determined structural differences between visual pigments may be linked to their molecular evolution, and the proposal of secondary retinoid binding to visual pigments may function as a regulatory mechanism of dark adaptation in the phototransduction process. As the crystal structure of these pigments is yet to be resolved, the identified key structural determinants, in the regeneration process, should be helpful in designing novel therapeutic strategies for congenital retinal cone dysfunction.

ABBREVIATIONS, ACRONYMS AND SYMBOLS

11CR	11-*cis*-retinal
7TM	seven transmembrane
9CR	9-*cis*-retinal
a.u.	arbitrary unit
ABCA4	ATP-binding cassette subfamily A member 4
Abs	absorbance
Amax	absorption maximum
ATP	adenosine-5'-Triphosphate
ATR	all-*trans*-retinal
BN-PAGE	blue native PAGE
bp	basepair
BSA	bovine serum albumin
BTP	bis-tris propane
c	concentration
cDNA	complementray DNA
cGMP	cyclic Guanosine 5'-monophosphate
CI / CIII	cytoplasmic loop I/III
cpm	counts per minute
CRALBP	cellular retinaldehyde binding protein
DAPI	4', 6-diamidino-2-phenylindole
DDHAPC	1, 2-didocosahexaenoyl-*sn*-glycero-3-phosphocholine
DHPC	L-α-1, 2-dihexanoyl-*sn*-glycero-3-phosphocholine
DM	n-dodecyl β-D-maltoside
DMEM	Dulbecco's modified eagle's medium
DMPC	1, 2-dimyristoyl-*sn*-glycero-3-phosphocholine
DNA	deoxy riboneuclic acid
dpm	disintegrations per minute
DTNB	5, 5'-dithio-bis-(2-nitrobenzoic acid)
E I / E III	extracellular loop I/III
FBS	fetal bovine serum
FITC	fluorescein isothiocyanate
GC	guanylate cyclase
GDP	guanosine-5'-diphosphate
GMP	guanosine 5'-monophosphate

GPCR	G-protein coupled receptor
GTP	guanosine 5'-triphosphate
$GTP\gamma S^{35}$	guanosine 5'-O- (3-thio) triphosphate
hν	quantum of light
ICL I / ICL III	intracellullar loop I / III
IPBR	interphotoreceptor binding protein
IPM	interphotoreceptor matrix
L-cone	long wavelength cone opsin / red cone opsin
l	length
LCA	Leber congenital amaurosis
LCR	locus control region
LN	long N-terminus
LRAT	lecithin: retinol acyl transferase
LWL	longer wavelength
M-cone	middle wavelength cone opsin / green cone opsin
MES	2-(N-morpholino) ethanesulfonic acid
MWL	middle wavelength
NADPH	nicotinamide adenine dineucleotide phosphate
NaPi	sodium phosphate buffer
NRPE	N-retinylidene phosphotidyl ethanolamine
P	promotor
PAGE	polyacrylamide gel electrophoresis
PBS	phosphate buffered saline
PCR	polymerase chain reaction
PDE	phosphodiesterase
PE	phosphotidyl ethanolamine
PEI	polyethylenimine
PSB	protonated Schiff base
PSB11	11-*cis*-retinal-prononated Schiff base
PSB13	13-*cis*-retinal-prononated Schiff base
PSB7	7-*cis*-retinal-prononated Schiff base
PSB9	9-*cis*-retinal-prononated Schiff base
PSBT	all-*trans*-retinal-prononated Schiff base
RDH	retinol dehydrogenase
REH	retinyl esterhydrolase
Rho	rhodopsin
ROS	rod outer segment

RP	retinitis pigmentosa
RPE	retinal pigment epithelium
RT	room temperature
RU	resonance unit
S-cone	short wavelength cone opsin / blue cone opsin
SB	Schiff base
SDS	sodium dodecyl sulfate
SPR	surface plasmon resonance
SWL	short wavelength
$t_{1/2}$	half-time
T2R	taste2 receptors
TBS	tris buffered saline
TM1 / TM7	transmembrane1/7
UV-vis	ultra violet – visble
WT	wildtype
λmax	wavelength maximum

Amino acids

A	alanine (Ala)
C	cysteine (Cys)
D	aspartate (Asp)
E	glutamate (Glu)
F	phenylalanine (Phe)
G	glycine (Gly)
H	histidine (His)
I	isoleucine (Ile)
K	lysine (Lys)
L	leucine (Leu)
M	methionine (Met)
N	asparagine (Asn)
P	proline (Pro)
Q	glutamine (Gln)
R	arginine (Arg)
S	serine (ser)
T	threonine (Thr)
V	valine (Val)
W	trptophan (Trp)
Y	tyrosine (Tyr)

TABLE OF CONTENTS

FIGURES

TABLES

1. INTRODUCTION

1.1. Cellular Communication

A cell is an open system, capable of receiving and transforming mass and energy through the plasma membrane. Structurally, cells are defined at their periphery by hydrophobic plasma membrane which is majorly composed of lipid and protein molecules that separate the contents of the cell from its surroundings (1). In multicellular organisms, the homeostasis is maintained by a coordinated communication with the exogenous/environmental mediators or through the mediators released by other cells within the living system into the extracellular milieu (2). The mediators, otherwise known as external stimuli with most of them being ligands, include light, gases, small molecules, amino acids, peptides, proteins, among others. These stimuli exert their functions by targeted interactions with specific, complementary, propagative molecules of the cells known as receptors. Based on the nature of these signaling molecules, the receptors are classified into two types including intracellular and cell surface receptors. The signaling molecules can be transported through the plasma membrane into the cell and exert their function by a complementary interaction with intracellular receptors. There are external ligands which can elicit a physiological response by interacting with cell surface receptors embedded within the plasma membrane (3).

A cell surface receptor is structurally composed of three domains namely, the extracellular domain, the transmembrane domain and the intracellular domain. The extracellular domain mainly consists of turns, a typical secondary structure of proteins, and the N-terminus of the receptor. This domain is important for the folding of the receptor and may participate in the interaction with ligands that may result in a conformational change of the receptor. The transmembrane domain is the membrane spanning structure of the receptor which is mainly made of hydrophobic residues and consists of α-helical segments, or β-sheet structure in the β-barrel structure. The intracellular domain is composed of loops and turns and the C-terminus of the protein. This is the functional part of the receptor which initiates the downstream process of signal transduction after receptor activation (4).

A typical mammalian cell can present cell surface receptors to more than 100 different types of extracellular signaling molecules. The ligand-imposed conformational changes on these cell surface receptors can stimulate various signaling mechanisms depending on the nature of the receptor. Based on the functional similarity between the signaling mechanism, the cell surface receptors are classified (5) as,

- *G-protein-coupled receptors:* these are receptors with seven transmembrane (TM) α-helices and an intracellular domain interacting with a heterotrimeric G protein. These receptors are activated by a wide range of signaling stimuli, such as light, ions, odorant molecules, neurotransmitters, hormones, etc.

- *Receptors associated with enzymatic activity:* these are receptors containing mainly a single transmembrane α-helix with an intracellular domain possessing either intrinsic enzymatic activity or associated with enzymes. Receptors associated with immunological functions belong to this category.
- *Ligand-gated ion channels:* these are receptors in which the transmembrane domain acts as an ion pore. Binding of ligand at the extracellular domain either opens or closes the ion pore thereby regulate the diffusion of ions into the cell.

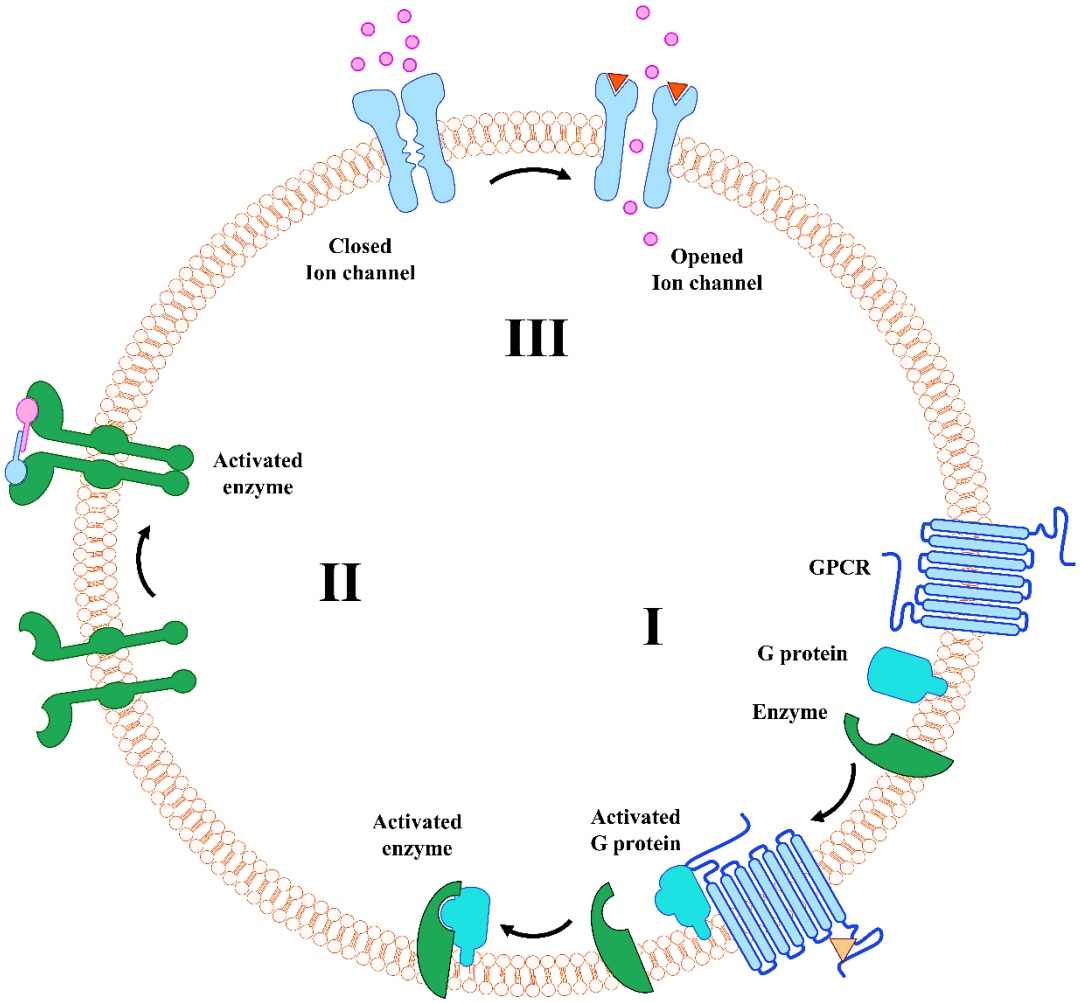

Figure 1.1. ***Cell surface receptors***. **(I)** *G-protein-coupled receptors*, the binding of ligand activates the G-protein which in turn engages in further downstream signaling **(II)** *Receptors associated with enzymatic activity*, binding of the ligand induces receptor dimerization which unleashes the intrinsic enzymatic activity of the receptor, **(III)** *Ligand-gated ion channels*, binding of a specific ligand opens the transmembrane ion channel.

1.2. G-protein-coupled receptors

The G-protein-coupled receptors (GPCRs) superfamily is one of the largest families of proteins in the mammalian genome (6). GPCRs are characterized by two main features. The first one relates to the presence of seven hydrophobic transmembrane α-helices embedded into the cell membrane lipid bilayer with each helical stretch of about 25 to 35 amino acids. This transmembrane core enables the binding of an extracellular ligand -or a chromophore- in order to exert a specific activity towards cellular function. The second principal feature is the ability of these seven transmembrane receptors to interact, upon activation, with G-proteins (7).

The total number of members for the GPCR superfamily is unknown, but it is estimated around 800 different human genes, of which approximately 350 are known for exhibiting their function by detecting hormones, pheromones, growth factors, neurotransmitters and other endogenous ligands (8,9). In human, all these GPCRs are classified in 5 major groups based on their sequence and functional similarity known as A-F classification (10,11) which include,

Class A. The rhodopsin family

Class B. The secretin family

Class C. The glutamate family

Class D . The Adhesion family

Class F. Frizzled/Taste2 family

The typical mechanism of action of GPCRs involves activation by a ligand (or light in the specific case of rhodopsin) which causes a conformational change in the inactive receptor, allowing the activated conformation to bind and activate a heterotrimeric G-protein. This process encompasses GDP for GTP exchange and dissociation of the α-subunit of the G-protein for further signaling (12).

Class A. The Rhodopsin-like GPCRs: class A or rhodopsin family, is the largest group of GPCRs containing around 701 receptors and the family is further divided into four subgroups – α, β, γ, and δ from which the α subgroup contains visual opsins. These family of GPCRs is highly heterogeneous in terms of primary structure and the preference of ligand. Most of the rhodopsin-like receptors are primarily activated by interactions between the ligand and the transmembrane regions and extracellular loops owing to their short N−terminal stretch of amino acids (7,13).

Class B. The Secretin family GPCRs: the secretin family is a small family of GPCRs, containing an extracellular binding domain, possessing hormones and peptide hormones as ligands. All the receptors from this family contain conserved cysteine residues in the first and second extracellular

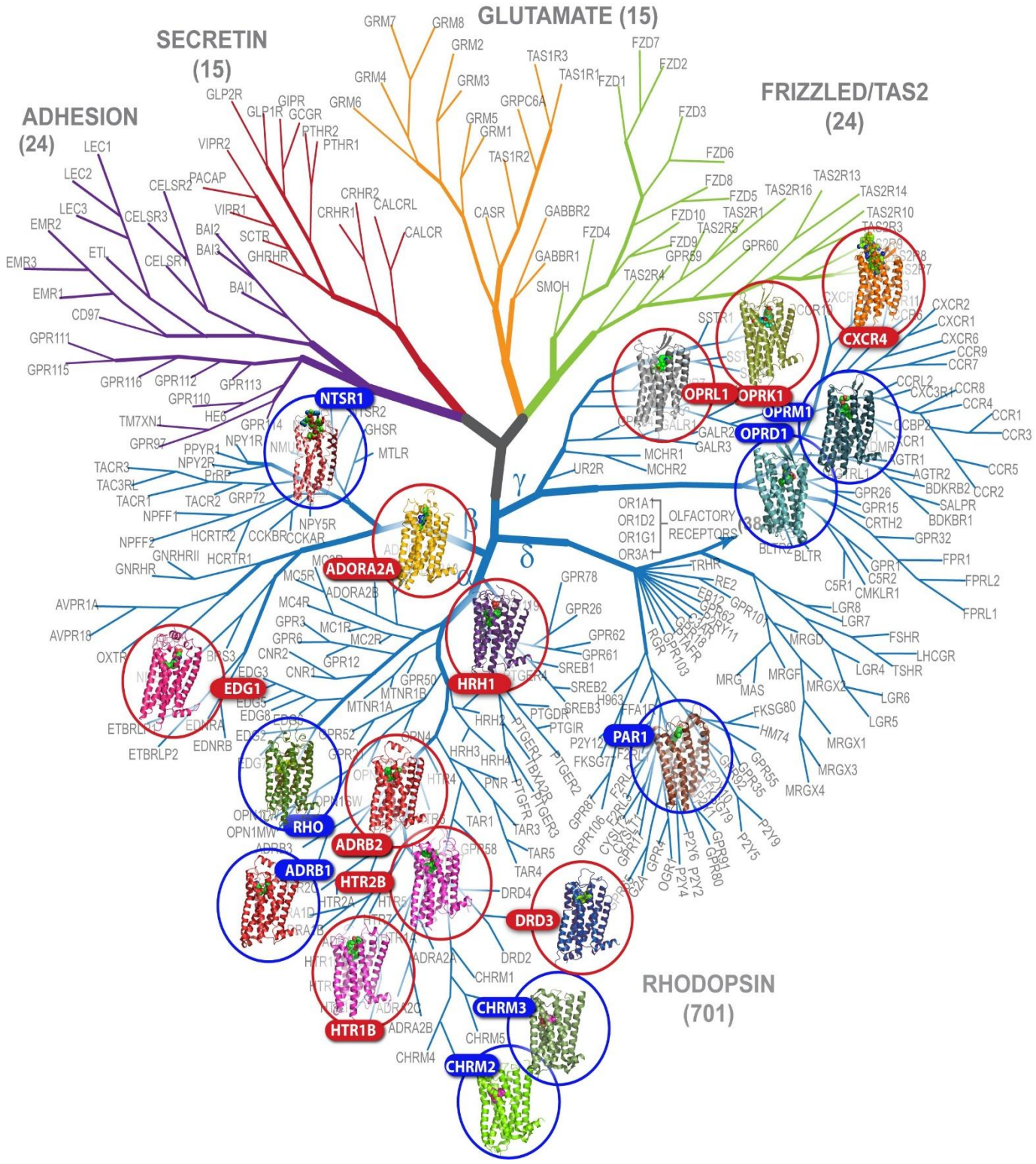

Figure 1.2. ***Classification of GPCR***. The 5 major groups of GPCRS with the number of receptors in each group are stated in brackets and the resolved structures are shown in circles. (*adapted from GPCR network-The Scripps Research Institute*)

loops of the transmembrane regions. Calcitonin like receptors, glucagon-like peptide receptors are some of the members of this family. This class of receptors are the major targets for hypercalcaemia, hypoglycaemia and osteoporosis (14,15).

Class C. The glutamate family GPCRs: calcium sensing receptors, the taste and umami taste receptors and several orphan receptors belong to the glutamate family GPCRs. Most members of this family of receptors bind their endogenous ligand within the N-terminal region. The ligand-binding mechanism of receptors of this family has been compared to a Venus flytrap mechanism, in which the two lobes of the ligand binding region form a cavity where glutamate binds and thereby activates the receptor (16,17).

Class D. The adhesion family GPCRs: the adhesion family receptors contain a proteolytic domain which gets activated on binding of the ligand. This family is also referred as LNB7TM receptors, where LN refers to Long N-terminal and the rest denotes the sequence similarity between transmembrane regions of class B receptors. The diverse N terminal regions of the adhesion family GPCRs may contain several domains that can also be found in other proteins, such as adhesion molecules include cadherin, lectin, laminin, olfactomedin, immunoglobulin and thrombospondin domains (18,19).

Class F. Frizzled/Taste2 family GPCRs: this family includes two distinct clusters of receptors, the frizzled receptors and the taste2 receptors. The frizzled receptors control cell fate, proliferation, and polarity during metazoan development upon activation by secretary glycoproteins called Wnt. These receptors have a 200-amino acid N terminus with conserved cysteines that are enabling the binding of Wnt. Human genome contains 25 functional taste2 receptors (T2R) which are clustered on chromosomes 7q31 and 12p13. The structural diversity noted within T2Rs helps to sense the thousands of bitter compounds which can interact with the extracellular loops (7,20).

1.2.1. GPCR numbering system

Based on the sequence and structural homologies, Ballesteros and Weinstein proposed a numbering scheme for GPCRs in order to relate the site-defined properties of amino acids at a particular helix of this seven transmembrane superfamily (BW numbering system) (21). Such conservation analysis was developed based on the quantitation of the global degree of sequence conservation among amino acids at each helix. Among the various numbering schemes that were also proposed for GPCRs, in the BW system there are three numbers assigned to each amino acid of the GPCR which is known as identifier. The identifier is noted as X.YY notation, where X is the helix identifier and YY, a number that defines the residue based on the most conserved residue in the helix. The highly conservative reference residue of each helix is assigned as 50 for YY. For example, the most conserved amino acid in TM6 is proline of which the identifier would be P6.50

and written as $P^{6.50}$. A tryptophan residue which is two amino acids above this proline is represented as $W^{6.48}$ and a threonine which is two amino acids below that proline would be written as $T^{6.52}$. The table shows the general numbering scheme for the GPCR sequences which are used in this thesis.

TM helix	amino acid	BW number	amino acid number in rhodopsin
TM1	Asn (N)	1.50	55
TM2	Asp (D)	2.50	83
TM3	Arg (R)	3.50	135
TM4	Trp (W)	4.50	161
TM5	Pro (P)	5.50	215
TM6	Pro (P)	6.50	267
TM7	Pro (P)	7.50	303

Table 1.1. ***Ballesteros and Weinstein numbering model for GPCR***. The conservative residue from each transmembrane helices has denoted as integer of the helix, followed by a decimal point as 50 and the corresponding amino acid and its positions in rhodopsin are presented.

1.3. Visual Pigments

Vision provides an animal with an instantaneous ability to detect, perceive, and act around its environment and it is believed that vision of vertebrates evolved about 500 million year ago (22). The retina is a thin tissue layer of the eye that converts visual signals into electrical impulses which are transmitted to the brain. The vertebrates retina contains two kinds of photoreceptor cells, rods and cones which were distinguished from each other on the basis of the morphological shape of their outer segments. Rods are abundant and distributed throughout the retina, whereas cone cells are much scarcer and concentrated mainly on the fovea of the eye (23). It was soon established that rod and cone cells are responsible for scotopic and photopic vision mediated by rhodopsin and cone opsins, respectively. These photoreceptor cells have membrane invaginations, on which the visual pigments are embedded (24).

The visual pigments found in retinal photoreceptor cells belong to the GPCR superfamily, and consist of a heptahelical transmembrane apoprotein, opsin, covalently linked to its natural

chromophore, the vitamin A derivative, 11-*cis*-retinal (11CR), acting as an inverse agonist. The opsin pigments get activated by a specific wavelength of photons and intiate the phototransduction cascade (25). Photoactivation-induced conformational changes allow the active intermediate opsin to bind transducin, the specific heterotrimeric G-protein. Binding of the pigment to transducin causes dissociation of its α-subunit which, in turn, activates a cGMP phosphodiesterase (23). The physiological response of both rhodopsin and cone opsins is different, with cone opsins showing lower sensitivity to light than rhodopsin, which allows rhodopsin to mediate sensitive dim light vision whereas cone opsins mediate bright daylight vision (26). This is evident from the fact that the rate of transducin activation -by cone opsins- was found to be 5 fold lower than that of rhodopsin (27).

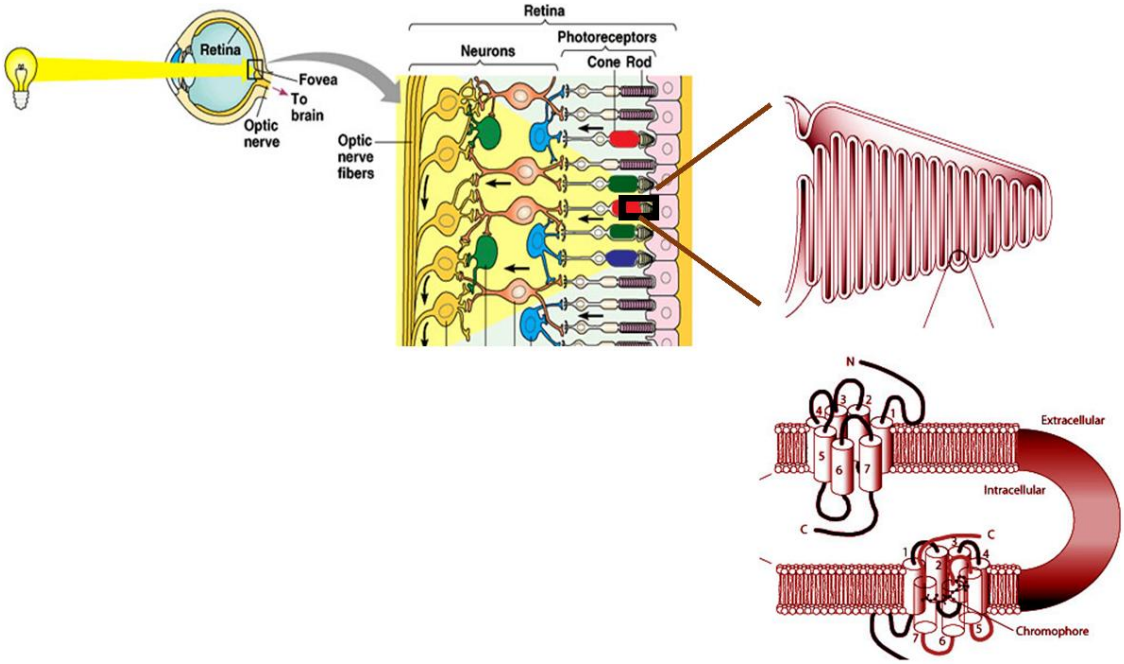

Figure 1.3. ***Process of vision.*** The hierarchy of vision: from eye to visual pigments. The bright light focused on the fovea of retina where the cone photoreceptor cells are populated. The membrane invaginations of photoreceptor cells, on which the visual pigments are embedded, can be observed. (*adapted from (28)*)

1.3.1. Rhodopsin

Rhodopsin mediates dim light vision by converting photons into chemical signals that can trigger the biological processes which enable the brain to sense the light stimulus (29). The visual pigment rhodopsin is found in the rod outer segments (ROS) of the rod photoreceptor cells from the retinal layer. ROS is a specialized compartment that consists of a stack of 1000 – 2000 distinct

discs of membrane invaginations enclosed in a plasma membrane. The major protein component of these bilayer discs is rhodopsin, which absorbs light and initiates photo-transduction cascade, followed by phospholipids and cholesterol. It has been estimated that there are around 8 x 10^4 rhodopsin molecules per disc (30,31). The length or ROS increases and the concentration of rhodopsin rises, when the light is reduced for an extended time. Such phenomenon is known as *photostasis*, "where the photoreceptor outer segment length and its rhodopsin content vary depending on environmental lighting" (32).

In human, rhodopsin is expressed from the gene RHO/OPN2 that contains five exons spanning 5 kb which are interrupted by four introns, located cytogenetically at 3q22 chromosome (33). Rhodopsin gets activated by the conformational change elicited by the isomerization of 11CR, the inverse agonist caused by photons of a wavelength maximum of 500 nm. The rod phototransduction system is extremely sensitive so that even a single photon can be detected (34). Retinal photoisomerization caused by absorption of a single photon of light is accompanied by a shift in the absorption maximum (λ_{max}) from 500 nm to 380 nm. A number of studies address this shift in wavelength that results from the opsin conformational change ensuing illumination. This shift is a very sensitive parameter, and a number of short-lived photointermediate conformations can be detected until all-*trans*-retinal (ATR) release. The photoactivated intermediates of rhodopsin have been shown to be affected by several parameters such as ionic strength, pH, glycerol, and temperature affects. As a result, these intermediates can be trapped at low temperature and their lifetime can be determined (35).

The photosensitivity of rhodopsin is associated with its molar extinction coefficient which was calculated to be 40,600 $M^{-1}cm^{-1}$ (36) with a quantum yield of 0.65 (37) which is a refined value from the long-time accepted number of 0.67 (38). The measured sensitivity of rhodopsin is twice higher than its free chromophore and also the rate of isomerization is much faster when the retinal is bound to the protein than when the chromophore is free in solution. The opsin apoprotein enhances the speed of retinal isomerization and suppresses the competitive relaxations (39).

1.3.2. Cone opsins

Human color perception is mediated by cone photoreceptor cells which mainly locate on the fovea of the retina (40,41). Bright light activates the photosensitive opsin pigments which are embedded in the outer segment membrane discs of cone retinal cells thereby initiating the complex process of photopic vision with a fast response (42). The cone visual pigments correspond to blue opsin (SWL, short wavelength), green opsin (MWL, medium wavelength) and red opsin (LWL, long wavelength). Red and green cone opsins present a 96% of sequence identity differing merely in 15 amino acids. This very high sequence identity has prompted the assumption that both green and red pigments share the same structural and functional features. The blue pigment, however,

shows a lower degree of homology to the red and green opsins. Thus, aside from their specific role in spectral-tuning into different absorption wavelengths, the differences in structure-function relationships caused by this minor sequence variance have not been previously elucidated. Furthermore, most of the mechanistisc insights into cone phototransduction are extrapolated from the rod photoreceptor cell system, responsible for dim-light scotopic vision, and its visual pigment rhodopsin which has been much more extensively studied (25).

It was first observed that cones are less sensitive than rod by studying the difference in dark adaptation between rods and cones (43) by means of biophysical, biochemical and functional approaches

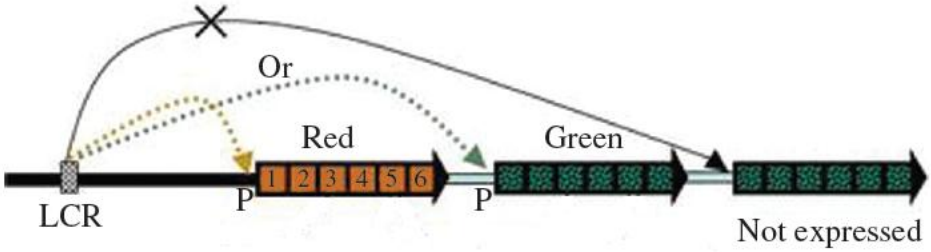

Figure 1.4. ***Gene array of human red and green cone opsins***. multiple green cone opsin genes are found in retinal cone cells, at chromosome X, followed by a single red cone opsin gene copy,. The LCR determines the expression of the particular gene by coupling to its P. Numbers in boxes denote the 6 exons of the opsin gene. (*adapted from (44)*)

Similar to rhodopsin, blue cone opsin (*OPN1SW*) is located at an autosome, 7q32.1, whereas the red cone opsin gene (*OPN1LW*) is arranged proximal to a green cone opsin gene (*OPN1MW*) in an array at Xq28 with 98% identical nucleotide sequences (44,45). The gene array of red and green cone opsin is composed of a single red cone opsin gene followed by one or more green cone opsin genes with 6 exons on each gene. However, the green cone opsin proximal to the red cone will be expressed and the other genes are inactivated. A locus control region (LCR) is located between 3.1 and 3.7 kb 50 of the gene array which is known as a "master switch". The LCR is essential for the expression of both the red and green cone opsin genes. Individuals with mutations at LCR have nonfunctional red and green cones (blue cone monochromats) (46).

In a single cone cell, the expression is exclusive to either one of the cone opsin genes. There is a permanent coupling between the LCR and the promoter (P) of either red or green cone opsin which is to be expressed (Fig. 1.4). This binding of LCR and P is mediated by certain DNA binding proteins. The LCR is inaccessible, at least from the third and more distal green pigment genes which are too distant from the LCR to be activated. Therefore, the LCR has a very low

probability to couple to the distal green promoters (44). Due to higher sequence similarity between red and green cone opsin genes and availability of multiple copies of the green cone opsin gene, intragenic crossing over may happen between L and M cone genes. Such crossing over may occur most likely within introns leading to a greater size of introns and resulting in hybrid M and L cone genes. If the hybrid gene begins with a red cone exon, sequences are known as 5'L-3'M (5'red-3'green) hybrid gene which express proteins that are similarly functional to green opsin genes with 6 exons on each gene, and would express a red cone functional protein (28).

```
Rho             ---------MNGTEGPNFYVP--------FSNATGVVRSPFEYPQYYLAEPWQFSMLAAY 43
Blue            ---------MRKMSEEEFYL---------FKNISSVG--PWDGPQYHIAPVWAFYLQAAF 40
Green           MAQQWSLQRLAGRHPQDSYEDSTQSSIFTYTNSNSTRG-PFEGPNYHIAPRWVYHLTSVW 59
Red             MAQQWSLQRLAGRHPQDSYEDSTQSSIFTYTNSNSTRG-PFEGPNYHIAPRWVYHLTSVW 59
                         :      : *          :.* ...   *:: *:*::*  * : : :.:

Rho             MFLLIVLGFPINFLTLYVTVQHKKLRTPLNYILLNLAVADLFMVLGGFTSTLYTSLHGYF 103
Blue            MGTVFLIGFPLNAMVLVATLRYKKLRQPLNYILVNVSFGGFLLCIFSVFPVFVASCNGYF 100
Green           MIFVVIASVFTNGLVLAATMKFKKLRHPLNWILVNLAVADLAETVIASTISVVNQVYGYF 119
Red             MIFVVTASVFTNGLVLAATMKFKKLRHPLNWILVNLAVADLAETVIASTISIVNQVSGYF 119
                *  :.  ..  * :.* .*::.**** ***:**:*::...:   : .    .  .  ***

Rho             VFGPTGCNLEGFFATLGGEIALWSLVVLAIERYVVVCKPMSNFRFGENHAIMGVAFTWVM 163
Blue            VFGRHVCALEGFLGTVAGLVTGWSLAFLAFERYIVICKPFGNFRFSSKHALTVVLATWTI 160
Green           VLGHPMCVLEGYTVSLCGITGLWSLAIISWERWMVVCKPFGNVRFDAKLAIVGIAFSWIW 179
Red             VLGHPMCVLEGYTVSLCGITGLWSLAIISWERWLVVCKPFGNVRFDAKLAIVGIAFSWIW 179
                *:*   * ***:  :: *    ***.::: **::*:***:.*.**. : *:  :  :*

Rho             ALACAAPPLAGWSRYIPEGLQCSCGIDYYTLKPEVNNESFVIYMFVVHFTIPMIIIFFCY 223
Blue            GIGVSIPPFFGWSRFIPEGLQCSCGPDWYTVGTKYRSESYTWFLFIFCFIVPLSLICFSY 220
Green           AAVWTAPPIFGWSRYWPHGLKTSCGPDVFSGSSYPGVQSYMIVLMVTCCITPLSIIVLCY 239
Red             SAVWTAPPIFGWSRYWPHGLKTSCGPDVFSGSSYPGVQSYMIVLMVTCCIIPLAIIMLCY 239
                .   : **: ****: *.**: *** * ::  .    :*:   :::     *: :* :.*

Rho             GQLVFTVKEAAAQQQESATTQKAEKEVTRMVIIMVIAFLICWVPYASVAFYIFTHQGSNF 283
Blue            TQLLRALKAVAAQQQESATTQKAEREVSRMVVVMVGSFCVCYVPYAAFAMYMVNNRNHGL 280
Green           LQVWLAIRAVAKQQKESESTQKAEKEVTRMVVVMVLAFCFCWGPYAFFACFAAANPGYPF 299
Red             LQVWLAIRAVAKQQKESESTQKAEKEVTRMVVVMIFAYCVCWGPYTFFACFAAANPGYAF 299
                 *:  ::: .* **:** :*****:**:***::*: :: .*: **: .* :   : .  :

Rho             GPIFMTIPAFFAKSAAIYNPVIYIMMNKQFRNCMLTTICCGKNPLGDDEASAT---VSKT 340
Blue            DLRLVTIPSFFSKSACIYNPIIYCFMNKQFQACIMKMVCGKAMTDESDTCSSQKTEVSTT 340
Green           HPLMAALPAFFAKSATIYNPVIYVFMNRQFRNCILQLFG-KKVDDGSELSSAS--KTEVT 356
Red             HPLMAALPAYFAKSATIYNPVIYVFMNRQFRNCILQLFG-KKVDDGSELSSAS--KTEVT 356
                   : ::*::*:*** ****:** :**:**: *::  .         .: .*:    .. *

Rho             ETSQVAPA- 348
Blue            ETSQVAPA- 348
Green           ETSQVAPA- 364
Red             ETSQVAPA- 364
                ********
```

Figure 1.5. ***Sequence alignment of rhodopsin and cone opsins***. Rhodopsin and cone opsins protein sequences were aligned, using ClustalW2 and the difference residues between red and green cone opsins are shown highlighted in red.

1.4. Structure of cone opsins using rhodopsin as template

All opsins are GPCRs that respond to photons and initiate intracellular signal transduction pathways that eventually result in visual perception (24,47). Various biophysical and biochemical investigations, at the molecular level, have carried out since the 1950s in order to refine our understanding of the molecular mechanisms involved in the sophisticated physiological process of vision. During the course of such continued research efforts, a milestone was achieved when the crystal structure of rhodopsin bound with 11CR was released in 2000 (48). This was the first resolved structure among GPCRs and later the ligand free opsin crystal structure was also elucidated (49). These structures of rhodopsin has been used as templates for various GPCRs in order to understand their molecular mechanisms, including those of cone opsins whose crystal structures have not been yet reported. The theoretical models for cone opsins were deposited as PDB files and their identifiers are 1KPN, 1KPW, 1KPX (50). The sequence comparison of rhodopsin and cone opsins was made using ClustalW2 (Fig. 1.5). In this approach, amino acids were aligned as sharing similar positions in the protein secondary structures. The overall secondary structure of cone opsins would apparently be very similar to that of rhodopsin (Fig. 1.6) which is composed of three domains, including an extracellular domain consisting of 3 loops E-I, E-II and E-III, a transmembrane domain with 7 TM helices and an intracellular domain made up by three cytoplasmic loops, C-I, C-II and C-III.

Extracellular domain*:* rhodopsin contains a compact extracellular domain, known as 'retinal plug', including two antiparallel β-sheets (β1 and β2) in the N terminus and loop E-II. The β1 strand, comprising G3 to P12, form a typical β-sheet fold running almost parallel to the expected plane of the membrane. Compared to the rhodopsin structure, at the similar positions where only G12 and Y19 are conserved in red/green cone opsins but other amino acids are different suggesting a potentially different interactions at the N-terminus of cone opsins. Loop E-II folds back into the protein to contribute residues SRYI from 186 to 189 for a β-strand (β2) which shares the similarity with red/green cone opsins containing SRYW. This whole retinal plug structure, with the antiparallel β-sheets is maintained in opsin which can be also observed from the theoretical model developed for cone opsins.

In the case of rhodopsin, the N-terminus is located just near the loop E-III, with the side chain of D282 close to that of N2, and this arrangement may also be possible with blue cone opsin by the residues R2 and G279 at the homologous positions. The N-terminus of red and green cone opsins contain 51 amino acids which are longer than rhodopsin. Two oligosaccharides at N2 and N15 are present in rhodopsin whereas N34 from red/green cone opsin suggest the presence of only one oligosaccharide chain which is similar in blue cone opsin containing N14. Cys from E-II forms a

disulfide bond with $C^{3.25}$ at the extracellular end of TM3. This disulfide is conserved in all opsins and also in most GPCRs. All other residues forming the loops are shown in Fig. 1.6.

Transmembrane domain*:* from the structure of frog rhodopsin, helices are found closely packed towards the intracellular side, and there is a cavity at the extracellular region for retinal binding formed by helices 3, 4, 5, 6 and 7. TM2 and TM3 keep TM6 and TM7 separated from TM4 (51) which has been also identified in the crystal structure of bovine rhodopsin (48). A relocation of conserved residues $W^{6.48}$ and $F^{6.44}$ towards $L^{5.51}$ and $P^{5.50}$, and of $L/G^{3.40}$ away from $P^{5.50}$. This transmission switch links ligand binding to the movement of TM5 and TM6 through the rearrangement of the TM3–TM5–TM6 interface, and possibly constitutes a common theme of GPCR activation(52). This region is believed to exhibit an irregular helicity, mainly around $K^{7.43}$ to which chromophore is covalently bound. The cytoplasmic ends of TM2 and TM4 are near to each other, but they diverge in the region of W161, one of the residues that are highly conserved among GPCRs. A salt bridge occurs between $R^{3.50}$ which is part of the conserved E(D)RY motif in GPCRs, and $E^{6.30}$. Together with $E^{3.49}$ and $T^{6.34}$, they form a more extended hydrogen-bonded network, called the 'ionic lock' (53,54). Residue 6.34 is conserved as Thr in rhodopsin, red and green cone opsins, but in the case of blue cone opsin, it is $S^{6.34}$ which also contains an OH functional group. The presence of the ionic interaction stabilizes TM6 within the helical bundle. TM7 has the $NPxxY(x)_{5,6}F$ motif which is linking TM7 with helix 8 (H8) and is conserved in all class A GPCRs including cone opsins. Though the major role of this motif is yet unclear, mutations at this motif are reported to affect ligand binding (55-57).

Intracellular domain: the intracellular domain of opsins consists of three loops with the C-I shorter than the other two and connected to TM2 by $N^{2.40}$. Specific amino acids contributing to the loops can be identified and compared (Fig. 1.6). C-III of rhodopsin is rigid at the site of a tetrapeptide from Q236 to E239, containing 3 Gln residues, but the polar side chains S240 to T242 pull the C-III towards the C-terminus. The C-III of red/green cone opsins, occupied by Q252-Q-K-E, has the presence of Lys instead of Gln compared to the rhodopsin sequence. However, this does not alter the rigidity of this structure and followed by polar amino acids also support that the C-III is closer to C-terminus of cone opsins similar to rhodopsin. It is known that the rhodopsin C-terminal amino acid sequence QVS(A)PA, functions as a structural motif which directs the sorting of visual pigments to the outer segment membrane.

C322 and C323 of rhodopsin project outside the protein and both the residues are palmitoylated (58). In contrast, only one Cys at position 320 can be found in blue cone opsin which is palmitoylated and no such Cys residues are present in red/green cone opsins.

Retinal binding site**:** the retinal binding of rhodopsin has been well elucidated from its crystal structure (48) and structural details on the rearrangement of specific residues upon illumination

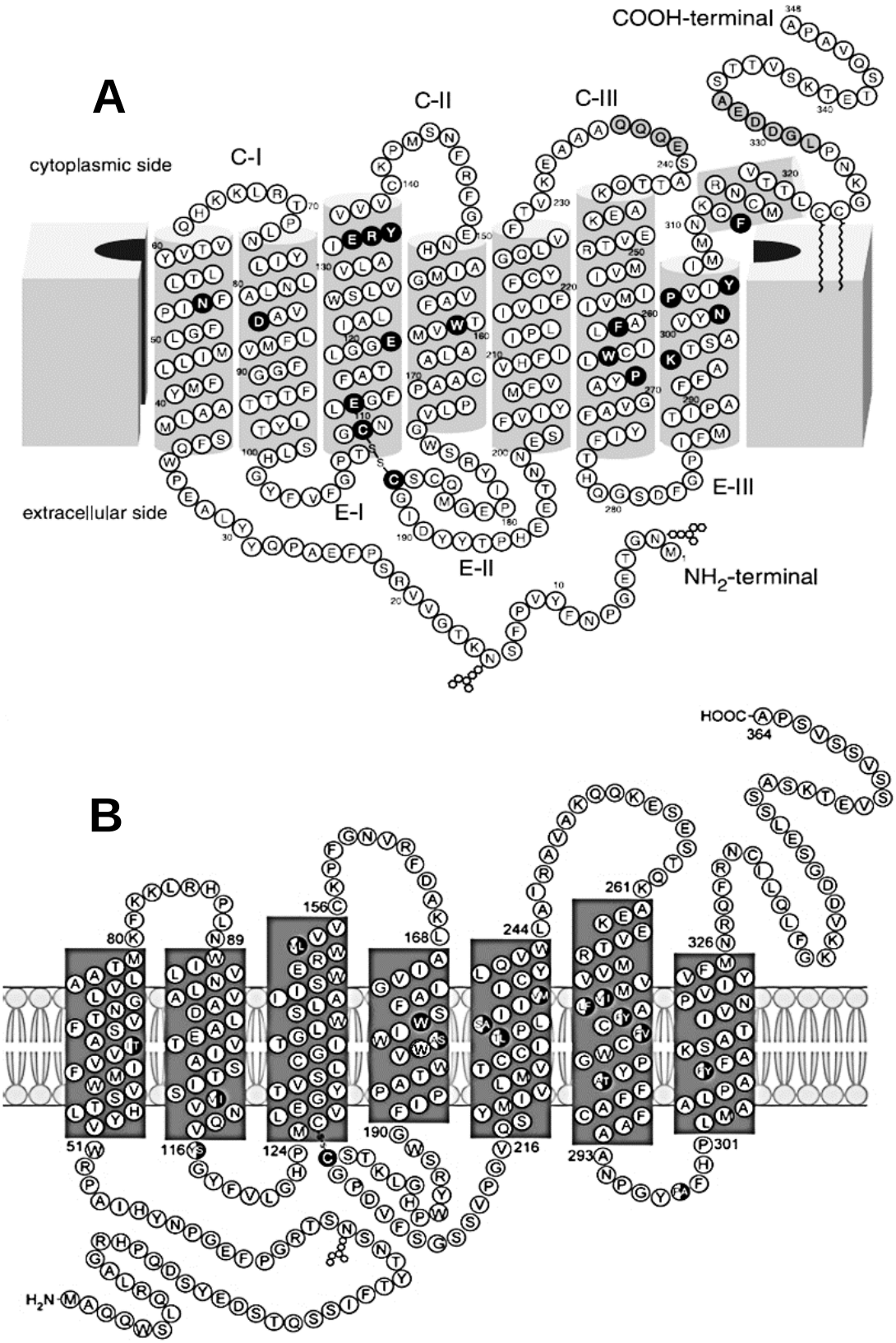
A
COOH-terminal
C-I
C-II
C-III
cytoplasmic side
extracellular side
E-I
E-II
E-III
NH2-terminal
B
HOOC-
364
80
89
156
168
190
216
244
261
293
301
326
51
116
124
H2N-

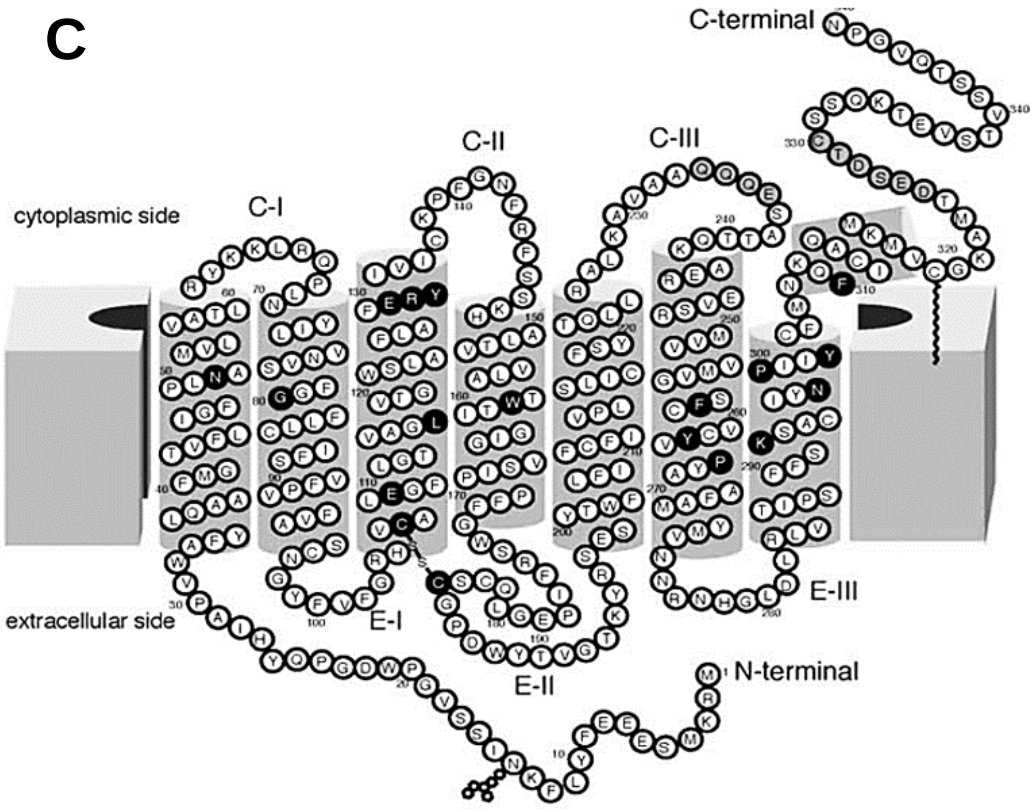

Figure 1.6. ***Secondary structure models of visual pigments.*** The secondary structure of rhodopsin **(A)** with the conservative residues marked in dark circles, (*adapted from (48)*). Red and green cone opsins **(B)**, with the amino acids differences between red (dark) and green (white) that are half circled, (*adapted from (59)*). The blue cone opsin **(C)** where the conserved residues are marked in a similar fashion to rhodopsin. (*adapted from (50)*)

has been determined (Fig. 1.7) (49). The amino acids that constitute the retinal binding site are mainly hydrophobic, which favors the accommodation and interactions with the polyene chain of the chromophore. F212$^{5.47}$ at TM5 and F261$^{6.44}$ at TM6 are near the ionone ring of the retinal. These residues are C228$^{5.47}$ in red and green cone opsin, and interestingly the other one is F277$^{6.44}$ in green cone opsin and the polar amino acid Y277$^{6.44}$ in red cone opsin.

The retinal bends towards the side chain of W265 at the ground state conformation of rhodopsin, which is W281 in red and green cone opsins but Y262 in blue cone opsin. The conformational changes ensuing illumination of the protein results in fluorescence changes in this Trp which is used in order to understand the dynamics of the retinal binding site (60). The Schiff base linkage between the retinal and Lys$^{7.43}$ is located near Glu$^{3.28}$ that serves as the counterion to the protonated Schiff base (PSB) in visual pigments. Another notable position is F293 of rhodopsin located near the PSB which undergoes a 120º rotation upon illumination moving away from the

binding pocket, and Y309 only in red cone opsin which is one of the major differences between red and green cone opsin at the retinal binding site.

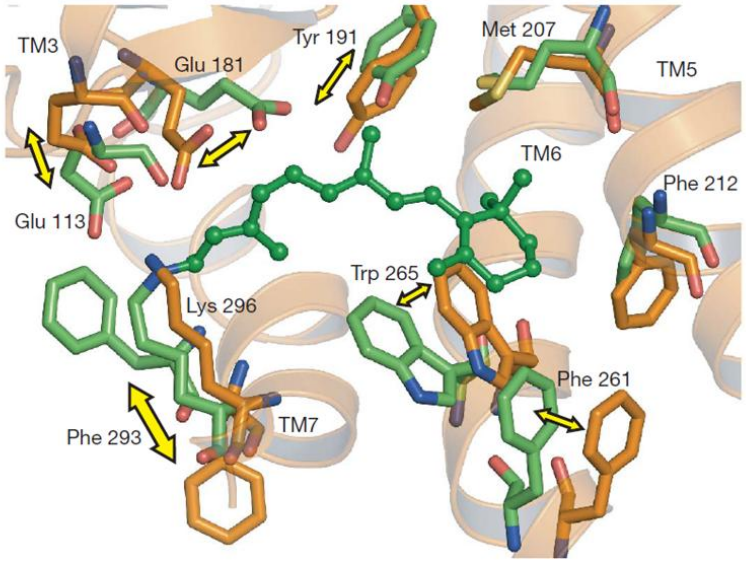

Figure 1.7. ***Retinal binding site of rhodopsin***. Residues of the retinal-binding pocket in rhodopsin in the inactive state (green) and active state (orange) are rendered as sticks. The yellow double arrows indicate differences in side-chain positions. Retinal in rhodopsin is shown as a ball-and-stick model for reference. (*adapted from (49)*)

1.5. Chromophore

The visual pigments are composed of a light-absorbing 11CR chromophore, a vitamin A derivative, covalently bound to the ε-amino group of a Lys residue of the opsin apoprotein via a PSB linkage thereby maintaining the inactive conformation (23,48). The 11CR chromophore has been conserved throughout evolution, because of its highly specialized role in vision, which includes a high quantum yield and a very fast response for photon-triggered isomerization. Retinal analogs, other than the natural 11-*cis* chromophore, such as 7-*cis*, 9-*cis*, 13-*cis*, and all-*trans*, have been investigated for their binding properties to the visual pigments in order to unravel the structural features of the retinal binding site and the details of the opsin-ligand recognition process (Fig. 1.8) (61-63). 9-*cis*-retinal (9CR) is often used as an exogenous analog to study the structure and function of visual pigments (64,65).

Schiff-base linkage with $K^{7.43}$ of visual pigments, thereby maintaining the inactive conformation (23,48). The fluorescence emission of $W^{6.48}$ (in red and green cones opsins) /$Y^{6.48}$ (only in blue cone opsin), which is located very close to the β-ionone ring of the retinal, and $W^{3.41}$ (66) are quenched by the bound retinal of these dark-adapted visual pigments. Hydrolysis of the retinyl-

idene linkage by photoisomerization causes the release of retinal and the parallel increase in fluorescence due to the fact that these aromatic residues, particularly that at position 6.48 (60), are no longer quenched.

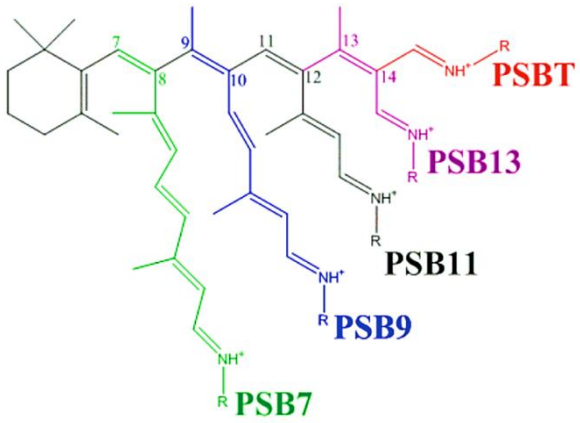

Figure 1.8. ***PSBs with retinal analogs***. Schematic representation of 7-*cis*- (PSB7, green), 9-*cis*- (PSB9, blue), 11-*cis*- (PSB11, black), 13-*cis*- (PSB13, purple), and all-*trans*-retinal (PSBT, red). R refers to $Lys^{7.46}$ from opsin. (*adapted from (67)*)

1.5.1. The retinoid cycle

The active photointermediate (MetaII) of visual pigment activates the α-subunit of a heterotrimeric G protein, transducing, which is the first event leading to closure of cGMP-gated cation channels in the ROS and resulting in photoreceptor cell membrane hyperpolarization. A surge of neurotransmitters from the photoreceptor cell neutralizes the polarization and the MetaII intermediate of the visual pigments decays subsequently by yielding free opsin and ATR. The isomerized retinal is replenished by the retinoid cycle, an enzymatic pathway by which ATR is converted back to 11CR. Various proteins are involved in this process thus ensuring the required 11CR supply to the photoreceptor cells. The proteins involved in the retinoid cycle can be categorized into transporter proteins which are retinoid binding proteins and the isomerizing enzymes (68). Mutations in these proteins, some of them with recessive inheritance, can lead to vision impairment associated with several retinal diseases, like Leber congenital amaurosis (LCA), Stargardt macular degeneration, congenital cone-rod dystrophy, and retinitis pigmentosa (RP) (69).

Upon decay of the MetaII intermediate, ATR readily condenses with phosphotidyl ethanolamine (PE) to form N-retinylidene-PE (NRPE). By binding to ABCR (a retina specific ATP binding cassette transporter), NRPE is transported across the membrane discs to the cytoplasmic side of the photoreceptor cells where it is reduced to all-*trans*-retinol by dehydrogenases with the

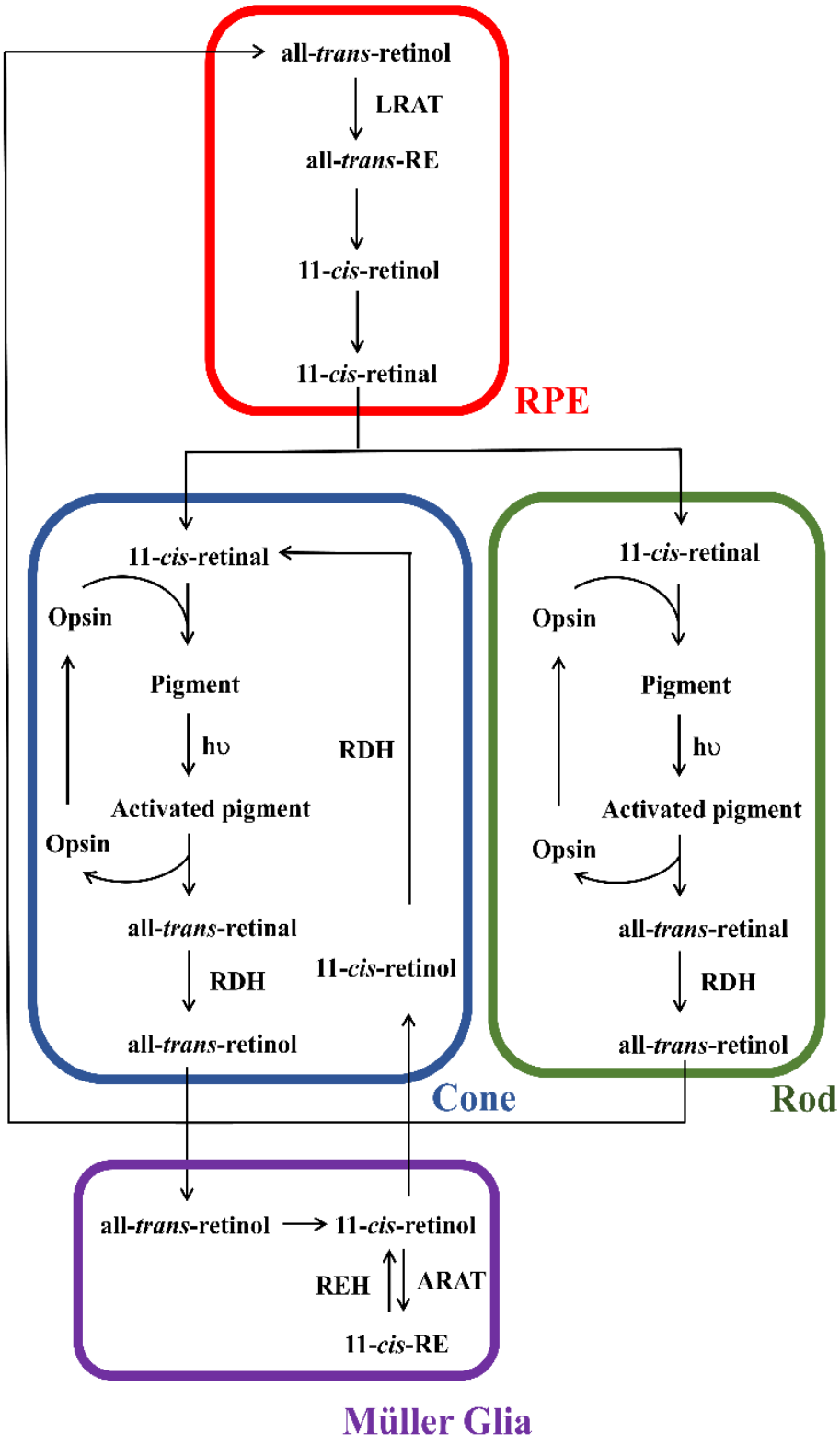

Figure 1.9. ***The retinoid cycle in rod and cone photoreceptor cells.*** The isomerized ATR from rod and cone photoreceptor cells, is transported across RPE and Müller glia and with the help of various oxidizing enzymes (LRAT - lecithin/retinol acyl transferase, RDH - retinol dehydrogenase, REH - retinyl ester hydrolase, ARAT - acyl-CoA-retinol acyl transferase) is converted back to 11CR

expenditure of NADPH. Photoreceptor cells release the all-*trans*-retinol into interphotoreceptor matrix (IPM) and the retinol is protected from oxidation and isomerization by binding to an interphotoreceptor binding protein (IPBR) and transported to the retinal epithelium (RPE) by endocytosis.

Within the RPE, retinol is esterified by lecithin/retinol acyl transferase (LRAT) producing retinyl esters. Rpe65, a RPE specific 65kDa isomerase using Fe^{2+} as co-factor converts the all-*trans*-retinoids to 11-*cis*-retinol. 11-*cis*-retinol is preserved by binding to cellular retinal binding protein (CRALBP) which can also bind to 11CR. 11-*cis*-retinol is either readily oxidized to 11CR and released to photoreceptor cells or it can be stored by being converted to 11-*cis*-retinyl esters by LRAT. These stored esters are again hydrolyzed by 11-*cis*-retinyl ester hydrolase (11-*cis*-REH) (68).

An alternate pathway has also been identified for cone photoreceptor cells in which the all-*trans*-retinol from cone photoreceptor cells are transported to müller cells and converted to 11-*cis*-retinol which in turn is converted to 11CR inside the cone photoreceptor cells by retinol dehydrogenase (RDH).

1.6. Trafficking, activation and signaling of visual pigments

1.6.1. Trafficking

Rod and cone photoreceptor cells have evolved into highly specialized cells consisting of three distinct areas that include the outer segment containing membrane discs where the visual pigments and other signaling proteins involved in phototransduction are located, the inner segment in which biosynthesis and other cellular processes occur, and the synaptic terminal that transmits the signal via neurotransmitter to downstream neurons. There is continuous renewal of the rod and cones in the outer segments in approximately, and every 10 days a complete renewal happens (70) through a narrow cilium connecting the outer segments to the cell body. A mouse rod outer segment is estimated to contain between $5x10^7$ and $7x10^7$ rhodopsins (71). Therefore, 80 rhodopsin molecules have to be synthesized and delivered each second which require an effective biosynthesis of the retinal proteins, with reliable transport and targeting pathways (72,73).

The opsins are transported from the endoplasmic reticulum, the biosynthetic site to Golgi complex and a trans-golgi network where they are sorted into vesicles with the help of interactions with various proteins and destined to the outer segment via the cilium (42). The last four amino acids at the C-terminal of opsins are known as VXPX motif which serves as an intracellular targeting signal (74), and also the Phe-Arg doublet at H8, known as FR signal, is also characterized to play a major role in protein targeting (75). The opsin assembly into the outer segments depends on an intraflagellar transport which is a highly conserved process, characterized as a bi-directional trafficking pathway along a microtubule backbone known as the ciliary axoneme (76,77).

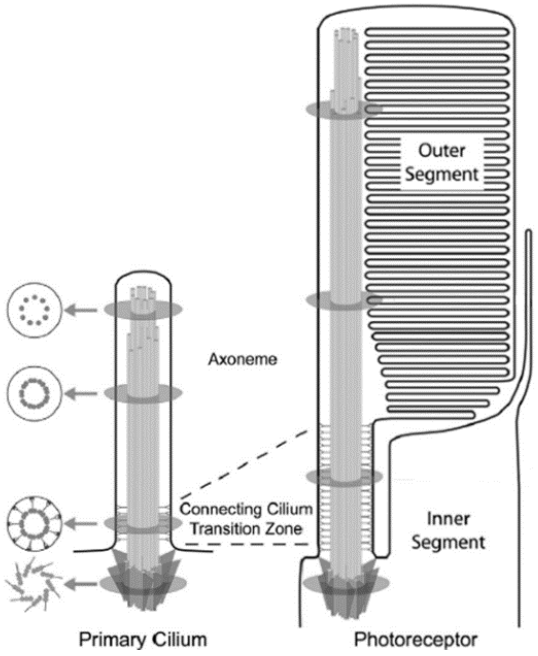

Figure 1.10. ***Axoneme and photoreceptor outer segment.*** Schematic drawings of the primary cilium depict tangential sections through the sub-ciliary compartments: basal body, transition zone, axoneme doublets, and axoneme singlets. (*adapted from (42)*)

1.6.2. Oligomerization

Oligomerization in GPCRs have been well established by various studies stating its importance for receptor activation. Homo or hetero oligomerization of GPCRs modulate the ligand binding selectivity and potency (78). AFM studies visualized the densely packed rhodopsin oligomers in the native membrane which also argued for a potential role of dimerization on G-protein recognition, binding kinetics, and signal amplification (79). Though the molecular mechanism of cone opsins dimerization is yet unclear, rhodopsin dimers in the dark state could be formed in a "head to head" orientation interfacing the TM1 of each monomer and a close interaction with H8 at the C-terminal (80). In the photoactivated rhodopsin a parallel dimer with the similar interface at TM1 and H8, and the involvement of TM2, has been proposed (81). The photoactivated rhodopsin and transducin can freely diffuse through the membrane milieu and a single trimeric G-protein can bind to a dimer of rhodopsin (82) which may also be asymmetric where the rhodopsins are at unequal activated states (83,84). Structurally, the opsin dimers are the building blocks of a hierarchical supramolecular architecture in membranes. Such higher order architecture of the pigments exhibits an efficient and faster signaling. A higher order organization of oligomerized rhodopsin has been observed in a recent study stating a four level structural organization in which rhodopsin dimerizes, and at least ten dimers form a row in native

membrane. A pair of rows, known as tracks would be aligned parallel to form disk incisures. These parallel alignments would be necessary for the sensitivity of visual pigments, and the rhodopsin tracks may trap the preassembled G-protein molecules (85).

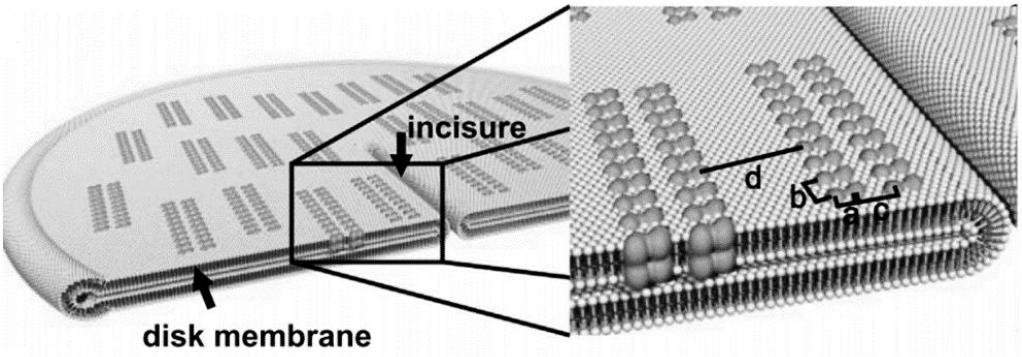

Figure 1.11. ***Oligomerization and higher order organization of rhodopsin*****.** Four levels of organization of rhodopsin (purple) in the intact disk membrane: The dimerization of rhodopsin monomers with a center-to-center distance of 4 nm (a); dimers form rows with a dimer-to-dimer distance of 5 nm (b); rows come in pairs separated by 5 nm (c); two pairs of rows (tracks) are separated by 15 nm. (*adapted from (85)*)

1.6.3. Activation

The main difference between the visual pigments and other GPCRs is the specific nature of the light-induced conformational isomerization with a faster photointermediate conformation that activates the G-protein. In the inactive dark-adapted state of cone opsins, the retinal chromophore is covalently bound to these visual pigments through its aldehyde group via a PSB linkage to the ε-amino group of $K321^{7.43}$ for red/green cone opsins and $K293^{7.43}$ for blue cone opsin at TM7, similar to rhodopsin. The PSB is stabilized by a salt bridge with the carboxylic group of the counterion, $E^{3.28}$ at TM3 (86). A PSB is a structural feature of visual pigments and the corresponding visible spectrum of a free PSB would show an absorption maximum at 440nm. However, the characteristic differences in visual sensitivities are due to specific amino acid variations at the retinal binding pocket which result in different absorption maxima -as a result of the so-called opsin shift effect- corresponding to 560nm for the red cone pigment, 530nm for the green cone pigment, and 420nm for the blue cone pigment (87-89).

The first step in the phototransduction process involves photon absorption by the visual pigments that causes 11CR isomerization to ATR (23). This activates the receptor by eliciting a conformational change, with formation of the active MetaII conformation resulting in binding and activation of the G-protein, transducin (90). There is a subsequent breakage of the PSB linkage

of the isomerized chromophore which no longer fits into the retinal binding cavity and leaves the binding pocket eventually exiting the protein. Visual pigment photoactivation changes the pKa of the PSB and induces deprotonation which is the primary molecular event of the visual transduction cascade after retinal isomerization (91). This is accompanied by a small displacement of the PSB away from the counterion which would result in a red-shifted absorption maximum (92). Upon photoactivation, isomerization of 11CR results in a series of short-lived photointermediates (photo- , batho-, lumi-) that lead to the MetaI opsin intermediate conformation which still shows a PSB linkage. Subsequence deprotonation of the PSB results in the formation of the MetaII intermediate with typical absorbance at 380 nm. MetaII decay is accompanied by disruption of the salt bridge between the isomerized chromophore and the free opsin apoprotein.

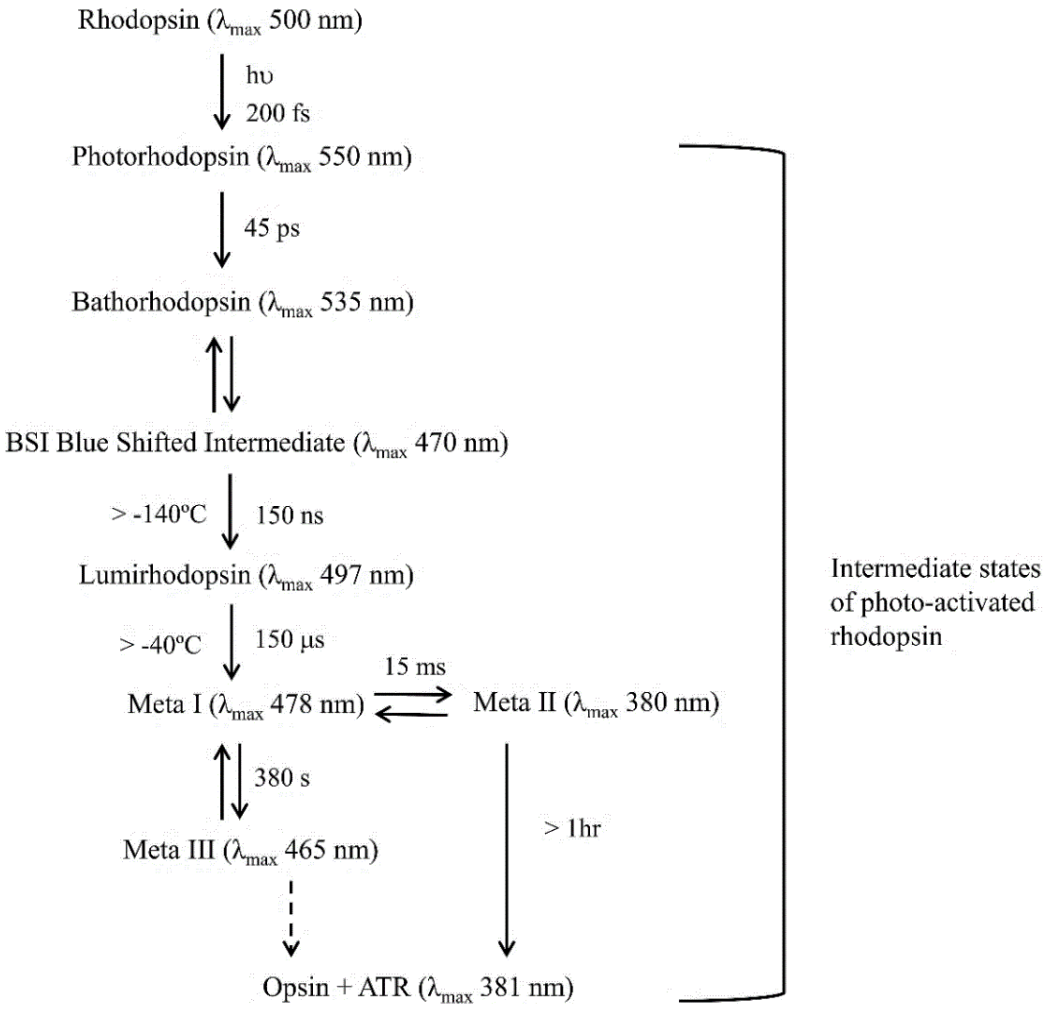

Figure 1.12. ***Photoactivated intermediates of rhodopsin***. The intermediates of photoactivated rhodopsin with their absorption maximum and their conversion kinetics at the given temperature.

The MetaII active photointermediate of cone opsins is short lived compared to that of rhodopsin (93-96). Overall, the photoactivated cone opsins are prone to spontaneous fast dissociation into free opsin and ATR.

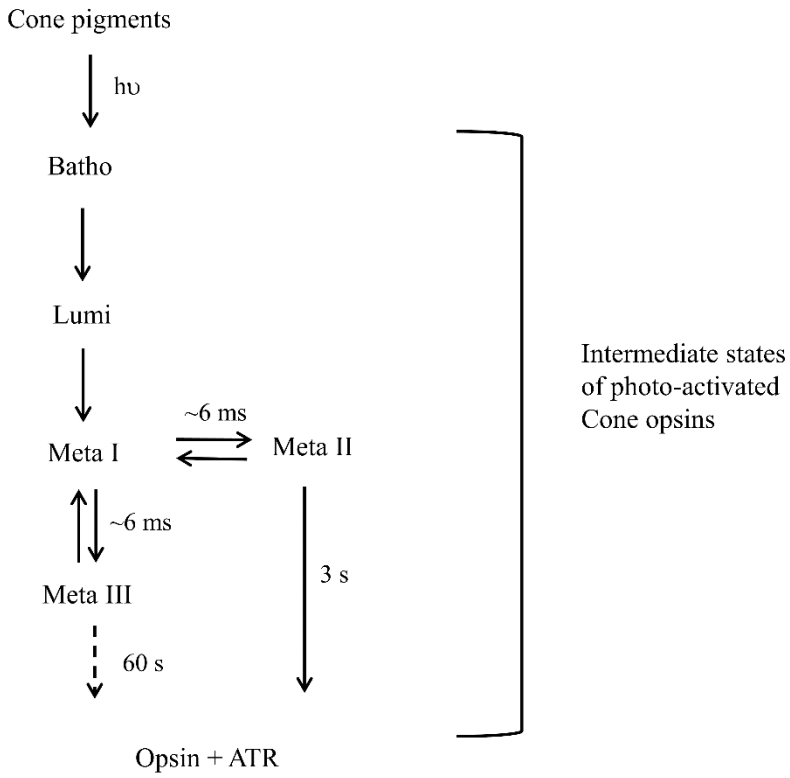

Figure 1.13. ***Photoactivated intermediates of cone opsins***. The intermediates of photoactivated cone opsins include batho-, lumi-, and, meta- intermediates.

1.6.4. Signaling

The G-proteins of the GPCRs superfamily comprise various isoforms including 16 G_{α} (four subfamilies: $G_{\alpha s}$, $G_{\alpha i}$, $G_{\alpha q}$, and $G_{\alpha 12}$), 5 G_{β} and 12 G_{γ} subunits (97). Both rods and cones mediate their function via G_i class of G proteins. The G-protein binding to rhodopsin is transducin, composed of $G_{\alpha t1}$ (39 kDa) and the $G_{\beta\gamma}$ dimer complex ($G_{\beta 1}$, 36 kDa, and $G_{\gamma 1}$, 8 kDa). Cone opsins activate $G_{\alpha t2\beta 3\gamma 8}$ trimer (98-100). The G-protein complexes activating both rod and cone opsins share a high degree of homology, i.e., $G_{\alpha t1}$ is 78% identical to $G_{\alpha t2}$, $G_{\beta 1}$ is 80% identical to $G_{\beta 3}$, and $G_{\gamma 1}$ is 64% identical to $G_{\gamma 8}$. The α-subunit of the G-protein possesses GTP-binding and GTP-hydrolyzing properties. The type of the nucleotide bound to α-subunit controls the activation process with the GDP-bound state being inactive and the GTP-bound form the active state. The photoactivated active state conformation of rhodopsin, MetaII (R*), characterized by the unprotonated Schiff-base linkage, enables the binding of transducin and catalyzes the exchange

of the bound GDP with GTP (101). It is believed that a single molecule of R* can activate 20–100 molecules of G_t (102).

Immediately after formation of R*-$G_{t\alpha\beta\gamma}$-GTP complex, $G_{\beta}\gamma$ dissociates and the dissociation of $G_{\beta\gamma}$ is essential for production of free $G_{t\alpha}$-GTP, which is capable of interacting with a phosphodiesterase (PDE). The lifetime of the active $G_{t\alpha}$-GTP is controlled by the GTPase activity of $G_{t\alpha}$. The basal GTPase activity is relatively slow and it is accelerated when the $G_{t\alpha}$ interacts with other regulatory protein by forming a complex with PDE/RGS9 (regulator of G-protein signaling 9). The GTPase reaction is crucial for the kinetics of the photoresponse (103).

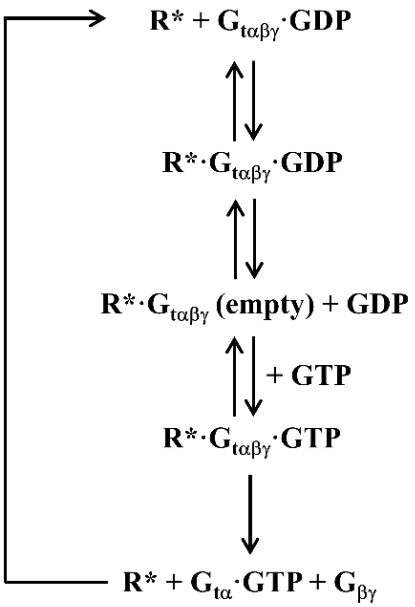

Figure 1.14. ***Activated opsins and G-protein***. The schematic representation of initial events of the phototransduction of visual pigments. (R* - activated visual pigments, $G_{t\alpha\beta\gamma}$ - trimeric G-protein complex).

Two $G_{t\alpha}$·GTP subunits bind to the two inhibitory γ subunits of PDE, thereby activating the catalytic subunits and enhancing the hydrolysis of cGMP to GMP. The subsequent decrease in the concentration of cGMP leads to the closure of cyclic nucleotide gated ion channels, and blockage of the influx of Na^+ and Ca^{2+} causing a hyperpolarization which is neutralized by the release of neurotransmitters from the synaptic endings of photoreceptor cells. The response of activated opsin is small and faster with cone opsin compared to that of rhodopsin as the MetaII intermediate is short-lived in cone opsins which also lowers the sensitivity of the pigments (25,104).

The rod and cone pigments are equivalent with respect to downstream signaling upon activation. Though the lifetime of the functionality of activated pigments is regulated by the decay of MetaII intermediate, phosphorylation and arrestin binding also play a major role in shutting off the signal. The rhodopsin kinases which phosphorylate the activated pigments and enables the binding of arrestin to opsin (105).

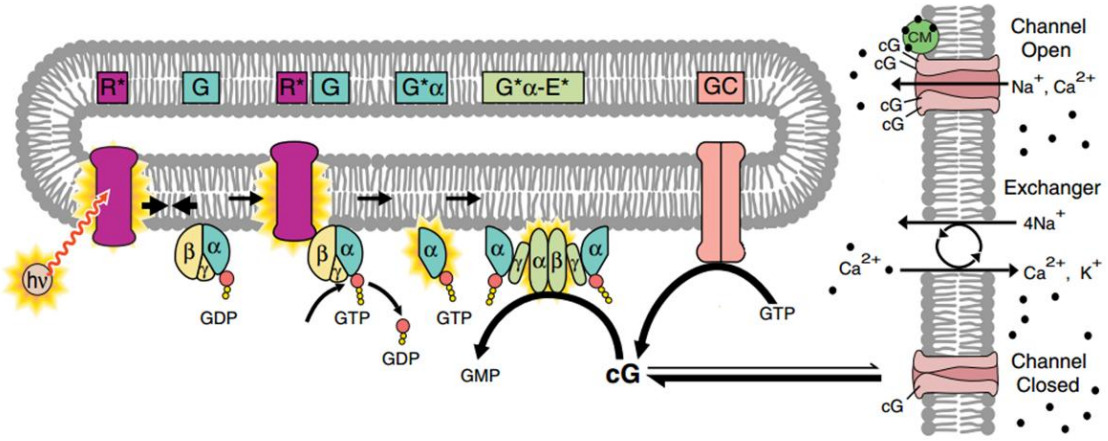

Figure 1.15. ***Signal transduction of visual pigments***. Photoactivated opsins (R*) exhibit conformational changes which activate transducin (G) by interacting with and replacing the bound GDP with GTP (R*G). GTP bound α-subunit dissociates and activates PDE (G*α-E*). PDE converts cGMP (cG) produced by guanylate cyclase (GC) to GMP which leads to the closure of cGMP gated ion channels. (*adapted from (104)*)

1.7. Cone opsin mutants

Adaptive evolution is the key to the switch from red cone pigments to green cone opsin pigments in which the specific positively selected point mutations give rise to green cone opsin. These positively selected green cone opsin pigments are found in animals with red-green color vision but some of these random mutations may also have adverse effects and lead to red/green color blindness in animals. Evolutionary genetic analysis have identified that both the constructive adaptive mutations responsible for color vision and the deleterious mutations causing retinal disorders have been strongly selected independently in different lineages (106,107).

Trichromatic color vision requires the absorption of photons from different visible wavelengths. The loss of function of one of the cone pigments, caused by certain congenital disorders, limits vision to dichromacy and the loss of two cone pigments leads to monochromacy (108). Table 1.2 shows some important clinically identified mutants of cone opsins which are known to cause visual alterations ranging from simple polymorphism, which only shift the absorption maximum wavelength by a few nm, to degenerative cone dystrophies.

1.7.1. Retinal disorders associated with blue cone opsin mutations

Tritanopia: tritanopia is an autosomal dominant disorder linked to blue cone opsin gene at 7q32.1 and associated to a selective deficiency of blue spectral sensitivity. The amount of functional loss varies from minor to complete depending on the position of the mutation. Six mutations have been identified to cause tritanopia that include L56P, G79R, T190I, S214P, P264S, and R283Q (109-113). Tritanopes are unable to differentiate light blues and greys, dark purples and black, mid-greens and blues, and oranges and reds.

Blue Cone Pigments	Green Cone Pigments	Red Cone Pigments
G79R	N94K	S180A
T190I	W177R	C203R
S214P	C203R	R247ter
	R330Q	G338E

Table 1.2. ***Cone opsin mutants causing retinal disorders.*** Clinically identified point mutations of blue, green and red cone opsins causing retinal disorders.

1.7.2. Retinal disorders associated with green cone opsin

Deuteranopia: loss of functional green cone pigments, due to point mutations at the green cone opsin gene, can lead to a dichromatic condition known as deuteranopia. N94K, R330Q are mutations causing deuteranopia previously identified. It was suggested that N94K disrupts opsin folding and R330Q affects the functionality of the pigment but shows absorption maximum similar to native green cone pigment (114).

C203R in green cone opsin is identified to cause the condition known as deuteranomaly where the defect implies a shift in the spectral sensitivity. Surprisingly, this mutation was found to be presented in 2% of the population -which is fairly common- but apparently it was not always expressed. In analogy with the lack of expression of some 5' green-red hybrid genes in persons with normal color vision, it was suggested that failure to manifest occurs when the mutated gene is located at a distal (3') position among several green opsin genes. This mutation might also predispose to certain X-linked retinal dystrophies (115).

X-linked cone dystrophies: these are a heterogenous group of disorders showing dysfunction and degeneration of cone photoreceptor cells. W177R mutation on exon 3 of chromosome Xp21 is the most common cause for cone photoreceptor degeneration. The affected individuals tend to develop a variable degree of photophobia in childhood or early adult life, reduced central vision,

and color-vision disturbance. W177 is highly conserved in visual and non-visual opsins across species. This mutation W177R in green cone opsin is equivalent to W161R mutation in rhodopsin which results in protein misfolding and retention in the endoplasmic reticulum. In addition to W177R, mutations in 11 other genes, including GUCA1A, a guanylate cyclase activator, peripherin, and ABCA4, retinal transporter protein have been identified to cause degenerative cone dystrophies (59,116).

Figure 1.16. ***Visual perception of congenital dichromats***. Comparison between the normal vision and visual perception of protanopes, deuteranopes and tritanopes. (*adapted from http://www.colourblindawareness.org*)

1.7.3. Retinal disorders associated with red cone opsin

Protanopia: purified G338E red cone mutant does not show any absorbance indicating the complete loss of functional red cone pigment, known as protanopia (114).

S180A is a polymorphism that exists over the population (60% serine, 40% alanine) which is characterized by shifting the absorption spectrum by 7 nm. Hence, individuals with different residue at position 180 tend to visualize the color red with a slight difference (117,118).

Blue cone monochromancy: C203R in green cone opsin and C203R in red cone opsin can be identified in certain individuals as well. In such condition, the affected individuals are

monochromats with only blue spectral sensitivity. This may be a consequence of LCR deletion adjacent to the red and green cone opsins gene array. In the R247ter mutant, the red cone pigment gene carries a point mutation (C to T) at the amino acid coding position 247 in exon 4 resulting in termination of protein synthesis beyond amino acid 246 (119).

2. OBJECTIVES

The main aim of this thesis are to characterize the structure and function of human cone opsins in their purified form and to anaylze the retinal binding behavior in comparison with rhodopsin. To this aim the regeneration of red, green and blue cone opsins with retinal analogs and the possible conformational differences -other than those known associated with spectral tuning- will be investigated. The present study is also aimed at characterizing specific mutations in cone opsins associated with retinal disorder and to investigate the alterations in their structure-function relationships when compared to the respective non-mutated recombinant pigments. These main objectives can be broken down in the following specific objectives:

1. To characterize purified recombinant human red, green and blue cone pigments and to compare their biochemical and biophysical properties with those of rhodopsin.

2. To investigate the ligand binding specificity of a selected photoactivated cone pigment and to compare it with chromophore regeneration of photoactivated rhodopsin at a late photoactivation state.

3. To compare the nature of chromophore regeneration with retinal analogs between red, green and blue cone opsins immediately after photoactivation.

4. To construct the clinically identified mutants of human cone opsins and to characterize the biochemical and biochemical features in comparison with their respective wild type pigments and to identify the possible alterations in structure-function relationships.

5. To stablize a cone opsin mutant, which cannot regenerate with its natural ligand in its purified form, by means of different stabilizing strategies, like introducing a new disulfide bond..

3. EXPERIMENTAL PROCEDURES

3.1. Materials

Red, green and blue cone opsin genes, which were cloned into pMT4 plasmid vector, were kindly provided by Prof. Kevin D. Ridge.

Dulbecco's modified eagle medium (DMEM) (Sigma, Spain) supplemented with fetal bovine serum (FBS) (Sigma, Spain), L-glutamine (Sigma, Spain), and penicillin-streptomycin (Sigma, Spain) was used to culture COS-1 cells (ATCC no. CRL-1650). Opti-MEM (Fisher scientific, France), DMEM-F12 (lab clinics, Spain) supplemented with FBS and penicillin- streptomycin were used to culture HEK-293s-GnTi^{-} cells.

11-*cis*-retinal (11CR) was provided by the National Eye Institute, National Institutes of Health (USA). Purified mAb rho-1D4 was obtained from Cell Essentials (Boston, USA) and was coupled to CNBr-activated Sepharose beads (Sigma, Spain). n-dodecyl-β-D-maltoside (DM) was purchased from Affymetrix (Germany). The nonamer-peptide H-TETSQVAPA-OH was obtained from Unitat de Tècniques Separatives i Síntesi de Pèptids, Universitat de Barcelona (Barcelona, Spain). The 9-*cis*-retinal (9CR), hydroxylamine, protease inhibitor cocktail, and phenylmethanesulfonyl fluoride (PMSF) were purchased from Sigma (Spain), and polyethyleneimine (PEI) was purchased from Polysciences Inc. (USA).

Dark adapted bovine retinas were purchased from W L Lawson Company (NE, USA). The cellulose membrane and manifold used for G-protein activation assay were purchased from Millipore (France). GTPγS^{35} (250 μCi) from Perkin Elmer, (Spain), and biodegradable scintillation fluid from GE healthcare life sciences (Spain).

Acrylamide/Bisacrylamide mix, 1.5 mM Tris-HCl, (pH 8.8), 0.5 mM Tris-HCl (pH 6.8) and other electrophoretic materials and reagents were purchased from BioRad (USA).

1, 2-didocosahexaenoyl-*sn*-glycero-3-phosphocholine (DDHA-PC), 1, 2-dihexanoyl-sn-glycero-3-phospho choline (DMPC), and 1, 2-dimhexanoyl-sn-glycero-3-phospho choline (DHPC) were purchased from Avanti polar lipids (Alabama, USA)

The oligonucleotides used to introduce the desired mutations, as well as those used for DNA sequencing, were purchased from Sigma (Spain). *Pfu* ultraII fushion hsDNA polymerase, and *dpnI* were purchased from Agilent technologies, (CA, USA)

All other chemicals and reagents were purchased from Sigma, Spain

3.2. Methods

3.2.1. Cell culture methods

Cells maintenance: COS-1 cells were routinely cultured in complete DMEM supplemented with 10% FBS, 2 mM L-glutamine, 100 units/ml penicillin, and 100 μg/ml streptomycin. When the cells attained 95% confluence, the mono-layer of adherent cells was passaged by trypsinization. The media was removed using a suction pump under a pre-UV-sterilized laminar flow hood, washed using sterile 1x PBS (137 mM NaCl, 2.7 mM KCl, 10 mM Na_2HPO_4, and 1.8 mM KH_2PO_4) in order to remove the dead cells and residual media which may inhibit the action of trypsin. Cells were treated with 1% trypsin (0.05% trypsin in 1x PBS), incubated for 3-4 min and 5 ml of complete DMEM was added in order to inactivate the trypsin, and the cells were spun down by centrifuging at 300g for 5 min. Cells were then suspended into fresh complete DMEM and dispensed in culture plates, and replenished with media to cover the cell monolayer. Plates were incubated in a 37ºC humid incubator with circulating CO_2 (5%).

HEK293S-GnTi$^-$ cells, in which the genes of glycosylating enzymes were silenced, were cultured using DMEM-F12 supplemented with 10% FBS, 2 mM L-glutamine, 100 units/ml penicillin, and 100 μg/ml streptomycin. These cells were passaged without trypsin, as the adherence is weak on the cell culture plates. After washing the plate gently using 1x PBS, 10 ml of complete DMEM-F12 was added to the plate and the cells were flushed carefully by pipetting the media. The detached cells were suspended in fresh media and cultured on new plates. The cultured plates were incubated in a 37ºC / 5% CO_2 incubator.

Freezing and thawing of cells: cells that were not immediately needed were frozen for long term storage in order to avoid senescence and genetic drift. After trypsinization, the cells were spun down and resuspended in 1ml/plate of freezing media (DMEM supplemented with 20% FBS, 10% DMSO). The cells were aliquoted in 1ml labeled cryotubes and kept at 4ºC for 2 h followed by treatment at -20ºC for 1 h and then the frozen cryotubes were transferred to -80ºC for overnight storage. Next day the frozen cells were transferred to a liquid nitrogen container.

The cells were recovered by thawing the cryotubes at 37ºC in a water bath. After thawing, the cryotubes were cleaned using 70% ethanol and cells were added aseptically into a cell-culture plate containing complete DMEM. The thawed cells were incubated in a 37ºC / 5% CO_2 incubator and the media was replaced after 24h.

3.2.2. Expression of opsins

The opsin genes were expressed in transiently transfected COS-1 cells by chemical transfection using polyethylenimine (PEI) reagent according to the manufacturer's instructions. PEI powder was dissolved in distilled water and the pH was adjusted to 7.0 (the solution becomes clear as the

pH is adjusted). After PEI was completely dissolved, the final concentration was adjusted to 1mg/ml and filtered through a 0.22 μM filtering unit. The prepared PEI regent can be aliquoted and stored at -20ºC. Once a PEI aliquot is thawed, it should be maintained at 4ºC.

500 μl of PEI (1 mg/ml) was added in a 50 ml sterile tube containing 12.5 ml of Opti-MEM, and in another sterile tube, 150 μg of plasmid was mixed with 12.5 ml of Opti-MEM. Both tubes were incubated separately for 5 min at room temperature (RT), and then the tubes were mixed and incubated for 20 min at RT. 5 ml of Opti-MEM/PEI/DNA was added to each plate of 80% confluent COS-1 cells, together with 5 ml of fresh complete DMEM. The transfected plates were incubated for 48 h in a 37ºC / 5% CO_2 incubator.

3.2.3. Purification of visual pigments

The CNBr-activated Sepharose beads were coupled to the 1D4 antibody according to the manufacturer instructions (GE Healthcare).

The transfected cells were harvested 48-60 h after transfection and regenerated with 10 μM 11CR in 1x PBS buffer by overnight incubation at 4°C. Regenerated cells were subsequently solubilized using 1% DM with PMSF and protease inhibitors, and the pigments were purified by immunoaffinity chromatography using Sepharose coupled to the rho-1D4 antibody. After 5 times washing the beads using 1x PBS containing 0.05% DM in order to remove the free retinal, the bound proteins were eluted in PBS containing the nonamer peptide and 0.05% DM (elution buffer). COS-1 cells were used for the expression of the recombinant proteins in all experiments except for samples used in the electrophoretic analysis.

Rhodopsin can be purified using either PBS buffer or sodium phosphate (NaPi) buffer (2 mM sodium dihydrogen phosphate and disodium hydrogen phosphate mixed to pH 7.4). Cone opsins were purified only using PBS buffer as chloride plays a role in the stability of cone opsins.

3.2.4. UV-visible spectroscopy

Spectroscopy deals with the electromagnetic radiation of a particular frequency, or a range of frequencies, that is allowed to impinge on the sample under study. The radiation coming out of the sample is then analyzed in terms of the intensity at different frequencies which will indicate which particular frequencies are absorbed by the molecule, thus giving a picture of the molecular energy levels. These, in turn, can be interpreted in terms of the chemistry or stereochemistry of the molecule.

If a beam of light of intensity I_0 falls on the sample, the emergent radiation intensity I is less intense than the incident radiation, since a portion of it is absorbed by the sample. The absorption wavelengths depend on the characteristic of the sample. This characteristic quantity is called the absorbance and may be calculated from the Beer-Lambert principle. The Beer- Lambert law states

that in a sample, each successive portion along the path of the incident radiation, containing an equal number of absorbing molecules absorbs an equal fraction of the radiation that traverses it. If we consider an infinitely thin slice of the sample (*dl*), the light traversing it may be considered a constant. Then the fraction of the light absorbed is simply proportional to the number of absorbing molecules,

$$-dI/I = C\varepsilon' dl$$

where *C* is the concentration of the molecule in moles per litre, ε' is a proportionality constant called the molar extinction coefficient and the negative sign indicates a diminution of the intensity of the radiation as it traverses the sample. ε' is a constant for a given wavelength for a given molecule and is independent of the concentration. Integrating this equation over the entire sample thickness 1, then

$$A = \log(\frac{I_0}{I}) = C\varepsilon(\lambda)l$$

where $\varepsilon = \varepsilon'/2.303$ i.e. molar extinction coefficient converted to log base 10 and expressed as a function of wavelength λ. The term $\log(\frac{I_0}{I})$ is called the absorbance A. The wavelength at the maximal extinction and the extinction coefficient at this wavelength are used to characterize the sample. A double beam spectrophotometer has a beam splitter that splits the beam into two equidistant paths. The sample is placed in the path of one half of the beam and the reference in the other (120).

The assay is non-destructive as the protein in most cases is not consumed and can be recovered. Secondary, tertiary and quaternary structures all affect absorbance; therefore, factors such as pH, ionic strength, etc. can alter the absorbance spectrum. The aromatic rings in the protein (mainly tryptophan, but to a lesser extent also tyrosine) absorb UV light at an absorbance maximum of 280 nm (121). The unique absorbance property of proteins could be used to estimate the level of proteins and their interactions and binding to the chromophore.

Purified pigments were spectroscopically characterized using a Varian Cary 100 Bio spectrophotometer (Varian, Australia), equipped with a water-jacketed cuvette holder connected to a circulating water bath. Temperature was controlled by a peltier accessory connected to the spectrophotometer. All the spectra were recorded in the 250 nm-650 nm range for rhodopsin and green cone opsin, 250 nm-600 nm for blue cone opsin and 250 nm-700 nm for red cone opsin, with a bandwidth of 2 nm, a response time of 0.5 s, and a scan speed of 400 nm/min.

The concentration of the visual pigments was calculated using the measured absorption maximum (Amax) at visible region λmax, using the formula,

$$c = \frac{A}{\varepsilon l}$$

c – concentration of the sample,

A – Amax at the λmax at the visible region

ε – molar extinction coefficient

The estimated molecular extinction coefficients of cone opsins include those of chicken red cone opsin, 47,200 (122), green cone opsin, 40,800 (123), and mouse blue cone opsin 41,760 (124) which have used during the course of the present study to calculate the concentration of the purified cone opsins.

l – length of the cuvette.

Photoactivation: the samples of rhodopsin, red and green cone opsins were illuminated with a 495 nm cut-off filter for 30 s using a Dolan-Jenner MI-150 fiber optic illuminator, and the blue cone opsin was illuminated without the cut-off filter because the Amax of blue cone opsin is at 420nm.

Thermal decay: the thermal stability of visual pigments was monitored as previously described (125). The thermal stability rates of visual pigments were measured by monitoring the decrease of absorbance at λmax of the visible spectral band as a function of time at 37°C. Spectra were recorded every min and half-life times were determined by fitting the experimental data to single exponential curves using Sigma Plot version 10.0 (Systat Software, Chicago, IL,USA).

Chemical decay: hydroxylamine can readily access the binding pockets of cone opsins and cleave the Schiff base linkage of 11CR which results in retinaloxime release in solution (126). A solution of 1M hydroxylamine, adjusted to pH 7, was added to dark-adapted samples in a spectroscopic cuvette (final concentration of 50 mM). The successive spectra were recorded every min to monitor the loss of pigment (Amax) and formation of retinaloxime (A365 nm). Reactions were carried out in the dark at 20°C (127). The half-time of the decay process was determined by fitting the experimental data to single-exponential curves using SigmaPlot version 10.0 (Systat Software).

Regeneration experiments: for regeneration experiments, 2-2.5-fold molar concentration of retinal over pigment was added to the purified pigments in the spectroscopic cuvette and thoroughly mixed. Retinal was added either before or after photoactivation which will be indicated at the particular results section. The volume of the retinal stock added to the protein sample represented a maximum of 1% of the total sample volume so the effect of the carrier (ethanol in which the retinal stock was dissolved) on the observed results may be negligible.

Acidification: acidifying the visual pigments, using 3-4 μl of 2N H_2SO_4, which yields a pH ~ 2.0, and reprotonates the Schiff base shifting Amax to 440 nm (128). This assay would help in identifying the presence of Schiff-base linked species during the course of the regeneration experiments.

3.2.5. Fluorescence spectroscopy

Fluorescence is a phenomenon by which light is absorbed by a system at one wavelength and emitted by it at a different, and longer, wavelength. The basic principle of fluorescence can be understood in terms of the electronic energy levels in one of which, according to quantum mechanics, the molecule is usually found (Fig. 3.1). Each of these electronic levels themselves has a so-called 'fine structure' due to the vibrational motion of the molecules, i.e. each electronic level is not a single energy value but consists of a band of closely spaced energies which arise due to the different vibrational modes. The molecule usually exists in the ground state. When a beam of light (visible or UV) falls on it, some of the energy is absorbed and electrons jump up to the excited state where they can go to any of the vibrational levels. So far the experiment is the same as UV-vis spectroscopy. However, now the electron in the upper electronic level can lose some of its energy in many ways. One of these is by going to a lower vibrational level within the same electronic level. When now the electron jumps back to the ground state, it does so by emitting radiation, but the radiation is of less energy and therefore longer wavelength than the incident light. The molecule is said to fluoresce. A study of the intensity of the fluorescent radiation as a function of the wavelength is known as fluorescence spectroscopy (120).

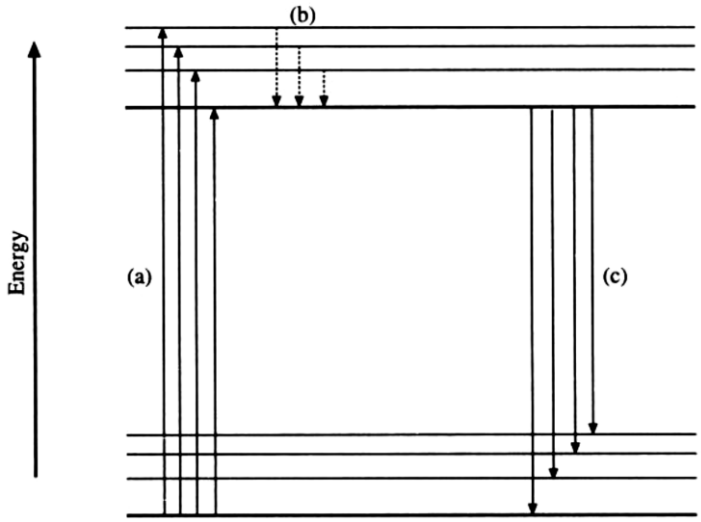

Figure 3.1. ***Energy levels in a molecule.*** (a) Transition from ground state to excited state. (b) Non-radiative loss of energy. (c) Radiative transitions to lower state.

A QuantaMaster 4 spectrofluorimeter (Proton Technology International, New Jersey, US) was employed to measure the Trp fluorescence emission from $W^{6.48}$ which is located close to the β-ionone ring of the retinal. These fluorescence changes are a measure of the retinal release and retinal uptake processes in rhodopsin, and red and green cone opsins. The excitation wavelength was 295 nm, and the emission wavelength was 330 nm, measuring 1 point per second for 2 s followed by 28 s pause (with the help a beam shutter to prevent sample bleaching by the fluorimeter lamp), the excitation slit settings were 0.5 nm, and emission 10 nm. In blue cone opsin, amino acid at 6.48 is a Tyr, and in this case the fluorescent changes of Tyr were measured with the setup of excitation wavelength at 285 nm and the emission wavelength adjusted to 335 nm.

A purified pigment was added to the micro cuvette and Trp fluorescence was monitored over time, in the dark, until a steady baseline was obtained. Then, the sample was photobleached with or without a 495 nm cut-off filter for 30 s using a Dolan-Jenner MI-150 fiber optic illuminator and the change in fluorescence was recorded.

Regeneration experiments and hydroxylamine treatment were also carried out by means of fluorescence spectroscopy under the same experimental conditions mentioned for UV-vis spectroscopy.

3.2.6. Surface Plasmon Resonance (SPR) spectroscopy

Surface plasmon resonance (SPR) spectroscopy is a biosensor technology that allows monitoring molecular interactions between two or more molecules in real time. SPR biosensors are sensitive to changes in mass of the molecule bound on the sensor surface and measures the changes in refractive index. Therefore, the interactions of visual pigments with transducin can be studied using this technique. In this technique, the visual pigments can be immobilized on a sensor chip surface whereas the G-protein, transducin, is injected in a mobile phase that is flushed into a miniature flow cell. The interactions between transducin and immobilized opsin on the surface lead to a change in refractive index. The time dependent changes in refractive index are recorded as sensograms which provides information about the binding kinetics and affinity of the interactions (129).

All the steps involved in measuring the SPR signals, arising from the interaction between transducin and visual pigments, were performed with a Biocore 1000 using the BIAcore control software 1.2 as previously described (130). The surface of the sensor chip (XanTec CMD50d) contains carboxymethylated dextran on which the 1D4-antibody is immobilized via amine coupling. De-gased HBS buffer (0.01 M Hepes pH 7.5, 150 mM NaCl, 3 mM EDTA, and 0.005% Tween 20 (v/v)) was used as running buffer in a constant flow of 5 μl/min. A mixture of 80 μl of 50 mM N-hydroxysuccinimide (NHS) and 80 μl of 200 mM N-ethyl-N′-[(dimethylamino)propyl]

carbodiimide (EDC) was used for activating the surface which eases the covalent linkage of 1D4-antibody to the surface. The antibody was diluted to 0.1 mg/ml in 10 mM sodium acetate pH 4.3, and it was injected producing an increase of 725 RU (Fig. 3.2). The surface was blocked with two injections of 35 µl of 1 M ethanolamine, pH 8.5. The visual pigments were immobilized, in the dark, on the 1D4 surface of the sensor chip, and 35 µl of 300 nM transducin was injected as mobile phase.

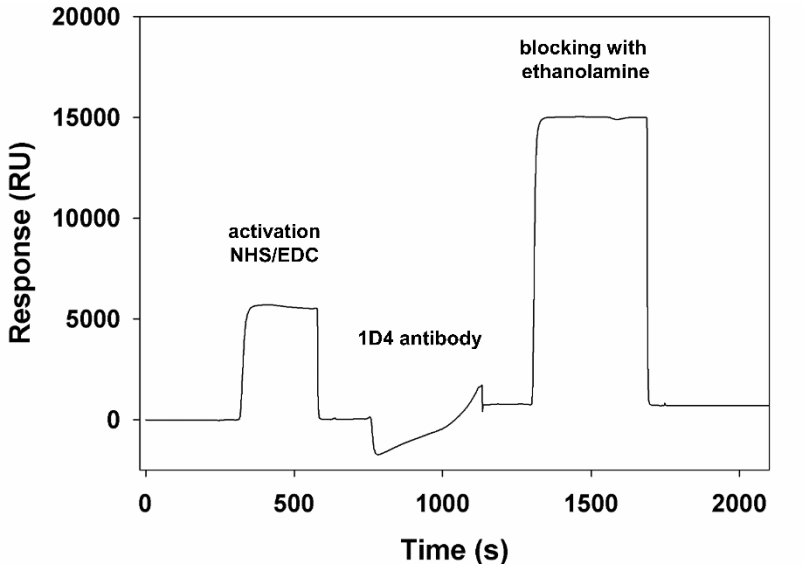

Figure 3.2. ***SPR sensogram of 1D4 antibody coupling on an activated sensor chip surface.*** The dextran surface of the sensor chip was activated by NHS/EDC mix and coupled with 1D4 antibody via amine coupling. The unbound surface of the chip was blocked using ethanolamine.

3.2.7. Blue Native-Polyacrylamide Gel Electrophoresis (BN-PAGE)

BN-PAGE allows separation and identification of proteins in their native form. BN-PAGE was performed as previously described (131,132) with few modifications. For electrophoresis, a Bio-Rad Mini-PROTEAN 2 gel running apparatus was used with the corresponding gel running buffer (50 mM Tricine, 15 mM Bis-Tris, 0.02% Coomassie blue G, pH 7.0). The gel was composed of 13% separating gel and 4% stacking gel as per table 3.1. Here, the opsin genes were expressed in transiently transfected HEK293S-GnTi- cells -which lack glycosylation- in order to avoid the smeary appearance of protein bands due to differences in glycosylation patterns (133).

Concentrations of the purified samples were normalized using A_{280nm} in the UV-visible spectra. Equal amount of protein samples in sample buffer (5% glycerol and 0.01% Ponceau-Red) were loaded onto the gel. After 4hr of electrophoresis, the gel was destained (30% methanol and 10%

glacial acetic acid in distilled water) and visualized using a gel documentation system, Chemidoc XRS, BioRad.

Reagents	Stock	Separating gel (ml)	Stacking gel (ml)
Acrylamide/Bisacrylamide	37.5% / 0.8%	3.5	0.7
Bis-Tris	1M, pH 7.0	0.4	0.25
Distilled water	-	4.0	4.0
APS	10%	0.1	0.05
TEMED	10%	0.05	0.05

Table 3.1. ***Protocol for casting BN-PAGE gel***

3.2.8. SDS-PAGE

Equal concentrations of purified visual pigments in DM were analyzed based on their electrophoretic mobility which depends on the molecular weight of the protein by SDS-PAGE as described earlier (134). Sodium dodecyl sulfate (SDS), an anionic detergent, is used to reduce proteins to their primary (linearized) structure and coat them with uniform negative charges so that the mobility of the proteins is solely based on molecular weight. The gel was casted with a composition of 12% separating gel and 4% stacking gel as indicated in table 3.2. The protein sample to be analyzed was diluted with a sample buffer (0.4 M dithiothreitol (DTT), 62.5 mM Tris, 2% SDS, 10% glycerol, 0.1% bromophenol blue). The prepared samples, and a 10 µl-sample of the protein molecular weight marker, were loaded onto the gel and the electrophoresis was carried out using a gel running buffer (25 mM Tris, 192 mM glycine, 0.1% SDS) at 100 v for 2 h. The run gel was stained overnight using a staining solution (0.025% Commassie R-250, 40% methanol, 10% glacial acetic acid diluted in distilled water). The stained gels were destained until visualizing the bands using destaining solution (40% methanol, 10% glacial acetic acid diluted in distilled water).

3.2.9. Western blot analysis

After separating the proteins using SDS-PAGE, the proteins from the gel were transferred onto a nitrocellulose membrane and detected using 1:10,000 dilution of the rho-1D4 anti-mouse antibody and 1:5,000 dilution of goat anti-mouse IgG conjugated to horseradish peroxidase (Santa Cruz biotechnology, California, US). The blots were developed using substrate SuperSignal West Pico Chemiluminescent Substrate (Luminol/H_2O_2) (Thermo Fisher scientific, France).

Reagents	12% Separating gel		5% Stacking gel	
	Stock	Volume (ml)	Stock	Volume (ml)
Distilled water	-	1.25	-	2.9
Tris-HCl	1.5M, pH 8.8	5.0	0.5M, pH 6.8	1.25
Acrylamide/Bisacrylamide	37.5% / 0.8%	3.2	37.5% / 0.8%	0.67
SDS	10%	0.1	10%	0.05
APS	10%	0.1	10%	0.05
TEMED	10%	0.05	10%	0.05

Table 3.2. ***Protocol for casting SDS-PAGE gel***

3.2.10 Isolation of transducin from bovine retina

Transducin was purified from bovine retinas as previously described (135). Briefly, 100 dark adapted frozen bovine retinas were thawed overnight at 4ºC under room light. The retinas were diluted with 47% sucrose (with 2 mM DTT, 0.1 mM PMSF) and homogenized. After a centrifugation at 42,000xg for 20 min at 4ºC, ROS membrane stuck on the walls were carefully taken and washed using buffer A (20 mM Tris, pH 7.4, 1 mM $CaCl_2$, 2 mM DTT, 0.1 mM PMSF). ROS membranes were resuspended in buffer A and layered on top of a sucrose density gradient (1.2 mM / 1.0 mM / 0. 8 mM). The orange layer was taken out carefully and washed using buffer C (10 mM Tris, pH 7.4, 100 mM NaCl, 5 mM $MgCl_2$, 2 mM DTT, 0.1 mM PMSF) followed by bufferD (10 mM Tris, pH 7.4, 0.1 mM EDTA 3 mM DTT, 0.1 mM PMSF) in order to remove the sucrose and the excess salts were chelated by buffer D. The final pellet was homogenized in 50 ml of buffer D with 40 μM GTP and rotated for 30 min at 4ºC. The supernatant was collected after centrifugation and filtered via 0.2 μm filter to remove traces of membrane. The collected sample was concentrated and dialyzed using buffer E (10 mM Tris, pH 7.4, 2 mM $MgCl_2$, 50% glycerol, 1mM DTT). The harvested transducin was stored at -20ºC. The concentration and quality of the purified transducin were analyzed using SDS-PAGE with bovine serum albumin (BSA) standards (Fig. 3.3).

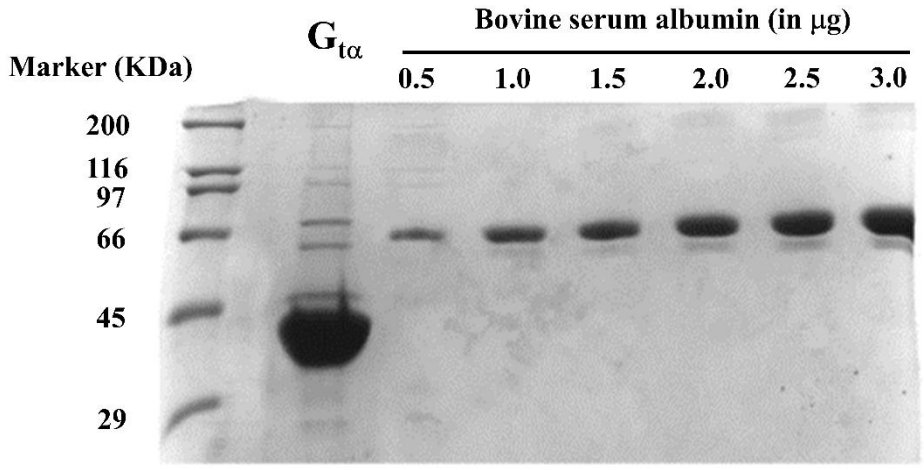

Figure 3.3. ***SDS-PAGE of transducin extracted from bovine retina.*** SDS-PAGE was carried out with extracted transducin and 0.5, 1.0, 1.5, 2.0, 3.0 μg standards of BSA.

3.2.11. Transducin activation assay

For the transducin activation assay, 10 nM concentration of rhodopsin and red cone opsin or 300 nM cone pigments were used, depending on the experiment. The samples were added to a mixture of 500 nM transducin in assay buffer (25 mM Tris, pH 7.5, 5 mM $MgCl_2$, 100 mM NaCl, 2.5 mM DTT, and 0.013% DM) containing 5 μM GTPγS^{35} (0.156 mCi/mmol). The reaction mixture was incubated at room temperature for 20min in the dark and transferred onto a 96-well cellulose membrane plate. The plate was fixed to a manifold filtering unit and the membrane was washed thoroughly with assay buffer. Bound GTPγS^{35} was measured by means of a Tri Carb 2100TR liquid scintillation counter (Perkin-Elmer, The Netherlands).

The activity measured as cpm which is converted by pmol using the formula,

$$Concentration = \frac{dpm}{2.22\ x\ 10^{12}\ x\ radioactivity\ of\ ligand}$$

Where,

$dpm = \frac{cpm}{counter\ efficiency}$;

counter efficiency = 55%

1Ci = 2.22 x 10^{12} dpm

radioactivity of the ligand = 1250 Ci/mMol

3.2.12. Site directed Mutagenesis

3.2.12.1. Plasmid details

The working plasmid containing the opsin gene was the pMT4 vector which is 6.2 kbp. The vector has ampicillin resistance and EcoRI and NotI cloning sites are at the two ends of the opsin gene. A nine amino acid epitope for anti-rhodopsin monoclonal antibody rho-1D4 is inserted at the C-terminus of all three cone opsins in order to facilitate immunopurification. The plasmid is resistant to ampicillin and hence the cells transformed with this plasmid will exhibit the colony selection on growth media supplemented with ampicillin.

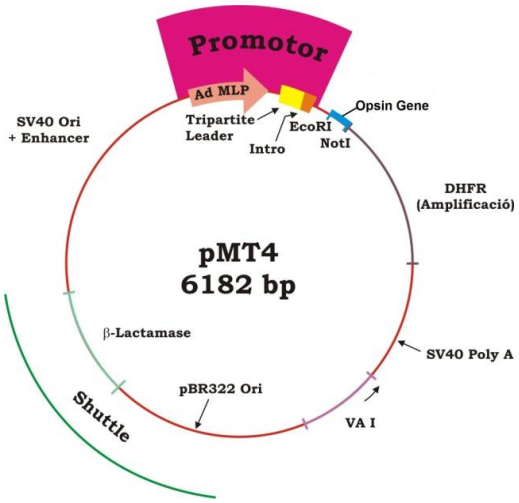

Figure 3.4. ***pMT4 plasmid containing the opsin gene.*** The opsin gene was inserted between the restriction sites EcoRI and NotI. β-lactamase confer the antibiotic resistance to the bacteria carrying this plasmid which would aid for artificial selection of the transformed cells on an ampicillin supplemented media.

3.2.12.2. Introducing the mutations into the opsin gene

Quickchange mutagenesis protocol (Stratagene) was employed to introduce the mutations into the opsin gene. This protocol involves the following steps:

Mutagenic primer designing: mutagenic primers are oligonucleotides containing the desired mutation which can anneal to the same sequence on opposite strands of the gene. The primers should be 25 to 45 bp with a melting temperature (Tm) of > 78ºC. The GC content of the primers should be more than 40% and the desired mutation should be located in the middle of the primer. By taking into account of all these parameters, the mutated primers for forward and backward strands were designed using a DNA codon table.

PCR amplification: the mutated opsin genes were synthesized using a thermal cycler by a polymerase chain reaction (PCR). The reaction mix for synthesizing and amplifying the mutated plasmid is shown in table 3.3.

Reagents	Volume (µl)
10x reaction buffer*	5.0
pMT4 plasmid (100 ng/µl)	1.0
Forward primer (125 ng/µl)	1.0
Reverse primer (125 ng/µl)	1.0
dNTP mix (100 mM)	1.0
Double-distilled water	41.0
PfuTurbo DNA polymerase (2.5 U/µl)	1.0

Table 3.3. ***PCR mix for site directed mutagenesis***. *10x reaction buffer (100 mM KCl, 100 mM $(NH_4)_2SO_4$, 200 mM Tris-HCl (pH 8.8), 20 mM $MgSO_4$, 1% Triton® X-100, 1mg/ml nuclease-free bovine serum albumin (BSA)).

The reaction mix was prepared in a microfuge tube and was subjected to a thermocycler with a specific protocol (Table 3.4.).

Step	Temperature	Time
Initial denaturation	95ºC	30 s
18 cycles	95ºC	30 s
	60ºC	60 s
	68ºC	6 min (1 min/bp of plasmid)
Final extension	68ºC	5 min
Hold	4ºC	

Table 3.4. ***Thermo-cycle conditions for a mutagenic PCR.***

dpnI digestion: in order to digest the temple plasmid, l μl of the *Dpn* I restriction enzyme (10 U/μl) was added and mixed well by pipetting the solution up and down several times. The contents were incubated at 37°C for 2 h.

The resulting DNA was analyzed by 0.8% agarose gel electrophoresis.

3.2.12.3. Transformation, DNA miniprep and DNA sequencing

Competent cells preparation: competent cells are treated cells which can easily uptake foreign DNA. E coli DH5α was used to transform pMT4 plasmid. In order to prepare competent cells, DH5α cells were cultured until the absorbance at 600 nm reached 0.6. The cultured cells were incubated on ice for 30 min and the cell pellet was mixed with 100mM autoclaved $CaCl_2$. After incubating on ice for 30 min, the cell pellet was resuspended in 20% glycerol and 80% $CaCl_2$. The prepared competent cells were stored at -80ºC until use.

Transformation: 5 μl of the PCR amplified plasmid was added a 50 μl aliquot of competent cells, and incubated on ice for 30 min. The cells were subject to heat-shock treatment at 42ºC for 42 s and the tube was immediately transferred to ice for 5 min. 500 μl of autoclaved 2YT media (16 g/L tryptone, 10 g/L yeast extract, 5 g/L NaCl) was added to the transformed cells and incubated at 37ºC, shaking for 1 h. The cells were plated on an ampicillin (100 mg/ml) supplemented LB agar plate which was incubated at 37ºC overnight.

Miniprep: a single colony from the transformed plate was inoculated into 10 ml of LB broth supplemented with 100 mg/ml ampicillin was and incubated at 37ºC by overnight shaking. The DNA was purified from the transformed cells using QIAprep spin Miniprep kit (Qiagen plasmid purification kits, La Jolla, CA). Concentration and quality of the sample of DNA were measured using UV-Vis Spectrophotometry at 260 nm.

The concentration of purified DNA was calculated using the formula,

$$concentration\ of\ DNA\ (\mu g/ml) = A_{260nm}\ X\ 50\ X\ dilution\ factor$$

As 50 μg/ml of DNA contributes to the absorbance 1.0.

DNA sequencing: the mutation introduced into the opsin gene was confirmed by DNA sequencing. The primers for DNA sequencing were designed from the sequence which is at least 50bp upfront to the mutation site. The primers used for the cone opsins are:

red and green cone opsin mutants:

5’ GAATTACCACATCGCTC 3’

blue cone opsin mutants:

5’ GTCTTCCTTATAGGGTTC 3’

The purified cone opsin mutant DNA and their corresponding primers were outsourced to Servei de Genòmica, UAB, Barcelona or STAB-VIDA, Portugal for DNA sequencing.

3.2.12.4. Maxiprep

Large scale DNA purification for transient transfection was carried out using QIAGEN maxiprep kit (Qiagen plasmid purification kits, La Jolla, CA) which is based on alkaline lysis, followed by binding the DNA to a QIAGEN anion-exchange resin. The eluted DNA was resuspended in TE buffer (10 mM Tris-HCl, pH 7.5, 1 mM EDTA). The DNA yield was measured in a UV spectrophotometer at 260 nm. The purified plasmid was stored at -20ºC until use.

3.2.13. Sub-cellular localization

COS-1 cells were plated in 6-well plates containing sterile coverslips and incubated for 24 h to reach 90% confluence. After the old media was removed, the cells were washed with PBS and treated with 1.2 ml of complete media (DMEM supplemented with FBS). For each well, PEI mix contained: 400 µl of Opti-MEM, 15 µl PEI (1 mg/ml; pH 6.0); DNA mix: 400 µl of Opti-MEM, 1 to 3 µg DNA, were prepared and incubated separately for 5 min. DNA mix was added gently into PEI mix and incubated for 20 min at room temperature. This transfection mix was added to the cells and incubated for 36-48 h, and immunofluorescence analysis was carried out. After removing the media, 1 ml of 37% formaldehyde was added and incubated at 37ºC for 20 min in order to fix the transfected cells onto the coverslips. Cells were 3X washed with TTBS and incubated with 1D4-mouse monoclonal antibody (dilution 1:2000) for one h. After 3X washing with TTBS, goat anti-mouse-1D4 tagged with FITC (dilution 1:200) was added. Again, after 3X washing with TTBS, cover glasses containing cells were taken and mounted on a glass slide with a help of mounting media supplemented with DAPI, which stains the nucleus. Images were collected using a fluorescence microscopy system, Nikon eclipse T*i* equipped with the camera DS-QiMc.

3.2.14. Bicelle Preparation

Bicelles are bilayer-mimic structures which are composed of phospholipids such are DMPC and DHPC in a ratio of 1:1. As a stock, 2% (w/v) DMPC and 10% (w/v) DHPC were prepared in buffer A (pH 6.0, 10 mM Bis-Tris propane (BTP), 140 mM NaCl, 2 mM $MgCl_2$, 2 mM $CaCl_2$), vortexed well and stored at -20ºC. Prior to use, the DHPC stock was taken out and let warm up for 5 min. In contrast, DMPC was taken from ice and vortexed for 5 min and incubated at 42ºC for 15 min in order to dissolve completely. The clear DHPC sample should be maintained at 4ºC. 1% DMPC and 1% DHPC were prepared by diluting with buffer A. The mixture was vortexed

briefly for 1 min and incubated at 42ºC for 15 min. The bicelles mixture was subject to shaking at room temperature for 1 h. The prepared bicelles should be used within 36 h or stored at 4ºC until use.

3.2.15. Estimation of sulfhydryls

Quantifying the free sulfhydrals groups, functional group of Cys from a protein, could be used as an indirect measure of the presence of disulfide bonds in a protein (136). 5,5'-dithio-bis-(2-nitrobenzoic acid), or DTNB or Ellman's reagent, reacts with free sulfhydrals at the periphery of the protein and produces a mixed disulfide with protein and a yellow colored TNB^{2-} which can be measured at 412 nm (137).

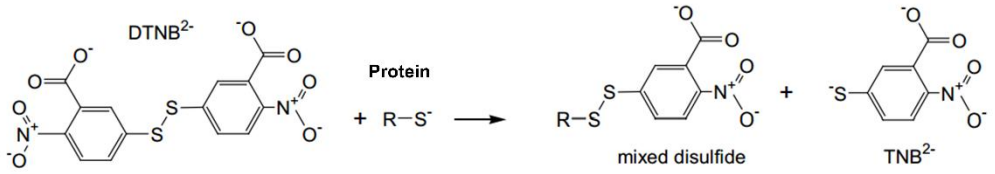

Figure 3.5. ***Reduction reaction with Ellman's reagent*.** DTNB (or Ellman's reagent) reacts with free sulfhydral groups of the protein producing mixed disulfides with the protein and a yellow colored TNB2- which is spectroscopically detectable.

25 µl of the protein sample was added to 0.25 ml reaction buffer (0.1 M sodium phosphate, pH 8.0, 1 mM EDTA and 5µl of Ellman's reagent solution (DNTB 4 mg/ml (w/v) in reaction buffer) in a tube, and incubated at RT for 15 min. Using the reaction buffer as control, the absorbance at 412 nm was measured by means of a UV-visible spectrophotometer. The concentration of free sulfhydryls in the protein sample was estimated by using the following formula:

$$C = \frac{A}{bE}$$

c - concentration of free sulfhydryls

A - absorbance average at 412 nm

b – path length of the cuvette (1 cm)

E – molar extinction coefficient of DTNB (14,150 $M^{-1}cm^{-1}$)

4. RESULTS AND DISCUSSION

4.1. Molecular characterization of human cone opsins

The biochemical and biophysical characterization of human cone opsin pigments is inevitable to unravel the structural subtleties of these pigments whose structural differences have been very little investigated. By studying these pigments we should obtain relevant information about the structure-function relationships of these photoreceptor proteins in comparison with the much better studied rhodopin from the rod photoreceptor cells. These characterization studies also help in identifying the similarities and variances in conformational aspects of functionally-relevant intra and intermolecular interactions among the three cone opsins. Such characterized parameters can be compared with those of cone opsin mutants which are responsible for inherited retinal disorders ranging from colorblindness to degenerative retinal dystrophies.

4.1.1. Purified recombinant human cone opsins

Plasmids containing human red, green and blue cone opsin genes were expressed in COS-1 cells. The expressed cells were harvested and regenerated with 11CR. Purification was carried out using 1D4 antibody coupled to a Protein A-Sepharose matrix. The purified cone pigments, in DM solution, were analyzed at room temperature using a UV-Vis spectrophotometer in which the absorbance spectra were measured from 250 nm to 700 nm. The measured spectra (Fig. 4.1) showed two main characteristic bands for all opsins, one at 280 nm characteristic of the opsin apoprotein and another one in the visible region at 564 nm, 532 nm, and 418 nm for red, green and blue cone opsins respectively corresponding to opsin regenerated with the chromophore. The peak at the 280 nm of wavelength corresponds to the total protein and it can include the regenerated protein, misfolded protein which cannot regenerate with 11CR, and protein species which lose the bound retinal due to the purification process (138).

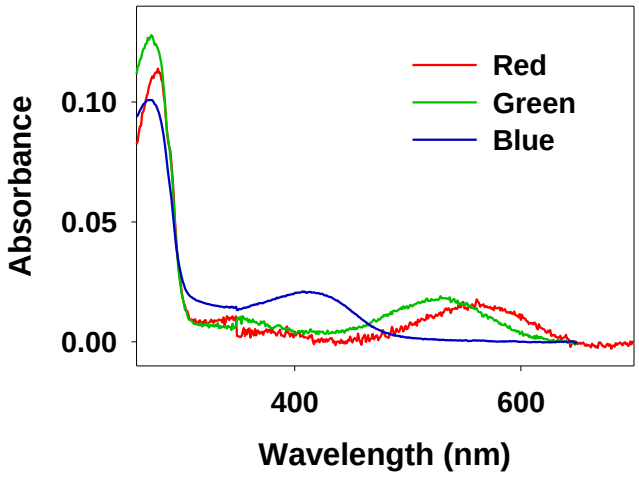

Figure 4.1. ***Purified recombinant human cone opsins.*** UV- Vis spectra of purified human red, green and blue cone pigments which were expressed by transfecting the pMT4 plasmid containing the cDNA of human cone opsins, (*OPNSW*, *OPNMW*, *OPNLW*) into COS-1 cells. The expressed cells were regenerated with 11CR and immunopurified using 1D4-Sepharose column.

In the case of rhodopsin, its UV-Vis spectrum shows its characteristic regenerated chromophoric band at 500 nm. Photoactivation of the rhodopsin shifts the absorbance to 380 nm (Fig. 4.2A) similarly, Illumination of the cone pigments lead to isomerization of the bound retinal to ATR which would no longer fit into the protein and leaves from the protein resulting a conformational change that shifts the absorption maximum of the pigments from their typical dark λmax to 380 nm (Fig. 4.2B) which is faster in the case of cone opsin than rhodopsin correlating with the physiological faster response to the light stimuli.

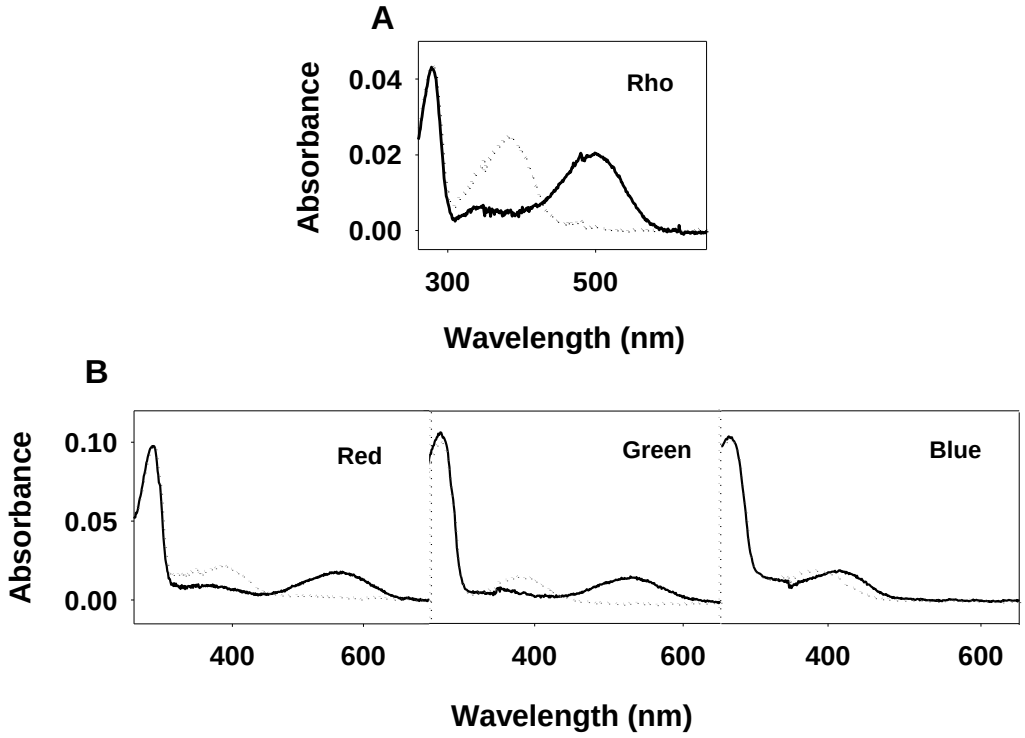

Figure 4.2. ***Photoactivation of recombinant visual pigments.*** **(A)** The purified recombinant rhodopsin in DM was a spectrophotometer was illuminated (dotted line) after measuring a dark spectrum (solid line). **(B)** UV-Vis spectra of red, green and blue cone opsins in dark (solid line), was illuminated (dotted line) causing a shift in peak to 380 nm.

4.1.2. MetaII decay of cone opsins

The isomerized chromophore, after illumination, causes a conformational change in the dark inactive state of visual pigments resulting to a series of short-lived photointermediates which lead to the formation of the active MetaII species. This active conformation decays with time yielding the protein ready for another retinal uptake and restoring the dark-adapted state in adaptation (visual cycle). The kinetics of this process is linked with the stability of the apo-protein with time. The decay of MetaII intermediate can be studied by means of fluorescence spectroscopy. This technique has been standardized for rhodopsin by measuring the fluorescence from W265$^{6.48}$

which is located in the ligand binding site. In the dark inactive state, the fluorescence of W265$^{6.48}$ is quenched by the β-ionone ring of the retinal, and upon illumination, the release of the isomerized retinal from the photoactivated pigment increases the fluorescence which can be followed with time and it can be a measure of the conformational change in the binding pocket involving W265$^{6.48}$ that can be used as a reporter amino acid. In order to measure the Trp fluorescence, the fluorimeter was set with an excitation wavelength of 295 nm and an emission wavelength of 330 nm and the fluorescence changes were monitored continuously with time (60,90).

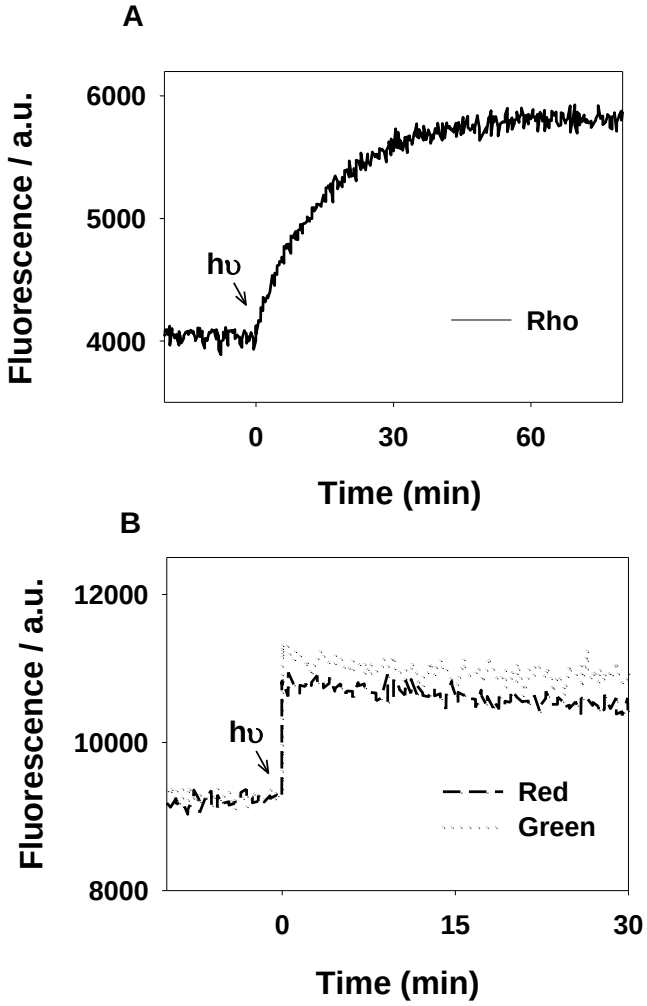

Figure 4.3. ***MetaII decay of rhodopsin, red, and green cone opsins.*** **(A)** Purified recombinant rhodopsin in DM was illuminated (>495 nm) and Trp fluorescence change was measured after a stable dark baseline was attained. **(B)** The same was carried out in red/green cone opsins to detect the photoactivation-induced fluorescence changes of Trp at the binding pocket.

The MetaII decay of the rod photoreceptor protein rhodopsin was studied in parallel to red and green cone opsins by means of fluorescence spectroscopy and fluorescence changes of Trp in the

retinal binding pocket are measured. In rhodopsin, the fluorescence increase upon illumination showed a slower rate with $t_{1/2}$ of 10.2 min for the process (Fig 4.3A) indicating that the photoisomerized retinal gets released from the protein at a slower rate.

This $W^{6.48}$ residue is also located in the binding pocket at the position 281 in red and green cone opsin sequences, and hence the same approach can be followed to study red and green cone opsins. Purified human recombinant red, or green, cone opsin in a fluorimetric cuvette at 20ºC, was illuminated (λ> 495 nm) after a stable fluorescence baseline was obtained in the dark. This causes a sudden increase in the fluorescence signal that immediately reaches a plateau (Fig. 4.3B) indicating a very fast response of red and green cone opsins to the light stimulus. The corresponding UV-Vis spectra of red, green cone opsins in dark and the spectral shift to 380 nm upon illumination the illumination shifting the peak to 380 nm indicate an analogous photobleaching behavior for these three proteins. (Fig. 4.2B).

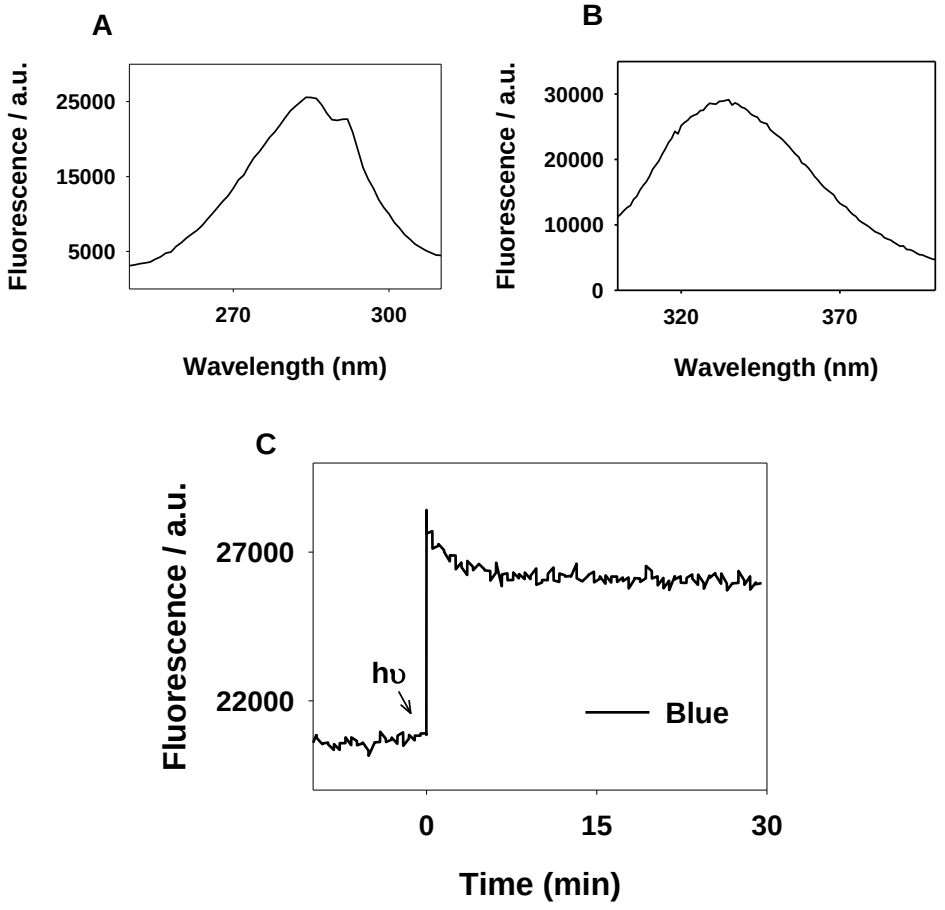

Figure 4.4. ***MetaII decay of blue cone opsin.*** **(A, B)** Using fluorescence spectroscopy, excitation (A) and emission (B) scans were carried out with purified blue cone opsin in DM which were measured as 285 nm and 335 nm as λmax of excitation and emission respectively in order to measure the fluorescence changes of Tyr in the retinal binding pocket of blue cone opsin. **(C)** Fluorescence change from Tyr was measured in the case of blue cone opsin metaII intermediate and resulting spectra represented as illuminated.

In blue cone opsin the bound chromophore quenching the fluorescence of $Y262^{6.48}$ which is also an aromatic amino acid located at the same position. Therefore, the MetaII decay of blue cone opsin upon illumination can be studied by measuring the Tyr fluorescence change in an analogous manner than measuring Trp for red and green cone opsins. It is known that, along with $W^{6.48}$, the fluorescence from $W^{3.41}$ which is W126 in rhodopsin and W142 in red/green cone opsins is also quenched by the retinal chromophore (66). The same residue is also located in human blue cone opsin as $W123^{3.41}$ which is believed to contribute to the fluorescence measurement of blue cone opsin MetaII decay. The optimal excitation and emission wavelengths were determined to be 285 nm and 335 nm (Fig 3.4A) for measuring maximum fluorescence emission from $Y262^{6.48}$ in blue cone opsin.

Purified blue cone opsin in DM was added to the fluorimetric micro-cuvette and illuminated using white light after a stable dark state baseline was obtained and an immediate increase in the fluorescence caused by $Y262^{6.4}$ was measured (Fig. 4.4B) This fluorescence increase may be contributed by $W123^{3.41}$ as the excitation and emission wavelengths of this Trp also fall within the range of Tyr absorbance. After the photoactivation-induced fluorescence increase (as seen with red and green cone opsin), a peculiar decrease in the fluorescence at a slower rate can been observed. This decrease in fluorescence after illumination may reflect a conformational change that can modify the retinal binding site accessibility hiding the exposed Tyr into the protein hydrophobic core.

4.1.3. Stability of cone opsins.

Thermal Stability

Visual pigments can be activated in dark by increasing the temperature that would promote opsin to a higher energy state and force chromophore isomerization. Such thermally-induced retinal isomerization is a two-step process, which includes Schiff base deprotonation followed by isomerization of 11CR to ATR and subsequent release of the retinal from the retinal binding pocket (139-141). Thermal stability of visual pigments is determined by measuring the absorbance decrease in the visible region over time, at a given temperature (142). Here, the thermal stability of cone opsins was determined at 37ºC. Purified red, green and blue cone opsins in DM were measured by means of UV-Vis spectrophotometry and the corresponding dark-state spectra were recorded at room temperature. Next, the temperature was increased to 37ºC and spectra were measured every min until complete loss of absorbance in the visible region was reached. The change of absorbance was plotted and fit with an exponential decay curve. The half-time for the thermal decay of each cone opsin was determined to be 10.25 ± 1.01 min for red cone opsin; 7.17 ± 0.98 min for green cone opsin; and 26.53 ± 2.24 for blue cone opsin (Fig. 4.1.5). Compared with the thermal stability of rhodopsin which was found to be 3100 ± 45 min (143),

red and green cone opsins are ~300 times less stable than rhodopsin at this temperature. It has been suggested that cone opsins undergo spontaneous dark activation as the activation energy required for isomerization of cone opsins is much lower than that for rhodopsin (144,145). The measured thermal decay half-time for blue cone is double than red and green cone opsin could be due to blue cone opsin sharing a more structural similarity with rhodopsin than others.

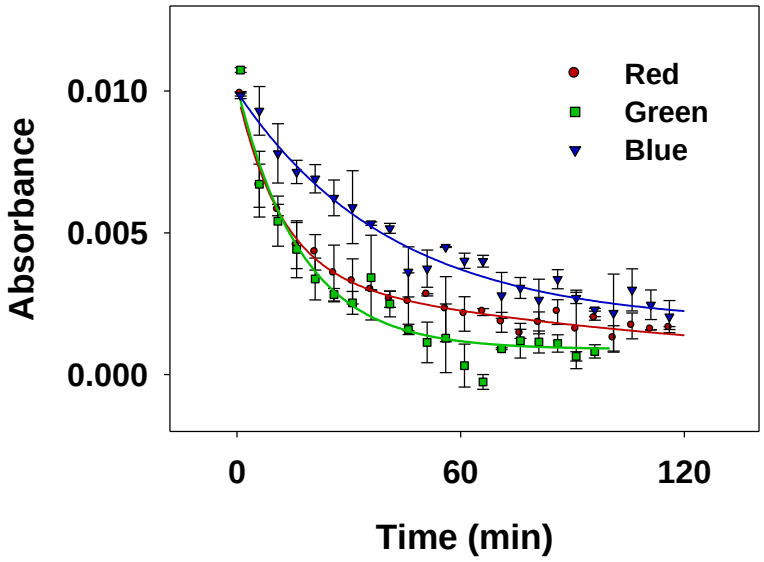

Figure 4.5. ***Thermal stability of cone opsins.*** Purified red, green, and blue cone opsins in DM were subject to thermal decay at 37ºC till the pigments had completely decayed. The thermal decay was measured by means of a UV-Vis spectrophotometer, the absorbance spectra were recorded every min and the Abs changes were plotted and fit to an exponential curve.

Chemical stability

The chemical reagent hydroxylamine can enter the retinal binding site of cone opsin in dark, break the Schiff base linkage and sequester the retinal molecule from the cone opsins resulting a retinaloxime and the opsin apo-protein. Hydroxylamine, added in dark, causes a decrease in the visible maximal absorbance, especially with cone opsins in which the binding pocket is quite open and accessible. In contrast, hydroxylamine does not react with rhodopsin even after 12 h of treatment in the dark (146). The retinal binding site accessibility –i.e. the chemical stability of cone opsins to hydroxylmine in the dark is a parameter that can be also compared with cone opsin mutants. Purified red, green and blue cone opsins in DM were treated with 50 μM hydroxylamine in dark and the UV-Vis spectra were recorded every min at 20ºC till the complete decay of the opsin visible band was recorded. The Abs change at the λmax in the visible region was plotted and fit with an exponential decay curve. The half-life times for the chemical stability of each cone opsin was determined to be 42.53 ± 2.68 min for red cone opsin; 38.65 ± 4.03 min for green cone opsin; and 4.71 ± 0.89 min for blue cone opsin (Fig. 4.6). It can be noted that blue cone

opsin is approximately 10 times more sensitive to hydroxylamine than red and green cone opsins. It is surprising that blue cone opsin, compare to red and green cone opsins, showed a slower thermal decay but a much faster hydroxylamine reactivity. These results may suggest that blue cone opsin has a very open retinal binding site with easy accessibility to the bound chromophore, but the activation energy required to thermo-isomerize the protein-bound retinal is higher than in the case of red and green cone opsins. The reason for these differences is not known but may be connected to the fact that red and green cone opsins are genetically more closely related than blue cone opsin which may have some features of rhodopsin.

The half-life times for the thermal and chemical decay of cone opsins are listed in Table 4.1.

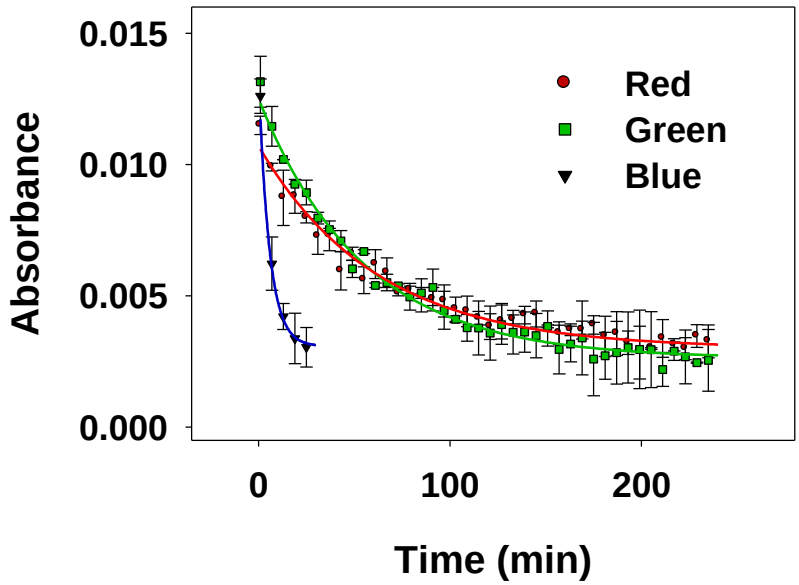

Figure 4.6. ***Hydroxylamine reactivity of cone opsins.*** Purified red, green, blue cone opsins in DM were added with 50mM hydroxylamine in a UV-Vis spectrophotometer. The absorbance spectra were recorded every min till the pigments were decayed completely and the λmax at each min were plotted and fitted in an exponential curve.

$T_{1/2}$ *(min)*	**Red cone opsin**	**Green cone opsin**	**Blue cone opsin**
Thermal Stability[a]	10.25 ± 1.01	7.17 ± 0.98	26.53 ± 2.24
Chemical Stability[b]	42.53 ± 2.68	38.65 ± 4.03	4.71 ± 0.89

Table 4.1. ***Stability of cone opsins.*** The estimated half-life times for the thermal and chemical stabilities of purified red, green, and blue cone opsins in DM measured in min, at 37ºC[a] and 50 μM hydroxylamine[b] respectively.

4.1.4. Functionality of purified recombinant cone opsins

The functionality of the purified cone pigments is tested by monitoring their ability to bind tranducin upon illumination. Activation of transducin by the cone pigments can be measured by means of a GTPγS^{35} binding assay. In a mixture containing transducin and GTPγS^{35}, 300 nM visual pigments were added, incubated and the amount of GTPγS^{35} bound to tranducin interacting with the photoactivated visual pigment could be determined by the radioactive binding assay.

After normalizing the activity data with regard to the basal activity of the pigments in the dark, the functionality of the photoactivated pigments is shown in fig. 4.7. The bound GTPγS^{35} was measured (see methods) in pmol as 0.73 ± 0.06 for red cone opsin, 0.8 ± 0.06 for green cone opsin, and 0.97 ± 0.41 for blue cone opsin, and the values are similar for the three cone opsins. In the case of rhodopsin, as the activity was 5.8 ± 0.16 pmol GTPγS^{35} bound which is 5 times higher than the average value for cone opsins. The activity of rhodopsin has been usually tested with a concentration of 10 nM (147). Here, 300 nM of rhodopsin has been used in order to compare the functionality of opsins at equal concentration, as the green and blue cone opsins do not show activity at this lower concentration although red cone opsin can show activity at 10 nM (148). It is also interesting to note that the transducin used for the experiment was isolated from bovine retina (that means from rod photoreceptor cells) and in addition the recombinant rhodopsin used

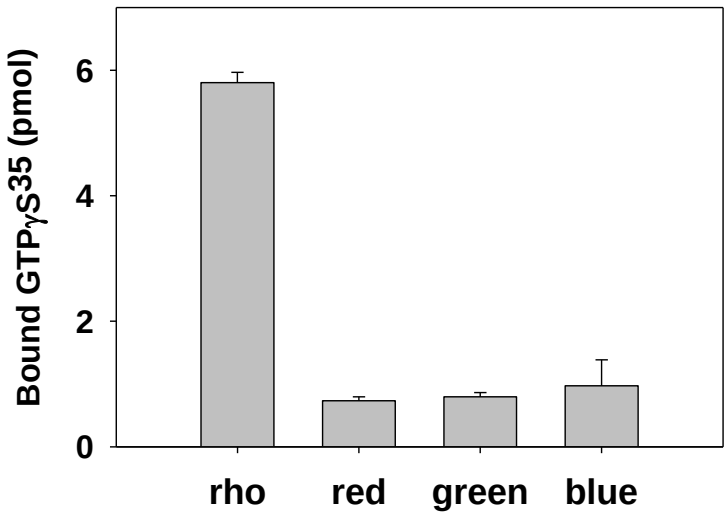

Figure 4.7. ***Transducin activation of cone opsins.*** 300 nM purified red, green, blue cone opsins and rhodopsin in DM were added with 500 nM transducin (purified from bovine retina), and GTPγS^{35} mix which was analyzed by a radioactive filter-binding assay. The basal dark activity was normalized to zero and the activity upon illumination was estimated by means of bound GTPγS^{35}.

in the assay was also from bovine origin. It has been known that rhodopsin shows greater transducin activation capacity than cone opsins due, in part, to the fact that the metaII intermediate, which is the active-state for transducin activation, of cone opsins is short-lived when compared to that of rhodopsin (27,149).

4.1.5. Surface plasmon resonance (SPR) spectroscopy of visual pigments

GPCR and G-protein interactions can be studied by immobilizing the receptor on a sensor chip and flowing the G-protein over the bound receptor. Binding of the G-protein onto the immobilized receptor would cause a change in refractive index that is measured as resonance units and reflects the specific protein-protein interaction which is the principle of SPR spectroscopy (150,151).

Rhodopsin in MES buffer, at different pH values, was immobilized and passed through the 1D4-coated SPR sensor chip, and the change of resonance units was compared (Fig 4.8A). This comparison shows that ΔRU was only around 100 at pH 6.0, whereas it was 1129 at pH 5.0. Therefore, the maximum binding of rhodopsin onto the 1D4-coated surface was obtained at pH 5.0. 0.585 μM transducin in MES pH 5.0 was passed through the rhodopsin immobilized surface which showed an increase in resonance units which denotes the dark binding of transducin to rhodopsin. Upon illumination there was no increase in the resonance observed and later washing with buffer removes the weak bound transducin showing the actual binding of around 5000 RU (Fig. 4.8B). Unlike the previous study which showed light induced binding of transducin with SPR immobilized rhodopsin (152), only the dark binding of transducin to rhodopsin was observed indicating that the experimental conditions destabilize the bound the rhodopsin which would activate the protein prior to illumination. Hence the buffer was changed to PBS for green cone opsin experiment in SPR

The same experiment was carried out for the first time with purified green cone opsin which showed a stable immobilization of ΔRU 4472 in PBS buffer pH 5.0 (Fig 4.9A). An increase in the resonance response was observed after transducin treatment of the opsin sample suggesting dark binding of transducin but no light induced binding was noticed upon illumination. Surprisingly, a slow dissociation of the bound transducin could be detected with a rate of 1.82 x 10^{-4} s^{-1} (Fig 4.9B) which is specific to the cone opsin and different from that of rhodopsin which was 4.7 x 10^{-4} s^{-1} (152). Such spontaneous dissociation without addition of GTP could be the reason behind the lower Gt activation ability observed with cone opsins (Fig. 4.7) when compared to rhodopsin.

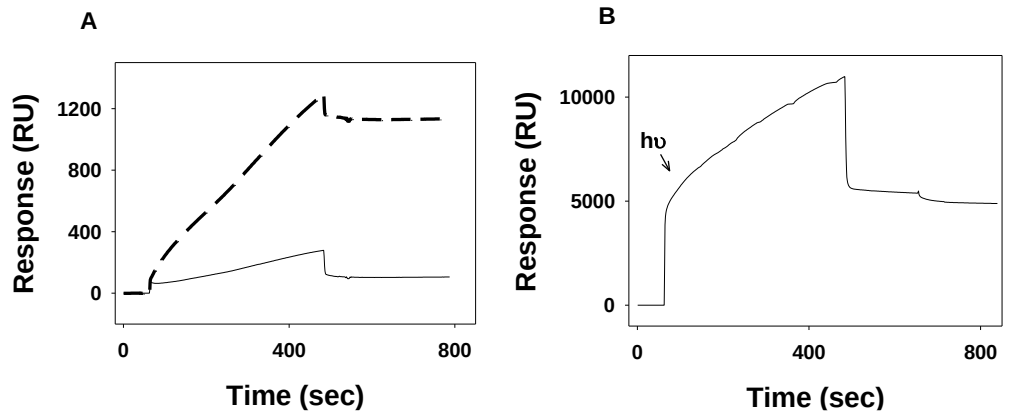

Figure 4.8. ***SPR of rhodopsin.*** **(A)** Immobilization of 1.25 μM purified rhodopsin in MES buffer containing 0.05% DM was carried out in pH 5.0 (dashed line) and pH 6.0 (solid line) on a 1D4 coated sensor chip of surface plasmon resonance spectroscopy and **(B)** Transducin, at a concentration of 1.25 μM, was passed through the rhodopsin bound surface and illuminated for 30 sec.

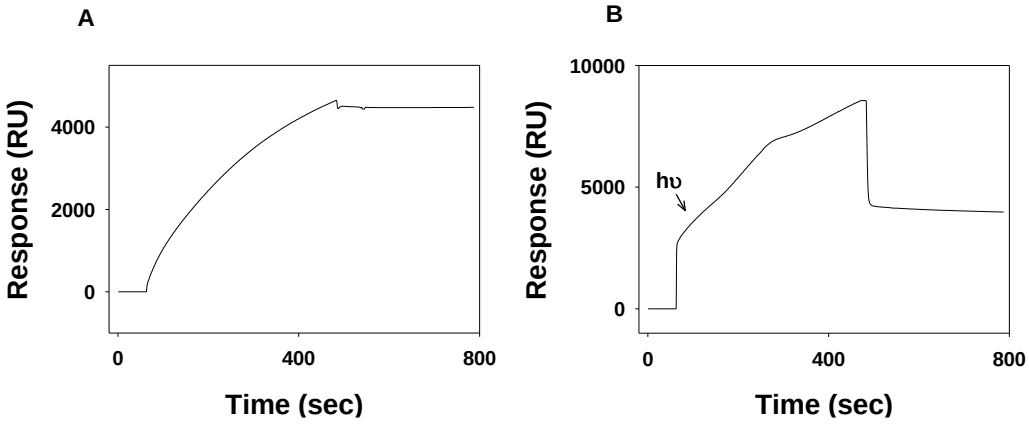

Figure 4.9. ***SPR of green cone opsin.*** **(A)** Immobilization of purified green cone opsin in MES buffer pH 5.0 containing 0.05% DM was carried out on a 1D4 coated sensor chip of surface plasmon resonance spectroscopy and **(B)** 1.25 μM Transducin was passed through the rhodopsin bound surface and illuminated for 30 sec.

.

4.2. Ligand binding specificity of photoactivated rhodopsin and red cone opsin

(The contents of this chapter have been published as

Srinivasan S, Ramon E, Cordomí A, Garriga P. Binding specificity of retinal analogs to photoactivated visual pigments suggest mechanism for fine-tuning GPCR-ligand interactions.Chemistry & Biology (2014) 21(3):369-378, PMID: 24560606, doi: 10.1016/j.chembiol.2014.01.006.)

Active state decay of visual photoreceptors has been extensively studied mainly for rhodopsin, and less for cone pigments. However, the receptor conformational properties at the post-bleaching phase are still unclear, particularly for cone opsin pigments. These properties can be used, for instance, to analyze in detail the structural and functional features of mutants associated with visual diseases, such as those associated with retinitis pigmentosa (RP) and congenital stationary night blindness (60,153-156). The effect of other factors such as lipids and salts on this decay has also been previously investigated (125,157). In this section, it was aimed at carrying out a detailed comparison of the regeneration differences of purified rhodopsin and red cone opsin, after photoactivation, with two retinal analogs.

4.2.1. Only 9CR can access the rhodopsin binding pocket at the post-Meta II phase

Upon illumination of purified rhodopsin, an increase in Trp fluorescence is observed due to the retinal release from its binding pocket (Fig. 4.2.1A) that closely parallels the MetaII decay process under the current experimental conditions. The fluorescence curve can be fit to a single exponential function with $t_{1/2}$ ~ 15 min in agreement with previously published data (125). Addition of 11CR, ~90 min after photobleaching (after complete decay of MetaII) did not decrease Trp fluorescence, indicating that 11CR is not able to enter opsin and reach the binding pocket (Fig. 4.10A). On the other hand, addition of 9CR resulted in a decrease of the fluorescence signal compatible with the presence of the exogenously added retinal in the binding pocket (Fig. 4.10B).

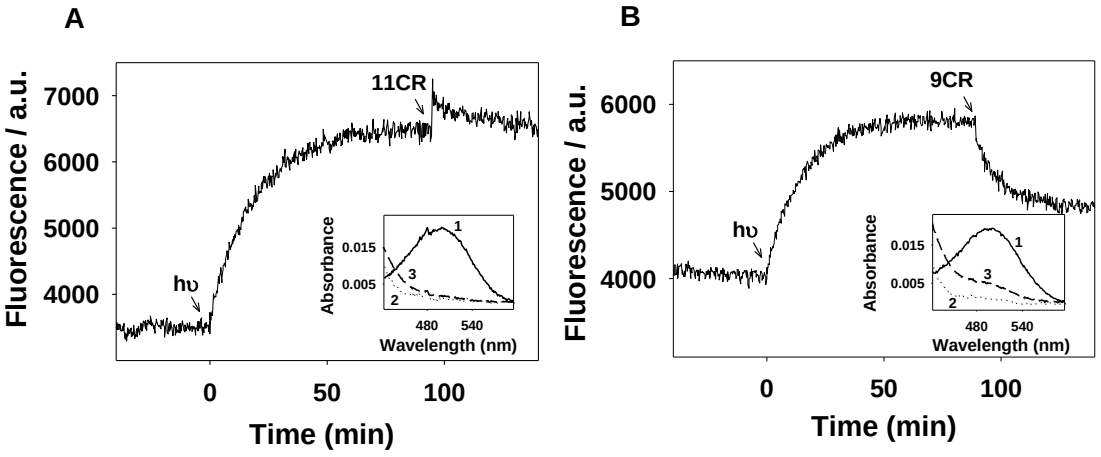

Figure 4.10. ***Regeneration of photoactivated rhodopsin with retinal analogs***. Purified recombinant rhodopsin added to the micro-cuvette was illuminated for 30 s (>495 nm) after the dark state spectra had stabilized. 2.5 fold of 11CR/9CR to the concentration of rhodopsin sample was added and mixed well **(A, B)**. Regeneration was also followed by UV-visible spectroscopy on the same fluorimetric samples (***inset*** A, B; 1; dark, 2; illuminated, 3; regenerated).

Parallel experiments, carried out using UV-visible spectroscopy, with identical experimental conditions to those of the MetaII decay fluorescence assay, showed the presence of the 500 nm band indicating regeneration of photobleached opsin. These spectra indicated no regeneration with 11CR (Fig. 4.10A, inset), whereas ~25% regeneration could be detected with 9CR (Fig. 4.10B, inset). These results are not only in agreement with the fluorescence measurements, but also prove that retinal binds covalently to opsin.

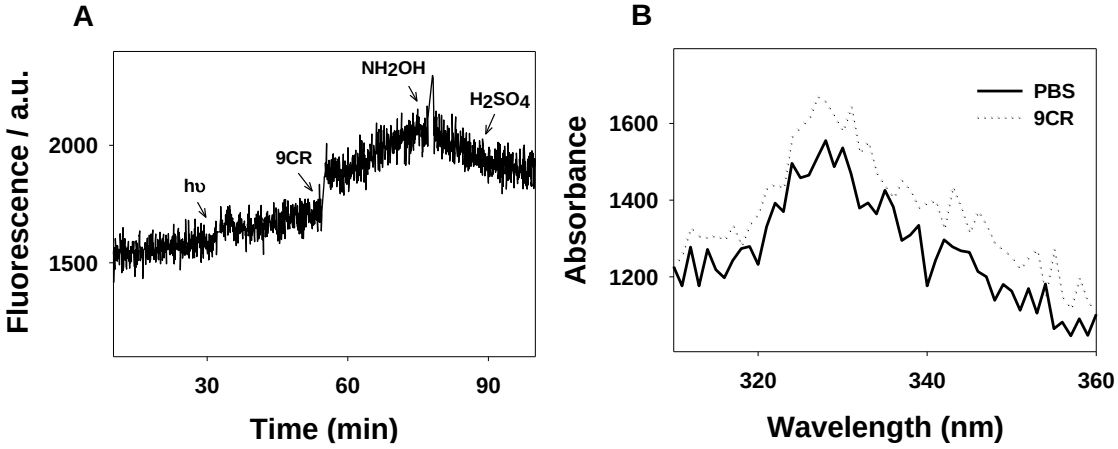

Figure 4.11. ***Intrinsic fluorescence of retinal does not interfere with the observed opsin fluorescence changes***. **(A)** PBS was initially measured and it was illuminated (hν), and 9-cis-retinal (9CR), hydroxylamine (NH_2OH), and sulfuric acid (H_2SO_4) were subsequently added. Fluorescence was continuously measured with the excitation at 295 nm and emission at 330 nm. **(B)** Fluorescence emission scan between 310 nm and 360 nm was measured for a PBS sample (—) and after addition of 9CR to the PBS buffer (•••).

Two control assays were carried out in order to discard that this behavior was due to intrinsic fluorescence properties of 9CR or other compounds present in the assay sample. First, the fluorescence of a sample of PBS buffer with 0.05% DM (elution buffer) was continually measured under different conditions: in the dark, upon photoactivation, addition of 9CR, addition of hydroxylamine, and addition of sulfuric acid, mimicking rhodopsin assays (Fig. 4.11A). The results show that there is no significant contribution of the buffer to the observed spectroscopic results and confirmed that there was no significant fluorescence change upon addition of retinal. Second, an emission scan from 310 nm to 360 nm was also performed to determine whether or not 9CR caused any contribution to the fluorescence observed in the experiments measured at 330 nm (Fig. 4.11B). The emission scan for 9CR in PBS buffer solution (excitation wavelength 295 nm) did not result in any significant increase in fluorescence. Additional controls such as adding 9CR or 11CR, immediately either after rhodopsin photobleaching or during the process of MetaII decay, are detailed below. In all cases this resulted in quenching of the fluorescence signal as expected and in agreement with previous reports (60), meaning that both retinals were able to bind the two visual receptors under these experimental conditions (Fig. 4.12).

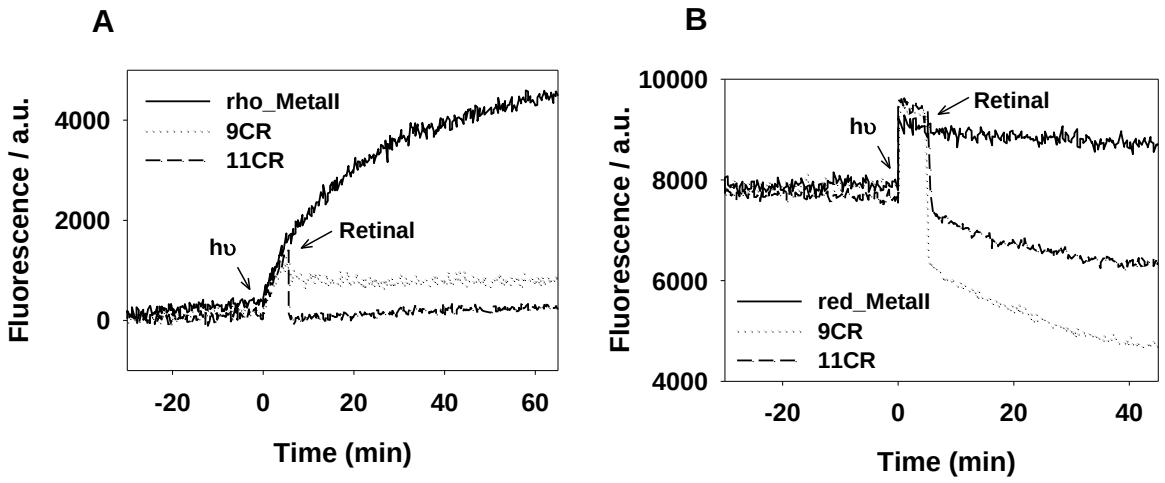

Figure 4.12. ***Effect of the addition of 11CR, or 9CR, to visual pigment shortly after photobleaching.*** Purified recombinant rhodopsin **(A)** and red cone opsin **(B)** were illuminated (λ>495 nm) for 30 s (hν) after a stable fluorescence baseline was obtained in the dark. Five minutes after illumination a 2.5 fold of 11CR, or 9CR, was added to the illuminated samples.

When 11CR is added immediately after photoactivation, i.e. while MetaII intermediate of rhodopsin has not decayed yet, similar results were observed to those previously published for 11CR (60) suggesting that rhodopsin is brought back to its native chromophore-regenerated state. In the case of red cone opsin, of which the $t_{1/2}$ of MetaII decay is in the ms time range (156), addition of retinal immediately after photoactivation led to a considerable decrease in Trp fluorescence suggesting the regeneration of red cone opsin with both retinals (Fig. 4.12). It is well established that rhodopsin visual pigment shows maximum regeneration when retinal is added immediately after photobleaching, and that the regeneration ability is gradually lost with time due to the formation of opsin conformations which impair retinal acceptance into the binding pocket (158).

An experiment was also performed in which 9CR was previously mixed with hydroxylamine before adding it to the photobleached rhodopsin sample. In this case, a fast decrease in fluorescence was observed, (Fig. 4.13A) suggesting that 9CR could enter the binding pocket without formation of a Schiff base linkage (which would not be possible with the retinaloxime formed with hydroxylamine). Different kinetics could be observed when only 9CR (and no hydroxylamine) was added to the sample (Fig. 4.13B).

In order to track the loss of 11CR regeneration ability for rhodopsin after photoactivation, the regeneration experiment was carried out at different time points after photobleaching (0 min, 30 min, and 60 min). The spectroscopic analysis showed a minimal regeneration at 30 min after photoactivation which was virtually abolished at 60 min. Hence the loss of 11CR regeneration was gradual, but in the case of 9CR, a significant regeneration level could be detected throughout this time period (Fig. 4.14). These data suggest that opsin stability plays a role -in addition to -

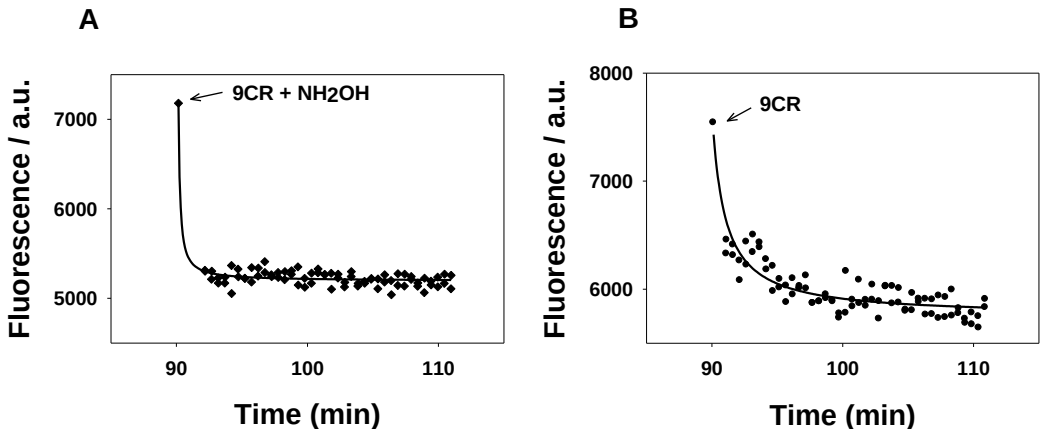

Figure 4.13. ***Binding kinetics of 9CR to photobleached rhodopsin.*** **(A)** 9CR (0.4μM) was previously mixed with 50 mM hydroxylamine to form retinaloxime and added to photobleached rhodopsin similar to Fig4.10B and the measured fluorescence was fit with an exponential curve. Note the faster decay compared to (A) which may indicate fast entering of the retinal into the opsin binding pocket. **(B)** The fluorescence decrease observed in Fig 4.10B, after 9CR addition to the photobleached rhodopsin sample, was fit to a single exponential function.

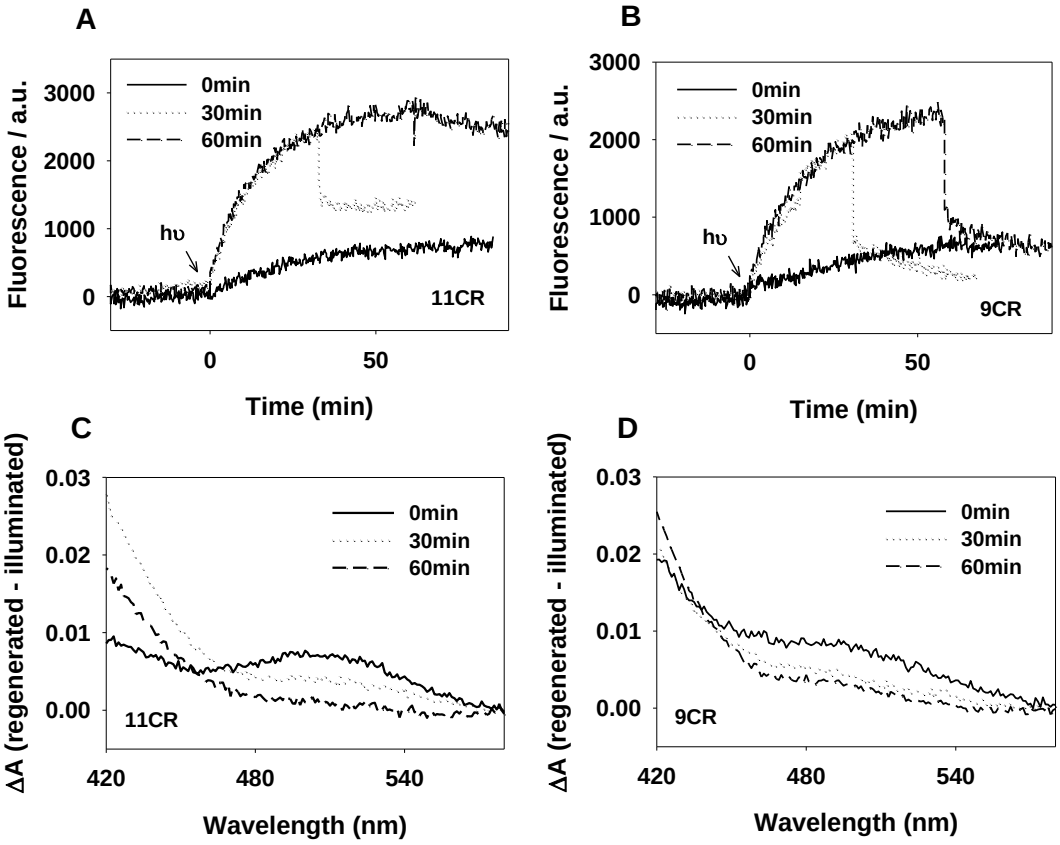

Figure 4.14. ***Timeline of rhodopsin regeneration.*** Purified recombinant rhodopsin added to the micro-cuvette was illuminated for 30 s (>495 nm) after the dark state spectra had stabilized. In a series of experiements, 2.5 fold of 11CR **(A)** or 9CR **(B)** with regard to the concentration of rhodopsin was added and mixed well at 0 min, 30 min and 60 min. The regeneration process was also followed by UV-visible spectroscopy on the same fluorimetric samples **(C, D)**.

retinal accessibility to the retinal binding pocket- in the observed pigment behavior.

4.2.2. 11CR and 9CR can access red cone opsin binding pocket at the post-MetaII phase

Upon illumination of the red cone opsin sample, a sudden fluorescence increase is detected (Fig. 4.15), compatible with a faster retinal release in cone pigments when compared to rhodopsin (155). Once the complete retinal release was observed (Trp fluorescence reached a plateau), the addition of either 11CR or 9CR resulted in a decrease in intensity suggesting that the two analogs could occupy the red cone binding pocket (Fig. 4.15). As in the case of rhodopsin, UV-visible spectroscopy was performed in order to monitor purified red cone pigment regeneration after photoactivation. The spectra showed a typical absorbance band with a maximum wavelength at 560 nm indicating red cone chromophore formation. Up to a ~60% of regeneration was observed with photoactivated red cone opsin with both retinals (Fig 4.15, insets). The post-bleaching regeneration shows a two phase kinetics which includes a sudden drop in fluorescence suggesting the fast entry of retinal into the binding pocket, and a slower decaying component suggesting the actual binding of retinal to the active site of the pigment. The fact that the fluorescence signal decreases to a level below that of the original pigment baseline may be due to the presence of non-regenerated opsin resulting from the immunopurification process. In this case, the retinal can also enter this non-regenerated opsin. Alternatively, this large decrease can also be partly due to the quenching of other Trp residues in addition to W281 in the retinal binding pocket. In the case of the 9CR, this isomer may be a better quencher because of the position it adopts in the binding pocket and its increased interaction with Trp residues.

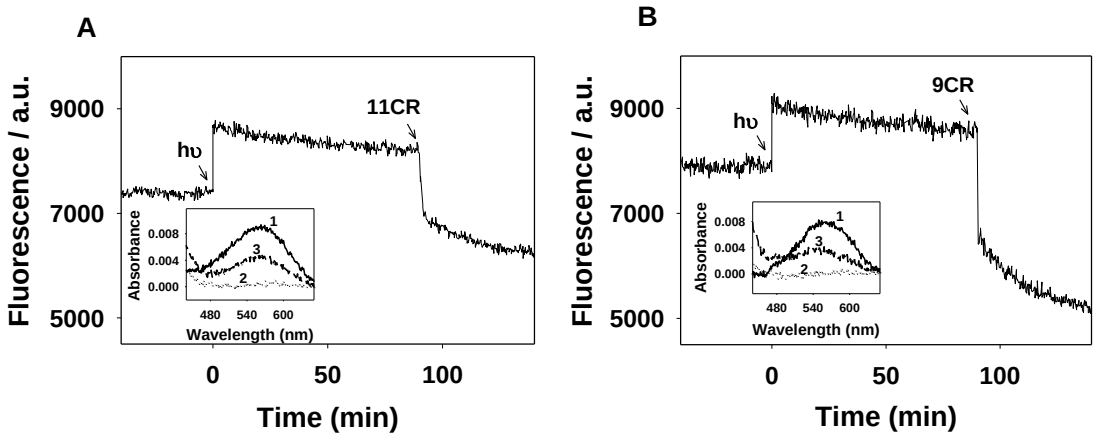

Figure 4.15. ***Regeneration of photoactivated red cone opsin with retinal analogs.*** Analogous to rhodopsin regeneration experiments, red cone opsin was illuminated (>495 nm) after a stable dark-state spectrum was obtained, followed by 11CR/9CR addition **(A, B)**. UV-visible spectroscopy of red cone opsin was also measured as in the rhodopsin case (***inset*** A, B; 1; dark, 2; illuminated, 3; regenerated).

In order to understand how retinal regeneration occurs at a molecular level it is important to understand the structural changes associated with the transition from the inactive to the active states and *vice versa*. In rhodopsin, K296$^{7.43}$ and W265$^{6.48}$ represent important residues of the retinal binding pocket. The aldehyde group of retinal covalently binds to K296$^{7.43}$, whereas W265$^{6.48}$ remains proximal to the β-ionone ring of retinal (90). Comparison of the extracellular region in the dark-state (11CR-bound) and active rhodopsin structures (159,160) reveals structural differences between them.

Two homology models for the red cone opsin were constructed based on the crystal structures of dark-state rhodopsin and opsin soaked with ATR. 11CR and 9CR retinals were docked to the opsin forms of rhodopsin and red cone opsin (148). There is no structure of bovine rhodopsin available with 9CR. However, squid rhodopsin has been crystallized with both 11CR and 9CR revealing only one minor differences between them: a shift in the localization of the C10 and C11 atoms by ~1 Å. (161,162). Accordingly, it was assumed in that study that the same mimicry should apply to rhodopsin and to the red cone opsin.

Fig. 4.16A-B represent an initial state of 11CR or 9CR rhodopsin and red cone opsin regeneration prior covalent binding to K296/312$^{7.43}$. Similar binding scenarios, for both retinals in both rhodopsin and red cone opsin, can be observed. According to the molecular model, a remarkable difference between the two photoreceptor proteins is the presence of W183$^{4.56}$ in red cone opsin (corresponding to C167$^{4.56}$ in rhodopsin), which may contribute to the stabilization of the retinal-opsin complexes (163). Therefore, W183 can help preserving the native conformation of the opsin binding pocket -in the absence of retinal- and facilitate increased accessibility of the retinal to red cone opsin binding pocket by favoring retinal-protein interactions. This specific Trp residue may prevent the red cone opsin binding pocket from becoming unstructured, and it can also contribute to the large drop in fluorescence caused by 9CR addition in the fluorimetric experiments. The main difference between the two retinals is that the 9-cis isomer makes more favorable contacts with W265/281$^{6.49}$ and Y268/284$^{6.51}$ than the 11-*cis* isomer in the two receptors in the region in the vicinity of the C13 methyl group. Thus, it is likely that 9CR benefits from higher stabilization energy than 11CR in the two photoreceptors (148). The modeling results show only remarkable changes in TMs 3, 6 and 7. In specific, a decrease from 8.5 Å to 6.5 Å in the distance between TM5 and TM6 (measured as the distance between the α-carbons of F208$^{5.43}$ and A269$^{6.52}$) is observed. In turn, TM7 becomes closer to TM6 (from 5.5 Å to 4.9 Å, measured between the α-carbons of P267$^{6.50}$ and P291$^{7.51}$. On the other side, the distance between TM3 increases (from 10.7 Å to 13.4 Å, measured between E113$^{3.28}$ and K296$^{7.43}$). Thus, without the inverse agonist 11CR, TM6 packs more tightly with TM5. Since TM7 moves closer to TM6, the distance to TM3 increases. A major consequence of these changes is that the main counter-charge of K296$^{7.43}$ changes between the dark and the active forms from E113$^{3.28}$ to E181$^{C\text{-}6}$. Table 4.1 shows a comparison between residues forming the retinal binding sites in rhodopsin and red cone photo-

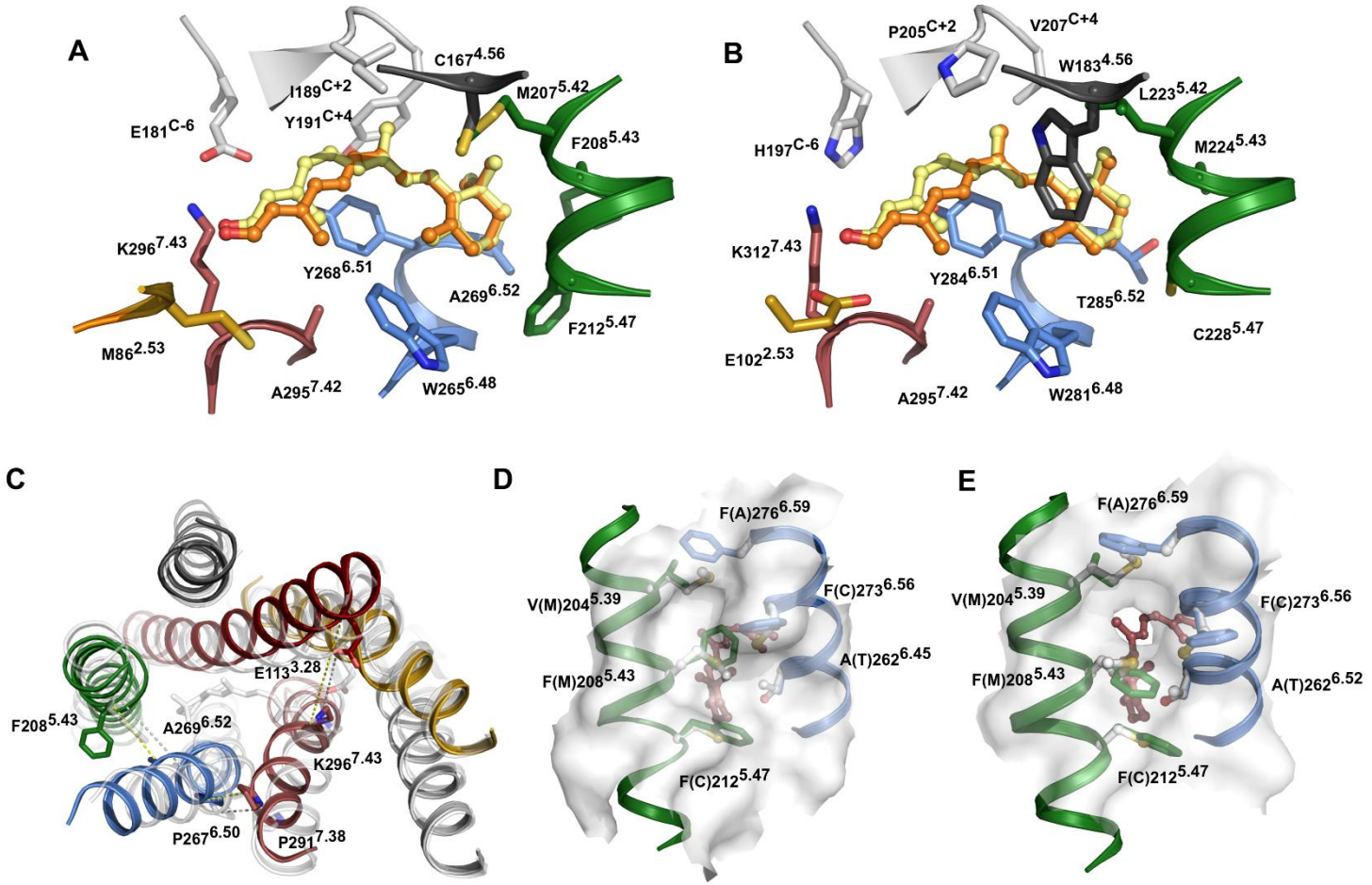

Figure 4.16. ***Molecular models of rhodopsin and red cone opsin.*** **(A, B)** Molecular complexes for 11-*cis* (pale-yellow) and 9-*cis* (orange) retinal bound to rod (A) and red cone (B) opsins. **(C)** Comparison between helical arrangements in dark-state rhodopsin (PDB id: 1GZM, shown as white transparent cartoon) (2) and opsin soaked with ATR (PDB id: 2X72, shown as colored cartoons) (3). The color-code for opsin helices is TM1: light-gray, TM2: gold, TM3: red, TM4: dark-gray, TM5: green, TM6: blue and TM7: pale-red. Dashed lines display the distances between the shown amino acids (see Text; dark-state rhodopsin: white, active opsin: yellow). D, E) The entrance site for retinals in the dark (D) and opsin (E) states. Rod opsin residues are shown in colors, whereas residues in red opsin are shown in white.

-receptors. Despite the fact that they share the same endogenous ligand, only a third of the residues are conserved between rhodopsin and the red cone opsin. Crystal structures reveal also the existence of different networks of interactions close to the retinal. This suggests specific recognition mechanisms at the molecular level. Retinal has been proposed to enter the opsin binding pocket between either TM1 and TM7 (called opening A) or TM5 and TM6 (called opening B). This opening B region is flanked by V204$^{5.39}$, F208$^{5.43}$, F212$^{5.47}$, A269$^{6.52}$, F273$^{6.56}$ and F276$^{6.59}$ (49,53). In the dark state these residues constitute a zipper between the two helices that keeps the access to the protein interior closed. A similar zipper is observed in the molecular model of the red cone opsin, though stabilized mainly by Met/Cys-Met/Cys interactions instead of aromatic-aromatic and aromatic-aliphatic interactions. These sulfur-containing residue interactions, which are of the same magnitude an even higher than aromatic-aromatic interactions can act as molecular gears in GPCRs (164). In the activated rhodopsin, F208$^{5.43}$ exhibits a conformational change that, together with the translation of TM5, opens a cavity within the zipper and allows the retinal into the retinal binding site (Fig 4.16D, E). The molecular model shows clearly that this cavity is conserved in red cone opsin, except that the opening of the zipper would be controlled by M214$^{5.43}$ instead of F208$^{5.43}$ (Fig. 4.16E). In addition, substitution of four Phe residues by residues with smaller volume (Met, Cys and Ala) may facilitate the entrance of retinal. The molecular models of opsin forms in complex with 11CR and 9CR, without formation of the Schiff base with K296$^{7.43}$, suggest that 9CR benefits from stronger interactions with W265$^{6.49}$ and Y268$^{6.51}$ than 11CR. In the red cone opsin, in addition to Y281$^{6.49}$ and W284$^{6.51}$ positions, W183$^{4.56}$ also contributes to maximal higher stabilization energy towards both retinals. The opening of TM6 after photoactivation shows that W265$^{6.49}$ presumably favors binding of 9CR which has shorter C9 to β-ionone ring length than 11CR. This would favor the 9-*cis* isomer to enter the retinal binding site. The previous finding that 9-demethyl retinal could inhibit the formation of active MetaII conformation of rhodopsin (165), but not of red cone opsin (166), suggests that the retinal binding site of red cone opsin is more accessible and more versatile than that of rhodopsin. The specific interaction of residues W265 and Y268 may contribute to enhance 9CR quenching observed in the fluorescence spectroscopic measurements. This is compatible with the present results of retinal regeneration long time after photobleaching. More versatile the ligand binding site, less constriction within the retinal entry and exit channels, hence either of retinal analogs, added exogenously after photoactivation, may be accommodated into the retinal binding site as observed in our fluorimetric measurements.

4.2.3. Accessibility of retinal binding sites of rhodopsin and red cone opsin by retinal analogs

In order to prove the hypothesis of different accessibility of the two retinal analogs to the binding pocket, 11CR or 9CR were added to rhodopsin and red cone pigment, prior to illumination and

the fluorescence intensity was monitored (Fig 4.17). No significant change in rhodopsin fluorescence in the dark upon addition of 11CR was detected, whereas only a minimal increase could be detected after illumination (with light >495 nm) (Fig 4.17A). This increase is much smaller than the typical MetaII decay curve (see Fig 4.10A) and may be due to the presence of excess amount of 11CR around MetaII that may replenish the activated pigment with ligand as previously reported (60). Addition of hydroxylamine resulted in a slight increase in the fluorescence signal. However, in the case of 9CR added to rhodopsin in the dark, an appreciable decrease in fluorescence intensity could be detected (Fig. 4.10B). Illumination only slightly altered the Trp fluorescence, though to a much smaller extent as compared to 11CR. Addition of hydroxylamine somehow increased the retinal release from the rhodopsin binding pocket (Fig. 4.10B).

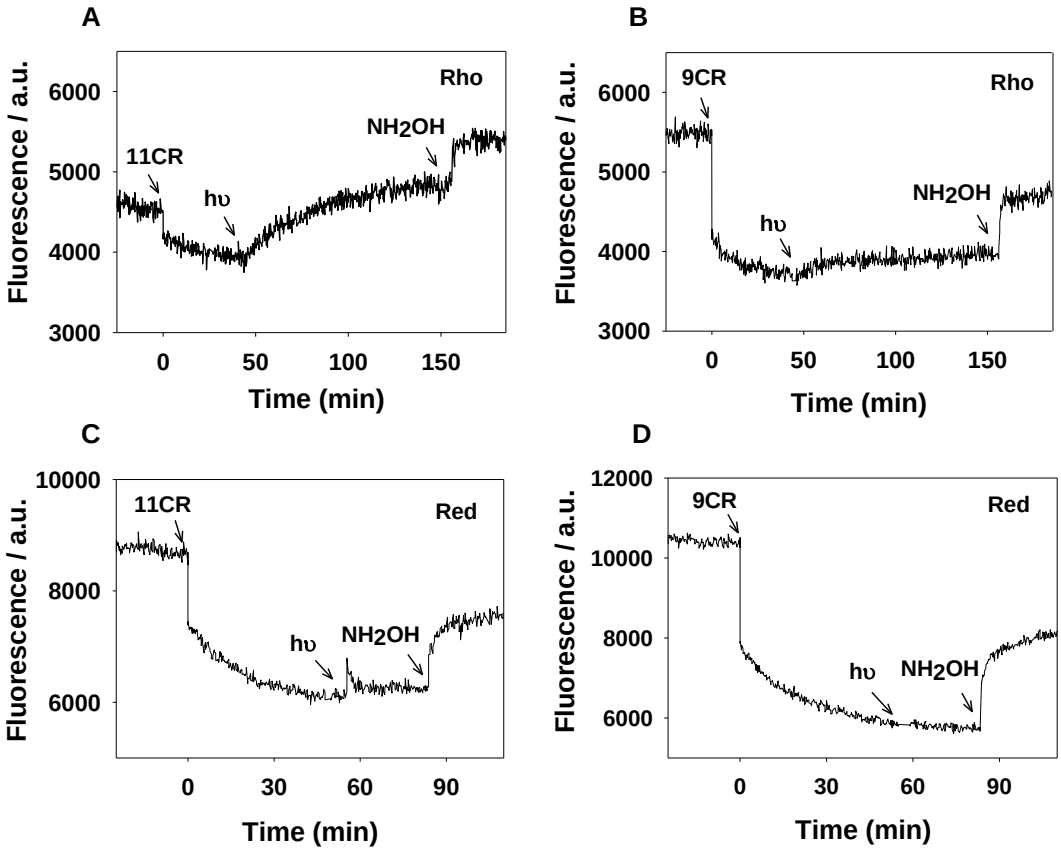

Figure 4.17. ***Difference in accessibility of retinal binding sites of rhodopsin and red cone opsin with retinal analogs.*** 11CR and 9CR (2.5 fold than rhodopsin concentration) were added to purified rhodopsin, followed by illumination (>495 nm), and 50mM hydroxylamine addition in the same sample when the stable spectra was obtained after each treatment **(A, B)**. Same experiment was carried out with purified red cone opsin **(C, D)**.

In the case of red cone pigment, the addition of either 11CR or 9CR caused a decrease in the fluorescence intensity indicating entry of both retinals into the binding pocket of free opsin. Upon

illumination, the fluorescence intensity was not affected, and subsequent treatment with hydroxylamine resulted in a saturation curve with $t_{1/2}$ of ~3 min that would reflect the formation of retinaloxime which would be released from the red cone pigment.

Strikingly, the decrease in fluorescence was observed with either retinal, and subsequent illumination did not alter the fluorescence intensity. UV-visible spectra of the dark state purified visual pigments indicate that, along with the peak of regenerated pigment in the visible region, the characteristic protein peak at 280 nm can also be detected which may account for the presence of both regenerated opsin and free opsin. At least a fraction of this opsin can be non-misfolded opsin as has already been previously reported (138,167). The A_{280}/A_{560} ratio of red cone opsin, from the UV-visible spectrum, indicates the presence of non-regenerated opsin in the eluted purified sample. The decrease in fluorescence observed in both red cone opsin and rhodopsin, in the dark before photoactivation, could be due to the presence of free opsin that can accept the exogenously added free retinal during the fluorimetric experiments. The lack of a classical photo-response upon illumination (Fig. 4.17) can be explained by the presence of excess free retinal in the sample. Interestingly, a saturation curve is obtained upon hydroxylamine addition which may reflect additional retinal release from the binding pocket. The $t_{1/2}$ of this process is ~3 min and this parameter can be used to assess the regeneration properties of red cone opsin mutants (associated with visual disorders). The observation of similar features in the case of rhodopsin with the addition of 9CR -except the fact of faster formation of retinaloxime-, and the lack of effect with 11CR conclusively supports the hypothesis that the binding pocket of free opsin from rhodopsin can be accessible by 9CR but not by 11CR under our experimental conditions. A recent study on the thermal properties of rhodopsin reports that exogenous addition of 11CR 10 min after photoactivation shows a decrease in Trp fluorescence intensity which is 20% of the total fluorescence increase observed after photobleaching. However, the conditions used in this study are different from those in the present study, namely that they used a 1:1 retinal:opsin ratio, a temperature of 55°C and a shorter post-bleaching time (142).

4.2.4. Improvement of rhodopsin regeneration with 9CR using low salt buffer

In order to determine the possible effect of buffer conditions on rhodopsin regeneration, recombinant rhodopsin was purified in sodium phosphate (NaPi) buffer (see Methods) and photoactivated in the spectrofluorimetric cuvette. The fluorescence increase was measured until it reached a plateau indicating complete MetaII decay and after addition of 2.5 fold concentration of 9CR (over rhodopsin). An immediate decrease in fluorescence intensity was detected after the addition of 9CR, suggesting a faster regeneration of photoactivated rhodopsin (Fig. 4.18). A parallel sample monitored by UV-visible spectrophotometry showed a regeneration which was

quantitatively larger (~70%) than the case of the experiment performed with rhodopsin purified with PBS elution buffer (Figure 4.18A, inset; compare to inset in Figure 4.10A).

The results indicate that photoactivated rhodopsin in NaPi buffer shows improved post-bleaching regeneration with 9CR. An interesting aspect was to find out whether oligomerization could alter retinal binding to the receptors. To this aim the receptors were purified using two different buffers, PBS or NaPi buffers, which may affect the regeneration abilities of the receptors. Blue native polyacrylamide gel electrophoresis (BN-PAGE) was carried out with equal concentration of rhodopsin expressed in HEK-293S-GnTi$^-$ cells. Rhodopsin purified using NaPi buffer clearly show the predominant presence of oligomeric forms (dimer and less intense trimer bands; Fig. 4.18B).

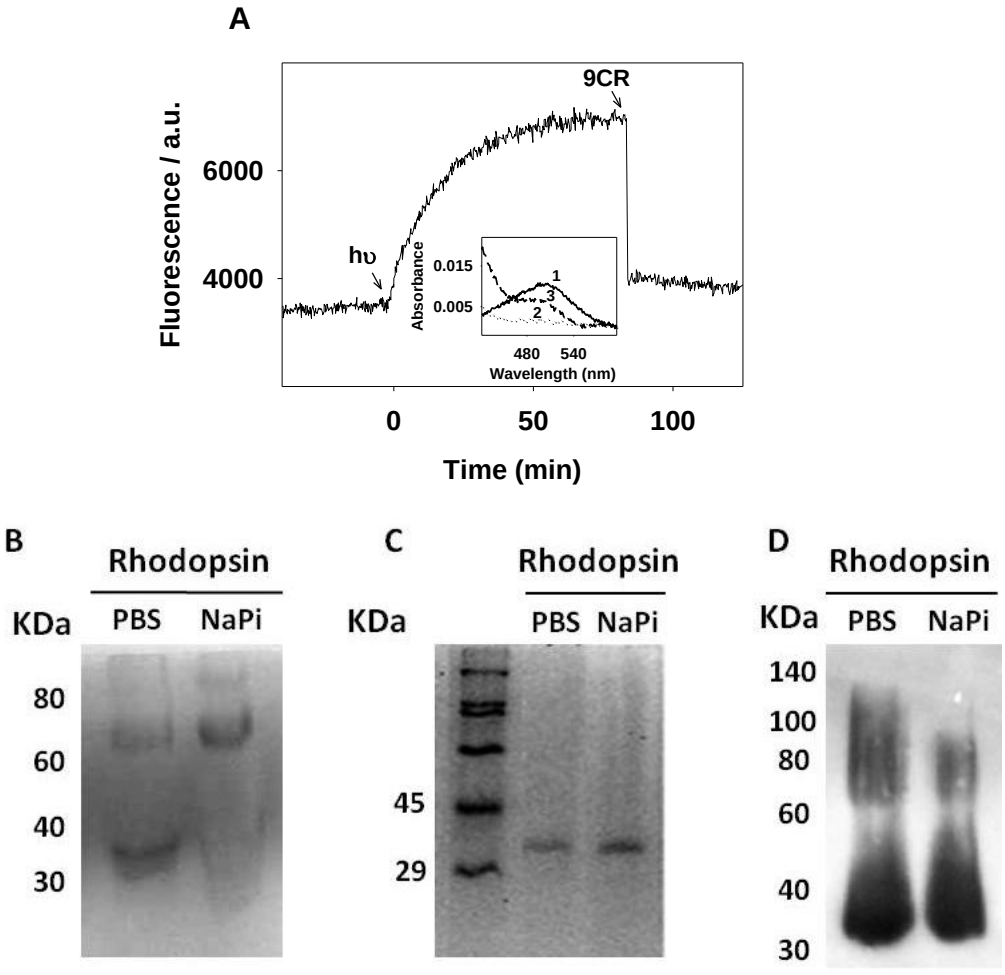

Figure 4.18. ***Phosphate buffer (low salt conditions) improves 9CR regeneration of photoactivated rhodopsin.*** **(A)**Purified recombinant rhodopsin in 2 mM NaPi buffer (containing 0.05% DM) was illuminated (>495 nm) after the dark state spectra had stabilized. Then 2.5 fold of 9CR to the concentration of rhodopsin was added and mixed thoroughly. The experiment was also followed by UV-visible spectroscopy (***inset*** A; 1; dark, 2; illuminated, 3; regenerated). **(B, C)** Blue Native PAGE and SDS-PAGE was performed with rhodopsin purified PBS and in NaPi which was expressed in HEK293S-GnTi$^-$ cells. **(D)** The Western blot was carried out with rhodopsin, expressed in COS-1 cells and purified in PBS, in NaPi.

In contrast, rhodopsin purified using PBS buffer shows the presence of a strong monomeric band and a much less intense dimer band (Fig. 4.18B). SDS-PAGE was also carried out with rhodopsin expressed in HEK-293S-GnTi$^-$ cells and purified using PBS or NaPi. The results show that rhodopsin appears as a single monomeric band in both cases with no indication of oligomeric behavior due to the denaturing conditions of the gel (Figure 4.18C). The red cone pigment failed to show regeneration in NaPi, and this lack of regeneration, in the low ionic strength buffer, could be related to the requirement of chloride ions which are known to have a specific binding site in cone opsins (168). The Western blot of rhodopsin in both buffers, subsequent to a denaturing SDS-PAGE gel, resulted in a similar smeary pattern probably due to the glycosylation behavior of COS-1 cells (Fig. 4.18D).

In order to understand the nature of the improved regeneration of photoactivated rhodopsin in NaPi buffer, BN-PAGE was performed to identify the presence of rhodopsin oligomers in different buffers (169). High molecular weight bands, corresponding to oligomeric forms of rhodopsin, appear to be more intense in NaPi buffer (Fig. 4.18B). These oligomeric forms of rhodopsin may provide a better environment for post-bleaching regeneration of rhodopsin due to increased stability provided by dimeric opsin units. The differences in oligomerization may account for the different kinetics observed for rhodopsin regeneration in PBS and NaPi buffers. Recent studies have highlighted the influence of rhodopsin dimers on its capacity for regeneration with either 11CR or 9CR (83) and on the asymmetry of the rhodopsin dimer complex with transducin (84). Attempts to purify red cone opsin using NaPi buffer resulted in destabilized protein and no regeneration could be obtained. Thus, regenerated red cone opsin could only be obtained in PBS buffer consistent with the fact that a chloride ion in its binding site is crucial for the optimal conformation of cone pigments (168).

Overall, the observed different regeneration ability of rhodopsin and red cone opsin, with 9CR and 11CR, may be due to a combination of both stability and accessibility effects. These two effects may act in concert and may help explain the differences observed for the two visual pigments. In the case of samples in PBS buffer, the opsin protein would show lower stability - being predominantly monomeric- and this would alter the conformation of the retinal binding pocket thus affecting the accessibility of retinal to the pocket. In contrast, in NaPi buffer the presence of dimers would help stabilize opsin and this would better preserve the correct retinal binding conformation allowing a faster and better accessibility of retinal to the interior of the protein. Therefore, increased stability of the opsin retinal binding pocket structure would result in a better accessibility of the retinal and would facilitate its entrance to the pocket and chemical binding to the pigment.

An analogous experiment was performed with 11CR and the chromophore regeneration could be detected in NaPi buffer (Fig 4.19). This finding stresses the importance of the buffer (and the

corresponding monomeric or dimeric status of the pigment) on the chromophore regeneration of the pigment.

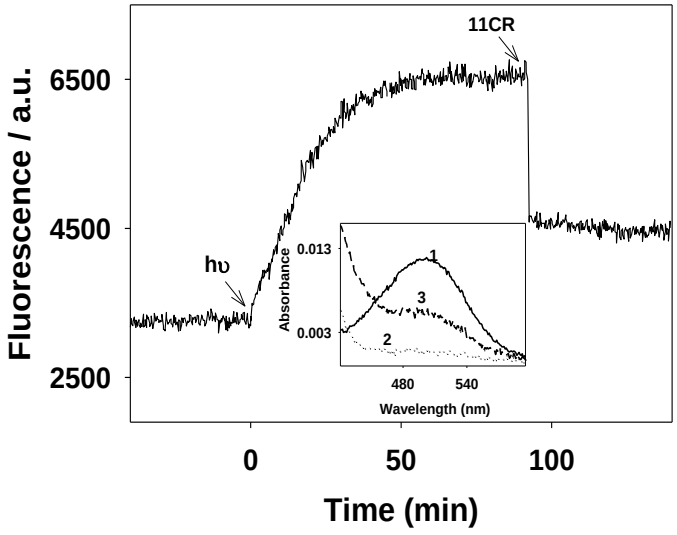

Figure 4.19. ***Photoactivated rhodopsin purified in NaPi shows regeneration with 11CR.*** Purified recombinant rhodopsin in 2 mM NaPi buffer (containing 0.05% DM) was illuminated (>495 nm) after the dark state signal had stabilized. Then, 2.5 fold of 11CR to the concentration of rhodopsin was added and mixed thoroughly. The experiment was also followed by UV-visible spectroscopy (inset: 1; dark, 2; illuminated, 3; regenerated).

4.2.5. Transducin activation of 9CR-regenerated rhodopsin and red cone opsin

To study the ability of regenerated pigments to activate transducin, purified visual pigments were tested in the dark, upon illumination, and after addition of 9CR under experimental conditions similar to those of the fluorimetric experiment (Fig. 4.20). To do this, different sample aliquots were taken from the cuvette during the fluorimeter measurements, added to the transducin mix immediately and the activation was measured by means of a radioactive GTPγS^{35} binding assay. In the case of rhodopsin, an increase in transducin activation immediately after photoactivation was observed, which decreases over time. However, the fact that upon subsequent addition of 9CR the functional activity of rhodopsin decreased may indicate regeneration of photoactivated rhodopsin with the added 9CR and formation of a dark-state pigment. Further illumination with white light of this regenerated pigment resulted in functional activation suggesting the formation of a small amount of functionally active regenerated rhodopsin from the whole sample (Fig. 4.20A, C). Importantly, the results show that photoactivated rhodopsin regenerated with 9CR is functionally active.

On the other side, transducin activation of red cone opsin samples taken along the fluorescence experiment was determined as mentioned above for rhodopsin. Unlike rhodopsin, red cone opsin

exhibited gradual transducin activation over time after illumination and a slower ability to activate transducin upon addition of 9CR (Fig. 4.20B, C).

On the functional side, rhodopsin appears to activate rod transducin more effectively than red cone opsin. This result is in line with a recent study where transducin activation by cone pigment is slowed immediately after photoactivation in contrast to the rhodopsin behavior (149). We also found that the photobleached regenerated rhodopsin retains more Gt activating capacity than red cone opsin.

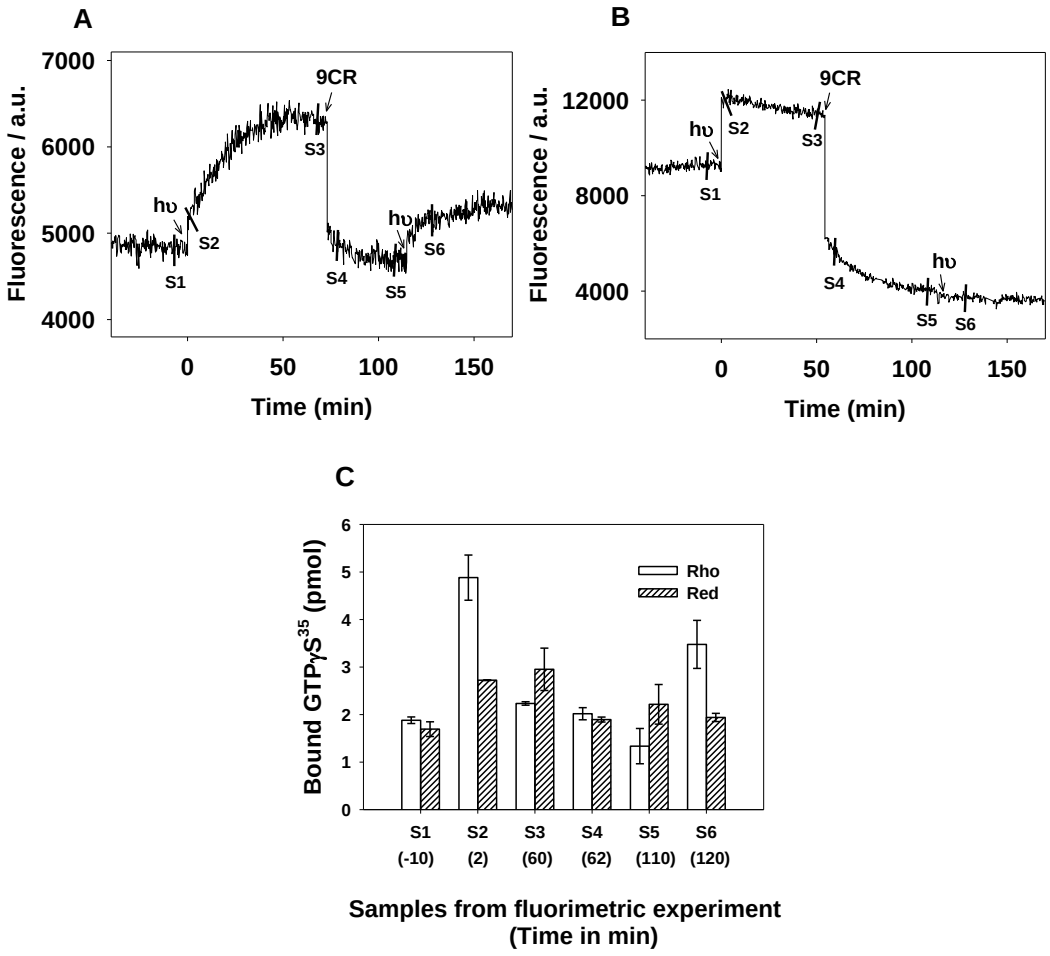

Figure 4.20. ***Transducin activation of 9CR regenerated visual pigments***. Rhodopsin **(A)** and red cone opsin **(B)** were monitored by means of fluorescence spectroscopy, and samples were treated by illumination (λ>495 nm), 9CR addition and a second illumination using white light. Rhodopsin and red cone opsin samples, taken at different time points from the experiments reported in panels A and B, and denoted as S1 – S6 (with the corresponding time in min) were analyzed for transducin activation **(C)**.

4.3. Beyond spectral tuning: functionally-relevant molecular differences between cone opsins

(The contents of this chapter have been published as
Srinivasan S, Cordomí A, Ramon E, Garriga P. Beyond spectral tuning: human cone visual pigments adopt different transient conformations for chromophore regeneration. Cellular and Molecular Life Sciences (2015) (accepted)

Srinivasan S, Ramon E, Garriga P. The photoactivated conformational change in blue cone opsin modulates the specificity of secondary retinal uptake. (to be submitted)

Specific amino acids at the retinal binding site, as well as their interactions with the retinal chromophore and surrounding water molecules, modulate spectral tuning of visual opsins (48,170,171). Cone opsin pigments have been much less characterized than the rod photoreceptor rhodopsin due to their lower availability and their higher conformational instability. With only 4% variance between red and green cone opsin sequences, these are believed to have analogous structure-function relationships, other than the well-established wavelength absorption modulation in the visible region of the spectrum. In this section, the regeneration behavior and kinetics of photoactivated green cone opsin and red cone opsin have been compared. Blue cone opsin has been studied separately because the typical regenerated absorbance is blue shifted to a position close to the free retinal absorbance.

4.3.1. Comparison of red and green cone opsin regeneration mechanism

4.3.1.1. Photoactivated green cone opsin regenerates with an unprotonated SB linkage with 11CR.

The dark state UV-vis spectrum of purified green cone opsin showed two typical characteristic absorbance bands with absorption maxima at 530 nm and 280 nm respectively (Figure 4.21A, continuous line). The amplitude of the band at 530 nm corresponds to the bound 11CR chromophore and reflects the amount of regenerated green cone pigment present, and the band at 280 nm corresponds to total opsin pigment. The regeneration experiment was done in the spectrophotometer cuvette by adding, in the dark, an aliquot of a concentrated stock sample of 11CR that corresponds to a 2.5- fold molar concentration with regard to opsin. This resulted in a spectrum which showed, in addition to the two dark absorbance bands in the visible and in the UV regions, another band at 380 nm corresponding to the added free 11CR (Fig. 4.21A, dashed line). Illumination of the sample was carried out by using a cut-off filter (λ>495 nm) which only bleaches the green cone opsin but not the added retinal, and the spectrum measured after 30 min showed an increase at 380 nm corresponding to photobleached opsin (Fig. 4.21A, dashed line). Illuminated sample, containing exogenously added 11CR, did not show any absorbance increase at 530 nm (Fig. 4.21A, dashed line) which suggests that the modified conformation of green cone opsin, immediately after photobleaching, is not the same as dark adapted green cone opsin and impairs 11CR binding. Conversely, a parallel experiment performed with 9CR, showed a visible region regenerated band around 495 nm with 85% maximal regeneration (Fig. 4.21B).

Photoactivated red cone opsin regenerates via a PSB with both 9CR / 11CR. An analogous regeneration experiment was carried out with purified red cone opsin, monitored using UV-vis spectrophotometry and extending the measuring range to 700 nm due to the fact that the typical absorption maximum of red cone opsin is 560 nm. In both experiments, 9CR and 11CR can bind opsin after illumination and regenerate the visible chromophore with PSB linkage indicated by

the presence of absorbance increase in the visible region above 440 nm. In particular, complete regeneration with 11CR was achieved as indicated by the re-appearance of the typical absorption maximum at 560 nm (Fig 4.21C) whereas ~70% regeneration with 9CR was recovered with an absorption maximum at ~520 nm (Fig 4.21D). The shifted absorption maximum of the protein is due to its different interaction with 9CR.

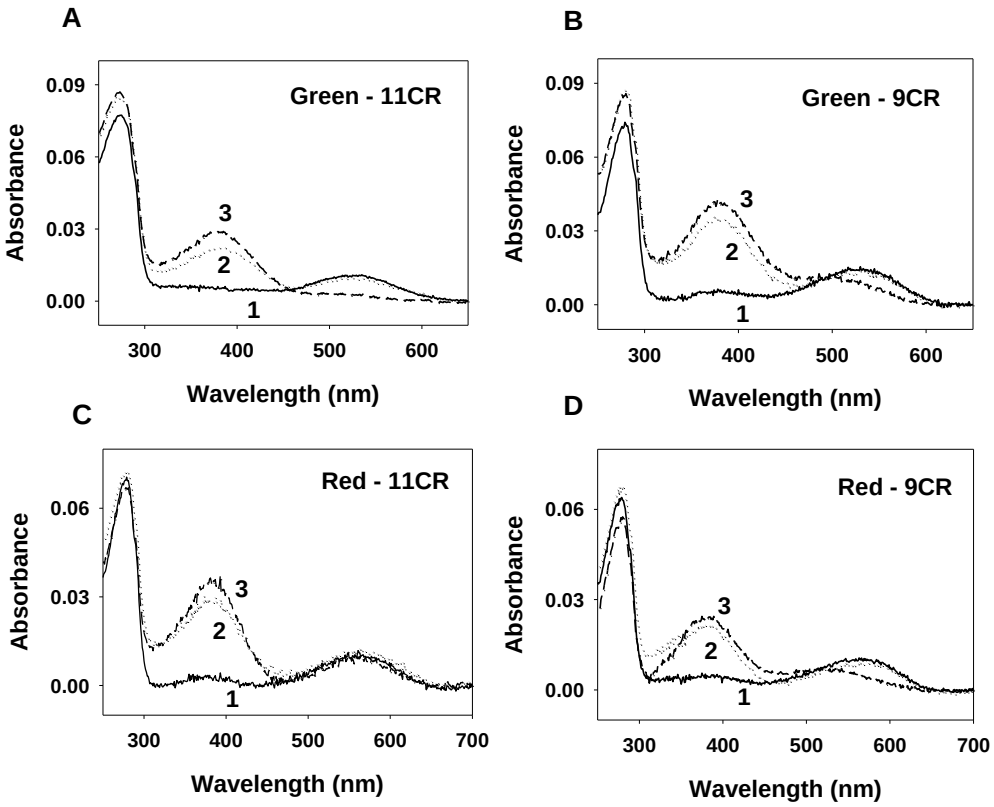

Figure 4.21. ***Regeneration of photoactivated green and red cone pigments with 11CR and 9CR.*** **(A, B)** Immunopurified human recombinant green cone opsin was analyzed by UV-visible spectrophotometry in the dark (1, solid line) and after addition of exogenous ligand, i.e. 2.5-fold of either 11CR (A) or 9CR (B) over opsin (2, dotted line). The pigment was then illuminated for 30 s (>495 nm) and a spectrum was recorded after 30 min (3, dashed line). **(C, D)** Red cone opsin was spectroscopically measured in an analogous way to green cone opsin and spectra were measured in the dark (1, solid line), after 11CR (C) or 9CR (D) addition (2, dotted line), and 30 min after illumination (3, dashed line).

11CR regenerates with photoactivated green cone opsin with an unprotonated SB linkage. The lack of absorbance increase in the visible region suggested lack of 11CR binding and prompted the question whether green cone opsin could be regenerating with 11CR by means of an unprotonated SB linkage. To test this hypothesis, the photobleached sample was acidified which resulted in a shift of the band to 440 nm characteristic of a PSB. This shift indicates that 11CR

was covalently bound to the protein but via an unprotonated SB (Fig 4.22A). In order to confirm this result, two parallel UV-vis spectroscopic experiments were carried out with the same green opsin sample that was illuminated and split into two aliquots. One of the aliquots was acidified immediately after photobleaching whereas the other was acidified 30 min after illumination. The difference spectrum between the two aliquots clearly showed a difference band at about ~450 nm (Fig 4.22B) which clearly indicated that the photoactivated green cone opsin formed an unprotonated SB linkage with 11CR.

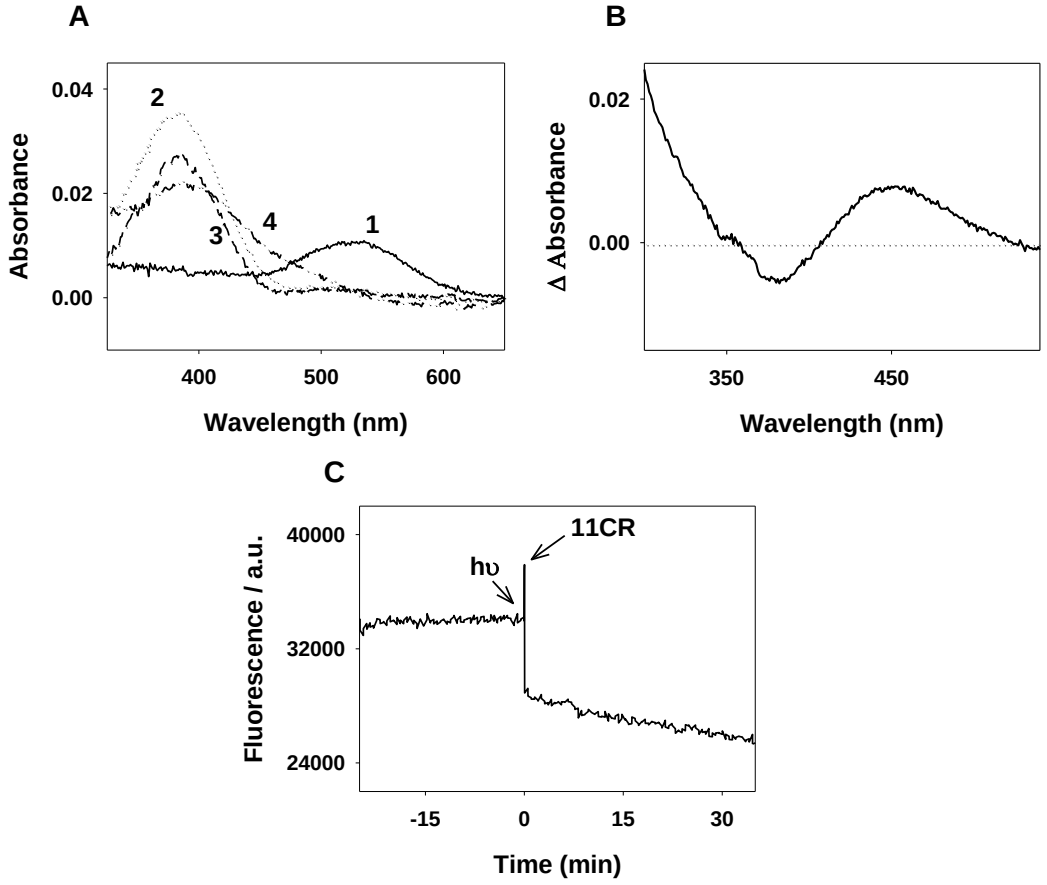

Figure 4.22. ***Photoactivated green cone opsin regenerates with 11CR by means of an unprotonated Schiff base linkage.*** **(A)** The UV-vis spectrum of purified green cone opsin was measured in the dark (1, solid line). After addition of 2.5 fold 11CR, it was illuminated for 30s (λ>495 nm) (2, dotted line). Then, the sample was split into two aliquots in which one was acidified with 2N H_2SO_4 immediately (3, dashed line) and the other 30 min (4, dot-dashed line) later. **(B)** A difference spectrum was obtained by subtracting the spectrum of the sample acidified after 30 min and the sample acidified immediately after photoactivation. **(C)** Green cone opsin, in a fluorimetric micro-cuvette was illuminated for 30s (λ >495 nm) after a stable baseline was obtained. Then, 2.5 fold of 11CR to the concentration of green cone opsin was added immediately after photoactivation and mixed thoroughly.

The photobleaching process was also measured by means of fluorescence spectroscopy by monitoring the Trp fluorescence increase upon green cone opsin illumination. In the dark state, the fluorescence from a specific Trp residue at the retinal binding pocket is quenched by the β-ionone ring of the retinal, and upon photoactivation and retinal release the Trp fluorescence is no longer quenched and an increase in fluorescence can be measured. Purified green cone opsin sample in the fluorescence cuvette was illuminated ($\lambda >$ 495 nm) after a stable dark baseline was obtained. The sudden increase in fluorescence, upon illumination of the green cone opsin sample, indicated a faster MetaII decay. Subsequent addition of exogenous 11CR (2.5 fold 11CR over protein) to the illuminated sample resulted in a decrease in the fluorescence signal confirming entry of 11CR into retinal binding site of activated green cone opsin (Fig 4.22C).

The conformation of opsin and the photochemistry of the chromophore determine the spectral properties of cone visual pigments and in turn the observed spectral behavior could provide hints about the structural details of the receptor proteins (172). When green cone opsin is regenerated with 9CR, the molecular coefficient of the pigment varies with regard to that of the protein regenerated with 11CR. Hence, the same opsin regenerated with different retinal analogs results in shifts in the wavelength of the visible absorption maximum and also differences in the maximum absorbance amplitude. The measured maximal chromophore regeneration of red and green cone opsin with 9CR was 85% and 70% respectively of the original dark spectra before illumination (Fig 4.21). Thus, it emphasizes that the different and specific behavior observed for 11CR and 9CR and the importance to take this into account in vision research.

It is striking that green cone opsin regenerates through an unprotonated SB intermediate conformation that eventually has to become protonated *in vivo* to regenerate the 530-nm absorbing chromophore. This novel intermediate conformation may have a decreased pKa of the SB nitrogen, in the case of green cone opsin, that could imply electrostatic changes at the SB linkage vicinity including changes in the SB-counterion distance. Green cone cells are less abundant in the human retina (the ratio of red cone cells to green cone cells in the human retina mosaic is estimated to be 1.5 to 1) and their response is believed to be analogous to that of red cone cells(28). Green and red cone opsins differ in only 14 residues, with most changes located in the central portion of TM5 and TM6. The similarity is remarkable in the retinal binding pocket (Fig 4.23), except the position $309^{7.40}$ in TM7 (Tyr and Phe in red and green opsins, respectively). Assuming a similar movement of this residue with activation as observed in the crystal structures of rhodopsin, in the dark-state red opsin $F309^{7.40}$ would form a hydrogen bond with T201 in ECL2. This interaction, which is not possible in green opsin, could underlie the observed differences in spectral and retinal regeneration properties.

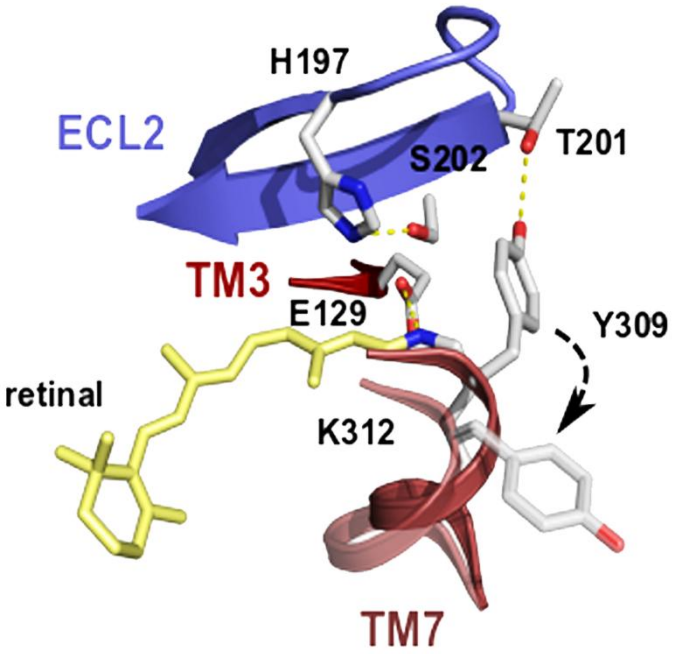

Figure 4.23. ***Molecular model of retinal binding site around SB region.*** Molecular model of inactive red opsin showing the proposed interaction between F309$^{7.40}$ (in TM7) and T201 (in ECL2). The cartoon of TM7 and the conformation of F309$^{7.40}$ in the active state are shown with a transparent representation, and the arrow indicates the movement.

To validate the modeling observation, F309Y mutation was introduced into green cone opsin and the 11CR regeneration experiment was carried out with the purified mutant pigment which showed a regenerated peak at 530 nm (Fig. 4.24A). The difference between the acidified and the regenerated spectra showed a clear band at 530 nm representing the PSB in 309Tyr mutant of green cone opsin, and the difference band at 440 nm corresponds to the amount of net SB from the regenerated pigment (Fig. 4.24B). The fact that the amplitude of the 530 nm band is lower than that of WT pigment regenerated with 11CR, suggests that other residues, like A285 (Thr in red cone opsin) and F279 (Tyr in red cone opsin) which are also in the vicinity of the retinal binding pocket, can also play a role in the formation of the PSB linkage for green cone opsin. However, the role of Y309 in modulating the process of protonation of photoactivated green cone pigment during 11CR regeneration has been substantiated.

A clear difference is found in the intermediate conformation after photoactivation of red and green cone opsins that may be related to differences arisen in the molecular evolution of these two genetically closely related visual pigments. Such transient intermediate conformations of the ligand free opsin during the process of the regeneration have also identified for rhodopsin (173). The unprotonated SB conformation detected could be involved in the dark adaptation process of the photoactivated receptor, in an excess of retinal environment, and consequently play a role in

the molecular basis of color vision by differentially modulating the chromophore regeneration and functionality of green and red cone photoreceptor cells.

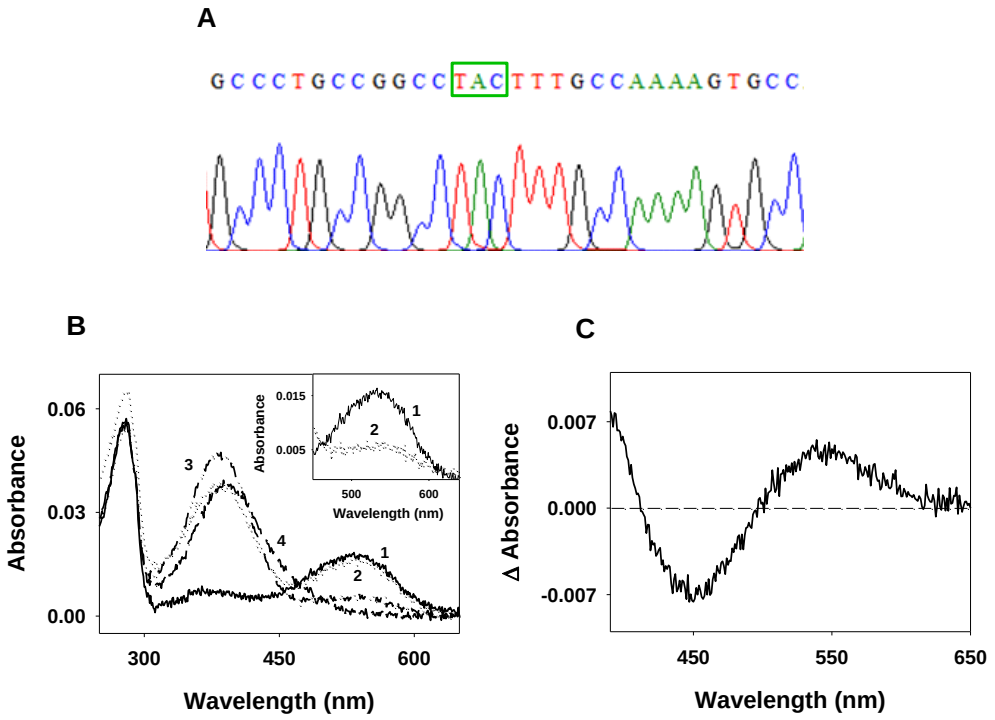

Figure 4.24. ***Phe309 regulates Schiff base protonation during 11CR regeneration of photoactivated green cone opsin.*** **(A)** DNA sequencing result showing the introduction of F309Y into green cone opsin by site directed mutagenesis using the primers (the forward primer - 5'GCCCTGCCGGCCTACTTTGCCAAAAGTGCC3'; and the reverse primer - 5'GGCACTTTTGGCAAAGTAGGCCGGCAGGGC3') **(B)** 11CR regeneration experiment was carried out with purified F309Y green cone opsin mutant. After measuring a dark state spectra (1), 11CR was added prior to illumination (2) and the regenerated spectrum was recorded after 30 min (3) showing a band at 530 nm and the sample was acidified (4). **(B, *inset*)** A closer look at the visible region of dark (1) and (2) regenerated spectra. **(C)** The difference spectrum, obtained by subtracting the acidified spectrum and the regenerated spectrum, shows a clear difference band at 530 nm.

However, these results suggest that there is a clear difference in the conformation after photoactivation of red and green cone opsins that may be related to differences arisen in the molecular evolution of these two genetically closely related visual pigments. The unprotonated SB conformation detected could be involved in the dark adaptation process of the photoactivated receptor, in an excess of retinal environment, and consequently play a role in the molecular basis of color vision by differentially modulating the chromophore regeneration and functionality of green and red cone photoreceptor cells. Furthermore, the proposal of unprotonated SB binding of 11CR to green cone opsin reflects a novel unreported conformational difference between photoactivated green and red cone opsins as discussed above.

4.3.1.2. Red and green cone opsins chromophore regeneration kinetics

The conformation of opsin and the photochemistry of the chromophore determine the spectral properties of cone visual pigments and, in turn, the observed spectral behavior could provide hints about the structural details of the receptor proteins (172). Illumination causes a decrease in absorbance of the regenerated pigment band in the visible region which would be apparently parallel to an absorbance decrease at 380 nm. The 380 nm absorbance decrease, upon chromophore regeneration, could reflect either 11CR binding to, or ATR release from, the opsin receptor. Each data point corresponding to the absorption maximum in the visible region and the retinal region of each regenerated spectra was plotted versus time. The data could be fit to the curves reflecting a fast regeneration process that rapidly reached a plateau.

Regeneration kinetics of green and red cone opsin with 9CR. In red and green cone opsins, the kinetics of the 9CR regeneration process gave $t_{1/2}$ of 1.0-1.5 min (Fig. 4.25A). The decrease in absorbance at 380 nm parallels the visible increase and represents entry of retinal into photoactivated opsin during the regeneration process (Fig. 4.25B) as expected. Parallel experiments were carried out with purified rhodopsin, in which the regeneration with 11CR and 9CR followed single saturation patterns which are significantly slower than those observed for cone opsins, and can be correlated with absorbance changes at 380 nm (Fig. 4.26).

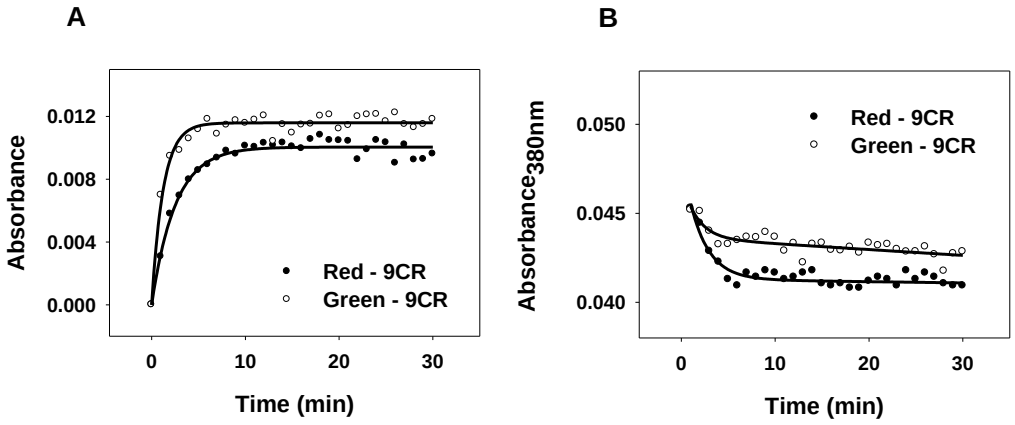

Figure 4.25. ***Regeneration and retinal release kinetics of green and red cone opsin with 9CR.*** **(A)** The absorbance increase at the λ_{max} in the visible region of each regenerated red/green pigment was plotted and fit with a saturation curve. Chromophore regeneration with 9CR was measured for red and green cone opsins for 30 min. The dark-state spectral values of red and green cone opsin were normalized to have equivalent dark absorbance and the regenerated absorbances were also normalized by the same factor. **(B)** Absorbance changes at 380 nm for the regenerated samples were plotted and fit to a single exponential decay curve.

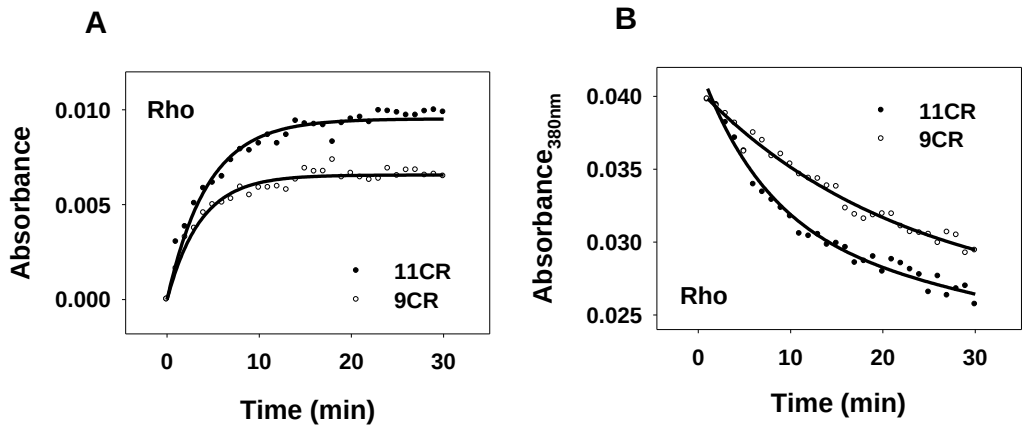

Figure 4.26. ***Regeneration kinetics process of rhodopsin with 11CR and 9CR.*** Regeneration experiments of rhodopsin with 11CR and 9CR were carried out by means of UV-visible spectrophotometry, in which retinal was added prior to illumination (λ>495 nm), and the regeneration was followed for 30 min. The dark-state spectra of rhodopsin were normalized to have equal dark state absorbance at λmax and the regenerated spectra were normalized by the same factor. **(A)** The visible λmax of each normalized regenerated spectrum was plotted and fit with a saturation curve and **(B)** the A380 nm change was also plotted and fit with an exponential decay curve.

4.3.1.3. Secondary retinal uptake kinetics by cone visual pigments after regeneration.

Analogous regeneration experiments were carried out with 11CR but only for red cone opsin as green cone opsin showed no absorbance increase in the visible region upon regeneration. A similar pattern to that observed for 9CR was obtained in the case of red cone opsin regenerating with 11CR with a $t_{1/2}$ less than 1.0 min, and the regeneration with 11CR was found to be even faster than with 9CR (Fig 4.27A). This behavior is in agreement with the complete fast regeneration observed for red cone opsin with 11CR (Fig. 4.21C).

Cone opsin regeneration is usually quantified by measuring the absorbance increase at the characteristic visible band, but in our case this was not possible for green cone opsin chromophore regeneration with 11CR. In order to estimate the regeneration kinetics, we measured the decrease in absorbance at 380 nm with time. This would reflect retinal entry into the binding site of cone opsins and was expected to parallel the regeneration process. In this regard, the change in absorbance at 380 nm after illumination was plotted and the data could be unexpectedly fit to a sigmoidal curve (Fig. 4.27B) which suggested entry of 11CR into visual pigments at a slower rate, with $t_{1/2}$ of 10.6 min for red cone and 13.7 min for green cone respectively. This behavior is in contrast to the faster binding kinetics of cone opsins regenerated with 11CR (Fig. 4.27A). This fast regeneration which is complete in about 1.0 min suggests that the slower process observed (Fig. 4.27B) cannot be due to retinal binding to the 11CR canonical pocket but suggested

additional uptake of 11CR into a secondary binding site facilitated by the presence of 11CR excess in the protein milieu.

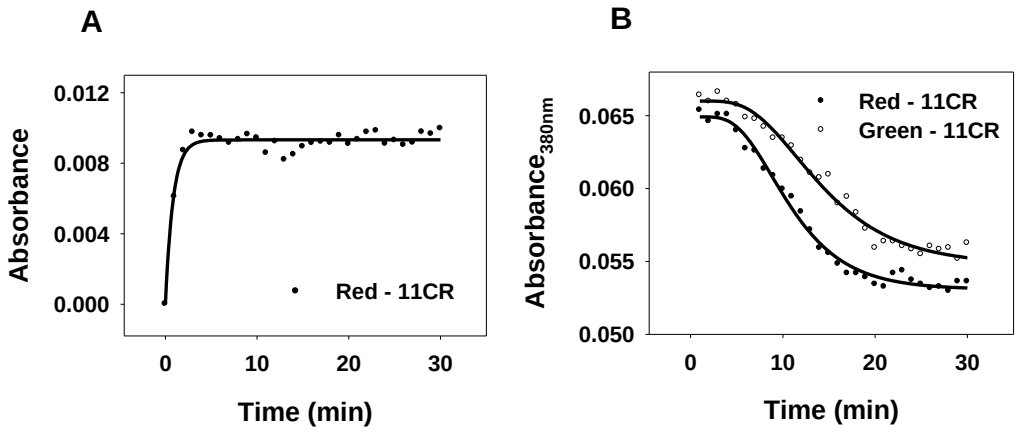

Figure 4.27. ***Regeneration and secondary retinal uptake kinetics of red and green cone opsins with 11CR.*** **(A)** 2.5 fold of 11CR to the concentration of red cone opsin was added in the dark and illuminated for 30s (λ>495 nm). UV-Visible spectra of the sample were obtained every min for 30 min. The λ_{max} at the visible region of each regenerated spectrum was plotted and fit with a saturation curve. **(B)** In the regeneration experiments with 11CR, the regeneration was followed at 380 nm and the absorbance change at this wavelength was monitored for 30 min and the data fit to a sigmoidal curve.

In the search for a possible secondary binding pocket for 11CR, we computed interaction potential maps for a hydrophobic probe in both inactive and active models of red and green opsins (see Methods). The maps revealed a cavity between TMs 1 and 7 in the active models of both red and green opsins with sufficient size to accommodate a second retinal molecule (Fig. 4.28). Because TM7 moves with activation, increasing the size of the cavity, only the active structures seem to allow binding of a second retinal in this region. This cavity is compatible with the proposed entry/exit channels for retinal (53) and with the presence of hydrophobic molecules observed in the crystal structures of rhodopsin, as we previously noted (147).

We interpret this phenomenon as a slower binding of a second 11CR molecule to the regenerated pigment to a site with lower affinity than that at the canonical ligand binding pocket. This secondary 11CR uptake might be potentially coupled with a delay in ATR release from the protein. We propose that this slower secondary retinal uptake is a distinct phenomenon to that of the fast regeneration of red and green cone opsins observed in a ~1 min time frame with 11CR. Such a behavior was not observed when photoactivated red and green cone opsins were regenerated with 9CR (Fig. 4.25B) suggesting that it is specific in the case of the native 11CR chromophore.

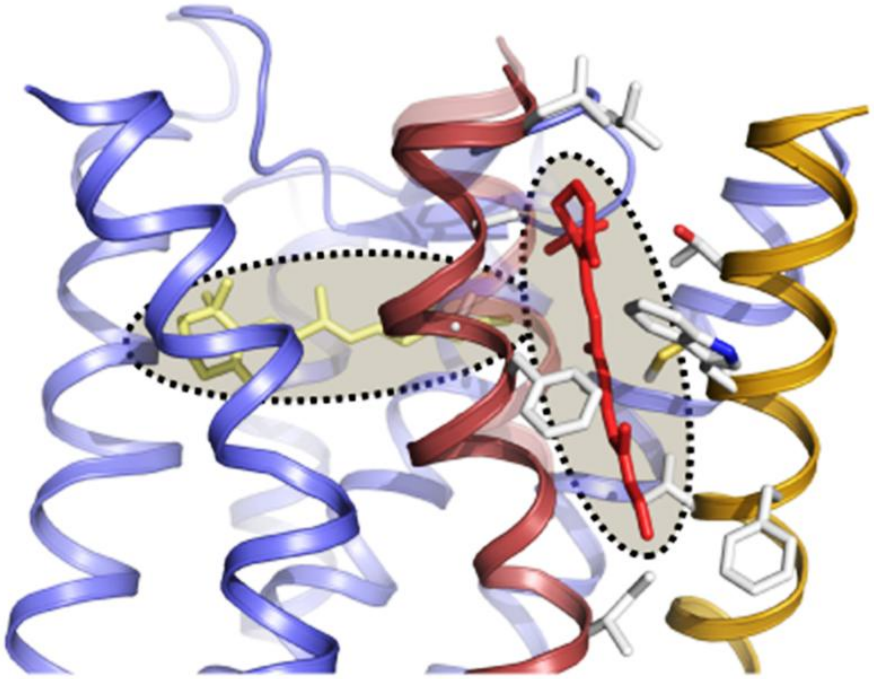

Figure 4.28. ***Model of red cone opsin with secondary retinal.*** Molecular model of the active red opsin showing the potential coexistence of two retinal molecules (yellow and red for the primary and secondary sites, respectively). The side-chains of neighboring hydrophobic residues are shown with sticks.

We believe that our spectral changes are not reflecting potential retinal binding to other regions on the surface, or external side of the protein, for several reasons. First, the secondary binding observed is not covalent, so binding to external Lys residues is excluded. It should also be pointed out that retinal binding to the protein surface is unlikely to cause the spectral change at 380 nm observed. Furthermore, such non-specific retinal-protein surface interactions would not be isomer specific but, in our case, only 11CR can induce the spectral behavior observed. Thus, the secondary binding site proposed shows specificity towards 11CR, but not 9CR, and such ligand specific accessibility would be difficult to explain if the secondary retinal binding would happen at the surface of the protein. All these arguments reinforce our proposal of secondary retinal binding at the proposed site by our molecular modeling analysis.

These findings are in agreement and support the results of previous studies proposing that more than one retinoid can interact with visual opsins (174) which strongly suggests the presence of functionally-relevant secondary binding sites of retinoids in opsin (175). Furthermore, previous experimental evidence showed an important role for non-covalent 11CR binding to opsin prior to regeneration (176) and in its ability to bind to a selective conformation of the protein among various conformational modes of visual pigments prior and after photoactivation (173).

In addition to the secondary 11CR binding event, changes at 380 nm could also be reflecting changes in ATR release that could alter the rate of retinoid recycling thus regulating dark state adaptation after photoactivation for cone opsins. Retinoid binding protein, ABCA4, is an ATP dependent transporter of ATR from the luminal side to the cytoplasmic side of photoreceptor cells. At the cytoplasmic side, ATR is converted to all-*trans*-retinol by RDH8 which is then released to Müller cells or retinal pigment epithelium (for the retinoid cycle) and further converted to 11CR which in turn diffuses into photoreceptor cell and results in dark adaptation of visual pigments (177-179). Stargardt disease is an autosomal recessive disorder characterized by mutations at ABCA4, in which vision loss is associated with accumulation of ATR and its derivatives that can be toxic by causing oxidative stress that can result in damage of the retinal cells (180,181). It is also known that transportation of ATR by ABCA4 is a multi-step process and that the substrate for ABCR4 is N-retinylidene-phosphotidyl ethanolamine (NRPE) formed from the interaction of ATR with phosphotidyl ethanolamine. NRPE is a reversible product, and the conversion process of RDH8 from ATR to all-*trans*-retinol is slow (177,182). Hence, the controlled release of ATR after photoactivation, coupled to 11CR binding to a secondary binding site other than the canonical retinal binding pocket, would help regulating the effective transport of ATR, from cone opsins. This may suggest a temporary entrapment of ATR to the same or other secondary binding site, and this may be connected to a slower movement of the hydrophobic retinal molecule along the ligand channel proposed between openings A and B which would be perpendicular to the helices axis. A secondary retinal binding site in cone visual pigments can accommodate a retinal molecule in addition to the one bound to the classical retinal binding pocket (174). We propose that this second binding site which would be specific for 11CR, and not for 9CR, may function as a retinal buffer, in cone opsins, rather than playing an allosteric role for retinal binding to its primary site. The different behavior for 11CR and 9CR is also evident from the faster initial velocity for the chromophore regeneration observed with 11CR than 9CR (Figs. 4.25 and 4.27). This secondary binding site may allow retinal pre-binding and subsequent fast transfer of this retinal molecule to the primary retinal binding pocket for covalent binding and dark-adapted pigment regeneration ready for another light stimulus.

4.3.2. Blue cone opsin regeneration mechanism

4.3.2.1. Regeneration of photoactivated blue cone opsin with 11CR

The dark-state UV-Vis spectrum of purified blue cone opsin in DM shows its characteristic regenerated protein band at 420 nm and the total opsin protein band at 280 nm. Upon illumination using white light, the release of isomerized 11CR shifts the peak from 420 nm to 380 nm. The regeneration experiments in blue cone opsin were carried out only after illumination, unlike red/green cone opsin where the retinal was added prior to illumination, as the absorption

maximum of blue cone opsin is closer to the λmax of retinal. First, the 11CR regeneration experiment was carried out with photoactivated blue cone opsin immediately after illumination. In order to do that, after measuring the dark-state spectrum of blue cone opsin in the 250-650 nm range, 11CR was added immediately after the sample was illuminated using white light, and the regeneration was followed for 60 min. The regeneration of photoactivated blue cone opsin cannot be observed because the band corresponding to the exogenously added retinal completely masks the overall regenerated band of blue cone opsin (Fig. 4.29A). Hence, the sample was acidified with H_2SO_4 and a shift in the λmax and an increase in absorbance at 440 nm could be detected which would account for the presence of Schiff-base linked material from the regenerated sample. For the better observation of the acidified spectrum of the regenerated sample, a difference spectrum was obtained by subtracting the acidified spectrum with the regenerated spectrum and this difference spectrum

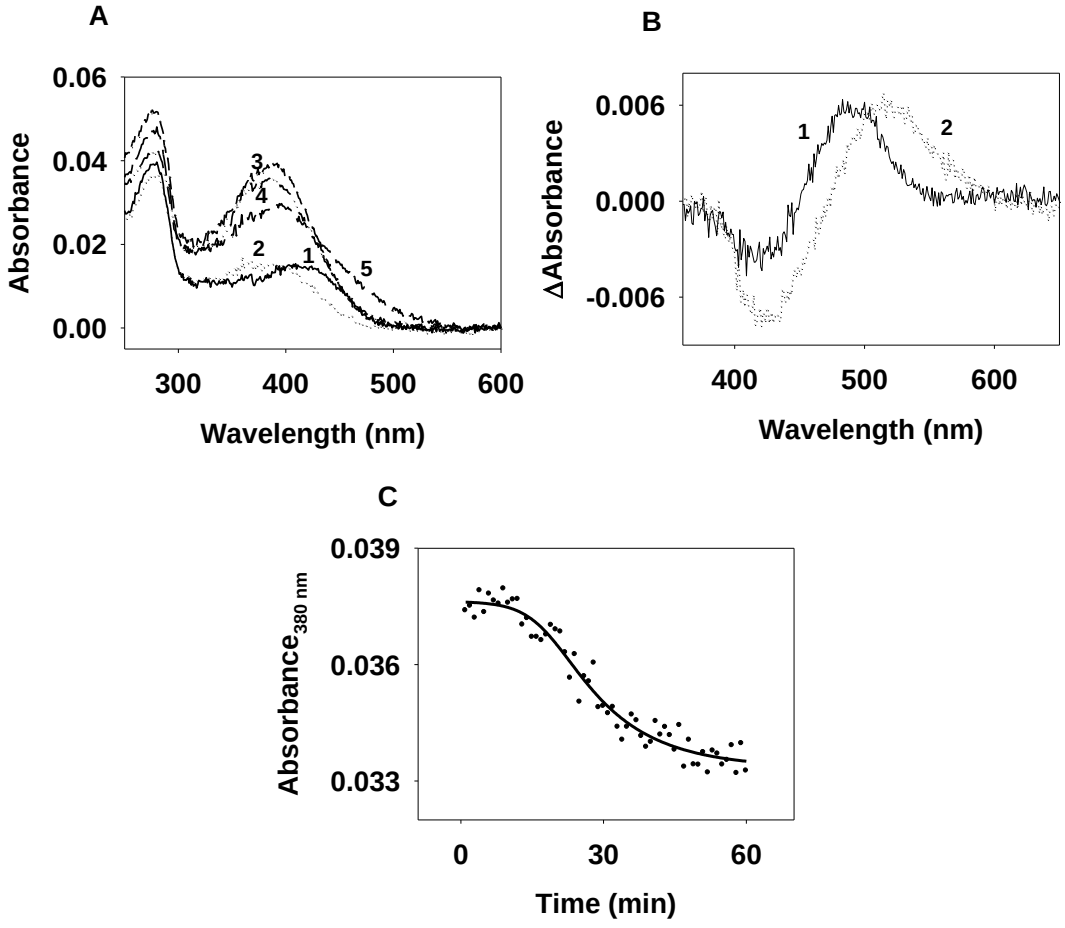

Figure 4.29. ***Photoactivated blue cone opsin regenerates with 11CR immediately after illumination***. **(A)** The UV-vis spectrum was measured in the dark (1, solid line). Immediately after illumination (2, dotted line) 2.5 fold 11CR was added (3, short dashed line), and followed for 60 min (4, dotted-dashed line) and acidified 30min later (5, long dashed line). **(B)** Difference spectra between dark and illuminated, and between acidified and regenerated. **(C)** Absorbance change at 380 nm was monitored for 60 min and the data fit to a sigmoidal curve.

was compared with the difference spectrum between dark and illuminated sample of the same blue cone opsin (Fig. 4.29B). This experiment distinctly shows the regeneration of photoactivated blue cone opsin with 11CR immediately after illumination. Unlike red/green cone opsin estimating the regeneration kinetics is not possible in the case of blue cone opsin as the added free retinal overlaps with the protein regeneration region of the spectrum. In any event, the changes at 380 nm were measured by plotting the absorbance change at this wavelength from 0 min to 60 min. This process showed a sigmoidal pattern similar to that observed in the case of red and green cone opsins (Fig. 4.29C). The estimated $t_{1/2}$ of the process is 26.6 min which is longer than that for the other cone opsins. It was reasonable to assume that blue cone opsin would show a fast regeneration process similar to green and red cone opsins, which is also supported by the high reactivity to hydroxylamine (Fig. 4.6) suggesting a more "open" retinal binding pocket than red/green cone opsins.

Considering the observation of slower fluorescence decrease in blue cone opsin after photoactivation (Fig. 4.4C), regeneration of blue cone opsin, after a stable post-photoactivated phase could be obtained, could be compared with the behavior of the protein immediately after dark adaptation. From this comparison, the structural changes associated with the regeneration mechanism can be elucidated.

In order to do that, regeneration of blue cone opsin with 11CR was carried out 15 min after illumination. All the experimental conditions were the same as those in the previous experiments, and the results showed that, upon acidification at the end of the regeneration experiment, the appearance of a shoulder in the 440 nm-520 nm region (Fig. 4.30A) which was similar to that obtained in the regeneration experiment carried out immediately after illumination. The difference spectrum between acidified and regenerated samples suggested a similar regeneration behavior (Fig. 4.30B) to that previously obtained. In contrast, there was no change in absorbance at 380 nm (Fig. 4.30C) suggesting no secondary retinal uptake when the regeneration is carried out 15 min after illumination. Furthermore, the regeneration at the primary binding site appeared to be unaltered.

The fluorescence decrease, observed after illumination of blue cone opsin, could be interpreted as reflecting a conformational change taking place with a slower kinetics that impairs secondary retinal uptake by the photoactivated receptor. These results would also be compatible with the assumption of a fast regeneration kinetics with 11CR (with maximal obtained regeneration) and the lack of absorbance changes at 380 nm.

The 11CR regeneration experiments with blue cone opsin, immediately and 15 min after illumination, were also carried out by means of fluorescence spectroscopy. In these experiments,

the samples of purified blue cone opsin were illuminated with white light after a stable baseline was obtained and the same amount of 11CR as that used for the UV-Vis regeneration experiment

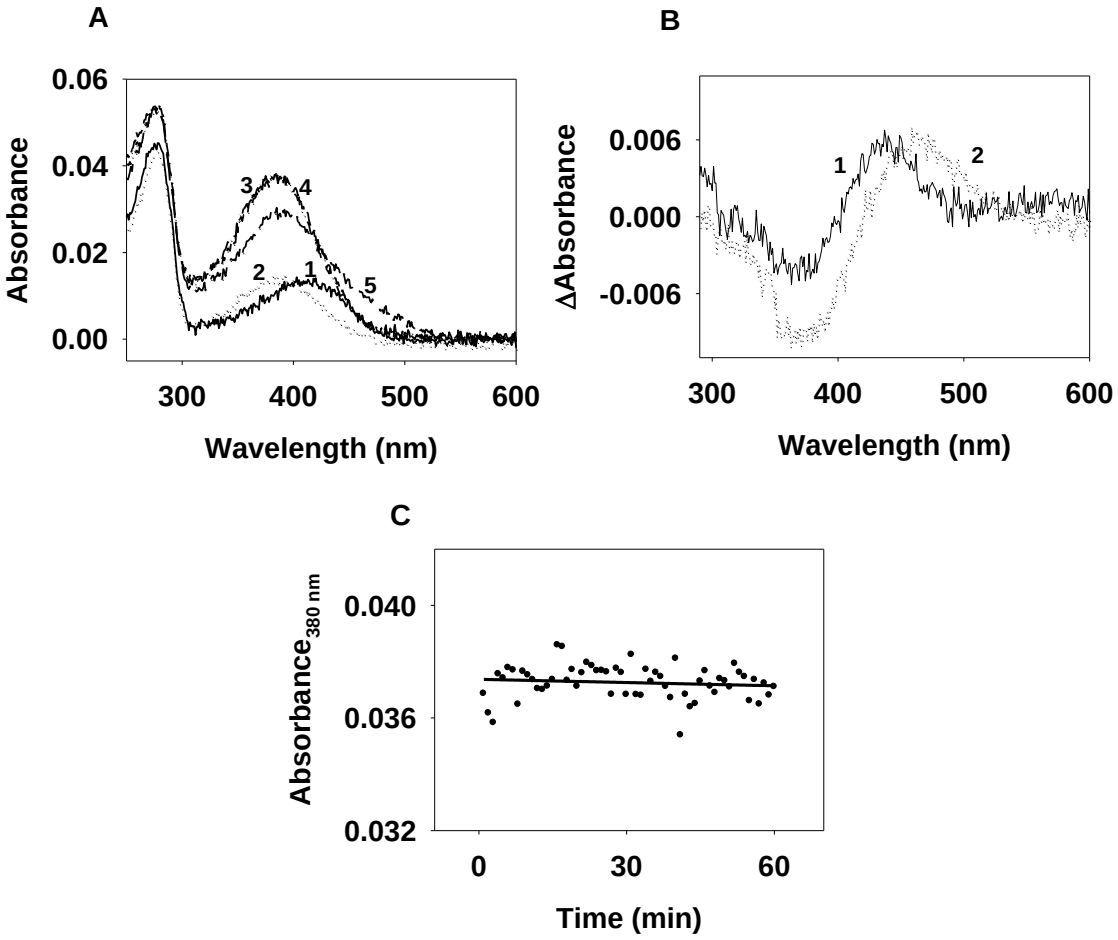

Figure 4.30. ***Photoactivated blue cone opsin regenerates with 11CR 15 min after illumination***. **(A)** The UV-vis spectrum was measured in the dark (1, solid line). 15min after illumination (2, dotted line) 2.5 fold 11CR was added (3, short dashed line), and followed for 60 min (4, dotted-dashed line) and acidified 30min later (5, long dashed line). **(B)** Difference spectra were plotted dark against illuminated and acidified against regenerated. **(C)** Absorbance change around 380 nm was monitored for 60 min and the data fit to a linear pattern.

was added immediately, and 15 min, after illumination. In both cases a decrease in fluorescence was observed suggesting blue cone opsin regeneration (Fig. 4.31). Particularly, the net fluorescence change observed in both cases was different but the fluorescent decrease seen during the regeneration of 11CR after 15 min of photoactivation would reflect a conformational change and the subsequent regeneration of the dark-adapted state. In contrast, the regeneration of the protein immediately after illumination would reflect only the occupancy of retinal binding site by the exogenous retinal and no additional imposed conformational change (observed only 15 min after photoactivation of the receptor). These result may suggest that the conformational change

exhibited by the blue cone opsin leads to the formation of a specific conformation that would prevent binding of 11CR to the postulated secondary site (Fig. 4.30C).

Overall, this behavior might lead the understanding that the fluorescence decrease observed after illumination may be due to a major conformational change happening in the blue cone opsin in a slower fashion which disables the secondary retinal uptake by the photoactivated blue cone opsin. This is also consistent with the recent study that analyzes the real time conformational dynamics of rhodopsin which identified a major conformational change with photoactivated rhodopsin with an extended larger movements of H5 and H6 about 80% larger than any helical movements observed earlier (183).

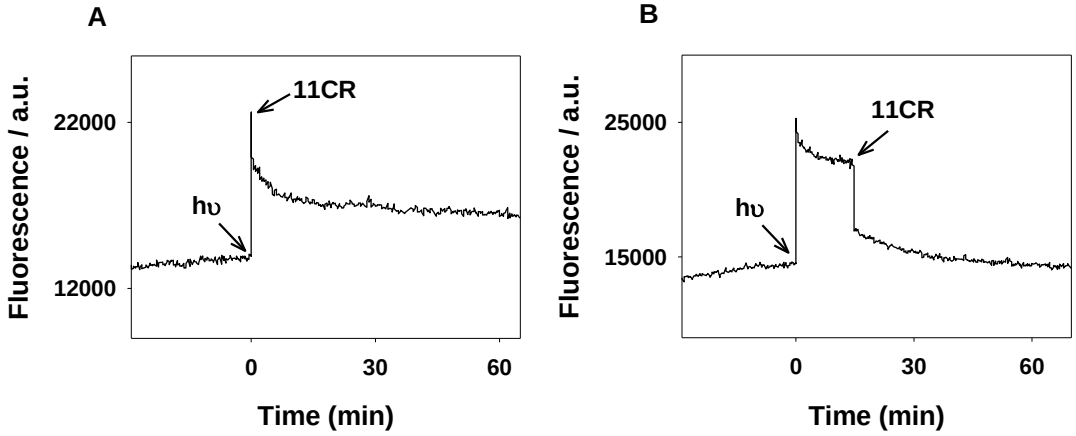

Figure 4.31. ***Fluorescent changes during the regeneration of blue cone opsin with 11CR.*** Purified blue cone opsin in DM added to the micro-cuvette was illuminated for 30 s after the stable baseline was obtained. 2.5 fold of 11CR to the concentration of blue cone opsin sample was added, either immediately **(A)** or 15 min after illumination **(B)**.

4.3.2.2. Regeneration of photoactivated blue cone opsin with 9CR

In an analogous experiment to that of regeneration with 11CR, photoactivated blue cone opsin was regenerated with 9CR immediately and 15 min after illumination. Blue cone opsin was photobleached and acidified in a similar manner. The result showed that blue cone opsin can regenerate with 9CR immediately after illumination in a similar fashion as what was observed in the case of regeneration with 11CR (Fig. 4.32A, B). However, in this case, the changes observed at 380 nm, which follow a sigmoidal pattern (Fig. 4.32C), suggest a secondary retinal uptake unlike other cone opsins (Fig. 4.25B) which do not show secondary retinal uptake with 9CR. This behavior highlights the specificity of the retinal binding site of blue cone opsin when compared to those of red and green cone opsins. The measured half-time of the kinetics of this secondary 9CR uptake is 34.7 min which is significantly longer than that for 11CR suggesting that,

immediately after illumination, the secondary retinal binding site has more affinity for binding 11CR than 9CR.

Blue cone opsin shares merely 43% homology when compared to the higher homology of red-green pigments, and with that of the red cone pigment and rhodopsin which is 41% (184). It evolved from a different pathway than red/green cone opsins exhibiting a differential molecular basis of spectral tuning (185,186) with significant differences in key amino acids at the retinal binding pocket. Particularly relevant appears to be Y262, which is W281 in the case of red/green cone opsins (23), in the proposed secondary 9CR uptake during blue cone opsin regeneration immediately after illumination.

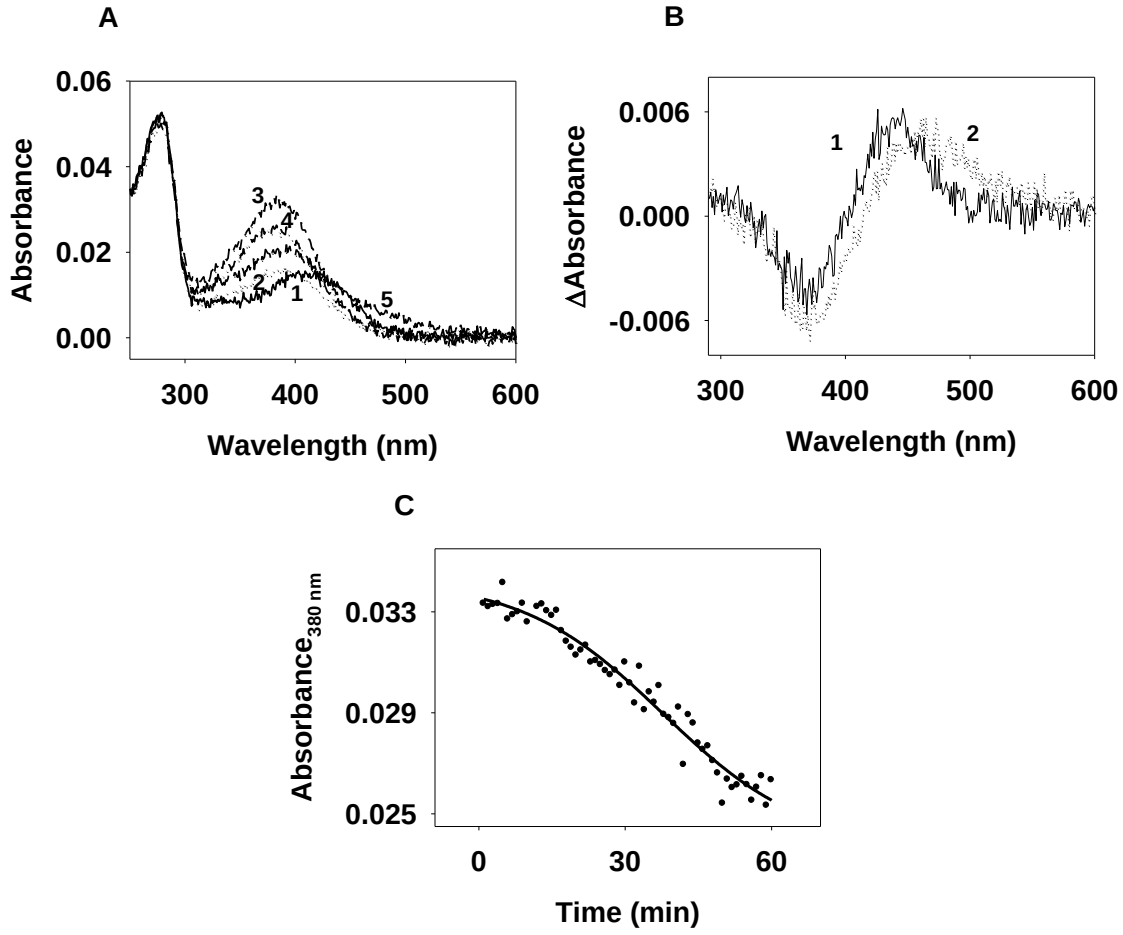

Figure 4.32. ***Regeneration of blue cone opsin with 9CR immediately after illumination***. **(A)** The UV-vis spectrum was measured in the dark (1, solid line). Immediately after illumination (2, dotted line), 2.5 fold 9CR was added (3, short-dashed line), and spectra recorded up to 60 min (4, dotted-dashed line), and subsequently acidified 30 min later (5, long-dashed line). **(B)** Difference spectra were obtained from the dark minus illuminated spectra and acidified minus regenerated spectra respectively. **(C)** Absorbance change at 380 nm was monitored for 60 min and the data was fit to a sigmoidal curve.

The regeneration behavior of blue cone opsin was also analyzed with 9CR at the post-illuminated phase, i.e. 15 min after illumination. The results showed that 9CR can still regenerate chromophore with photoactivated blue cone opsin in a similar fashion that 11CR. Surprisingly, what we attribute to a secondary retinal uptake was observed with $t_{1/2}$ 28.8 min (Fig. 4.33C) which is faster than the kinetics of 9CR binding immediately after illumination. This behavior is also different in the case of 11CR which does not appear to have secondary retinal entry into the binding pocket of the 15 min post-illuminated conformation of blue cone opsin.

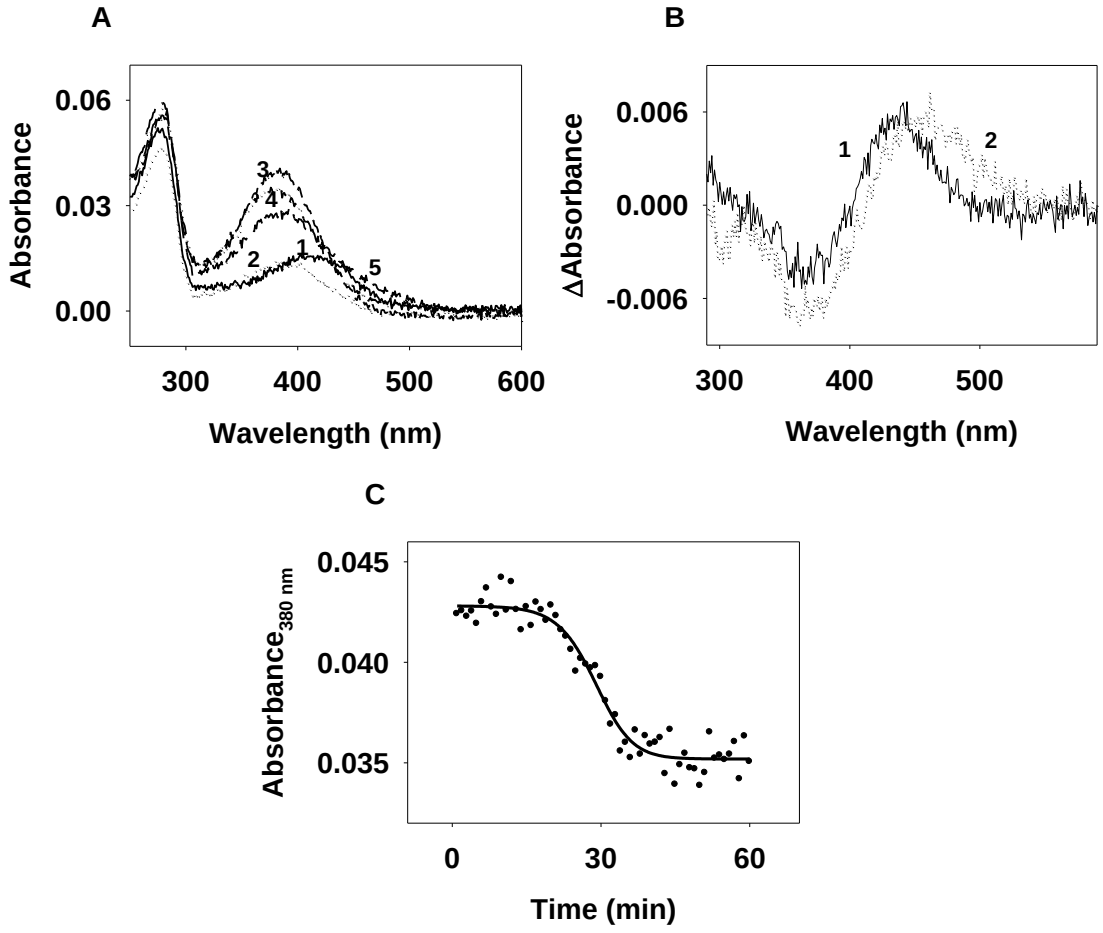

Figure 4.33. ***Regeneration of blue cone opsin with 9CR 15 min after illumination***. **(A)** The UV-vis spectrum was measured in the dark (1, solid line), and 15 min after illumination (2, dotted line), 2.5 fold 9CR was added (3, short-dashed line), and spectra were recorded up to 60 min (4, dotted-dashed line), and subsequently acidified 30min later (5, long-dashed line). **(B)** Difference spectra were obtained from the dark minus illuminated spectra and acidified minus regenerated spectra respectively. **(C)** Absorbance change at 380 nm was monitored for 60 min and the data was fit to a sigmoidal curve with a $t_{1/2}$ of 28.8 min.

Overall, the regeneration experiments of photoactivated blue opsin, with retinal analogs, at different time points after illumination, suggest a conformational change (other than the canonical

photoactivated conformation obtained after retinal photoisomerization) that would be coupled with a sophisticated fine-tuning mechanism that involves a secondary retinal binding site which does not withhold 11CR, 15 min after photoactivation, but only 9CR and with a faster kinetics. This previously unreported phenomenon may show mechanistic similarities to the rearrangement events observed in the primary binding site of rhodopsin (chapter 2 of this thesis) (148). Thereby, differences in intragenic epistatic interactions among these structurally similar red, green and blue cone opsins may justify the different functionally-relevant conformations observed (187,188).

An intriguing correlation can be made between the estimated secondary retinal uptake t1/2 for the binding kinetics with 11CR, immediately after illumination, versus the typical absorption maximum of cone opsins. Interestingly, the data perfectly match a linear pattern that suggests a relationship between the energetics of the pigments (the differences in energy for the electronic levels associated with the maximal wavelength absorption) and the kinetics of the secondary binding event (Fig. 4.34). Though the interpretation of this correlation is yet unclear, coupling of thermodynamic properties of the cone pigments (and the isomerized retinal leaving the protein), and the kinetics of the entry of a secondary retinal molecule at a specific site of the protein might help explain the perfect correlation observed and the connection to the wavelength maximum detected. A shorter wavelength may be correlated with a higher energy level and suggest a less stable pigment and this could be linked to a longer time needed for retinal binding to the proposed putative secondary binding site. An interesting possibility arises to further analyze additional opsins with different wavelength maxima and check if they could adjust to the obtained line.

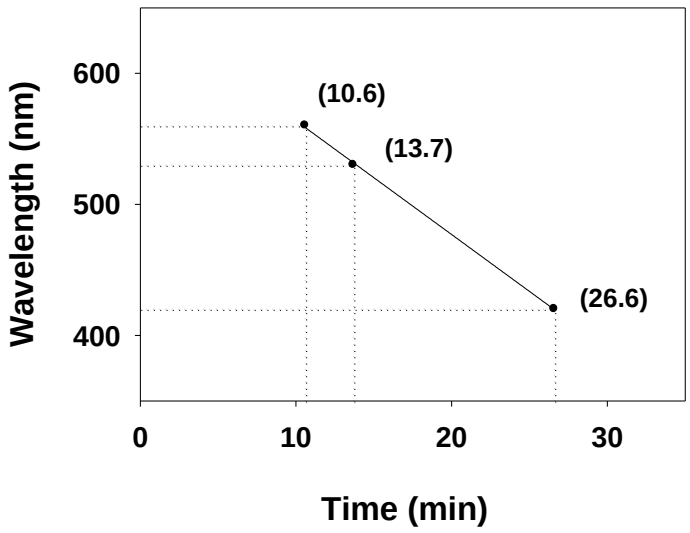

Figure 4.34. ***Correlation between secondary retinal uptake kinetics and absorption maximum of cone opsins***. The estimated $t_{1/2}$ for secondary 11CR uptake kinetics for red (10.6 min), green (13.7 min) and blue (26.6 min) cone opsins, immediately after illumination, were plotted against their characteristic λmax at the visible region.

4.4. Molecular investigation of cone opsin mutants associated with retinal disorders

(The contents of this chapter are in preparation for a publication as
Srinivasan S, Ramon E, Garriga P. Molecular mechanism of green cone opsin mutants associated with color blindness (in preparation))

Natural selection depends on adaptive evolution from the genetic variability within species. Point mutations give rise to variability in genes which can be either neutral (synonymous mutations which do not alter the amino acid sequence of the protein), favorable (optimizing the functionality of the protein), or deleterious (non-synonymous mutations which are amino acid-altering and can potentially disrupt the protein structure) (189-191). Adaptive evolution of the visual system serves to accumulate constructive mutations yielding enhanced spectral tuning capabilities thus stabilizing the well-functioning trichromatic color vision system. However, from time-to-time various missense mutations have been identified in humans which lead to abnormalities in the visual system ranging from minor polymorphisms with modified spectral tuning to severe retinal degenerative cone dystrophies (44,192).

4.4.1. Blue cone opsin mutants

The major intention in studying tritanopic mutants, causing inherited blue color vision deficiency is to reveal the conformational changes in the protein that could justify the malfunction of the pigment. Site directed mutagenesis was employed to introduce the point mutations, associated with retinal disorders, into the WT of blue cone pigment. Such mutations were G79R, T190I, and S214P. The mutated plasmids were sequenced in order to confirm the successful introduction of the mutations (Fig 4.35).

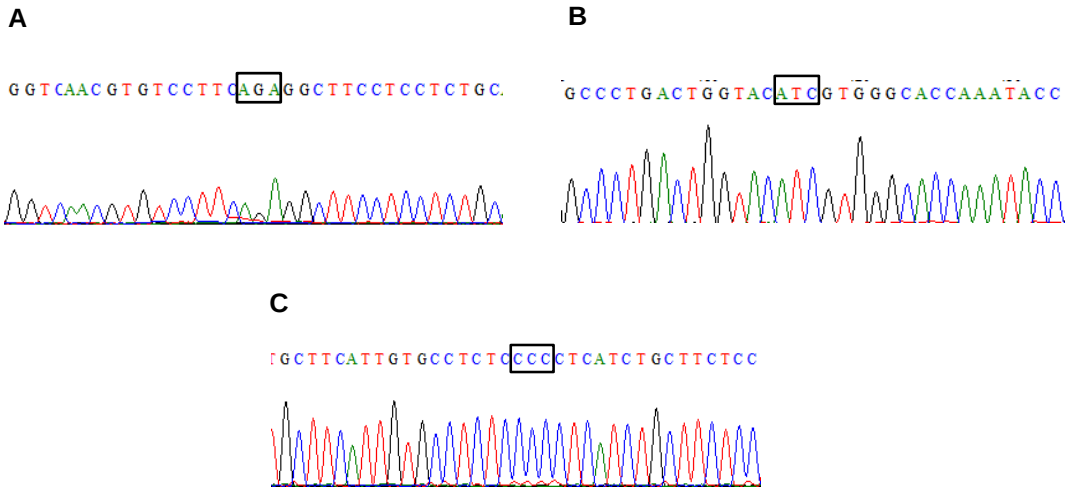

Figure 4.35. ***Mutagenesis of blue cone mutants.*** Mutagenic primers used contained the mutations for the G79R mutant **(A)**, 5'GGTCAACGTGTCCTTCAGAGGCTTCCTCCTCTGC3', 5'GCAGAGGAG GAAGCCTCTGAAGGACACGTTGACC3'; for the T190I mutant **(B)**, 5'GCCCTGACTGGTACAT CGTGGGCACCAAATACC3', 5'GGTATTTGGTGCCCACGATGTACCAGTCAGGGC3'; and for the S214P mutant **(C)** 5'GCTTCATTGTGCCTCTCCCCCTCATCTGCTTCTCC3', 5'GGAGAAGC AGATGAGGGGGAGAGGCACAATGAAGC 3'. The mutations were constructed by a thermocyclic PCR method. The resulting mutants were subject to DNA sequencing and the mutated codons are shown boxed.

WT and mutants of blue pigments were expressed and immunopurified, and the UV-visible spectra were measured. The UV-visible spectrum of WT blue cone pigment showed a characteristic absorption maximum at 420 nm (Fig. 4.36). On the other hand, the clinically identified mutants G79R, T190I and S214P did not show this characteristic retinal band, meaning that there was no regeneration with the chromophore, and aggregation of the protein was also presumably observed, determined by the shift from 280 nm to 260 nm at the opsin protein band. This result confirms that the structural alterations caused by the replaced amino acid destabilize the protein preventing retinal binding to the protein.

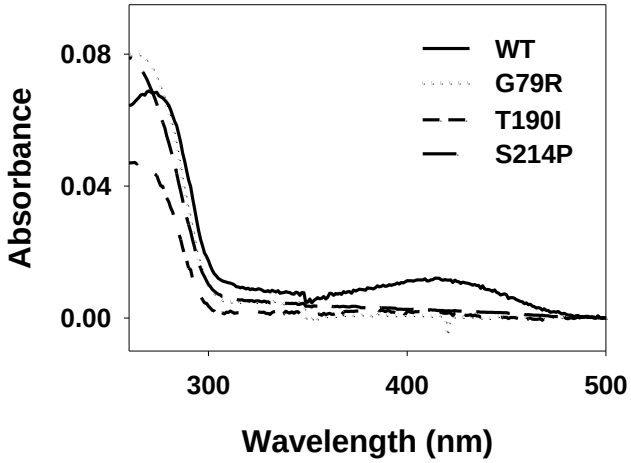

Figure 4.36. ***Expression of blue cone opsin mutants*.** The UV-Vis Spectra of purified blue cone pigment WT and their mutants, G79R, T190I, S214P in the dark, which were expressed in COS-1 cells and regenerated with 10μM 11CR.

The protein band of all the purified mutants of blue cone opsins has shifted to ~260 nm suggesting protein aggregation as a consequence of protein misfolding. It is assumed that the replacement of the bulkier, positively charged Arg against the non-polar and smaller Gly, in the G79R mutant, would affect folding and compromise the stability of blue cone opsin. The corresponding position in rhodopsin is A82$^{2.49}$, located at TM2, which is a small and non-polar residue not reported as being important for protein folding or stability. This position is next to the highly conserved D83$^{2.50}$ which is however a Gly in the blue cone opsin. S214P mutation is also believed to disrupt the optimal functional conformation of blue cone opsin by afftecting protein folding and stability of the protein (110).

T190 is present at the EII and it has been reported to have a significantly different behavior than other deutan or protan mutants during light- and dark-adapted conditions, in the sense that this S-cone mutant results in mild to moderate S-cone dysfunction and loses its sensitivity at low light levels (113). T193 of rhodopsin is the homologous position in rhodopsin and the mutation T193M

has been identified to cause RP in humans (193). T193M was classified as a Class II rhodopsin mutant that showed poor chromophore regeneration with 11CR, and inefficient transport to the plasma membrane (194,195).

4.4.2. Red cone opsin mutants

Mutations in red cone opsin genes lead to dichromatic clinical condition, in which the spectral sensitivity of affected individuals lies within the green region of the visual spectrum. The clinically identified mutants that cause protanopia include, S180A, R247Ter, and G338E which are the point mutations in the red cone opsin gene. In the case of R247Ter, the nucleotide position, CGA 739 is mutated to TGA, a stop codon. Hence the protein will be truncated at the position of 247 and it could not be immunopurified because it would lack the epitope for 1D4 antibody which is at the C-terminal end of the protein. Mutations S180A and G338E were introduced into the WT red cone opsin and the corresponding mutated plasmids were sequenced in order to verify the correct introduction of the mutations (Fig 4.37).

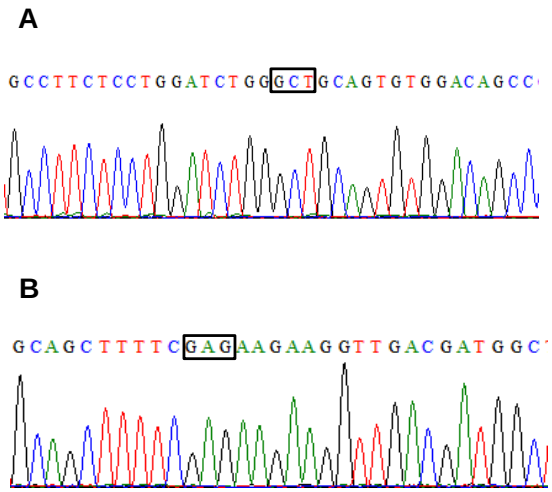

Figure 4.37. ***Mutagenesis of red cone mutants.*** Mutagenic primers used contained the mutations for the S180A mutant (A), 5' GCCTTCTCCTGGATCTGGGCTGCAGTGTGGACAGCC 3', 5'GGCTGTCCACACTGCAGCCCAGATCCAGGAGAAGGC3'; and for the G338E mutant (B), 5'GCAGCTTTTCGAGAAGAAGGTTGACGATGGC3', 5'GCCATCGTCAACCTTCTTCTCGAA AAGCTGC3'; were constructed by a thermocyclic PCR method. The resulting mutants were subject to DNA sequencing and the mutated codons are shown boxed.

WT and S180A were regenerated and no aggregation problems were observed (Fig. 4.4.4). This result is expected because S180A is a polymorphism, being Ser present in 62% of Caucasian males, and causing only little variations in normal color vision (about 4-5 nm blue-shift in the

absortion maximum). S180 is one of the residues involved in spectral tuning of the pigment (44,196).

In the case of G338E, the introduction of a negatively charge at the C-terminal end of the protein appears to dramatically affect protein regeneration ability and probably induces some aggregation as observed by the shift from the typical protein opsin band at 280 nm to 260 nm.

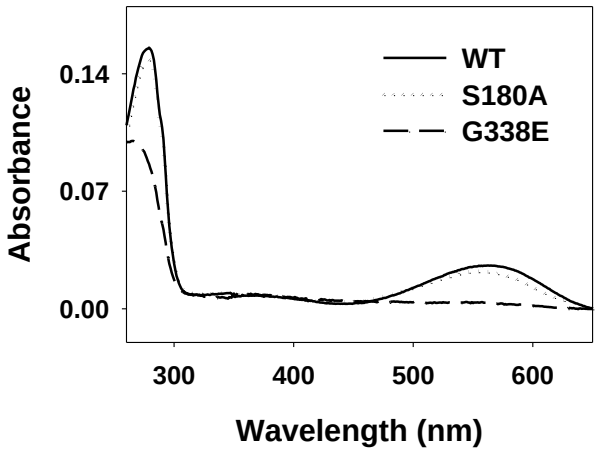

Figure 4.38. ***Expression of red cone opsin mutants*****.** The UV-Vis Spectra of purified red cone WT pigment and its mutants, S180A and G338E, in the dark, which were expressed in COS-1 cells and regenerated with 10μM 11CR.

4.4.3. Green cone opsin mutants

Though red and green cone opsin genes are located in an array at chromosome X sharing a high degree of homology, the frequency and prevalence of deuteranopia is slightly higher than protanopia (197). Red/green cones are allelic variants from a single gene, hence some of the mutations associated with red/green cone genes can be combined. These mutations can lead to different conditions, ranging from dichromacy to cone monochromacy in which the affected individuals possess only functional blue cone opsin (198,199).

Green cone mutants N94K, W177R, C203R, and R330Q were introduced into the WT plasmid of green cone pigments by site directed mutatgenesis using mutagenic primers carrying the required mutations. The sequencing results of the mutant products confirm that green cone mutant opsin plasmids were generated for subsequent characterization studies (Fig 4.39). Expression of these mutants was carried out in COS-1 cells. The transfected cells were harvested and regenerated with 11CR and immunopurified using 1D4 antibody. The UV-Spectra of W177R and C203R showed that there was no regeneration in the visible region of the spectra (Fig 4.40A) suggesting that the

mutated conformations of W177R and C203R are altered preventing entry and/or covalent binding of 11CR by means of a Schiff base to K312.

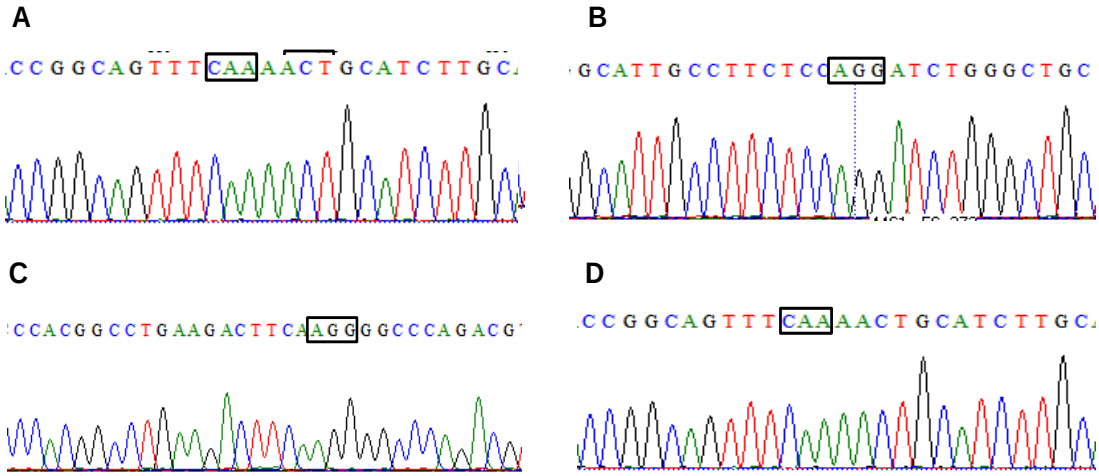

Figure 4.39. ***Mutagenesis of green cone mutants.*** The primers used containing the mutations for the N94K mutant **(A)**, 5'GGATCCTGGTGAAGCTGGCGGTCGC3', 5'GCGACCGCCAGCTTCACCA GGATCC 3'; for the W177R mutant **(B)**, 5'GCATTGCCTTCTCCAGGATCTGGGCTGC3', 5'GCA GCCCAGATCCTGGAGAAGGCAATGC3'; for the C203R mutant **(C)**, 5'CCACGGCCTGAAGAC TTCAAGGGGCCCAGACG3', 5'CGTCTGGGCCCCTTGAAGTCTTCAGGCCGTGG3'; and for the R330Q mutant **(D)** 5'CCGGCAGTTTCAAAACTGCATCTTGC3', 5'GCAAGATGCAGTTTTG AAACTGCCGG3'. The mutations were constructed by a thermocyclic PCR method. The resulting mutants were subject to DNA sequencing and the mutated codons are shown boxed.

The UV-Vis spectrum of R330Q shows a band at 530 nm indicating the ability of the mutant to regenerate with 11CR. Even though N94K does not show regeneration in the vision region, a peculiar peak at 360 nm was observed (Fig 4.4.6B).

Green cone proteins behaved differently depending on the localization of the mutation. WT and R330Q showed the characteristic green pigment visible peak, at 530 nm, as reported elsewhere (89,200,201). On the other hand, W177R and C203R, showed no protein regeneration, as previously described (59). Green W177R is associated with X-linked cone dystrophy and the behavior of W177R was expected because of the dramatic replacement of an aromatic and hydrophobic residue to a positively charged at a highly conserved position (202).

The C203R mutation would interfere with the formation of the Cys-Cys conserved disulfide bridge present in all G protein coupled receptors superfamily and important for their stability and integrity (202). C203R has been observed in some individuals identified as dichromats (deuteranopia) with a single mutation at the active green cone opsin in the gene array at

chromosome X, whereas it was also identified to cause blue cone monochromancy in which the mutation was identified in red/green cone hybrids (115,203,204). C203R is also associated with disruption of the cone mosaic and lower pigment density in the retina than normal (205). Mutation C187Y, at the homologous site in rhodopsin has been found to disrupt the protein folding and decrease its stability resulting in a severe and early onset form of RP (206).

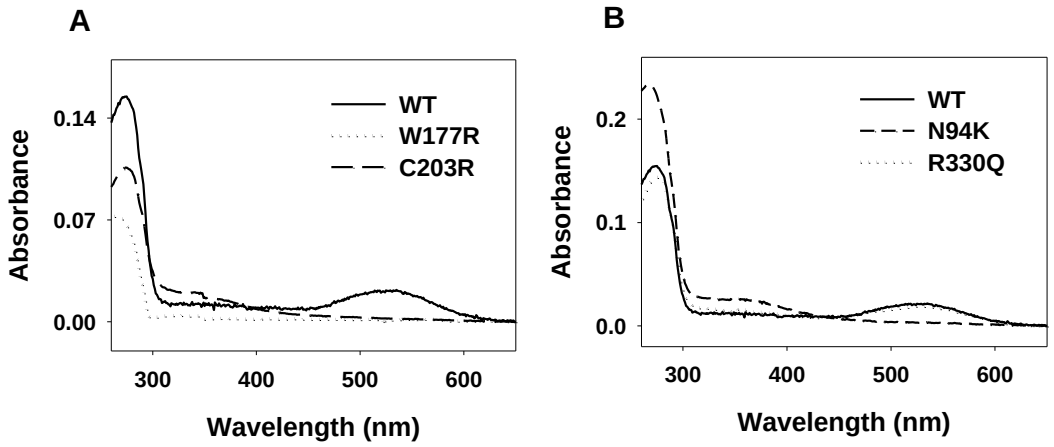

Figure 4.40. ***Expression of green cone opsin mutants.*** UV-Vis spectra of purified WT green cone pigment and its mutants, in the dark. The mutants were expressed in COS-1 cells, regenerated with 10μM 11CR. **(A)** Spectra of the mutants W177R and C203R with WT; and **(B)** spectra of the mutants N94K and R330Q with WT.

In the deutan mutant R247Ter, cytidine[1233] at exon 4 of the green cone opsin gene is converted to thymidine, which turns the amino acid position at 247 to a stop codon and hence the translated protein gets truncated after TM5 of the WT protein (119).

The observation of a clear band at 360 nm, led to think about the possibility of formation of an unprotonated Schiff base linkage with the protein by N94K. The protein band observed below 280 nm would suggest some potential aggregation of the mutant protein. R330Q, which shows regeneration at the visible region, and N94K have with its atypical absorbance band at 360 nm, were chosen in order to further analyze the structure-function differences exhibited by these mutants and to shed some light into the associated retinal dysfunction. In the case of the R330Q mutant, located at the C-terminal domain of the protein, it does not appear to alter protein expression, regeneration and purification.

Green N94K and green R330Q were identified as causing deutanopia and first studies showed that R330Q can regenerate with retinal and that N94K does not show any regeneration with the natural chromophore (114) but no detailed molecular characterization was performed. Now, it was aimed to carry out a detailed characterization of the spectral properties of these mutants.

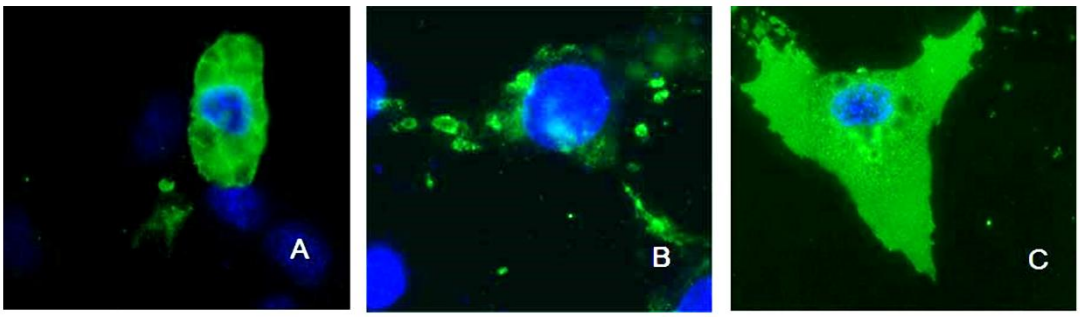

Figure 4.41. ***Localization of green cone mutants.*** Images from immunofluorescence of COS-cells transfected with green WT **(A)**, green N94K **(B)**, and green R330Q **(C)**. The transfected cells were subject to mouse rho-1D4 antibody as the primeray antibody (1:5,000) followed by goat anti-mouse tagged with FITC (1:200).

Fig. 4.41 shows pictures taken of WT, N94K and R330Q green cone pigment and their trafficking in COS-1 cells. The fluorescent images confirm the WT-like behavior of R330Q which is located to the plasma membrane, whereas opsin is being spread in the cell cytosol, and inclusion bodies can be detected for the N94K mutant.

4.4.3.1. Green N94K mutant

In order to examine the nature of the band at 360 nm of the purified N94K mutant of green cone pigment, by means of UV-vis spectrophotometer, a purified sample was measured in the dark and after acidification of the sample (Fig 4.42A). It shows a shift in the peak from 360 nm to 440 nm suggesting the presence of an unprotonated Schiff base linkage between retinal and the green opsin mutant. This was confirmed by plotting the difference spectra of the two spectra in Fig. 4.42A. The difference spectrum (Fig. 4.42B) shows a positive band at ~440 nm and a negative band around 360 nm which indicates that the pigment is clearly red shifted with acidification.

In spite of this Schiff base presence it is important to note that the opsin band suggests potential aggregation that would result from partial misfolding of the protein. The detailed study of the stability and regeneration ability of this mutant is presented in the next chapter this thesis.

4.4.3.2. Green R330Q mutant

Among all the mutants of cone pigments causing retinal disorders constructed and expessed, only green R330Q shows regeneration in the visible region. Therefore, it is of interest to further characterize this mutant because it can reveal the possible structure-function differences with the wild type green cone pigment resulting in receptor malfunction which could be linked to the molecular basis of the clinical condition.

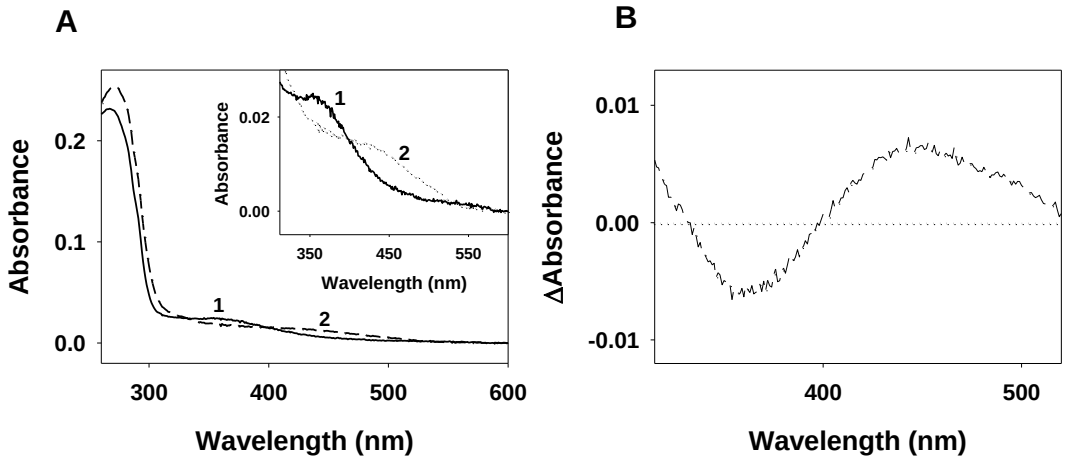

Figure 4.42. ***Characterization of green N94K.*** **(A)**The UV-Vis Spectra of purified Green N94K dark, which were expressed in COS-1 cells, regenerated with 10μM 11R, and acidified using 2N H_2SO_4 (***insest***,A) closer look at the visible region of the spectra distinctively showing the dark-state (1) and acidified state (2) of the mutant. A difference spectra was plotted by subtracting the time course absorbance of Green N94K acidified with Green N94K dark (B).

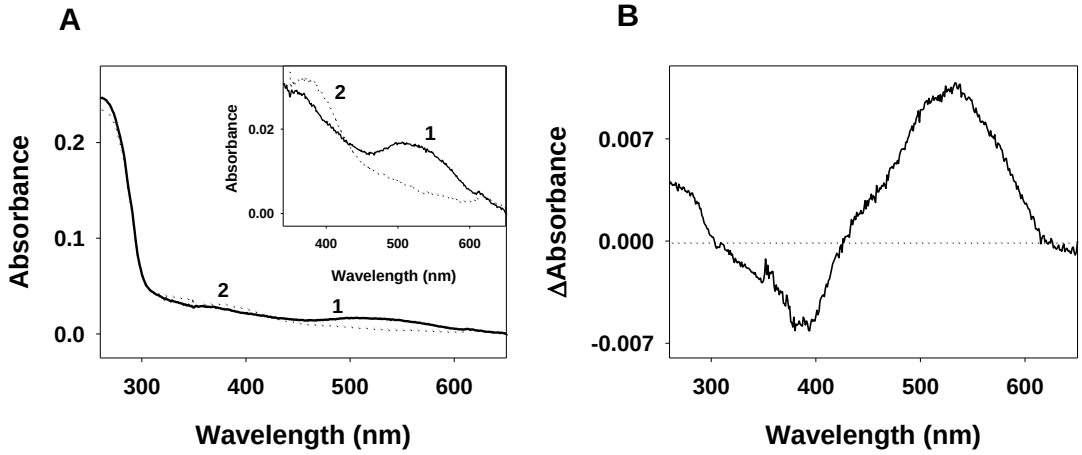

Figure 4.43. ***Characterization of green R330Q*****. (A)** The UV-Vis Spectra of purified green R330Q in the dark, which were expressed in COS-1 cells, regenerated with 10μM 11R, and illuminated (>495 nm). (***inset***, **A**) A closer look at the visible region showing the dark-state and illuminated state of the spectra. **(B)** A difference spectrum was obtained by subtracting the dark spectrum minus the illuminated spectrum of R330Q.

Expression and purification of green R330Q. Green R330Q mutant was expressed in COS-1 cellsand immunopurified in PBS buffer containing 0.05% DM. The dark state spectrum shows a band at 530 nm indicating that the mutant can regenerate with 11CR in the visible region unlike

other cone mutants tested. Illumination of the sample shifts the band to 380 nm (Fig 4.43A). A difference spectrum was obtained by subtracting the absorbance between illuminated and dark which clearly indicates the band at 530 nm (Fig 4.43B).

Meta II decay. The process of Meta II decay can be well studied by means of fluorescence spectroscopy. Similar to WT cone pigment, a Trp residue at the retinal binding site quenches the fluorescence of the retinal chromophore. Upon photoactivation, and as a result of retinal release, there will be an increase in the Trp fluorescence which can be recorded. The kinetics of this fluorescence increase reflects the Meta II decay process and subsequent retinal release. The purified green R330Q sample was illuminated after a stable baseline was obtained and the fluorescent changes were recorded. It showed a sudden increase in the fluorescence immediately after illumination similar to WT green cone pigment (Fig 4.44) suggesting a fast decay of the Meta II photointermediate.

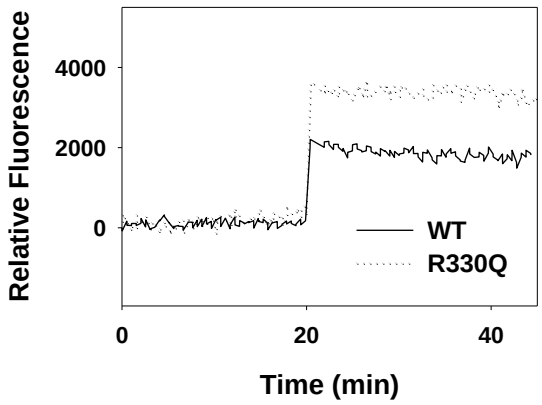

Figure 4.44. ***MetaII decay of green WT and green R330Q.*** Trp fluorescence was measured for green WT and green R330Q in the dark and after illumination (λ>495 nm).

Thermal stability. By measuring the behavior of the regenerated visual pigment at a given temperature, the stability of the protein can be determined which is on the correct folding and the thermodynamic properties of the visual pigments. Measuring the time taken for the complete decay of the chromophoric visible band and comparing it with the WT pigment would provide information on the effect of the introduced mutation on protein conformational stability. Green R330Q mutant thermal stability was measured by UV-Vis spectrophotometry at and compared with WT green cone opsin. The measured $t_{1/2}$ for R330Q thermal decay was 7.91± 0.32 min (Fig. 4.45A) which is similar to that of the WT green cone pigment (7.17± 0.98 min). This result confirms that the R330Q has the same thermal stability than WT and rules out important structural defects for the protein.

Chemical stability. The chemical reagent hydroxylamine, added in the dark, decreases the visible maximal absorbance. This is due to the more open retinal conformation in the binding pocket of cone opsins, when compared to rhodopsin, which leads to a more exposed SB linkage that can be broken and the retinal sequestered from the binding pocket. The half time obtained for this process was 38.65 ± 4.03 for green WT and 30.0 ± 1.72 from green R330Q mutant (Fig. 4.45B). This result suggests that the binding pocket of the R330Q mutant is more susceptible to hydroxylamine than green WT.

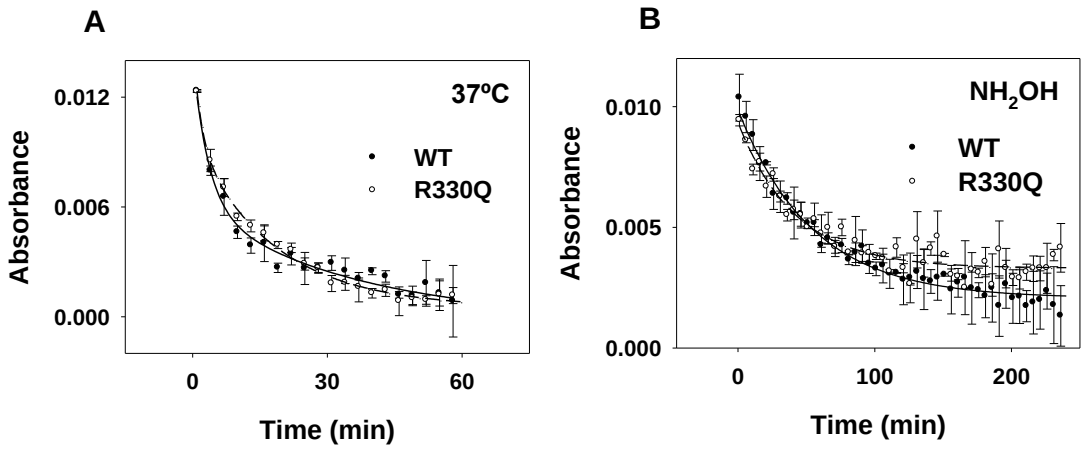

Figure 4.45. ***Thermal and chemical decay of green WT and green R330Q.*** Thermal stability assay was carried out at 37ºC with green WT and R330Q purified in DM. The plot showing the decrease of absorbance at the λmax in the visible region over time (A). Green WT and R330Q were treated with 50 mM hydroxylamine pH 7.0 at 20ºC for the chemical stability assay. (B) Chemical reagent stability was determined by monitoring the decrease at λmax over time.

Transducin activation. The functionality of the pigments was studied by testing their ability to activate rod transducin. To do this, a sample of green R330Q and WT were mixed with transducin and the activation was measured by means of a radioactive GTPγS^{35} assay before and after illumination. Upon illumination, there is a binding of transducin with R330Q pigment which is reduced when compared to WT green cone opsin (Fig 4.46). Thus the C-terminal mutant R330Q of green cone pigment presents impaired transducin binding which may cause deficiencies in green cone functionality and can help explain the resulting color blindness.

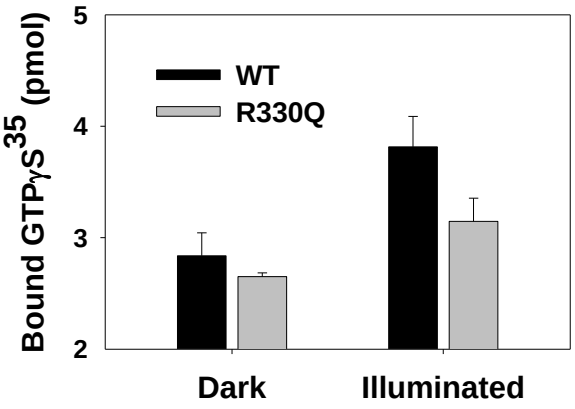

Figure 4.46. ***Transducin activation of green WT and green R330Q***. Functionality of green WT and R330Q mutant were determined by measuring bound $GTP\gamma S^{35}$ to an opsin-transducin complex in a radionuecleotide filter-bound assay. This was carried out with 300 nM green WT and R330Q in the dark and after illumination. The SD of the experiments is shown by error bars.

4.5. Strategies for stabilizing the deuteranopic N94K mutant

From the previous results section, it was identified that green N94K (which causes deuteranopia in humans), was shown to bind retinal by means of an unprotonated Schiff base linkage but the low protein yield, and a UV absorbance band for opsin shifted to 260 nm suggested an unstable conformation of the protein and possible aggregation. Therefore, providing a stable environment for the protein in solution would possibly keep the protein in an optimally folded state that could be used for further studies. Changes in buffers, the chemical nature of the chromophoric isomer of retinal, and introducing positive changes into the structure of the proteins are the key aspects to be considered in this section.

4.5.1. Purification of green N94K mutant using 9CR

Green cone opsin was expressed in COS-1 cells and the transfected cells were regenerated overnight with 50μM 9CR. The cell membrane was solubilized using DM and the protein was immunopurified using 1D4 antibody. The obtained sample was analyzed by UV-vis spectrophotometry. The resulting spectrum (Fig. 4.47) did not show any regenerated band in the visible region suggesting that there is no regeneration of green N94K with 9CR in the visible region, but it showed a smaller band around 380 nm which is similar to Green N94K purified with 11CR.

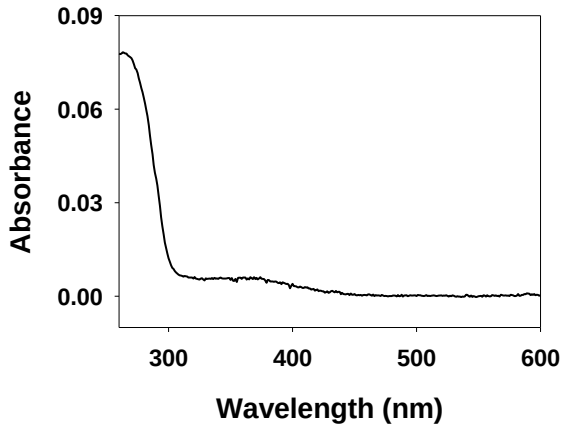

Figure 4.47. ***Green N94K purified with 9CR*****.** The UV-Vis Spectrum of purified Green N94K mutant in the dark, which was expressed in COS-1 cells and regenerated overnight with 50μM 9CR.

4.5.2. Effects of lipids on green N94K

The effective molecular characterization of membrane proteins can be achieved by studying them in a detergent-solubilized form, but this state compromises the stability of the proteins. The detergents used to solubilize biological membranes, form a micelle around protein thereby preserving the main structural and functional features of the membrane proteins. Membrane proteins are quite unstable in the micelles of detergent and denature during the course of time,

especially the mutants of integral membrane proteins which possess an altered conformation compared to the wild type. Moreover, the membrane-mimic support provided by the detergent micelles may expose certain surfaces of the protein which were previously buried into the lipid bilayer membrane, potentially leading to protein aggregation (207). Hence, it is known that membrane proteins can be successfully stabilized when reconstitute into lipid systems. We thought that this approach would increase the stability of the green N94K mutant and would help in its chromophore regeneration for subsequent characterization.

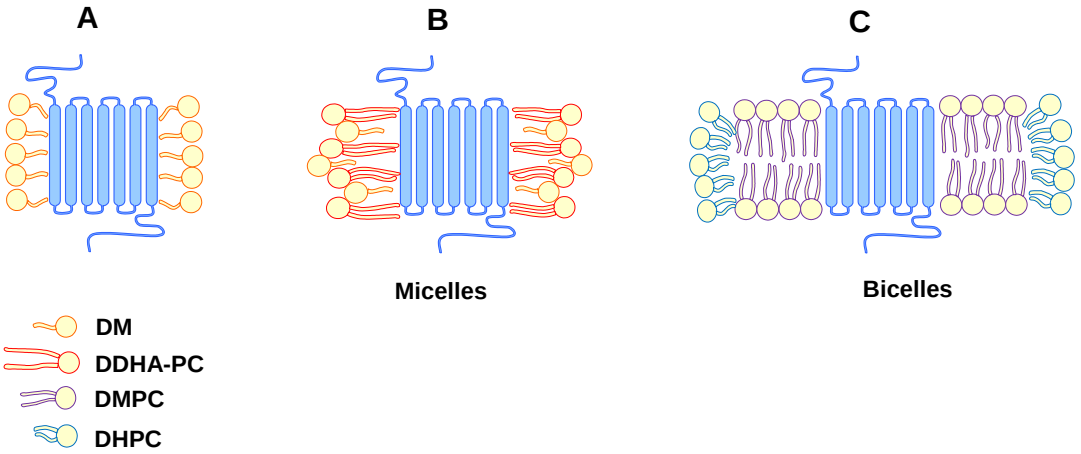

Figure 4.48. ***Schematic lipid environments in membrane proteins*****. (A)** The membrane protein was integrated into a micelle of DM. **(B)** Mixed micelles were formed by DDHA-PC and DM which would cover the hydrophobic transmemebrane helices of the receptor. **(C)** The protein was embedded into a bilayer of DMPC and capped by DHPC at the rim region, which is known as DMPC/DHPC bicelle.

Purification of green N94K regenerated with 11CR and 9CR in DDHA-PC / DM mixed micelles.

In general, the visual pigments are purified and stored in a buffer containing the mild neutral detergent DM. DM is a non-ionic detergent, which forms a micelle (Fig 4.48A.) around the protein (208,209). It is known that the retina is rich in docosahexaenoic acid (DHA), a specific lipid which has been proposed to interact directly with opsin visual pigments (210). In a previous study, 1, 2-didocosahexaenoyl-*sn*-glycero-3-phosphocholine (DDHA-PC) was reported to stabilize rhodopsin (157), and therefore the same strategy could be employed along with DM to form a mixed micelles which would provide an improved support for the membrane protein.

DDHA-PC was dissolved in chloroform ($CHCl_3$): methanol (CH_3OH) in 1:1 ratio, mixed well and the organic solved completely evaporated with nitrogen gas. To that 1 ml of PBS with 0.05% DM was added and sonicated for 1 min at 30% in order to break the DDHA-PC liposomes and enabling the formation of mixed micelles of DDHA-PC and DM (Fig 4.48B.).

COS-1 cells expressing the green N94K mutant were harvested and regenerated overnight with 11CR. The visual pigment was purified using 1D4-antibody. The protein bound Sepharose beads were washed using PBS containing mixed micelles and eluted into the same buffer containing the C'-terminal nonapeptide. The same protocol was carried out by regenerating the sample with 9CR. The purified sample was analyzed by UV-Vis spectrophotometry (Fig 4.49A) which shows that green N94K mutant fails to regenerate in the visible region with either retinal analog. A faint peak at 360 nm region was observed with the sample regenerated with 11CR, which is similar to the mutant purified in DM alone. Hence, the mixed micelles cannot promote chromophore regeneration for the mutant.

Purification of green WT and N94K in DMPC / DHPC bicelles

Bicelles are disc-like bilayer-mimic structures that are composed of a long tailed phospholipid such as 1,2-dihexanoyl-sn-glycero-3-phospho choline (DMPC) which assemble as bilayer surrounding the membrane protein and a short tailed phospholipids like, 1,2-dimhexanoyl-sn-glycero-3-phospho choline (DHPC) which orient as a rim to DMPC bilayer (Fig. 4.48C.). Because of their bilayer morphology, solubility in water, and likely to stabilize the protein in their optimal folding (207), bicelles have been employed in various studies from functional analysis like the one suggesting rhodopsin incorporated with bicelles show inproved functional efficiency with transducin (211) to crystallizing the membrane proteins (212).

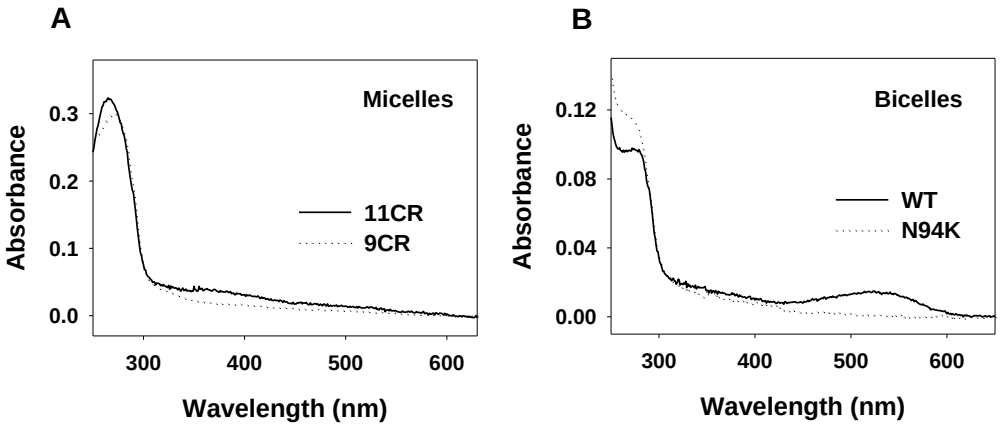

Figure 4.49. ***Effects of lipds on green N94K.*** **(A)** The UV-Vis spectra of purified green N94K mutant in the dark, which was expressed in COS-1 cells, regenerated overnight with 10μM 11R / 50μM of 9CR, and eluted in PBS containing DDHA-PC/DM mixed micelles. **(B)** Green WT and Green N94K were purified using DMPC:DHPC bicelles.

Green WT and N94K mutant were expressed in COS-1 cells and immunopurified using Sepharose-1D4 beads. The protein bound beads were washed using buffer A) added with 0.05%

DM and the purified pigments were eluted in 1:1; DMPC:DHPC bicelle mixture also containing 100μM nonapeptide (see Methods section). The measured UV-Vis Spectra of the purified pigments in bicelles show that the conformation of green N94K is not able regenerate with 11CR and thus bicelles are not able to improve the stability of the mutant *per se* the regeneration (Fig 4.49B). This finding suggests that the Lys introduced in the membrane imposes, without any counterion, a high energetic cost impairing optimal protein folding and visible chromophoric regeneration.

4.5.3. Co-transfection of green N94K with a rhodopsin triple mutant

Co-expression of a mutant together with WT would result in alterations in the folding, trafficking and behavior of each one (213,214). Rhodopsin is more stable than cone opsins in solution, so it is possible that formation of rhodopsin and cone opsin dimers (215) could improve the stability and regeneration of cone opsins. If both the receptors of opsin-dimer regenerate with 11CR, the regenerated peaks at UV-Vis would overlap which would question the significance of the experiment and hence it was decided to mutate the Lys of rhodopsin which binds the retinal molecule, i.e. K296. It is known that mutating the K296 of rhodopsin would affect the stability of the receptor. Therefore, the stable rhodopsin mutant N2C/N282C was used which is more stable even in the ligand free form (216). N2C/N282C/K296G mutations were introduced into rhodopsin which turns WT opsin into a very stable opsin structure which cannot covalently bind the retinal molecule.

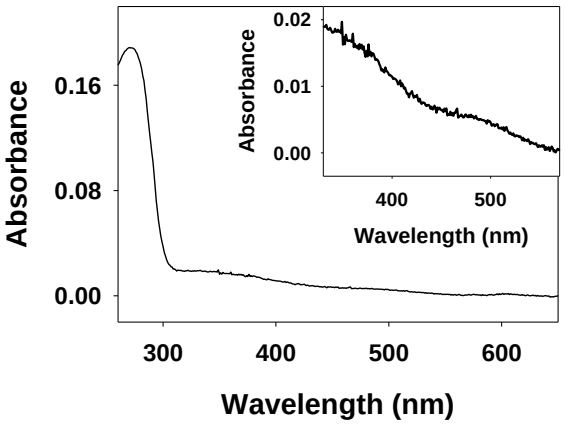

Figure 4.50 ***Green N94K co-transfected with a triple mutant of rhodopsin*****.** The UV-Vis Spectrum of purified Green N94K co-transfected with rhodopsin N2C/N282C/K296G in the dark, which was expressed in COS-1 cells and regenerated with 11CR. The inset shows the same spectrum at the wavelength from 350 nm-550 nm which was magnified.

This rhodopsin triple mutant was co-transfected with green N94K into COS-1 cells and the transfected cells were harvested after 48 h. The cells were regenerated with 10μM 11CR and the

pigments were immunopurified using Sepharose-1D4 beads in PBS with 0.05% DM. UV-Vis spectrum of the purified sample was measured (Fig 4.50) which shows that a distinct band around 360 nm which has been already noticed with the previous purification methods and also a less intense band in the 500 nm region (Fig 4.50 *inset*).

In order to identify the band at 500 nm, the rhodopsin triple mutant alone was expressed in COS-1 cells, harvested, and regenerated with 11CR and immunopurified. The purified sample was analyzed in a Spectrophotometer in dark and followed by the sample was illuminated. Interestingly, there was a shift in the absorbance from ~490 nm to ~374 nm upon illumination Fig 4.51A.) which can be clearly visualized from the difference spectrum between dark and illuminated states (Fig 4.51B). This result suggests that in a stable ligand free rhodopsin K296G mutant, still the retinal molecule can occupy the binding pocket which support the idea of covalent bond between the protein and retinal is not necessary for the activation of the visual pigment (217) and translocation of active-site Lys (218).

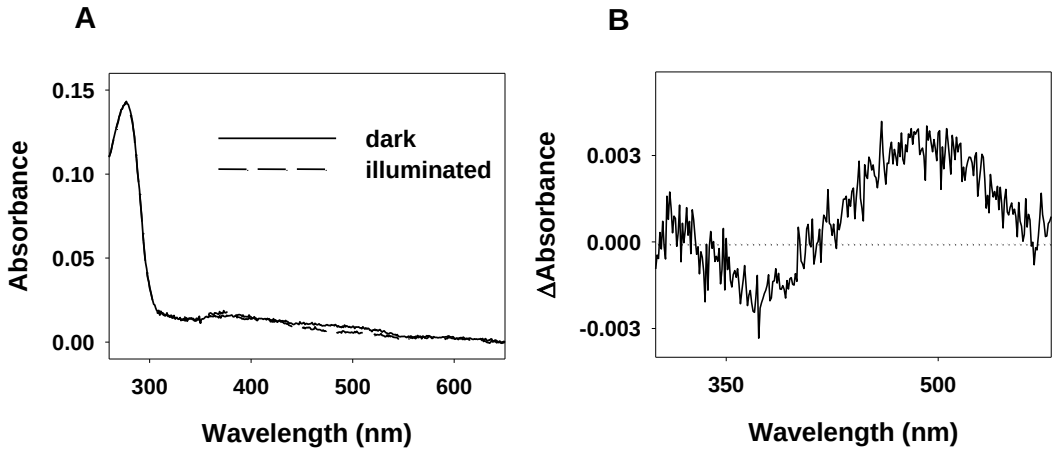

Figure 4.51. ***Rhodopsin triple mutant N2C/N282C/K296G*****. (A)** The UV-Vis Spectra of purified rhodopsin triple mutant in dark (solid line), and after illumination (λ> 495 nm) (dashed line). **(B)** Difference spectrum between the dark and illuminated rhodopsin triple mutant.

4.5.4. Expression of N94K introduced into a double Cys green mutant

One of the problems of cone pigments that complicates our understanding of cone opsins structure-function relationships, is their low stability in their purified form. Such intrinsic instability may affect structure-function relationship determinations for purified pigments during the course of time. Introducing Cys residues in membrane proteins at positions which are structurally closer enough to form disulfide linkages is an established approach for rhodopsin (216). This approach can be a good strategy to stabilize these membrane receptors and also to acquire further insights into their structure-function relationships. This system can facilitate the

study of the conformational alterations and molecular properties of opsin mutants associated with retinal dysfunctions.

Construction of a stable green cone pigment by introducing two Cys mutations

Using the theoretical model for green cone opsin, 1KPW (50) in PyMol molecular visualization system, the residues close to each other but distant in sequence were analyzed and the potential amino acids which can form disulfide linkage, when mutated to Cys, were identified. One of such pairs is W90 at TM2 and A169 at TM4 from the cytoplasmic domain of the receptor (green SS) (Figure 4.52).

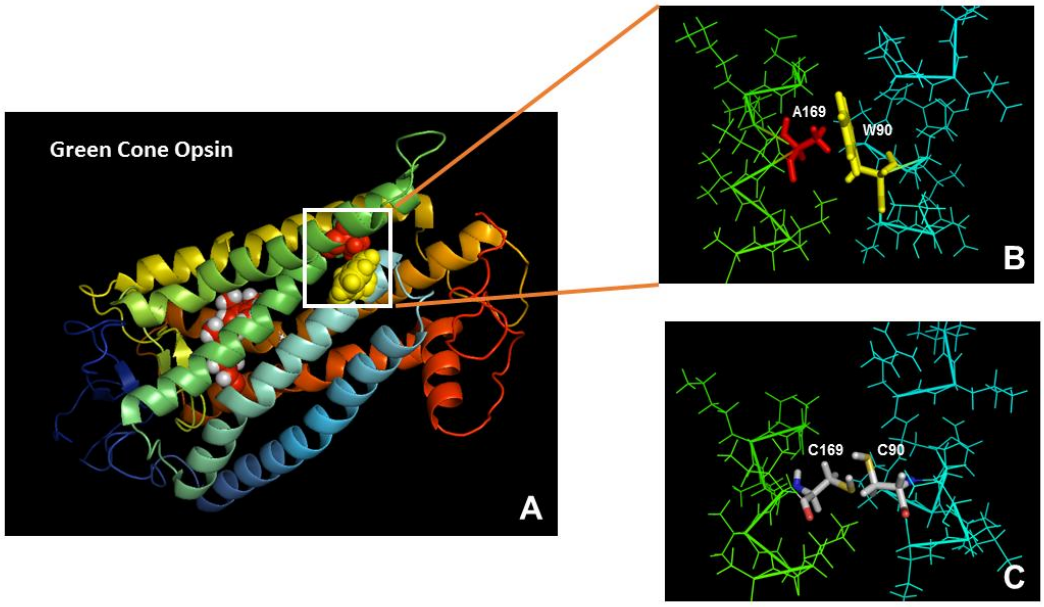

Figure 4.52. ***Green W90C/A169C model.*** Using PyMol, 1KPW, green cone pigment **(A)** was magnified at the C-terminal side around TM2 and TM4 showing W90 and A169 residues **(B)** which were mutated to Cys thus could form a disulfide linkage between W90C and A169C **(C).**

Expression of green SS

The green cone opsin double mutant (green SS) containing W90C and A169C was constructed by site directed mutagenesis of the green WT gene cloned into the pMT4 plasmid. The double mutant was sequenced in order to confirm the successful introduction of the mutations. The obtained sequence was aligned and the introduced mutations were validated (Fig 4.53A). Green SS was expressed and immunopurified as usual and the UV-vis spectrum measured. The UV-vis spectrum of the purified sample, in the dark, indicates that the double Cys mutant could successfully regenerate with 11CR showing the typical absorbance band at 530 nm. In addition some absorbance at 380 nm could be detected suggesting the presence of some amount of unprotonated Schiff base species. Acidification shifted the absorbance to 440 nm confirming the

presence of protonated Schiff Base species and reflecting a covalent linkage between the double Cys mutant opsin and 11CR (Figure 4.53B).

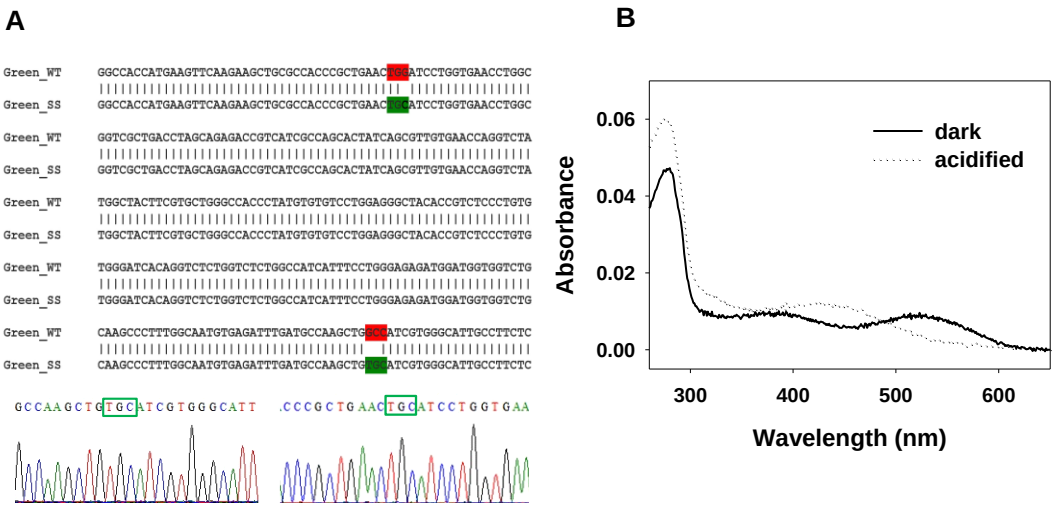

Figure 4.53. ***Mutagenesis of green cone opsin to introduce the double cysteines and expression*** **(A)** The sequence alignment of WT and SS confirming the introduction of Cys mutations. Using the primers containing the mutations for the W90C mutation, 5'CCCGCTGAACTGCATCCTGGTGAA3', 5'TTCACCAGGATGCAGTTCAGCGGG 3'; and for the A169C mutation, 5'GCCAAGCTGCATCG TGGGCATT3', 5'AATGCCCACGATGCAGCTTGG C3', green SS was constructed by a thermocyclic PCR method. The mutants were sequenced, the sequences aligned and the mutated codons were shown boxed. **(B)** Expression of green SS. Green SS gene was expressed in COS-1 cells, regenerated with 11CR and purified using Sepharose-1D4 beads. UV-Vis spectra of the protein were measured in the dark (solid line) and after acidification using 2N H_2SO_4 (dotted line).

Estimation of sulfhydryl groups

The actual presence of the disulfide bond could be confirmed by quantifying the free sulfhydryl groups that could be labeled in the protein (136). 5,5'-dithio-bis-(2-nitrobenzoic acid) or DTNB or Ellman's reagent reacts with free sulfhydrals at the periphery of the protein and produces a mixed disulfide with protein and a yellow colored TNB^{2-} (see methods) which can be measured at 412 nm (137).

Measuring the free sulfhydryl groups of green SS and comparing this number with that for green WT would confirm that the introduced Cys amino acids are involved in forming a disulfide bond. Equal concentrations of green WT and green SS were taken in duplicates and mixed separately with Ellman's reagent and incubated for 15 min. Absorbance at 412 nm was measured and the average was calculated. Using the following formula, the amount of free Cys amino acids present in green SS was calculated and compared with green WT.

$$c = \frac{A}{bE}$$

c - concentration of free sulfhydryls

A - Average of absorbance at 412 nm (green WT: 0.0135; green SS: 0.01705)

b - pathlength of the cuvette (1 cm)

E – Molar extinction coefficient of DTNB (14,150 $M^{-1}cm^{-1}$)

Free sulfhydryl groups in green WT:

$$c = \frac{0.0135}{(1)(14{,}150)}$$

$$= 9.54 \times 10^{-7}\ M$$

25 μl of green WT was added to total volume of 280 μl reaction mixture

$$\text{Therefore, } \frac{280}{25} \times 9.54 \times 10^{-7}\ M$$

$$= 10.6848\ \mu M$$

The concentration of free sulfhydryl groups in 25 μl of green WT is 10.6848 μM which accounts from two Cys residues present at the cytoplasmic side of the protein which are the ones that can be labeled only with the Ellman's reagent. The other Cys in opsin are not accessible to the reagent.

Free sulfhydryl groups in green SS:

$$c = \frac{0.01705}{(1)(14{,}150)}$$

$$= 1.2 \times 10^{-6}\ M$$

25 μl of Green SS was added to total volume of 280 μl reaction mixture

$$\text{Therefore, } \frac{280}{25} \times 1.2 \times 10^{-6}\ M$$

$$= 13.44\ \mu M$$

The concentration of free sulfhydral groups in 25 μl of green SS is 13.44 μM.

If the presence of two Cys residues in green WT accounts for 10.6848 μM free sulfhydryls, addition of two more Cys residues into the protein would result in double the concentration of sulfhydryls in green SS if this were not forming a disulfide bond. The concentration calculated, 13.44 μM, is merely 1.25 fold that of WT free sulfhydryl groups when it should be double. This

proves that W90C and A169C are forming a disulfide linkage between TM2 and TM4 of green cone opsin.

Thermal and chemical stability of green SS

The decay kinetics of green SS at 37ºC was measured and compared with that for green WT. This comparison can provide information about the stability of the helical structures favoring the optimal functionality of the protein. In order to do that, after measuring the dark spectra, green WT and green SS spectra were recorded at 37ºC continually every min until the complete decay of the sample was attained. The absorbance maximum at the visible region of each spectra was plotted and fit to an expontential decay curve (Fig. 4.54A.). Green WT follows a decay kinetics with a $t_{1/2}$ of 7.17±0.98 min whereas green SS shows a $t_{1/2}$ of 12.05±3.4 min. This suggests only a slight stabilization in the case of the double cysteine mutant.

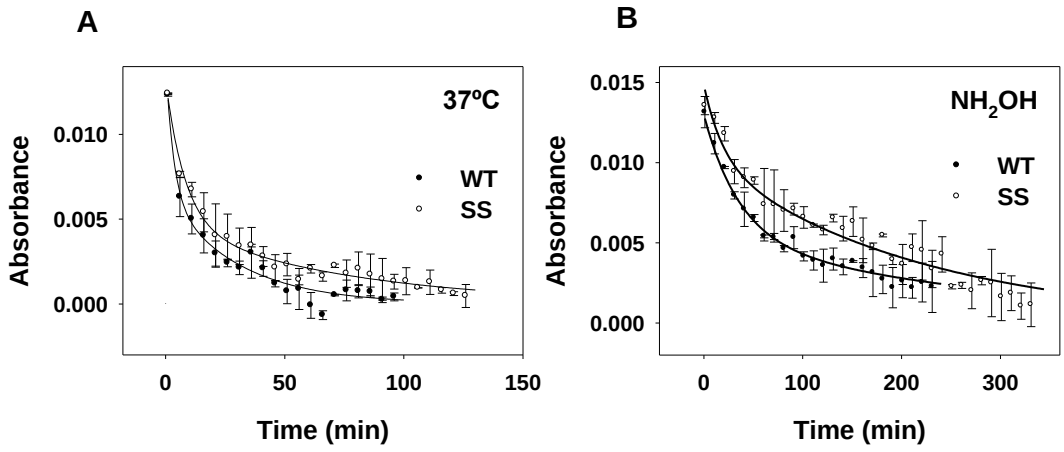

Figure 4.54. ***Thermal and chemical stability of green SS*****. (A)** Thermal stability assay was carried out at 37ºC with green WT and green SS in DM. Plot showing the decrease of absorbance at the λmax in the visible region over time. **(B)** Green WT and Green SS were treated with 50 mM hydroxylamine pH 7.0 at 20ºC for the chemical stability assay. Chemical reagent stability was determined by monitoring the decrease of λmax over time.

The binding pocket of cone opsins is more "open" or "flexible" than that of rhodopsin (148,200) allowing hydroxylamine to get into the binding pocket and react with retinal forming retinaloxime and shifting the absorbance to ~360 nm. After measuring the dark state spectra of green WT and green SS at room temperature, 50 μM hydroxylamine was added, mixed well and the spectra were recorded every min until the complete decay of the visible band could be attained. The kinetics of the chemical decay process was measured by plotting the absorbance maximum versus time (Fig. 4.54B). Interestingly, the $t_{1/2}$ of the hydroxylamine decay kinetics for green WT is 34.65± 4.03, and for green SS is 44.7±3.25. This shows that the disulfide bond introduced can

slightly increase the chemical stability of the chromophore. Therefore, green SS may be a good candidate to study the molecular properties of cone pigments as, biochemical and biophysical properties are similar, or even better, to those of green WT.

Green SS-N94K

After establishing that green SS binding pocket is stable, it would be interesting to introduce the N94K mutation into green SS and compare the results with green SS and green WT. Site directed mutagenesis was carried out using green SS as a template with N94K mutagenic primer. The resulting product was sequenced and the corresponding mutation was validated. Green SS-N94K gene was expressed in COS-1 cells. The transfected cells were harvested and regenerated with 11CR and immunopurified using 1D4-Sepharose beads. The purified sample was analyzed by means of UV-Vis spectrophotometry. The dark spectrum showed a similar behavior to that previously seen, with a band around 360 nm and a non-aggregated protein peak at 280 nm (Fig. 4.55). It suggests that N94K mutation at the TM2 of green cone opsin has an altered conformation which is very hard to revert.

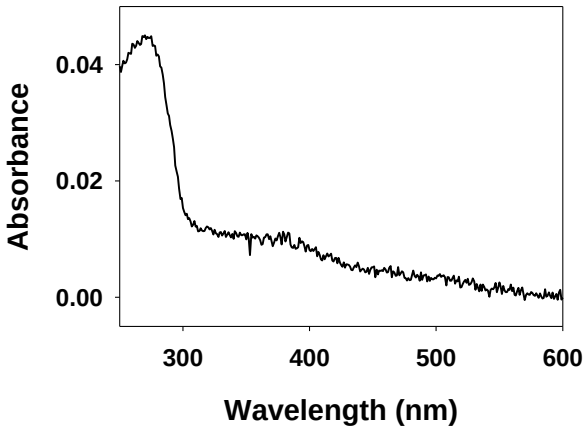

Figure 4.55. ***Expression of green SS-N94K.*** The UV-Vis Spectrum of purified Green SS-N94K in the dark, which was expressed in COS-1 cells and regenerated with 11CR.

4.5.5. Comparison of green cone N94K mutant with a sectoral Retinitis Pigmentosa (RP) mutant of rhodopsin

Retinitis Pigmentosa (RP) is a group of inherited heterogenous retinal degenerative diseases clinically characterized by progressive night blindness, visual field restriction, tunnel vision, and eventually complete blindness and they are prevalence in 1 in 4000 worldwide (219). Sectoral RP is an atypical form of RP, characterized by pigmented retinopathy and initially restricted to the

inferior quadrant of the retina and further progressive over time (147,220). Though several point mutations are known to cause such sectoral RP, N78I mutant of rhodopsin (Rho N78I) has been identified to cause sectoral RP and this mutation is located at the corresponding analogous position to that of N94K in the case of green cone opsin, $N^{2.45}$ of TM2 (221). Considering the structural instability of green N94K, comparing the molecular properties of rhodopsin N78I with green N94K may shed some light into the structural defects underlying the disease phenotype.

Rhodopsin N78I

Site directed mutagenesis was employed to introduce the N78I mutation into the pMT4 plasmid containing the rhodopsin gene. After validating the sequence of the N78I mutated gene, it was expressed into COS- cells using PEI transfection and incubated for 36-48 hrs. The transfected cells were harvested, regenerated with 11CR, solubilized with DM and immunopurified using rho-1D4-Sepharose beads. The purified sample was spectrally analyzed in the dark, and after illumination and acidification. The results showed that N78I can regenerate with 11CR at 500 nm similar to WT rhodopsin. The illuminated and acidified samples of rho N78I also behave as WT rhodopsin (Fig 4.56).

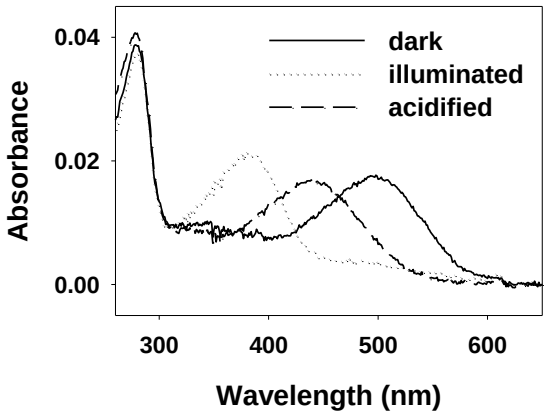

Figure 4.56. ***Characterization of rhodopsin N78I.*** The UV-Vis Spectrum of purified rhodopsin N78I in dark, which was expressed in COS-1 cells and regenerated with 11CR. The sample was illuminated (>495 nm) followed by acidification using 2N H_2SO_4.

Rhodopsin N78K

To the aim of comparing $N^{2.45}$ of rhodopsin and green cone opsin, and obtain further information it was decided to construct the mutant of rho N78K.

Using site directed mutagenesis, rho N78K was constructed and the sequence was validated. The mutant was transfected into COS-1 cells and regenerated with 11CR. The expressed rho N78K was immunopurified and the sample was spectrally analyzed. The dark state spectrum of the

sample consists of a peak at 360 nm which is similar to Green N94K and upon acidification the peak is shifted to 440 nm suggesting binding or 11CR to opsin by means of an unprotonated Schiff base linkage (Fig 4.57).

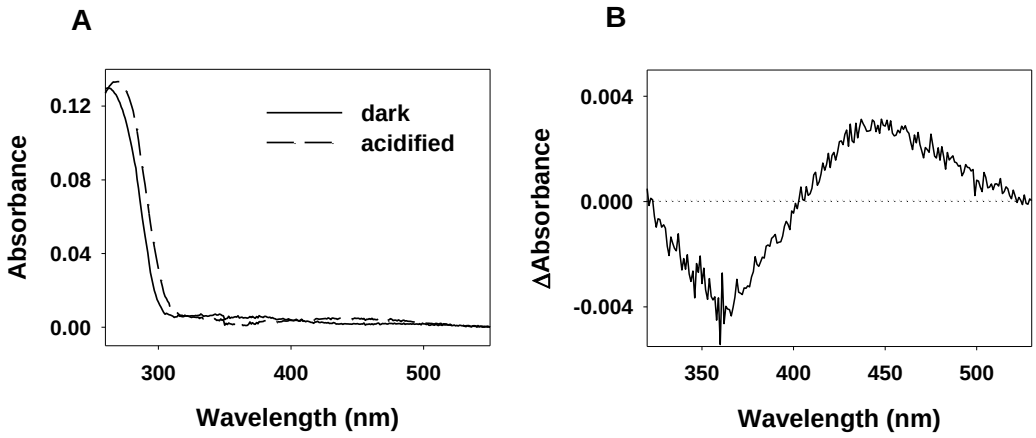

Figure 4.57. ***Characterization of Rhodopsin N78K.*** **(A)** The UV-Vis Spectra of purified rhodopsin mutant in dark (solid line), and acidified by 2N H_2SO_4 (dashed line). **(B)** Difference spectrum between the acidified - dark N78K rhodopsin.

It is worth noting that the Lys residue introduced may alter specific amino acid interactions disrupting the functional conformation of visual pigments around the region of $N^{2.45}$. In the case of a similar mutation in rhodopsin, N55K, also causing sectoral RP and located at TM1, the introduced Lys impairs the retinal release from the binding pocket of rhodopsin (147).

Overall, from the different experimental approaches undertaken in order to analyze the structural alterations behind the lack of chromophore regeneration for the N94K green mutant, it can be concluded that the lysine in green N94K encompasses a structural instability by the introduced Lys mutation which cannot be successfully compensated by any of these strategies. Further studies should be carried out in order to obtain more insights that can provide meaningful information that can be of therapeutic interest for cone opsin mutations associated with vision disorders.

5. GENERAL DISCUSSION

Rhodopsin is the most thoroughly studied GPCR and the first GPCR whose crystal structure was elucidated (48) which confirmed the basic structural features of the receptor shared by the diverse GPCR superfamily. Later, in the past eight years, various active and inactive conformations of GPCRS were determined by successive crystallizations and this lead to an important advance in our understanding of the mechanism of GPCR function, and the specific roles of individual amino acids (49,81,222). Among the ~700 identified members of the rhodopsin-like family of GPCRs, >20 of them have been crystalized and their structures have been solved at atomic resolution. These structures have been used as templates to study the behavior of other members of the GPCRs, from which, most of them could be of therapeutic interest (223-225). As the crystal structure of the cone pigments is yet to be resolved, identifying the key structural and functional features of these pigments (which are different from those of rhodopsin) should provide useful clues on the color vision process and would help in finding novel therapeutic strategies for congenital retinal disorders associated with cone dysfunction. In that aspect, the present study has determined novel molecular properties of these cone pigments by means of biochemical and biophysical methods. The current study also highlights key differences in the structural determinants of cone opsin function and regeneration which has been traditionally believed to be similar to that of rhodopsin.

Concerning the stability of opsins, it is commonly accepted that the ligand-free opsin species are highly unstable in solution, and the chromophore accessibility is questionable in the later phase of photoactivation. The fate of purified opsin after photoactivation was examined in a previous study (158) where the regeneration ability of photoactivated rhodopsin gets abolished with time and this effect was correlated with the stability of ligand-free opsin in detergent solution. The results of the present study are in agreement with the previous finding in a way because we find that 11CR is not able to regenerate with rhodopsin 90 min after photoactivation, but interestingly we observed that it can regenerate with 9CR under the same experimental conditions (Fig. 4.10). More interestingly, cone opsins which are believed to have a less stable opsin conformation than rhodopsin (chapter 1, results and discussion) can regenerate better than rhodopsin with both retinal analogs (Fig. 4.15). These findings lead to a reevaluation of the criteria on the stability of ligand-free opsin, particularly for cone opsins.

The structure-function relationships of the photoreceptor proteins from cone cells have been classically compared to those of rhodopsin, and only differences in spectral tuning have been proposed. Thus, the structure of rhodopsin served, until now, as a template for understanding the molecular mechanisms of cone opsins (50). Similarly, from part of the thesis, the regeneration process of photoactivated red cone opsin was compared to that of rhodopsin at a later phase after illumination, where the flexible red cone opsin regenerates with 11CR and 9CR, but rhodopsin appears to restrict the entry of 11CR. Red cone opsin was also compared with green cone opsin

for the regeneration process immediately after illumination. Intriguingly, different regeneration behavior was observed which has led to the proposal of different regeneration modes for the two highly homologous red and green cone opsins regenerating with both the analogs as mentioned above. These findings are schematically represented in Fig. 5.1 with a red cone opsin central model and attributing a more versatile conformational nature of red (and green) cone opsin conformation in the regeneration process when compared to rhodopsin.

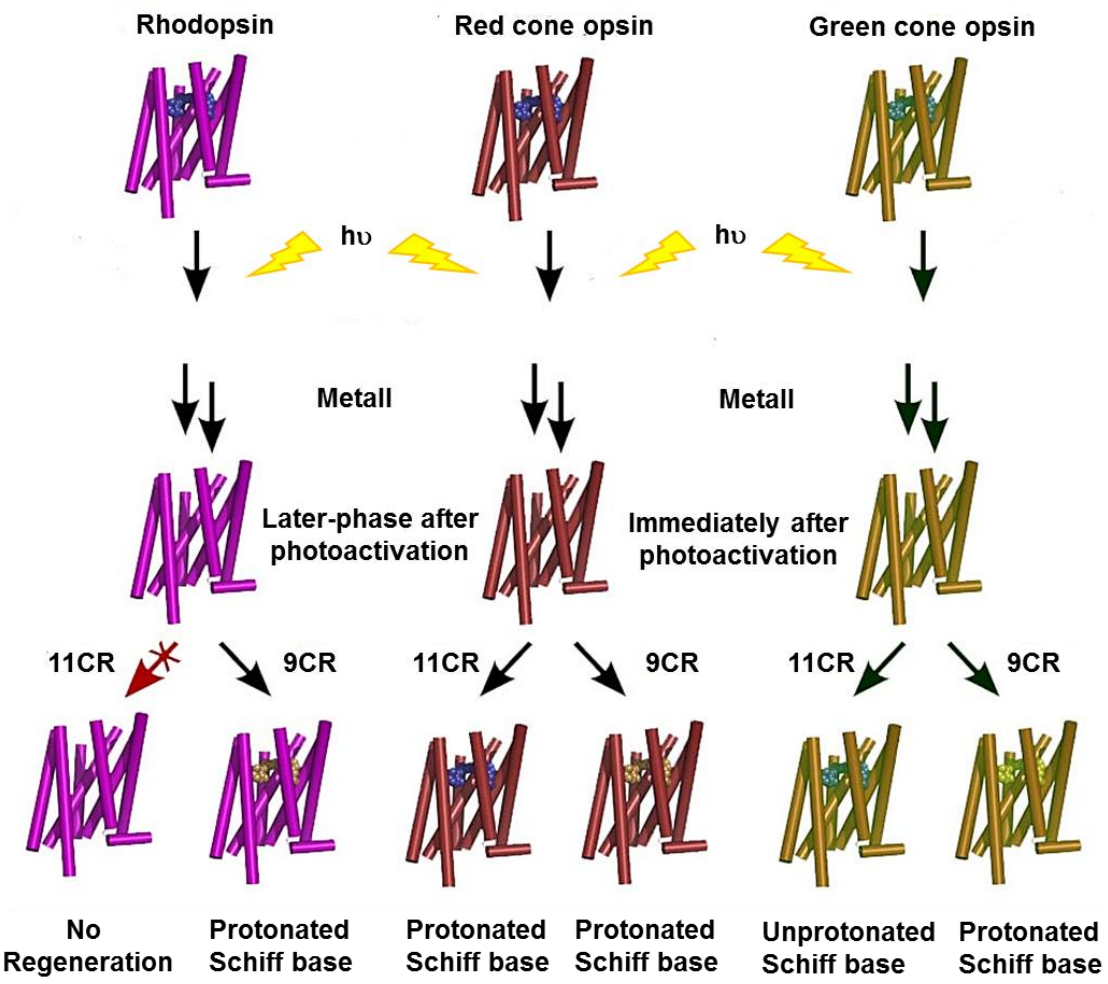

Figure 5.1. ***Schematic representation of regeneration of visual pigments with retinal analogs.*** The regeneration experiments with retinal analogs were carried out with rhodopsin and red cone opsin at a later phase of photoactivation suggesting the versatile nature of red cone opsin binding pocket. The same was compared between red and green cone opsins but immediately after illumination, reveal different retinal binding modes but the behavior of red cone opsin unaltered.

Leber's congenital amaurosis (LCA) is a group of retinal degenerative disorders, in which vision loss is associated with abolished 11CR synthesis but featuring relatively preserved retinal cells (226,227). QLT, an undisclosed 9-*cis*-retinoid analog, has been tested as a potential therapeutic

molecule for the clinical abnormalities associated with LCA (228). In the present study, it was also found that 9CR has better regeneration properties in various time-points after photoactivation as well as with all the visual pigments examined. These results are coherent with the view that 9CR, or chemically modified analogs of 9CR, could eventually be employed for the treatment of various visual disorders in which mutations impair chromophore regeneration of visual opsins.

A recent study has identified a proposed mechanism for conformational selection of retinal isomers by opsins (173). This study can be correlated with the present study in which the regeneration experiments performed with cone pigments and rhodopsin at immediately and later phase after photoactivation using 11CR and 9CR. We postulate that the fine-tuning mechanism mediated by the activated transient conformations (which are able to regenerate differently with different specific retinal analog) would depend on the complementary combination of accessibility and specificity of the chromophore towards a specific transient intermediate opsin conformation. This would provide a mechanistic, a possible functional, difference between the cone opsins and rhodopsin.

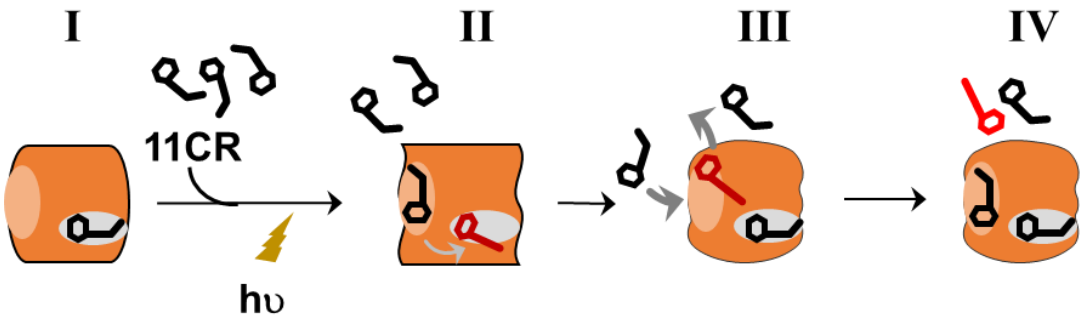

Figure 5.2. ***Molecular mechanism of chromophore regeneration in photoactivated cone opsins.*** The cone pigments heterologously expressed in mammalian cells are regenerated with 11CR and immunopurified (I). Exogenous 11CR is added in the dark, to the immunopurified regenerated sample, and the sample is subsequently illuminated. This causes the isomerization of opsin-bound 11CR to ATR resulting in a protein conformational change. This facilitates fast pre-binding of free 11CR to a secondary, lower affinity, retinal binding site followed by chomophore regeneration (II). Fast chromophore regeneration would be achieved by translocation and covalent binding of this pre-bound 11CR to the chromophoric binding pocket by displacing ATR which in turn would move out from the protein. Further, a secondary uptake of 11CR by the visual pigment, with a slower kinetics, may be associated with the conformational change of the regenerated protein coupled with the reduced availability of bulk 11CR that would synergistically decelerate 11CR binding to the secondary site (III). Under the experimental conditions of the present study this would lead, at this stage, to 11CR-regenerated visual pigment harboring an additional 11CR bound to the postulated secondary binding site (IV).

The molecular mechanism behind the transient conformation regenerating with 11CR is represented in the model depicted in Fig. 5.2. This secondary retinal uptake regeneration mechanism is not observed with 9CR in red/green cone pigments, but can be clearly identified in the case of blue cone opsin. This suggests that the secondary retinal uptake, by the photoactivated visual pigments, is not only modulated by the accessibility of the free retinal occupying the secondary site, but also to the specificity towards the functional groups of specific amino acids involved in ligand binding for the different opsins.

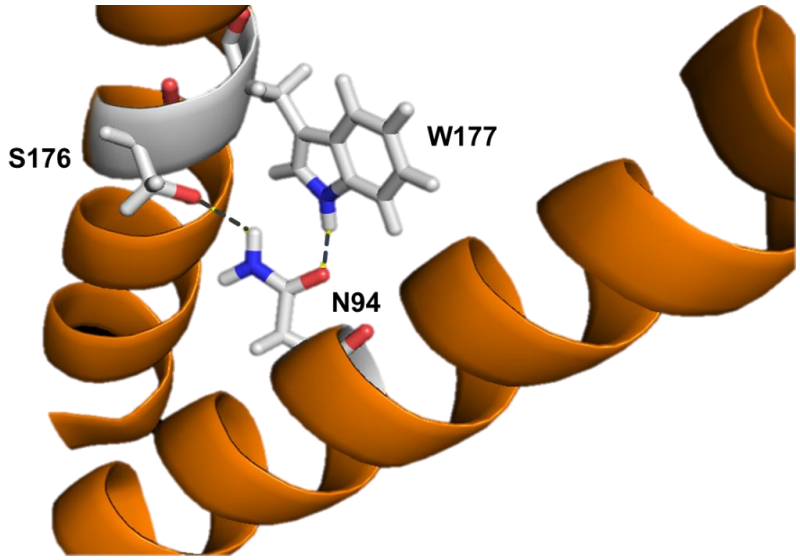

Figure 5.3. ***Interhelical interactions from green cone pigment.*** The interactions between S176, W177 and N94 was visualized using PyMOL showing a polar clamp hydrogen bonded network between TM2 and TM4. The hydrogen bonds are shown in dashed lines.

Molecular modeling of the native green cone pigment (Fig. 5.3) identified a polar clamp hydrogen bonded network between TM2 and TM4, formed by the residues $W177^{4.50}$, $S176^{4.49}$ and $N94^{2.45}$ where the OH of S176 hydrogen bonded with NH_2 of N94 and the C=O of N94 establishes a polar interaction with nitrogen from the indole ring of W177, similar to rhodopsin (229,230). $W^{4.50}$ is a highly conversed residue, among GPCRs, and the cytoplasmic ends of TM2 and TM4 diverge and TM3 penetrates towards TM5 enabling the counterion $E^{3.28}$ to position to the closer vicinity of the Schiff base by 3.5 Å for protonation (48,222). Disrupting the interhelical hydrogen bonding network which stabilizes the TM2 and TM4, may result in an unstable conformation. The role of $W177^{4.50}$ in the functional folding of green cone pigment has also been identified earlier (59). W177R mutation, in human green cone, causes protein misfolding and retention in endoplasmic reticulum, and purified mutant does not show any regeneration (Fig.4.40). This could be the underlying cause of degenerative cone dystrophy. The N94K may possibly disrupt

the polar interaction with W177 which may not as drastic as W177R (177 position is further away from the retinal binding site). Hence the Lys mutation destabilizing the optimal conformation of the green cone opsin with a structural alterations, either by steric hindrance exhibited by the bulkier functional group or by charged amino group polar contacting with neighboring residues. This may result in a shift of E129$^{3.28}$ counterion away from the Schiff base which could lead to an unprotonated Schiff base linkage.

6. CONCLUSIONS

The molecular investigation of human recombinant cone opsins, using various biochemical and biophysical approaches, unraveled novel molecular mechanisms underlying chromophore regeneration of these pigments. Clinically identified cone opsin mutants, associated with visual disorders have been characterized at the molecular level.

The main findings of the present study are:

General properties of human cone opsins

- The biophysical properties of human cone opsins, i.e. photoactivation, MetaII decay, thermal stability and hydroxylamine reactivity, have been compared with those of rhodopsin and confirm that cone opsins are less stable in solution and their retinal binding site is more accessible than that of rhodopsin.

- With regard to functional activity, cone opsins appear to activate rod transducin less efficiently, which would be consistent with the known physiological response for cone pigments.

Regeneration of red cone opsin compared with rhodopsin

- The constricted retinal binding site of rhodopsin (together with an inherently less-stable retinal binding pocket in the opsin conformation) restricts the entry of 11CR but permits the entry of 9CR into the retinal binding site a long time after photoactivation. In contrast, the flexible (and more stable in the opsin state) retinal binding site of red cone opsin is open to the entry of either retinal isomer.

- In red cone opsin, both retinals benefit from the interaction with W183$^{4.56}$ (lacking in rhodopsin), which favors the entry of 11CR and 9CR into the retinal binding site. However, 9CR interacts more favorably than 11CR with Y268/284$^{6.51}$ and W265/281$^{6.48}$. This would be justified by the stronger interaction energy acquired by the C-13 methyl group of 9CR from Y268 and W265, favoring the entry into the rhodopsin retinal binding site, which is lower in the case of the 11CR ligand.

- NaPi buffer improves the regeneration of rhodopsin by presumably favoring the oligomerization status of rhodopsin in detergent solution. This buffer lacks chloride (which is present in PBS buffer), and as chloride binding to opsin is important for the stability of cone opsins, these fail to regenerate with retinal when using NaPi buffer.

Mechanism of chromophore regeneration in red, green and blue cone opsins

- The photoactivated green cone opsin regenerates with 11CR via an unprotonated Schiff base linkage whereas red cone opsin forms a typical protonated Schiff base with its natural chromophore. It is possible that these two pigments regenerate with 9CR via a protonated Schiff base linkage.

- The lack of F309 hydrogen bonding with T201 in green cone opsin, and the fact that the Y309F mutant of green cone opsin can partially regenerate via a protonated Schiff base with 11CR, proves that these two highly homologous visual pigments adopt different transient intermediate conformations prior to dark adaptation.

- The retinal binding kinetics of red/green cone opsins is faster when compared to that of rhodopsin with both retinal analogs. Considering retinal entry into the protein, 11CR follows (unlike 9CR) a slow sigmoidal pattern which is in contrast to the faster retinal binding kinetics, suggesting a secondary retinal entry into photoactivated red/green cone opsins.

- In the case of blue cone opsin, the proposed secondary retinal uptake has been observed with both retinal analogs and 15 min after photoactivation. After this period of time, blue cone opsin loses the ability to bind 11CR to the secondary site but this is not the case with 9CR. This behavior would be due to the binding of 11CR to the canonical binding site of rhodopsin at a later phase after photoactivation.

Characterization of cone opsin mutants associated with visual dysfunction

- Most of the mutants of cone pigments which are associated with congenital visual disorders used in the present study fail to regenerate with retinal due to protein misfolding, defective trafficking and also aggregation of the corresponding apoproteins in solution.

- R330Q mutant of green cone opsin, causing deuteranopia in humans, is able to regenerate with 11CR. The characterization studies showed that the biochemical and biophysical properties of this mutant are similar to WT pigment except for an altered transducin activation ability.

- Another deuteranopic mutant, N94K shows a band at 360 nm which shifts to 440 nm upon acidification, suggesting the presence of unprotonated Schiff base binding of 11CR to the apoprotein with a compromised stability.

- Various stabilizing attempts performed with the N94K mutant include incorporating the mutant into micelles and bicelle environments, regenerating with retinal analogs, co-transfecting with a thermostable rhodopsin mutant, and introducing potentially stabilizing disulfide bonds. None of these attempts has been successful in stabilizing the opsin conformation so as to allow chromophore regeneration of the N94K mutant.

7. BIBLIOGRAPHY

1. Garrett, R. H., Grisham, C. H. (2013) *Biochemistry*, 5th ed., Brooks/Cole, Cengage Learning, Belmont, USA
2. Hanyaloglu, A. C., and von Zastrow, M. (2008) Regulation of GPCRs by endocytic membrane trafficking and its potential implications. *Annual review of pharmacology and toxicology* **48**, 537-568
3. Nelson, D., and Cox, M. (2005) *Lehninger Principles of Biochemistry* 4th ed., W.H. Freeman and Company, New York
4. Berg, J. M., Tymoczko, J. L., and Stryer, L. (2012) *Biochemistry*, W.H. Freeman, Basingstoke
5. Lodish, H., Berk, A., Kaiser, C. A., Krieger, M., Scott, M. P., Bretscher, A., Ploegh, H., Matsudaira, P. (2007) *Molecular Cell Biology*, 6th ed., W. H. Freeman and company
6. Lander, E. S., Linton, L. M., Birren, B., Nusbaum, C., Zody, M. C., Baldwin, J., Devon, K., Dewar, K., Doyle, M., FitzHugh, W., Funke, R., Gage, D., Harris, K., Heaford, A., Howland, J., Kann, L., Lehoczky, J., LeVine, R., McEwan, P., McKernan, K., Meldrim, J., Mesirov, J. P., Miranda, C., Morris, W., Naylor, J., Raymond, C., Rosetti, M., Santos, R., Sheridan, A., Sougnez, C., Stange-Thomann, N., Stojanovic, N., Subramanian, A., Wyman, D., Rogers, J., Sulston, J., Ainscough, R., Beck, S., Bentley, D., Burton, J., Clee, C., Carter, N., Coulson, A., Deadman, R., Deloukas, P., Dunham, A., Dunham, I., Durbin, R., French, L., Grafham, D., Gregory, S., Hubbard, T., Humphray, S., Hunt, A., Jones, M., Lloyd, C., McMurray, A., Matthews, L., Mercer, S., Milne, S., Mullikin, J. C., Mungall, A., Plumb, R., Ross, M., Shownkeen, R., Sims, S., Waterston, R. H., Wilson, R. K., Hillier, L. W., McPherson, J. D., Marra, M. A., Mardis, E. R., Fulton, L. A., Chinwalla, A. T., Pepin, K. H., Gish, W. R., Chissoe, S. L., Wendl, M. C., Delehaunty, K. D., Miner, T. L., Delehaunty, A., Kramer, J. B., Cook, L. L., Fulton, R. S., Johnson, D. L., Minx, P. J., Clifton, S. W., Hawkins, T., Branscomb, E., Predki, P., Richardson, P., Wenning, S., Slezak, T., Doggett, N., Cheng, J. F., Olsen, A., Lucas, S., Elkin, C., Uberbacher, E., Frazier, M., Gibbs, R. A., Muzny, D. M., Scherer, S. E., Bouck, J. B., Sodergren, E. J., Worley, K. C., Rives, C. M., Gorrell, J. H., Metzker, M. L., Naylor, S. L., Kucherlapati, R. S., Nelson, D. L., Weinstock, G. M., Sakaki, Y., Fujiyama, A., Hattori, M., Yada, T., Toyoda, A., Itoh, T., Kawagoe, C., Watanabe, H., Totoki, Y., Taylor, T., Weissenbach, J., Heilig, R., Saurin, W., Artiguenave, F., Brottier, P., Bruls, T., Pelletier, E., Robert, C., Wincker, P., Smith, D. R., Doucette-Stamm, L., Rubenfield, M., Weinstock, K., Lee, H. M., Dubois, J., Rosenthal, A., Platzer, M., Nyakatura, G., Taudien, S., Rump, A., Yang, H., Yu, J., Wang, J., Huang, G., Gu, J., Hood, L., Rowen, L., Madan, A., Qin, S., Davis, R. W., Federspiel, N. A., Abola, A. P., Proctor, M. J., Myers, R. M., Schmutz, J., Dickson, M., Grimwood, J., Cox, D. R., Olson, M. V., Kaul, R., Raymond, C., Shimizu, N., Kawasaki, K., Minoshima, S., Evans, G. A., Athanasiou,

M., Schultz, R., Roe, B. A., Chen, F., Pan, H., Ramser, J., Lehrach, H., Reinhardt, R., McCombie, W. R., de la Bastide, M., Dedhia, N., Blocker, H., Hornischer, K., Nordsiek, G., Agarwala, R., Aravind, L., Bailey, J. A., Bateman, A., Batzoglou, S., Birney, E., Bork, P., Brown, D. G., Burge, C. B., Cerutti, L., Chen, H. C., Church, D., Clamp, M., Copley, R. R., Doerks, T., Eddy, S. R., Eichler, E. E., Furey, T. S., Galagan, J., Gilbert, J. G., Harmon, C., Hayashizaki, Y., Haussler, D., Hermjakob, H., Hokamp, K., Jang, W., Johnson, L. S., Jones, T. A., Kasif, S., Kaspryzk, A., Kennedy, S., Kent, W. J., Kitts, P., Koonin, E. V., Korf, I., Kulp, D., Lancet, D., Lowe, T. M., McLysaght, A., Mikkelsen, T., Moran, J. V., Mulder, N., Pollara, V. J., Ponting, C. P., Schuler, G., Schultz, J., Slater, G., Smit, A. F., Stupka, E., Szustakowski, J., Thierry-Mieg, D., Thierry-Mieg, J., Wagner, L., Wallis, J., Wheeler, R., Williams, A., Wolf, Y. I., Wolfe, K. H., Yang, S. P., Yeh, R. F., Collins, F., Guyer, M. S., Peterson, J., Felsenfeld, A., Wetterstrand, K. A., Patrinos, A., Morgan, M. J., de Jong, P., Catanese, J. J., Osoegawa, K., Shizuya, H., Choi, S., Chen, Y. J., and International Human Genome Sequencing, C. (2001) Initial sequencing and analysis of the human genome. *Nature* **409**, 860-921

7. Fredriksson, R., Lagerstrom, M. C., Lundin, L. G., and Schioth, H. B. (2003) The G-protein-coupled receptors in the human genome form five main families. Phylogenetic analysis, paralogon groups, and fingerprints. *Molecular pharmacology* **63**, 1256-1272
8. Foord, S. M., Bonner, T. I., Neubig, R. R., Rosser, E. M., Pin, J. P., Davenport, A. P., Spedding, M., and Harmar, A. J. (2005) International Union of Pharmacology. XLVI. G protein-coupled receptor list. *Pharmacological reviews* **57**, 279-288
9. Gao, Q. B., and Wang, Z. Z. (2006) Classification of G-protein coupled receptors at four levels. *Protein engineering, design & selection : PEDS* **19**, 511-516
10. Kolakowski, L. F., Jr. (1994) GCRDb: a G-protein-coupled receptor database. *Receptors & channels* **2**, 1-7
11. Attwood, T. K., and Findlay, J. B. (1994) Fingerprinting G-protein-coupled receptors. *Protein engineering* **7**, 195-203
12. Wettschureck, N., and Offermanns, S. (2005) Mammalian G proteins and their cell type specific functions. *Physiological reviews* **85**, 1159-1204
13. Bockaert, J., and Pin, J. P. (1999) Molecular tinkering of G protein-coupled receptors: an evolutionary success. *The EMBO journal* **18**, 1723-1729
14. Harmar, A. J. (2001) Family-B G-protein-coupled receptors. *Genome biology* **2**, REVIEWS3013
15. Bazarsuren, A., Grauschopf, U., Wozny, M., Reusch, D., Hoffmann, E., Schaefer, W., Panzner, S., and Rudolph, R. (2002) In vitro folding, functional characterization, and disulfide pattern of the extracellular domain of human GLP-1 receptor. *Biophysical chemistry* **96**, 305-318

16. Bjarnadottir, T. K., Fredriksson, R., and Schioth, H. B. (2005) The gene repertoire and the common evolutionary history of glutamate, pheromone (V2R), taste(1) and other related G protein-coupled receptors. *Gene* **362**, 70-84
17. Kunishima, N., Shimada, Y., Tsuji, Y., Sato, T., Yamamoto, M., Kumasaka, T., Nakanishi, S., Jingami, H., and Morikawa, K. (2000) Structural basis of glutamate recognition by a dimeric metabotropic glutamate receptor. *Nature* **407**, 971-977
18. Bjarnadottir, T. K., Fredriksson, R., Hoglund, P. J., Gloriam, D. E., Lagerstrom, M. C., and Schioth, H. B. (2004) The human and mouse repertoire of the adhesion family of G-protein-coupled receptors. *Genomics* **84**, 23-33
19. Stacey, M., Lin, H. H., Gordon, S., and McKnight, A. J. (2000) LNB-TM7, a group of seven-transmembrane proteins related to family-B G-protein-coupled receptors. *Trends in biochemical sciences* **25**, 284-289
20. Lagerstrom, M. C., and Schioth, H. B. (2008) Structural diversity of G protein-coupled receptors and significance for drug discovery. *Nature reviews. Drug discovery* **7**, 339-357
21. Ballesteros, J. A., Weinstein, H. (1995) Integrated methods for the construction of three-dimensional models and computational probing of structure-function relations in G protein-coupled receptors. *Methods in Neurosciences* **25**, 366-428
22. Bowmaker, J. K. (2008) Evolution of vertebrate visual pigments. *Vision research* **48**, 2022-2041
23. Mustafi, D., Engel, A. H., and Palczewski, K. (2009) Structure of cone photoreceptors. *Progress in retinal and eye research* **28**, 289-302
24. Nickle, B., and Robinson, P. R. (2007) The opsins of the vertebrate retina: insights from structural, biochemical, and evolutionary studies. *Cellular and molecular life sciences : CMLS* **64**, 2917-2932
25. Shichida, Y., and Matsuyama, T. (2009) Evolution of opsins and phototransduction. *Philosophical transactions of the Royal Society of London. Series B, Biological sciences* **364**, 2881-2895
26. Kawamura, S., and Tachibanaki, S. (2008) Rod and cone photoreceptors: molecular basis of the difference in their physiology. *Comparative biochemistry and physiology. Part A, Molecular & integrative physiology* **150**, 369-377
27. Tachibanaki, S., Yonetsu, S., Fukaya, S., Koshitani, Y., and Kawamura, S. (2012) Low activation and fast inactivation of transducin in carp cones. *The Journal of biological chemistry* **287**, 41186-41194
28. Sharpe, L. T., Stockman A., Jägle H., Nathans J. (2001) Opsin genes, cone photopigments, color vision and color blindness. in *Color vision: From genes to perception.* (Gegenfurther, K. R., Sharpe, L. T. ed.), Cambridge University Press. pp

29. Hubbard, R., and Kropf, A. (1958) The Action of Light on Rhodopsin. *Proceedings of the National Academy of Sciences of the United States of America* **44**, 130-139
30. Jeon, C. J., Strettoi, E., and Masland, R. H. (1998) The major cell populations of the mouse retina. *The Journal of neuroscience : the official journal of the Society for Neuroscience* **18**, 8936-8946
31. Liang, Y., Fotiadis, D., Maeda, T., Maeda, A., Modzelewska, A., Filipek, S., Saperstein, D. A., Engel, A., and Palczewski, K. (2004) Rhodopsin signaling and organization in heterozygote rhodopsin knockout mice. *The Journal of biological chemistry* **279**, 48189-48196
32. Cunea, A., Begum, R., Reinisch, D., and Jeffery, G. (2013) Questioning photostasis. *Visual neuroscience* **30**, 169-174
33. Nathans, J., and Hogness, D. S. (1984) Isolation and nucleotide sequence of the gene encoding human rhodopsin. *Proceedings of the National Academy of Sciences of the United States of America* **81**, 4851-4855
34. Sampath, A. P., and Rieke, F. (2004) Selective transmission of single photon responses by saturation at the rod-to-rod bipolar synapse. *Neuron* **41**, 431-443
35. Palczewski, K. (2006) G protein-coupled receptor rhodopsin. *Annual review of biochemistry* **75**, 743-767
36. Wald, G., and Brown, P. K. (1953) The molar extinction of rhodopsin. *The Journal of general physiology* **37**, 189-200
37. Kim, J. E., Tauber, M. J., and Mathies, R. A. (2001) Wavelength dependent cis-trans isomerization in vision. *Biochemistry* **40**, 13774-13778
38. Dartnall, H. J. (1968) The photosensitivities of visual pigments in the presence of hydroxylamine. *Vision research* **8**, 339-358
39. Kandori, H., Katsuta, Y., Ito, M., and Sasabe, H. (1995) Femtosecond Fluorescence Study of the Rhodopsin Chromophore in Solution. *Journal of the American Chemical Society* **117**, 2669-2670
40. Hartridge, H. (1946) Colour receptors of the human fovea. *Nature* **158**, 97
41. Thomson, L. C., and Wright, W. D. (1947) The colour sensitivity of the retina within the central fovea of man. *The Journal of physiology* **105**, 316-331
42. Pearring, J. N., Salinas, R. Y., Baker, S. A., and Arshavsky, V. Y. (2013) Protein sorting, targeting and trafficking in photoreceptor cells. *Progress in retinal and eye research* **36**, 24-51
43. Hecht, S., Haig, C., and Chase, A. M. (1937) The Influence of Light Adaptation on Subsequent Dark Adaptation of the Eye. *The Journal of general physiology* **20**, 831-850
44. Deeb, S. S. (2005) The molecular basis of variation in human color vision. *Clinical genetics* **67**, 369-377

45. Nathans, J., Piantanida, T. P., Eddy, R. L., Shows, T. B., and Hogness, D. S. (1986) Molecular genetics of inherited variation in human color vision. *Science* **232**, 203-210
46. Nathans, J., Davenport, C. M., Maumenee, I. H., Lewis, R. A., Hejtmancik, J. F., Litt, M., Lovrien, E., Weleber, R., Bachynski, B., Zwas, F., and et al. (1989) Molecular genetics of human blue cone monochromacy. *Science* **245**, 831-838
47. Shichida, Y., and Imai, H. (1998) Visual pigment: G-protein-coupled receptor for light signals. *Cellular and molecular life sciences : CMLS* **54**, 1299-1315
48. Palczewski, K., Kumasaka, T., Hori, T., Behnke, C. A., Motoshima, H., Fox, B. A., Le Trong, I., Teller, D. C., Okada, T., Stenkamp, R. E., Yamamoto, M., and Miyano, M. (2000) Crystal structure of rhodopsin: A G protein-coupled receptor. *Science* **289**, 739-745
49. Park, J. H., Scheerer, P., Hofmann, K. P., Choe, H. W., and Ernst, O. P. (2008) Crystal structure of the ligand-free G-protein-coupled receptor opsin. *Nature* **454**, 183-187
50. Stenkamp, R. E., Filipek, S., Driessen, C. A., Teller, D. C., and Palczewski, K. (2002) Crystal structure of rhodopsin: a template for cone visual pigments and other G protein-coupled receptors. *Biochimica et biophysica acta* **1565**, 168-182
51. Unger, V. M., Hargrave, P. A., Baldwin, J. M., and Schertler, G. F. (1997) Arrangement of rhodopsin transmembrane alpha-helices. *Nature* **389**, 203-206
52. Deupi, X., and Standfuss, J. (2011) Structural insights into agonist-induced activation of G-protein-coupled receptors. *Current opinion in structural biology* **21**, 541-551
53. Hildebrand, P. W., Scheerer, P., Park, J. H., Choe, H. W., Piechnick, R., Ernst, O. P., Hofmann, K. P., and Heck, M. (2009) A ligand channel through the G protein coupled receptor opsin. *PloS one* **4**, e4382
54. Ballesteros, J. A., Jensen, A. D., Liapakis, G., Rasmussen, S. G., Shi, L., Gether, U., and Javitch, J. A. (2001) Activation of the beta 2-adrenergic receptor involves disruption of an ionic lock between the cytoplasmic ends of transmembrane segments 3 and 6. *The Journal of biological chemistry* **276**, 29171-29177
55. Fritze, O., Filipek, S., Kuksa, V., Palczewski, K., Hofmann, K. P., and Ernst, O. P. (2003) Role of the conserved NPxxY(x)5,6F motif in the rhodopsin ground state and during activation. *Proceedings of the National Academy of Sciences of the United States of America* **100**, 2290-2295
56. Hamamoto, A., Horikawa, M., Saho, T., and Saito, Y. (2012) Mutation of Phe318 within the NPxxY(x)(5,6)F motif in melanin-concentrating hormone receptor 1 results in an efficient signaling activity. *Frontiers in endocrinology* **3**, 147
57. Huynh, J., Thomas, W. G., Aguilar, M. I., and Pattenden, L. K. (2009) Role of helix 8 in G protein-coupled receptors based on structure-function studies on the type 1 angiotensin receptor. *Molecular and cellular endocrinology* **302**, 118-127

58. Ovchinnikov Yu, A., Abdulaev, N. G., and Bogachuk, A. S. (1988) Two adjacent cysteine residues in the C-terminal cytoplasmic fragment of bovine rhodopsin are palmitylated. *FEBS letters* **230**, 1-5

59. Gardner, J. C., Webb, T. R., Kanuga, N., Robson, A. G., Holder, G. E., Stockman, A., Ripamonti, C., Ebenezer, N. D., Ogun, O., Devery, S., Wright, G. A., Maher, E. R., Cheetham, M. E., Moore, A. T., Michaelides, M., and Hardcastle, A. J. (2010) X-linked cone dystrophy caused by mutation of the red and green cone opsins. *American journal of human genetics* **87**, 26-39

60. Farrens, D. L., and Khorana, H. G. (1995) Structure and function in rhodopsin. Measurement of the rate of metarhodopsin II decay by fluorescence spectroscopy. *The Journal of biological chemistry* **270**, 5073-5076

61. Schick, G. A., Cooper, T. M., Holloway, R. A., Murray, L. P., and Birge, R. R. (1987) Energy storage in the primary photochemical events of rhodopsin and isorhodopsin. *Biochemistry* **26**, 2556-2562

62. Harbison, G. S., Smith, S. O., Pardoen, J. A., Winkel, C., Lugtenburg, J., Herzfeld, J., Mathies, R., and Griffin, R. G. (1984) Dark-adapted bacteriorhodopsin contains 13-cis, 15-syn and all-trans, 15-anti retinal Schiff bases. *Proceedings of the National Academy of Sciences of the United States of America* **81**, 1706-1709

63. Fukada, Y., Kokame, K., Okano, T., Shichida, Y., Yoshizawa, T., McDowell, J. H., Hargrave, P. A., and Palczewski, K. (1990) Phosphorylation of iodopsin, chicken red-sensitive cone visual pigment. *Biochemistry* **29**, 10102-10106

64. Hubbard, R., and Wald, G. (1952) Cis-trans isomers of vitamin A and retinene in the rhodopsin system. *The Journal of general physiology* **36**, 269-315

65. Nakamichi, H., and Okada, T. (2007) X-ray crystallographic analysis of 9-cis-rhodopsin, a model analogue visual pigment. *Photochemistry and photobiology* **83**, 232-235

66. Hoersch, D., Otto, H., Wallat, I., and Heyn, M. P. (2008) Monitoring the conformational changes of photoactivated rhodopsin from microseconds to seconds by transient fluorescence spectroscopy. *Biochemistry* **47**, 11518-11527

67. Sekharan, S., and Morokuma, K. (2011) Why 11-cis-retinal? Why not 7-cis-, 9-cis-, or 13-cis-retinal in the eye? *Journal of the American Chemical Society* **133**, 19052-19055

68. Kiser, P. D., Golczak, M., and Palczewski, K. (2014) Chemistry of the retinoid (visual) cycle. *Chemical reviews* **114**, 194-232

69. Travis, G. H., Golczak, M., Moise, A. R., and Palczewski, K. (2007) Diseases caused by defects in the visual cycle: retinoids as potential therapeutic agents. *Annual review of pharmacology and toxicology* **47**, 469-512

70. Young, R. W. (1967) The renewal of photoreceptor cell outer segments. *The Journal of cell biology* **33**, 61-72

71. Lyubarsky, A. L., Daniele, L. L., and Pugh, E. N., Jr. (2004) From candelas to photoisomerizations in the mouse eye by rhodopsin bleaching in situ and the light-rearing dependence of the major components of the mouse ERG. *Vision research* **44**, 3235-3251
72. Williams, D. S. (2002) Transport to the photoreceptor outer segment by myosin VIIa and kinesin II. *Vision research* **42**, 455-462
73. Avasthi, P., Watt, C. B., Williams, D. S., Le, Y. Z., Li, S., Chen, C. K., Marc, R. E., Frederick, J. M., and Baehr, W. (2009) Trafficking of membrane proteins to cone but not rod outer segments is dependent on heterotrimeric kinesin-II. *The Journal of neuroscience : the official journal of the Society for Neuroscience* **29**, 14287-14298
74. Tam, B. M., Moritz, O. L., Hurd, L. B., and Papermaster, D. S. (2000) Identification of an outer segment targeting signal in the COOH terminus of rhodopsin using transgenic Xenopus laevis. *The Journal of cell biology* **151**, 1369-1380
75. Corbit, K. C., Aanstad, P., Singla, V., Norman, A. R., Stainier, D. Y., and Reiter, J. F. (2005) Vertebrate Smoothened functions at the primary cilium. *Nature* **437**, 1018-1021
76. Bhowmick, R., Li, M., Sun, J., Baker, S. A., Insinna, C., and Besharse, J. C. (2009) Photoreceptor IFT complexes containing chaperones, guanylyl cyclase 1 and rhodopsin. *Traffic* **10**, 648-663
77. Pazour, G. J., Baker, S. A., Deane, J. A., Cole, D. G., Dickert, B. L., Rosenbaum, J. L., Witman, G. B., and Besharse, J. C. (2002) The intraflagellar transport protein, IFT88, is essential for vertebrate photoreceptor assembly and maintenance. *The Journal of cell biology* **157**, 103-113
78. Tena-Campos, M., Ramon, E., Rivera, D., Borroto-Escuela, D. O., Romero-Fernandez, W., Fuxe, K., and Garriga, P. (2014) G-protein-coupled receptors oligomerization: emerging signaling units and new opportunities for drug design. *Current protein & peptide science* **15**, 648-658
79. Fotiadis, D., Liang, Y., Filipek, S., Saperstein, D. A., Engel, A., and Palczewski, K. (2003) Atomic-force microscopy: Rhodopsin dimers in native disc membranes. *Nature* **421**, 127-128
80. Ruprecht, J. J., Mielke, T., Vogel, R., Villa, C., and Schertler, G. F. (2004) Electron crystallography reveals the structure of metarhodopsin I. *The EMBO journal* **23**, 3609-3620
81. Salom, D., Lodowski, D. T., Stenkamp, R. E., Le Trong, I., Golczak, M., Jastrzebska, B., Harris, T., Ballesteros, J. A., and Palczewski, K. (2006) Crystal structure of a photoactivated deprotonated intermediate of rhodopsin. *Proceedings of the National Academy of Sciences of the United States of America* **103**, 16123-16128

82. Dell'Orco, D., and Schmidt, H. (2008) Mesoscopic Monte Carlo simulations of stochastic encounters between photoactivated rhodopsin and transducin in disc membranes. *The journal of physical chemistry. B* **112**, 4419-4426
83. Jastrzebska, B., Ringler, P., Palczewski, K., and Engel, A. (2013) The rhodopsin-transducin complex houses two distinct rhodopsin molecules. *Journal of structural biology* **182**, 164-172
84. Jastrzebska, B., Orban, T., Golczak, M., Engel, A., and Palczewski, K. (2013) Asymmetry of the rhodopsin dimer in complex with transducin. *FASEB journal : official publication of the Federation of American Societies for Experimental Biology* **27**, 1572-1584
85. Gunkel, M., Schoneberg, J., Alkhaldi, W., Irsen, S., Noe, F., Kaupp, U. B., and Al-Amoudi, A. (2015) Higher-Order Architecture of Rhodopsin in Intact Photoreceptors and Its Implication for Phototransduction Kinetics. *Structure*
86. Hofmann, K. P., Scheerer, P., Hildebrand, P. W., Choe, H. W., Park, J. H., Heck, M., and Ernst, O. P. (2009) A G protein-coupled receptor at work: the rhodopsin model. *Trends in biochemical sciences* **34**, 540-552
87. Kakitani, H., Kakitani, T., Rodman, H., and Honig, B. (1985) On the mechanism of wavelength regulation in visual pigments. *Photochemistry and photobiology* **41**, 471-479
88. Loppnow, G. R., Barry, B. A., and Mathies, R. A. (1989) Why are blue visual pigments blue? A resonance Raman microprobe study. *Proceedings of the National Academy of Sciences of the United States of America* **86**, 1515-1518
89. Merbs, S. L., and Nathans, J. (1992) Absorption spectra of human cone pigments. *Nature* **356**, 433-435
90. Borhan, B., Souto, M. L., Imai, H., Shichida, Y., and Nakanishi, K. (2000) Movement of retinal along the visual transduction path. *Science* **288**, 2209-2212
91. Peters, K., Applebury, M. L., and Rentzepis, P. M. (1977) Primary photochemical event in vision: proton translocation. *Proceedings of the National Academy of Sciences of the United States of America* **74**, 3119-3123
92. Honig, B., Greenberg, A. D., Dinur, U., and Ebrey, T. G. (1976) Visual-pigment spectra: implications of the protonation of the retinal Schiff base. *Biochemistry* **15**, 4593-4599
93. Matthews, R. G., Hubbard, R., Brown, P. K., and Wald, G. (1963) Tautomeric Forms of Metarhodopsin. *The Journal of general physiology* **47**, 215-240
94. Zaitseva, E., Brown, M. F., and Vogel, R. (2010) Sequential rearrangement of interhelical networks upon rhodopsin activation in membranes: the Meta II(a) conformational substate. *Journal of the American Chemical Society* **132**, 4815-4821

95. Knierim, B., Hofmann, K. P., Ernst, O. P., and Hubbell, W. L. (2007) Sequence of late molecular events in the activation of rhodopsin. *Proceedings of the National Academy of Sciences of the United States of America* **104**, 20290-20295

96. Kubli-Garfias, C., Salazar-Salinas, K., Perez-Angel, E. C., and Seminario, J. M. (2011) Light activation of the isomerization and deprotonation of the protonated Schiff base retinal. *Journal of molecular modeling* **17**, 2539-2547

97. Downes, G. B., and Gautam, N. (1999) The G protein subunit gene families. *Genomics* **62**, 544-552

98. Burns, M. E., and Arshavsky, V. Y. (2005) Beyond counting photons: trials and trends in vertebrate visual transduction. *Neuron* **48**, 387-401

99. Peng, Y. W., Robishaw, J. D., Levine, M. A., and Yau, K. W. (1992) Retinal rods and cones have distinct G protein beta and gamma subunits. *Proceedings of the National Academy of Sciences of the United States of America* **89**, 10882-10886

100. Fung, B. K., Hurley, J. B., and Stryer, L. (1981) Flow of information in the light-triggered cyclic nucleotide cascade of vision. *Proceedings of the National Academy of Sciences of the United States of America* **78**, 152-156

101. Kolesnikov, A. V., Kisselev, O. G., and Kefalov, V. J. (2014) Signaling by Rod and Cone Photoreceptors: Opsin Properties, G-protein Assembly, and Mechanisms of Activation. in *G Protein Signaling Mechanisms in the Retina* (Martemyanov, K. A., and Sampath, A. P. eds.), Springer New York. pp 23-48

102. Heck, M., and Hofmann, K. P. (2001) Maximal rate and nucleotide dependence of rhodopsin-catalyzed transducin activation: initial rate analysis based on a double displacement mechanism. *The Journal of biological chemistry* **276**, 10000-10009

103. Burns, M. E., and Pugh, E. N., Jr. (2010) Lessons from photoreceptors: turning off g-protein signaling in living cells. *Physiology* **25**, 72-84

104. Pugh Jr, E. N., and Lamb, T. D. (2000) Chapter 5 Phototransduction in vertebrate rods and cones: Molecular mechanisms of amplification, recovery and light adaptation. in *Handbook of Biological Physics* (D.G. Stavenga, W. J. D., and Pugh, E. N. eds.), North-Holland. pp 183-255

105. Kefalov, V. J. (2012) Rod and cone visual pigments and phototransduction through pharmacological, genetic, and physiological approaches. *The Journal of biological chemistry* **287**, 1635-1641

106. Yokoyama, S., and Takenaka, N. (2005) Statistical and molecular analyses of evolutionary significance of red-green color vision and color blindness in vertebrates. *Molecular biology and evolution* **22**, 968-975

107. Yokoyama, S. (2008) Evolution of dim-light and color vision pigments. *Annual review of genomics and human genetics* **9**, 259-282

108. Sharpe, L. T., Stockman, A., Jagle, H., Knau, H., Klausen, G., Reitner, A., and Nathans, J. (1998) Red, green, and red-green hybrid pigments in the human retina: correlations between deduced protein sequences and psychophysically measured spectral sensitivities. *The Journal of neuroscience : the official journal of the Society for Neuroscience* **18**, 10053-10069

109. Gunther, K. L., Neitz, J., and Neitz, M. (2006) A novel mutation in the short-wavelength-sensitive cone pigment gene associated with a tritan color vision defect. *Visual neuroscience* **23**, 403-409

110. Weitz, C. J., Miyake, Y., Shinzato, K., Montag, E., Zrenner, E., Went, L. N., and Nathans, J. (1992) Human tritanopia associated with two amino acid substitutions in the blue-sensitive opsin. *American journal of human genetics* **50**, 498-507

111. Weitz, C. J., Went, L. N., and Nathans, J. (1992) Human tritanopia associated with a third amino acid substitution in the blue-sensitive visual pigment. *American journal of human genetics* **51**, 444-446

112. Baraas, R. C., Carroll, J., Gunther, K. L., Chung, M., Williams, D. R., Foster, D. H., and Neitz, M. (2007) Adaptive optics retinal imaging reveals S-cone dystrophy in tritan color-vision deficiency. *Journal of the Optical Society of America. A, Optics, image science, and vision* **24**, 1438-1447

113. Baraas, R. C., Hagen, L. A., Dees, E. W., and Neitz, M. (2012) Substitution of isoleucine for threonine at position 190 of S-opsin causes S-cone-function abnormalities. *Vision research* **73**, 1-9

114. Ueyama, H., Kuwayama, S., Imai, H., Tanabe, S., Oda, S., Nishida, Y., Wada, A., Shichida, Y., and Yamade, S. (2002) Novel missense mutations in red/green opsin genes in congenital color-vision deficiencies. *Biochemical and biophysical research communications* **294**, 205-209

115. Winderickx, J., Sanocki, E., Lindsey, D. T., Teller, D. Y., Motulsky, A. G., and Deeb, S. S. (1992) Defective colour vision associated with a missense mutation in the human green visual pigment gene. *Nature genetics* **1**, 251-256

116. Michaelides, M., Hardcastle, A. J., Hunt, D. M., and Moore, A. T. (2006) Progressive cone and cone-rod dystrophies: phenotypes and underlying molecular genetic basis. *Survey of ophthalmology* **51**, 232-258

117. Winderickx, J., Battisti, L., Hibiya, Y., Motulsky, A. G., and Deeb, S. S. (1993) Haplotype diversity in the human red and green opsin genes: evidence for frequent sequence exchange in exon 3. *Human molecular genetics* **2**, 1413-1421

118. Matsumoto, Y., Hiramatsu, C., Matsushita, Y., Ozawa, N., Ashino, R., Nakata, M., Kasagi, S., Di Fiore, A., Schaffner, C. M., Aureli, F., Melin, A. D., and Kawamura, S. (2014) Evolutionary renovation of L/M opsin polymorphism confers a fruit

discrimination advantage to ateline New World monkeys. *Molecular ecology* **23**, 1799-1812

119. Nathans, J., Maumenee, I. H., Zrenner, E., Sadowski, B., Sharpe, L. T., Lewis, R. A., Hansen, E., Rosenberg, T., Schwartz, M., Heckenlively, J. R., and et al. (1993) Genetic heterogeneity among blue-cone monochromats. *American journal of human genetics* **53**, 987-1000
120. Pattabhi, V., and Gautham, N. (2002) *Biophysics*, Alpha Science International
121. Wenk, M. R., and Fernandis, A. Z. (2007) *A Manual for Biochemistry Protocols*, World Scientific
122. Okano, T., Fukada, Y., Shichida, Y., and Yoshizawa, T. (1992) Photosensitivities of iodopsin and rhodopsins. *Photochemistry and photobiology* **56**, 995-1001
123. Shichida, Y., Imai, H., Imamoto, Y., Fukada, Y., and Yoshizawa, T. (1994) Is chicken green-sensitive cone visual pigment a rhodopsin-like pigment? A comparative study of the molecular properties between chicken green and rhodopsin. *Biochemistry* **33**, 9040-9044
124. Vought, B. W., Dukkipatti, A., Max, M., Knox, B. E., and Birge, R. R. (1999) Photochemistry of the primary event in short-wavelength visual opsins at low temperature. *Biochemistry* **38**, 11287-11297
125. Reyes-Alcaraz, A., Martinez-Archundia, M., Ramon, E., and Garriga, P. (2011) Salt effects on the conformational stability of the visual G-protein-coupled receptor rhodopsin. *Biophysical journal* **101**, 2798-2806
126. Chinen, A., Matsumoto, Y., and Kawamura, S. (2005) Spectral differentiation of blue opsins between phylogenetically close but ecologically distant goldfish and zebrafish. *The Journal of biological chemistry* **280**, 9460-9466
127. Toledo, D., Ramon, E., Aguila, M., Cordomi, A., Perez, J. J., Mendes, H. F., Cheetham, M. E., and Garriga, P. (2011) Molecular mechanisms of disease for mutations at Gly-90 in rhodopsin. *The Journal of biological chemistry* **286**, 39993-40001
128. Sakmar, T. P., Franke, R. R., and Khorana, H. G. (1991) The role of the retinylidene Schiff base counterion in rhodopsin in determining wavelength absorbance and Schiff base pKa. *Proceedings of the National Academy of Sciences of the United States of America* **88**, 3079-3083
129. Koch, K. W. (2000) Identification and characterization of calmodulin binding sites in cGMP-gated channel using surface plasmon resonance spectroscopy. *Methods in enzymology* **315**, 785-797
130. Komolov, K. E., Senin, II, Philippov, P. P., and Koch, K. W. (2006) Surface plasmon resonance study of g protein/receptor coupling in a lipid bilayer-free system. *Analytical chemistry* **78**, 1228-1234

131. Schagger, H., and von Jagow, G. (1991) Blue native electrophoresis for isolation of membrane protein complexes in enzymatically active form. *Analytical biochemistry* **199**, 223-231

132. Wittig, I., Braun, H. P., and Schagger, H. (2006) Blue native PAGE. *Nature protocols* **1**, 418-428

133. Reeves, P. J., Kim, J. M., and Khorana, H. G. (2002) Structure and function in rhodopsin: a tetracycline-inducible system in stable mammalian cell lines for high-level expression of opsin mutants. *Proceedings of the National Academy of Sciences of the United States of America* **99**, 13413-13418

134. Laemmli, U. K. (1970) Cleavage of structural proteins during the assembly of the head of bacteriophage T4. *Nature* **227**, 680-685

135. Fukada, Y., Matsuda, T., Kokame, K., Takao, T., Shimonishi, Y., Akino, T., and Yoshizawa, T. (1994) Effects of carboxyl methylation of photoreceptor G protein gamma-subunit in visual transduction. *The Journal of biological chemistry* **269**, 5163-5170

136. Simpson, R. J. (2008) Estimation of Free Thiols and Disulfide Bonds Using Ellman's Reagent. *CSH protocols* **2008**, pdb prot4699

137. Ellman, G. L. (1959) Tissue sulfhydryl groups. *Archives of biochemistry and biophysics* **82**, 70-77

138. Reeves, P. J., Hwa, J., and Khorana, H. G. (1999) Structure and function in rhodopsin: kinetic studies of retinal binding to purified opsin mutants in defined phospholipid-detergent mixtures serve as probes of the retinal binding pocket. *Proceedings of the National Academy of Sciences of the United States of America* **96**, 1927-1931

139. Aho, A. C., Donner, K., Hyden, C., Larsen, L. O., and Reuter, T. (1988) Low retinal noise in animals with low body temperature allows high visual sensitivity. *Nature* **334**, 348-350

140. Barlow, R. B., Birge, R. R., Kaplan, E., and Tallent, J. R. (1993) On the molecular origin of photoreceptor noise. *Nature* **366**, 64-66

141. Birge, R. R., and Barlow, R. B. (1995) On the molecular origins of thermal noise in vertebrate and invertebrate photoreceptors. *Biophysical chemistry* **55**, 115-126

142. Liu, J., Liu, M. Y., Nguyen, J. B., Bhagat, A., Mooney, V., and Yan, E. C. (2011) Thermal properties of rhodopsin: insight into the molecular mechanism of dim-light vision. *The Journal of biological chemistry* **286**, 27622-27629

143. Janz, J. M., Fay, J. F., and Farrens, D. L. (2003) Stability of dark state rhodopsin is mediated by a conserved ion pair in intradiscal loop E-2. *The Journal of biological chemistry* **278**, 16982-16991

144. Barlow, H. B. (1957) Purkinje shift and retinal noise. *Nature* **179**, 255-256

145. Rieke, F., and Baylor, D. A. (2000) Origin and functional impact of dark noise in retinal cones. *Neuron* **26**, 181-186

146. Kawamura, S., and Yokoyama, S. (1998) Functional characterization of visual and nonvisual pigments of American chameleon (Anolis carolinensis). *Vision research* **38**, 37-44

147. Ramon, E., Cordomi, A., Aguila, M., Srinivasan, S., Dong, X., Moore, A. T., Webster, A. R., Cheetham, M. E., and Garriga, P. (2014) Differential Light-induced Responses in Sectorial Inherited Retinal Degeneration. *The Journal of biological chemistry* **289**, 35918-35928

148. Srinivasan, S., Ramon, E., Cordomi, A., and Garriga, P. (2014) Binding specificity of retinal analogs to photoactivated visual pigments suggest mechanism for fine-tuning GPCR-ligand interactions. *Chemistry & biology* **21**, 369-378

149. Imamoto, Y., Seki, I., Yamashita, T., and Shichida, Y. (2013) Efficiencies of activation of transducin by cone and rod visual pigments. *Biochemistry* **52**, 3010-3018

150. Heyse, S., Ernst, O. P., Dienes, Z., Hofmann, K. P., and Vogel, H. (1998) Incorporation of rhodopsin in laterally structured supported membranes: observation of transducin activation with spatially and time-resolved surface plasmon resonance. *Biochemistry* **37**, 507-522

151. Salamon, Z., Wang, Y., Brown, M. F., Macleod, H. A., and Tollin, G. (1994) Conformational changes in rhodopsin probed by surface plasmon resonance spectroscopy. *Biochemistry* **33**, 13706-13711

152. Komolov, K. E., Aguila, M., Toledo, D., Manyosa, J., Garriga, P., and Koch, K. W. (2010) On-chip photoactivation of heterologously expressed rhodopsin allows kinetic analysis of G-protein signaling by surface plasmon resonance spectroscopy. *Analytical and bioanalytical chemistry* **397**, 2967-2976

153. Toledo, D., Cordomi, A., Proietti, M. G., Benfatto, M., del Valle, L. J., Perez, J. J., Garriga, P., and Sepulcre, F. (2009) Structural characterization of a zinc high-affinity binding site in rhodopsin. *Photochemistry and photobiology* **85**, 479-484

154. Ramon, E., del Valle, L. J., and Garriga, P. (2003) Unusual thermal and conformational properties of the rhodopsin congenital night blindness mutant Thr-94 --> Ile. *The Journal of biological chemistry* **278**, 6427-6432

155. Chen, M. H., Kuemmel, C., Birge, R. R., and Knox, B. E. (2012) Rapid release of retinal from a cone visual pigment following photoactivation. *Biochemistry* **51**, 4117-4125

156. Estevez, M. E., Kolesnikov, A. V., Ala-Laurila, P., Crouch, R. K., Govardovskii, V. I., and Cornwall, M. C. (2009) The 9-methyl group of retinal is essential for rapid Meta II decay and phototransduction quenching in red cones. *The Journal of general physiology* **134**, 137-150

157. Sanchez-Martin, M. J., Ramon, E., Torrent-Burgues, J., and Garriga, P. (2013) Improved conformational stability of the visual G protein-coupled receptor rhodopsin by specific interaction with docosahexaenoic acid phospholipid. *Chembiochem : a European journal of chemical biology* **14**, 639-644

158. Sakamoto, T., and Khorana, H. G. (1995) Structure and function in rhodopsin: the fate of opsin formed upon the decay of light-activated metarhodopsin II in vitro. *Proceedings of the National Academy of Sciences of the United States of America* **92**, 249-253

159. Li, J., Edwards, P. C., Burghammer, M., Villa, C., and Schertler, G. F. X. (2004) Structure of bovine rhodopsin in a trigonal crystal form. *J. Mol. Biol.* **343**, 1409-1438

160. Scheerer, P., Park, J. H., Hildebrand, P. W., Kim, Y. J., Krauss, N., Choe, H. W., Hofmann, K. P., and Ernst, O. P. (2008) Crystal structure of opsin in its G-protein-interacting conformation. *Nature* **455**, 497-502

161. Murakami, M., and Kouyama, T. (2008) Crystal structure of squid rhodopsin. *Nature* **453**, 363-367

162. Murakami, M., and Kouyama, T. (2011) Crystallographic analysis of the primary photochemical reaction of squid rhodopsin. *Journal of molecular biology* **413**, 615-627

163. Nakayama, T. A., Zhang, W., Cowan, A., and Kung, M. (1998) Mutagenesis studies of human red opsin: trp-281 is essential for proper folding and protein-retinal interactions. *Biochemistry* **37**, 17487-17494

164. Cordomi, A., Gomez-Tamayo, J. C., Gigoux, V., and Fourmy, D. (2013) Sulfur-containing amino acids in 7TMRs: molecular gears for pharmacology and function. *Trends in pharmacological sciences* **34**, 320-331

165. Ganter, U. M., Schmid, E. D., Perez-Sala, D., Rando, R. R., and Siebert, F. (1989) Removal of the 9-methyl group of retinal inhibits signal transduction in the visual process. A Fourier transform infrared and biochemical investigation. *Biochemistry* **28**, 5954-5962

166. Das, J., Crouch, R. K., Ma, J. X., Oprian, D. D., and Kono, M. (2004) Role of the 9-methyl group of retinal in cone visual pigments. *Biochemistry* **43**, 5532-5538

167. Jager, S., Palczewski, K., and Hofmann, K. P. (1996) Opsin/all-trans-retinal complex activates transducin by different mechanisms than photolyzed rhodopsin. *Biochemistry* **35**, 2901-2908

168. Wang, Z., Asenjo, A. B., and Oprian, D. D. (1993) Identification of the Cl(-)-binding site in the human red and green color vision pigments. *Biochemistry* **32**, 2125-2130

169. Shukolyukov, S. A. (2009) Aggregation of frog rhodopsin to oligomers and their dissociation to monomer: application of BN- and SDS-PAGE. *Biochemistry. Biokhimiia* **74**, 599-604

170. Sekharan, S., Sugihara, M., and Buss, V. (2007) Origin of spectral tuning in rhodopsin--it is not the binding pocket. *Angewandte Chemie* **46**, 269-271

171. Okada, T., Fujiyoshi, Y., Silow, M., Navarro, J., Landau, E. M., and Shichida, Y. (2002) Functional role of internal water molecules in rhodopsin revealed by X-ray crystallography. *Proceedings of the National Academy of Sciences of the United States of America* **99**, 5982-5987

172. Blatz, P. E., and Liebman, P. A. (1973) Wavelength regulation in visual pigments. *Experimental eye research* **17**, 573-580

173. Schafer, C. T., and Farrens, D. L. (2015) Conformational selection and equilibrium governs the ability of retinals to bind opsin. *The Journal of biological chemistry* **290**, 4304-4318

174. Makino, C. L., Riley, C. K., Looney, J., Crouch, R. K., and Okada, T. (2010) Binding of more than one retinoid to visual opsins. *Biophysical journal* **99**, 2366-2373

175. Heck, M., Schadel, S. A., Maretzki, D., and Hofmann, K. P. (2003) Secondary binding sites of retinoids in opsin: characterization and role in regeneration. *Vision research* **43**, 3003-3010

176. Kefalov, V. J., Crouch, R. K., and Cornwall, M. C. (2001) Role of noncovalent binding of 11-cis-retinal to opsin in dark adaptation of rod and cone photoreceptors. *Neuron* **29**, 749-755

177. Tsybovsky, Y., Molday, R. S., and Palczewski, K. (2010) The ATP-binding cassette transporter ABCA4: structural and functional properties and role in retinal disease. *Advances in experimental medicine and biology* **703**, 105-125

178. Maeda, A., Maeda, T., Sun, W., Zhang, H., Baehr, W., and Palczewski, K. (2007) Redundant and unique roles of retinol dehydrogenases in the mouse retina. *Proceedings of the National Academy of Sciences of the United States of America* **104**, 19565-19570

179. Lamb, T. D., and Pugh, E. N., Jr. (2004) Dark adaptation and the retinoid cycle of vision. *Progress in retinal and eye research* **23**, 307-380

180. Allikmets, R., Singh, N., Sun, H., Shroyer, N. F., Hutchinson, A., Chidambaram, A., Gerrard, B., Baird, L., Stauffer, D., Peiffer, A., Rattner, A., Smallwood, P., Li, Y., Anderson, K. L., Lewis, R. A., Nathans, J., Leppert, M., Dean, M., and Lupski, J. R. (1997) A photoreceptor cell-specific ATP-binding transporter gene (ABCR) is mutated in recessive Stargardt macular dystrophy. *Nature genetics* **15**, 236-246

181. Chen, Y., Ratnam, K., Sundquist, S. M., Lujan, B., Ayyagari, R., Gudiseva, V. H., Roorda, A., and Duncan, J. L. (2011) Cone photoreceptor abnormalities correlate with vision loss in patients with Stargardt disease. *Investigative ophthalmology & visual science* **52**, 3281-3292

182. Molday, R. S. (2007) ATP-binding cassette transporter ABCA4: molecular properties and role in vision and macular degeneration. *Journal of bioenergetics and biomembranes* **39**, 507-517

183. Malmerberg, E., PH, M. B.-G., Katona, G., Deupi, X., Arnlund, D., Wickstrand, C., Johansson, L. C., Westenhoff, S., Nazarenko, E., GF, X. S., Menzel, A., de Grip, W. J., and Neutze, R. (2015) Conformational activation of visual rhodopsin in native disc membranes. *Science signaling* **8**, ra26

184. Nathans, J., Thomas, D., and Hogness, D. S. (1986) Molecular genetics of human color vision: the genes encoding blue, green, and red pigments. *Science* **232**, 193-202

185. Shi, Y., Radlwimmer, F. B., and Yokoyama, S. (2001) Molecular genetics and the evolution of ultraviolet vision in vertebrates. *Proceedings of the National Academy of Sciences of the United States of America* **98**, 11731-11736

186. Takahashi, Y., and Yokoyama, S. (2005) Genetic basis of spectral tuning in the violet-sensitive visual pigment of African clawed frog, Xenopus laevis. *Genetics* **171**, 1153-1160

187. Parera, M., and Martinez, M. A. (2014) Strong epistatic interactions within a single protein. *Molecular biology and evolution* **31**, 1546-1553

188. Yokoyama, S., Xing, J., Liu, Y., Faggionato, D., Altun, A., and Starmer, W. T. (2014) Epistatic adaptive evolution of human color vision. *PLoS genetics* **10**, e1004884

189. Hughes, A. L. (2007) Looking for Darwin in all the wrong places: the misguided quest for positive selection at the nucleotide sequence level. *Heredity* **99**, 364-373

190. Kimura, M. (1983) *The Neutral Theory of Molecular Evolution*, Cambridge University Press: Cambridge

191. Hahn, M. W. (2008) Toward a selection theory of molecular evolution. *Evolution; international journal of organic evolution* **62**, 255-265

192. Golding, G. B., and Dean, A. M. (1998) The structural basis of molecular adaptation. *Molecular biology and evolution* **15**, 355-369

193. Cideciyan, A. V., Hood, D. C., Huang, Y., Banin, E., Li, Z. Y., Stone, E. M., Milam, A. H., and Jacobson, S. G. (1998) Disease sequence from mutant rhodopsin allele to rod and cone photoreceptor degeneration in man. *Proceedings of the National Academy of Sciences of the United States of America* **95**, 7103-7108

194. Kaushal, S., and Khorana, H. G. (1994) Structure and function in rhodopsin. 7. Point mutations associated with autosomal dominant retinitis pigmentosa. *Biochemistry* **33**, 6121-6128

195. McKeone, R., Wikstrom, M., Kiel, C., and Rakoczy, P. E. (2014) Assessing the correlation between mutant rhodopsin stability and the severity of retinitis pigmentosa. *Molecular vision* **20**, 183-199

196. Yokoyama, S., Yang, H., and Starmer, W. T. (2008) Molecular basis of spectral tuning in the red- and green-sensitive (M/LWS) pigments in vertebrates. *Genetics* **179**, 2037-2043

197. Neitz, M., and Neitz, J. (2000) Molecular genetics of color vision and color vision defects. *Archives of ophthalmology* **118**, 691-700

198. Kawamura, S., Hirai, M., Takenaka, O., Radlwimmer, F. B., and Yokoyama, S. (2001) Genomic and spectral analyses of long to middle wavelength-sensitive visual pigments of common marmoset (Callithrix jacchus). *Gene* **269**, 45-51

199. Cideciyan, A. V., Hufnagel, R. B., Carroll, J., Sumaroka, A., Luo, X., Schwartz, S. B., Dubra, A., Land, M., Michaelides, M., Gardner, J. C., Hardcastle, A. J., Moore, A. T., Sisk, R. A., Ahmed, Z. M., Kohl, S., Wissinger, B., and Jacobson, S. G. (2013) Human cone visual pigment deletions spare sufficient photoreceptors to warrant gene therapy. *Human gene therapy* **24**, 993-1006

200. Ramon, E., Mao, X., and Ridge, K. D. (2009) Studies on the stability of the human cone visual pigments. *Photochemistry and photobiology* **85**, 509-516

201. Oprian, D. D., Asenjo, A. B., Lee, N., and Pelletier, S. L. (1991) Design, chemical synthesis, and expression of genes for the three human color vision pigments. *Biochemistry* **30**, 11367-11372

202. Strader, C. D., Fong, T. M., Tota, M. R., Underwood, D., and Dixon, R. A. (1994) Structure and function of G protein-coupled receptors. *Annual review of biochemistry* **63**, 101-132

203. Jagla, W. M., Jagle, H., Hayashi, T., Sharpe, L. T., and Deeb, S. S. (2002) The molecular basis of dichromatic color vision in males with multiple red and green visual pigment genes. *Human molecular genetics* **11**, 23-32

204. Reyniers, E., Van Thienen, M. N., Meire, F., De Boulle, K., Devries, K., Kestelijn, P., and Willems, P. J. (1995) Gene conversion between red and defective green opsin gene in blue cone monochromacy. *Genomics* **29**, 323-328

205. Carroll, J., Baraas, R. C., Wagner-Schuman, M., Rha, J., Siebe, C. A., Sloan, C., Tait, D. M., Thompson, S., Morgan, J. I., Neitz, J., Williams, D. R., Foster, D. H., and Neitz, M. (2009) Cone photoreceptor mosaic disruption associated with Cys203Arg mutation in the M-cone opsin. *Proceedings of the National Academy of Sciences of the United States of America* **106**, 20948-20953

206. Macke, J. P., Davenport, C. M., Jacobson, S. G., Hennessey, J. C., Gonzalez-Fernandez, F., Conway, B. P., Heckenlively, J., Palmer, R., Maumenee, I. H., Sieving, P., and et al. (1993) Identification of novel rhodopsin mutations responsible for retinitis pigmentosa: implications for the structure and function of rhodopsin. *American journal of human genetics* **53**, 80-89

207. McKibbin, C., Farmer, N. A., Jeans, C., Reeves, P. J., Khorana, H. G., Wallace, B. A., Edwards, P. C., Villa, C., and Booth, P. J. (2007) Opsin stability and folding: modulation by phospholipid bicelles. *Journal of molecular biology* **374**, 1319-1332

208. London, E., and Khorana, H. G. (1982) Denaturation and renaturation of bacteriorhodopsin in detergents and lipid-detergent mixtures. *The Journal of biological chemistry* **257**, 7003-7011

209. Ramon, E., Marron, J., del Valle, L., Bosch, L., Andres, A., Manyosa, J., and Garriga, P. (2003) Effect of dodecyl maltoside detergent on rhodopsin stability and function. *Vision research* **43**, 3055-3061

210. Mitchell, D. C., Niu, S. L., and Litman, B. J. (2003) Enhancement of G protein-coupled signaling by DHA phospholipids. *Lipids* **38**, 437-443

211. Kaya, A. I., Thaker, T. M., Preininger, A. M., Iverson, T. M., and Hamm, H. E. (2011) Coupling efficiency of rhodopsin and transducin in bicelles. *Biochemistry* **50**, 3193-3203

212. Ujwal, R., and Bowie, J. U. (2011) Crystallizing membrane proteins using lipidic bicelles. *Methods* **55**, 337-341

213. Rajan, R. S., and Kopito, R. R. (2005) Suppression of wild-type rhodopsin maturation by mutants linked to autosomal dominant retinitis pigmentosa. *The Journal of biological chemistry* **280**, 1284-1291

214. Mendes, H. F., and Cheetham, M. E. (2008) Pharmacological manipulation of gain-of-function and dominant-negative mechanisms in rhodopsin retinitis pigmentosa. *Human molecular genetics* **17**, 3043-3054

215. Liang, Y., Fotiadis, D., Filipek, S., Saperstein, D. A., Palczewski, K., and Engel, A. (2003) Organization of the G protein-coupled receptors rhodopsin and opsin in native membranes. *The Journal of biological chemistry* **278**, 21655-21662

216. Xie, G., Gross, A. K., and Oprian, D. D. (2003) An opsin mutant with increased thermal stability. *Biochemistry* **42**, 1995-2001

217. Zhukovsky, E. A., Robinson, P. R., and Oprian, D. D. (1991) Transducin activation by rhodopsin without a covalent bond to the 11-cis-retinal chromophore. *Science* **251**, 558-560

218. Devine, E. L., Oprian, D. D., and Theobald, D. L. (2013) Relocating the active-site lysine in rhodopsin and implications for evolution of retinylidene proteins. *Proceedings of the National Academy of Sciences of the United States of America* **110**, 13351-13355

219. Petrs-Silva, H., and Linden, R. (2014) Advances in gene therapy technologies to treat retinitis pigmentosa. *Clinical ophthalmology* **8**, 127-136

220. Van Woerkom, C., and Ferrucci, S. (2005) Sector retinitis pigmentosa. *Optometry* **76**, 309-317

221. Rivera-De la Parra, D., Cabral-Macias, J., Matias-Florentino, M., Rodriguez-Ruiz, G., Robredo, V., and Zenteno, J. C. (2013) Rhodopsin p.N78I dominant mutation causing sectorial retinitis pigmentosa in a pedigree with intrafamilial clinical heterogeneity. *Gene* **519**, 173-176

222. Choe, H. W., Kim, Y. J., Park, J. H., Morizumi, T., Pai, E. F., Krauss, N., Hofmann, K. P., Scheerer, P., and Ernst, O. P. (2011) Crystal structure of metarhodopsin II. *Nature* **471**, 651-655

223. Latek, D., Pasznik, P., Carlomagno, T., and Filipek, S. (2013) Towards improved quality of GPCR models by usage of multiple templates and profile-profile comparison. *PloS one* **8**, e56742

224. Chaudhari, R., Heim, A. J., and Li, Z. (2015) Improving homology modeling of G-protein coupled receptors through multiple-template derived conserved inter-residue interactions. *Journal of computer-aided molecular design* **29**, 413-420

225. Jang, J. W., Kim, M. S., Cho, Y. S., Cho, A. E., and Pae, A. N. (2012) Identification of structural determinants of ligand selectivity in 5-HT(2) receptor subtypes on the basis of protein-ligand interactions. *Journal of molecular graphics & modelling* **38**, 342-353

226. Chung, D. C., and Traboulsi, E. I. (2009) Leber congenital amaurosis: clinical correlations with genotypes, gene therapy trials update, and future directions. *Journal of AAPOS : the official publication of the American Association for Pediatric Ophthalmology and Strabismus / American Association for Pediatric Ophthalmology and Strabismus* **13**, 587-592

227. Chacon-Camacho, O. F., and Zenteno, J. C. (2015) Review and update on the molecular basis of Leber congenital amaurosis. *World journal of clinical cases* **3**, 112-124

228. Maeda, T., Dong, Z., Jin, H., Sawada, O., Gao, S., Utkhede, D., Monk, W., Palczewska, G., and Palczewski, K. (2013) QLT091001, a 9-cis-retinal analog, is well-tolerated by retinas of mice with impaired visual cycles. *Investigative ophthalmology & visual science* **54**, 455-466

229. Liang, J., Naveed, H., Jimenez-Morales, D., Adamian, L., and Lin, M. (2012) Computational studies of membrane proteins: models and predictions for biological understanding. *Biochimica et biophysica acta* **1818**, 927-941

230. Adamian, L., and Liang, J. (2002) Interhelical hydrogen bonds and spatial motifs in membrane proteins: polar clamps and serine zippers. *Proteins* **47**, 209-218

8. ACKNOWLEDGEMENTS

I would like to express my immense gratitude to Prof. Pere Garriga who has been very kind since the day he has accepted me in his lab. I am very much thankful for his constant support, guidence, and encouragement throughout the project. I also thank for the hourly discussions we had on the results which led me to the better understanding about the cone opsin system and eventually the present thesis.

My sincere thanks to Dr. Eva Ramon who has been like an another mentor to me. Her dedication towards science enhanced my perseverance and in a way motivated to do a better research. I also thank for her relentless support, guidence, discussions and encourgements throughout my research.

I wish to thank Prof. Karl Koch from University of Oldenburg, Germany, who had accepted me to work in his lab on SPR. I feel grateful for his kind guidence and assitance on working with SPR even in late hours and also thankful about the discussions regarding the obtained results. I would like to also thank his students Stefan and Astrid who had taken care on me during my stay.

I wish to thank Dr. Arnau Cordomí from UAB who have made models for our publications which I have also used in this thesis. I also thank for the discussions we had, which helped me to visualize the conformational changes observed from my studies.

This would not have been possible if there were not my labmates, Merce, Dong, Lupita, and Miguel who have made the working environment pleasant and funfilled. I am also thankful to them sparing their experimental schedules when there was a timely need for me. I extend my thanks to the former labmates Marlet, and Aram, who had helped in my initial settelement, other members of the lab and master students.

I wish to thank Prof. Margarita Morillo for her best wishes and support. I am also thankful to Prof. Tzanko Tzanov and his group Toni, Marga, Carlos, Petya, and Kristina who have been supportive, sharing the space and materials, and also running out off mouth along with us.

Diana, one of the best friends I have got during my stay. I am very much indebted for her friendship and kind support. I feel grateful for her willingness to help me even before I sought for. The memories of our lunches, chatters and drives are ever lasting and the most cherishable.

I wish to thank my flatmates who had been very much amiable especially Oscar for being generous to bear with me when I miss my cleaning schedules, catching their breath by my cooking, and loud musics. The time we have spent on parties, dinners, eat-outs, conversations, watching and discussing football were funfilled and exposed me to the culture in Catalonia.

I could never laugh so much unless I have been with my Barcelona friends Vinoth, Karthi, Rajagopal, Hasini, Shrikanth, Aswin, Sudhashu and Marta. I must thank for the time we have spent on trips, parties, hangouts, dinners, pub crawls, night walks, songs, stories, movies, football which will ever stay close to my heart.

My masters buddies Salini and Chaitanya who have been very much supportive, cheering with in my ups and motivating in my downs. You guys make me euphoric whenever I talk with you and I am immensely thankful for always being my side.

I take this oppurtunity to thank my previous boss from Anna university Dr. Suvro Chatterjee and his lab where I began my research carrer. I feel grateful for his encourging words and advises which are steadfast. I would also like to thank Majumdar, Swaraj, and Bindu who have been friendly, supportive and encourging in my persuits.

I wish to thank my fellowships FI-AGAUR and FPI-UPC which were financially supporting my stay and I would also like to thank university staffs who had been taking care of the all the bureaucratic process which enabled me a better concentration towards the project.

Finally, I wish to thank everyone who have supported me direclty and indirectly throughout the course of my research.